ADSORPTION CAPACITY OF CARBON DIOXIDE ON ARGONNE PREMIUM COALS

Karl Schroeder[1], Ekrem Ozdemir[1,2], and Badie I. Morsi[2]

[1] U.S. Department of Energy (DOE) - National Energy Technology Laboratory (NETL), P.O.Box 10940, Pittsburgh, PA 15236
[2] Chemical and Petroleum Engineering Department, University of Pittsburgh, 1249 Benedum Hall, Pittsburgh, PA 15261

Introduction

The sequestration of carbon dioxide (CO_2) in coal seams is one of the geologic strategies being considered to mitigate increasing atmospheric concentrations of CO_2. Historically, the adsorption of CO_2 on coals has been studied to estimate the coal surface area.[1] Usually, these measurements have been conducted at low pressures and low temperatures.[2] Although information obtained from measurements such as these is important to current sequestration efforts, low-pressure adsorption isotherm data may not represent high-pressure in-seam conditions. On the other hand, CO_2 adsorption data obtained at high pressure has been reported to poorly fit the conventional adsorption equations such as the Langmuir (monolayer), BET (multiplayer), and Dubinin (pore filling) equations.[3,4]

The inconsistency between the experimental data and the isotherm equations is proposed to be due to coal swelling.[5] We have derived an expression, which incorporates the effect of swelling and shrinkage of the coal on the CO_2 adsorption isotherm. Its generalized form is given in Equation 1,

$$n_{\exp} = n_{ads} + k\left(\frac{P}{z}\right) \qquad (1)$$

where n_{exp} is the amount of adsorbed gas calculated from the ΔP determined experimentally when the void volume of the sample chamber (V_o) is considered constant at the value estimated by the He-expansion method, n_{ads} is the amount of gas actually adsorbed on the coal sample, and k is a constant, which includes the effect of the volume change in the sample cell. The constant, k, explicitly accounts for the change in volume:

$$k = \frac{(\Delta V/w)}{RT} = \frac{(\Delta V/V_0)}{\rho_0 RT} \qquad (2)$$

where $DV/$w is the change in accessible volume per gram of sample, DV/V_o is the ratio of the change in accessible volume of the sample to the initial sample volume, as estimated by He-expansion, and ρ_o is the helium-density of the sample.

According to Eq.1, the measured adsorption isotherm has two contributing parts: (1) the physical adsorption of CO_2 on the coal sample, n_{ads}, and (2) an artifact of coal swelling caused by the change in accessible pore volume which is closed to helium but accessible to CO_2, $k(P/z)$. A number of equations, including the Langmuir and Dubinin, can be substituted for the physical adsorption term, n_{ads}, to give good correlations. Herein, we use the Langmuir equation. The increased volume available for gas compression we attribute to an opening of the restricted pores by CO_2 which increases the void volume of the sample cell beyond that measurable by helium.

In this study, we report on the adsorption capacity of CO_2 on some of the Argonne Premium coals employing the newly derived adsorption equation.

Experimental

Coal Samples. The proximate and ultimate analyses for the Argonne premium coal samples are shown in **Table 1**.[6] Minus 100 mesh samples were used in all experiments. Sample handling was performed in a helium-flushed glove bag under a positive pressure of helium. Each sample was dried *in-situ* at 80 °C under vacuum for 36 hours before measurements were performed.

Table 1. Proximate and Ultimate Analyses of the Argonne Premium Coal Samples

Coal Sample	Rank	Proximate Analysis (wt%) Moisture	Ash[a]	VM[b]	Ultimate Analysis (wt%, daf) C	H	O	S	N
Pocahontas No.3	Lvb.	0.65	4.74	18.48	91.0	4.4	2.0	0.7	1.27
Upper Freeport	Mvb.	1.13	13.2	27.45	85.5	4.7	7.5	0.74	1.55
Illinois No. 6	Hvb.	7.97	15.5	40.05	77.7	5.0	13.5	2.38	1.37
Wyodak	Subbit.	28.09	6.31	32.17	75.0	5.4	18.0	0.6	1.20
Beulah-Zap	Lignite	32.24	6.59	30.45	73.0	4.8	20.0	0.8	1.04

[a] dry basis
[b] volatile matter, dry basis

Gas adsorption apparatus. Gaseous carbon dioxide adsorption isotherms were obtained using a manometric gas adsorption apparatus described elsewhere.[7] Briefly, the manometric apparatus consists of a reference cell of approximately 13 ml and a sample cell of about 6 ml; both contained within a temperature-controlled bath (±0.1 °C). The cell volumes were estimated by the He-expansion method. The pressure within each of the cells was monitored using a pressure transducer (Omega PX300-5KGV), accurate to ± 0.25% full scale. An ISCO syringe pump was used to deliver pressurized CO_2.

Measurement Methods. Adsorption isotherms of CO_2 on the Argonne Premium coals were measured at 22, 30, 40, and 55 °C. The reference cell was pressurized to the desired level as indicated on a pressure transducer. Thermocouples within the cells showed that thermal equilibrium was established within 3 min. A portion of the gas was then transferred from the reference cell to the sample cell. It was found that 20-30 min was sufficient for the adsorption to reach equilibrium as evidenced by stable temperature and pressure readings. From the calculated volumes of the reference and sample cells, and the constant temperature, the amount of gas that was transferred from the reference cell to the sample cell was calculated using the real gas law, which accounts for the gas compressibility.[8] The difference between the moles transferred from the reference cell and the moles in the gas phase in the sample cell was accounted to the adsorption of CO_2 on the coal. The pressure in the reference cell was then increased and the process was repeated. Adsorption isotherms were plotted as the total amount of adsorbed gas at each equilibrium pressure.

Results and Discussion

The adsorption and desorption isotherms of CO_2 on the Argonne Premium coals were measured at 22, 30, 40, and 55 °C and at pressures up to 4 MPa. **Figure 1** shows the adsorption (open symbols) and desorption (closed symbols) isotherms for CO_2 on these coals at 22 °C. The lines were calculated by substituting the Langmuir expression for n_{ads} in Equation 1 and fitting the resultant equation to the entire range of adsorption data. In general, both adsorption and desorption data fall on the same line. Similar isotherm shapes but with a lower extent of adsorption were seen at the higher temperatures. A small amount of hysteresis was observed only for the Illinois No. 6 sample. The fact that the data for all 5 coals could be fit well using Equation 1 argues favorably for its general form although we recognize that the fit alone does not prove the underlying assumptions of the derivation.

Eq.1 can be employed to differentiate between the adsorbed CO_2 and the effect of coal swelling. This partitioning of the adsorbed amount is shown in **Figure 2** where the measured adsorption isotherm for the Pocahontas coal is divided into the two contributing parts. The portion of the missing gas apportioned to the physical adsorption of the CO_2 is shown as the solid-line Langmuir portion of Equation 1 and the effect of the change in accessible pore volume is displayed as the dashed line. Due to CO_2-induced swelling of the coal during adsorption, the accessible volume available for gas compression increases so that more volume becomes available to the CO_2 than the volume initially estimated by helium expansion. At low-pressures, the effect of swelling on the adsorption isotherm is small when compared with the amount of CO_2 actually adsorbed. At high pressures, however, the amount of gas in the additional void volume is considerably higher due to the compressibility of CO_2.

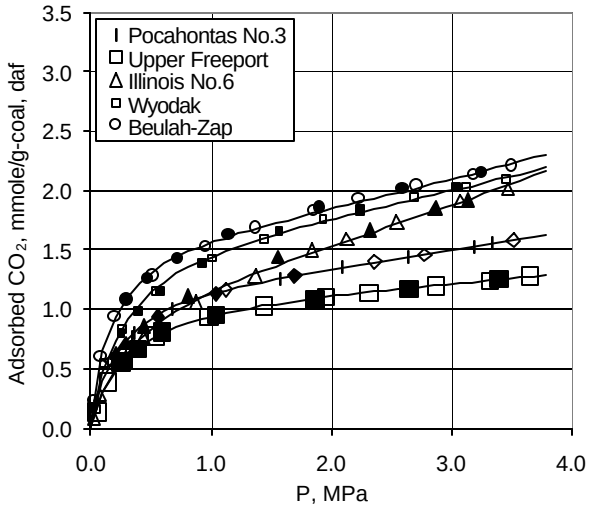

Figure 1. CO_2 adsorption (open symbols) and desorption (closed symbols) isotherms of several of the Argonne Premium.

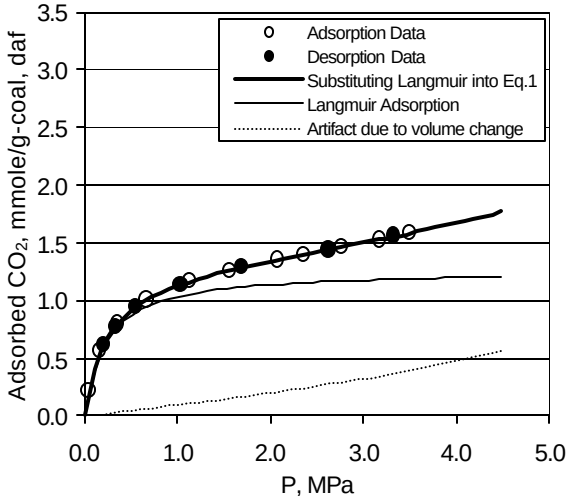

Figure 2. Best fit of Eq.1 (heavy solid line) to the adsorption (open symbols) and desorption (closed symbols) isotherms of the Argonne Premium Pocahontas No.3 coal showing the relative contributions of Langmuir adsorption (solid line) and swelling effects (dashed line).

By substituting the Langmuir or Dubinin-Astakhov equations for n_{ads} in Equation 1, the adsorption capacities were calculated. The heats of adsorption for CO_2 were calculated directly from the Dubinin-Astakhov equation and by using the Clausius-Clapeyron equation and the temperature dependence of the adsorption isotherms in the case of the Langmuir best-fits. These are shown as a function of maf carbon in **Figure 3**. Both decrease with maturation of the coal up to 80-86% C, and then increase with increasing maturation consistent with the U-shaped dependence typical of surface areas, densities, and porosities of coals of different rank.[9] However, the variations in the adsorption capacity and the characteristic heat of adsorption are not large. The adsorption capacities and characteristic heats of adsorption are 0.9-1.7 mmole/g-coal, daf-basis and –26 to –30 kJ/mole, regardless of coal rank.

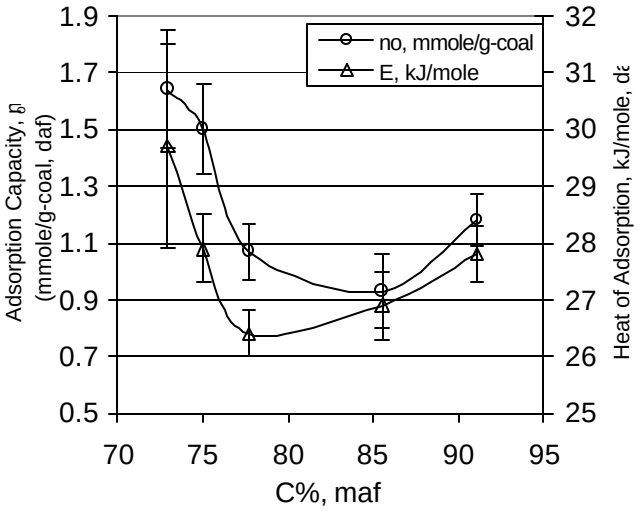

Figure 3. Adsorption capacity and heat of adsorption of CO_2 on several of the Argonne Premium coals.

References

[1] Ettinger, I.; Chaplinsky, A.; Lamba, E. and Adamov, V. *Fuel*, **1965**, 351-356.

[2] Walker, P.L. and Kini, K.A. *Fuel*, **1965**, 44, 453.

[3] Clarkson, C.R.; Bustin, R.M.; and Levy, J.H. *Carbon*, **1997**, 35 (12), 1689-1705.

[4] Duda, J.M.; Duda, J.; Nodzenski, A. and Lakatos, J. *Langmuir*, **2000**, 16, 5458-5466.

[5] Ozdemir, E.; Schroeder, K.; and Morsi, B.I. **2001**, in preparation.

[6] Vorres, K., *Energy Fuels,* **1990**, 4, 420-426.

[7] Ozdemir, E.; Schroeder, K. and Morsi, B.I. Prepr. Pap. - *Am. Chem. Soc., Div. Fuel Chem.*, **2001**, 46 (1), xxx.

[8] Span, R. and Wagner, W. *J. Phys. Chem. Ref. Data*, **1996**, 25(6), 1509-1596.

[9] Jones, A.H.; Bell, G.J. and Schraufnagel, R.A. In: Coalbed Methane, SPE Preprint Series, No.35, SPE, Richardson, TX, 1992.

CARBON DIOXIDE CAPTURE BY AMINES: INCREASING THE EFFICIENCY BY AMINE STRUCTURE MODIFICATION

Angela Dibenedetto, Michele Aresta and Marcella Narracci*

University of Bari and METEA Research Center
Department of Chemistry, Campus Universitario, 70126 - Bari, Italy,
fax +39 080 544 2083, e-mail: a.dibenedetto@chimica.uniba.it

Introduction

Carbon dioxide is the largest contributor to the greenhouse effect, being produced in the combustion of fossil fuels as oil, natural gas or coal, for energy production or heating, and in industrial processes.

Carbon dioxide can be recovered by using several technologies such as the absorption into an appropriate solution[1] or the membrane separation.[2] The former is used in several industrial applications such as CO_2 separation from power plants flue gases, natural gas treatment and landfill gas upgrading. The capacity of the amine to uptake/bind CO_2 is of fundamental importance for sizing the separation tower.

In this paper we consider the advantage of using new amines for capturing carbon dioxide from gas mixtures. The kinetics of CO_2 uptake using four new different amines is compared with that of absorption by MEA.

Experimental

All data were recorded under the same conditions: 1 atm of CO_2 and 298 K. The kinetics was followed in tetrahydrofuran (THF) as solvent. 8 mL of THF were saturated with CO_2 in the absorption flask, then the amine (0.90 mmol) was added. The uptake of CO_2 was followed using a gas burette.
Neat amines have been also used.

Results and Discussion

Aliphatic amines are known to react promptly with CO_2 [Eq 1] to afford an ammonium carbamate.[3]

$$2\ RNH_2 + CO_2 \longrightarrow RNH_3^{+-}O_2CNHR \quad (1)$$

We have investigated the behaviour of mono- (A, B, C) and di-amines (D, E)[4] towards CO_2 at various temperatures. Mono-amines A, B and MEA (C) react rapidly with CO_2 at 298 K in THF. Figure 1a-b-c show that the reaction is almost complete in 15 minutes and the amount of CO_2 taken up by the amine (*ca.* 0.55 mol/mol amine) says that one mol of CO_2 reacts with two moles of amine, as required by the stoichiometry of reaction 1, to afford ammonium carbamates.

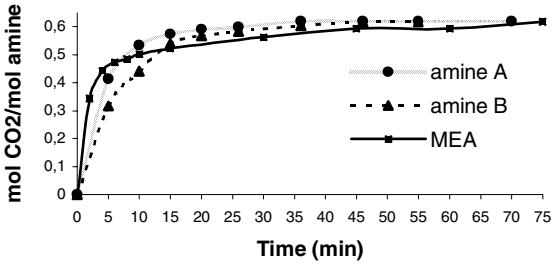

Figure 1. Kinetics of reactions of mono-amines with carbon dioxide

Amines A and B are as performing as MEA. In all cases, the solution at the end of the reaction is cloudy due to a fine suspension of a white solid. Interestingly, if the reaction is carried out at 273 K, the amount of CO_2 fixed by amines A and B, after a fast initial uptake, of ca. 0.50 mol/mol, increases slowly to 1 mol/mol within three hours. This feature can be explained assuming that at low temperature any of the ammonium carbamates $RNHCOO^{-+}H_3NR$ slowly converts into the dimeric form of the relevant carbamic $(RNHCOOH)_2$ acid. We have already shown that, in the same conditions, the carbamate/carbamic acid conversion takes place with benzylamine[5] and other N-compounds. (Eq.2) In the case of R=benzyl, the dimeric carbamic acid has been isolated and characterized by X-ray[5a].

$$RNHCOO^{-+}H_3NR + CO_2 \rightarrow (RNHCOOH)_2 \qquad R = \text{Benzyl} \qquad (2)$$

Carbamates of amines (A and B) do not release CO_2 easily upon heating. Therefore, they are not good candidates for the separation of carbon dioxide from other gases (e.g., from flue gases) as they can not advantageously operate in a cyclic system implying the uptake and release of carbon dioxide.
When diamine D or E is used, the CO_2 uptake curve (Fig. 2) at 298 K has a different shape with respect to that characteristic of monoamines.

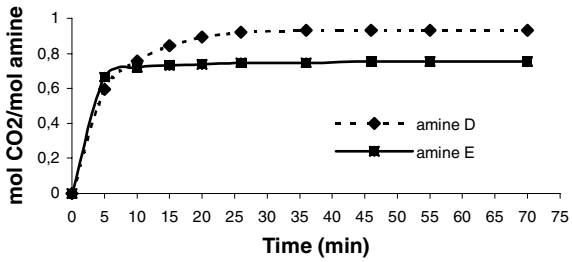

Figure 2. Kinetics of reactions of di-amines with carbon dioxide

Diamines D, E take up CO_2 with a 0.8-1 molar ratio, to afford a glassy material that occludes solvent. The reaction quickly takes place also in absence of solvent. The resulting carbamates have been isolated and characterised. Diamines are thus by far more efficient than monoamines for CO_2-capturing. This aspect is quite important as by using diamines it would be possible to reduce to half the amount of amine necessary for the separation of a given amount of CO_2, and thus the volume of the absorption tower. Interestingly, the carbamates of diamines easily release carbon dioxide at moderate temperatures, making such systems quite interesting candidates for CO_2 separation.

We are now working at some improvement of the amine molecular structure in order to further increase the separation efficiency.

Acknowledgement. This work was supported by MURST, Project no. 9803026360 and MM03027791

References

(1) Rangwala H.A. *J. Memb. Science* **1986**, 112, 229.
(2) RUCADI Project, BRRT-CT98-5089.
(3) a) Aresta, M. and Quaranta, E. *Tetrahedron*, **1991**, 47, 9489; b) Aresta, M. and Quaranta, E. *Ital. Pat.* 1237207, **1993.**

(4) The structure of the amines A, B, C, D will be discussed at the symposium.
(5) a) Aresta, M.; Ballivet-Tkatchenko, D.; Belli Dell'Amico, D.; Bonnet, M. C.; Boschi, D.; Calderazzo, F.; Faure, R.; Labella, L. and Marchetti, F. *Chem. Commun.* **2000**, 1099**;** b) Aresta, M.; Ballivet-Tkatchenko, D.; Bonnet, M. C.; Faure, R.; and Loiseleur, H. *J. Am. Chem. Soc.* **1985**, 107, 2994

CARBON SEQUESTRATION UTILIZING INDUSTRIAL SOLID RESIDUES

Daniel J. Fauth, Yee Soong, and Curt M. White

U.S. Department of Energy, National Energy Technology Laboratory
P.O. Box 10940, Pittsburgh, PA 15236-01940

Introduction

Increasing public concern related to the possible effects that anthropogenic emissions of CO_2 may have on global climate has led the Department of Energy (DOE) to embark on development of a number of carbon sequestration processes for mitigating carbon dioxide. Anthropogenic emissions of CO_2 generated by the combustion of fossil fuels are estimated at 6 GtC/year[1]. The intent of the Carbon Sequestration program is to significantly decrease emissions of greenhouse gases and stabilize atmospheric CO_2 concentrations at 550 ppm, by 2025. Complementary to traditional areas of energy research, such as improving energy efficiency or shifting to renewable or nuclear energy sources, carbon sequestration will allow continued use of fossil energy, buying decades of time needed for transitioning into less carbon-intensive and more energy-efficient methods for generating energy in the future.

Mineral carbonation, the reaction of CO_2 with non-carbonated minerals to form stable, benign, mineral carbonates, has been identified as a possible safe, long-term, and unmonitored option for storing carbon dioxide[2-7]. In this chemical approach, CO_2 reacts with alkaline earth containing silicate minerals, such as serpentine $Mg_3Si_2O_5(OH)_4$, forming magnesite, $MgCO_3$. Moreover, Goff and Lackner have shown the economics of using magnesium silicates for carbonation and their abundance are well matched concerning the scale of CO_2 storage[8]. Current studies using serpentine, a Mg-rich lamellar hydroxide based mineral, however, requires prior pulverization to the mineral, removal of iron oxide, magnetite, prior to carbonation, and thermal activation at high temperatures (630°C) to successfully achieve rapid and high rates of conversion to magnesite. Thus, alternative chemical and mechanical methods focusing on surface activation of serpentine to accelerate the carbonation reaction efficiency have been under investigation[9,10].

The objective of our study was to use industrial solid residues (FBC ash and FGD spray dryer ash) rather than natural minerals, for investigating their potential in permanently sequestering CO_2 as mineral carbonates. Although not available in sufficient quantities to make an impact on worldwide CO_2 emissions, these materials are readily available at low cost, easily gathered at or near energy and industrial sites, and readily accessible in fine particle sizes. Use of these alternative feeds were envisioned to provide a faster reaction pathway optimizing energy management along with providing an immediate incentive toward the development of a high-pressure direct carbonation method for processing these commercial by-products.

Experimental

Mineral Carbonation Experiments Initial proof-of-concept tests were conducted using samples obtained from Freeman United Coal Mining Company, Farmersville, Illinois, USA and Consol Energy, Library, PA, USA, respectively. Carbonation reactions were carried out in a 1-liter Hastelloy C-2000 continuous-stirred-tank-reactor (CSTR). In a representative experiment, a determined amount of solid reactant was mixed with an aqueous bicarbonate solution (0.5 M Na_2CO_3/0.5 M $NaHCO_3$; 1.0 M NaCl) and charged into the CSTR. The CSTR was sealed, and purged with gaseous carbon dioxide. A pre-determined amount of liquid CO_2 was then carefully injected through the side port of the CSTR. The solid reactant/bicarbonate solution/liquid CO_2 mixture was sufficiently agitated during both heat up and testing to prevent any settling of solid reactant. The carbonation studies were conducted at temperatures (155 &185°C) and CO_2 pressures (75 & 115 atm) for 1 hour at an agitation speed of 1000 rpm. At the conclusion of the test, the remaining CO_2 was vented, and the carbonated slurry was flushed from the CSTR and filtered to separate solids from the aqueous bicarbonate solution. The washed carbonated solid product was dried at 105°C in air overnight. A digital pH meter was used to determine the pH values of pre-and post-product solutions.

X-ray powder diffraction (XRD) XRD measurements of untreated and supercritical CO_2–treated solids were carried out using a Rigaku DAD-IIA powder diffractometer with a Cu-Kα X-ray source at 40kV and 25 mA. The powder sample was mounted on a glass sample holder. The XRD patterns were recorded over a 2θ range of 2° to 90° and compared with the JCPDS mineral powder diffraction file.

Scanning Electron Microscopy (SEM) SEM analyses were performed using an Aspex Personal SEM™ equipped with a Noran energy dispersive detector enabling x-ray detection of elements with atomic number 6 (carbon) and greater. Sample preparation involved mounting a portion of a representative sample in epoxy and polishing to obtain a cross section of the particles. Polished cross sections of supercritical CO_2-treated solid products were analyzed at an accelerating voltage of 20 KeV and working distance of 16-19 mm. Prior to analyses, samples were coated with a thin layer of carbon to provide an electrically conductive surface. The samples were examined in backscattered electron imaging (BSI) mode coupled with energy dispersive spectroscopy (EDS).

Results and Discussion

The chemical analyses of the major components were determined by ICP-AES, with a preliminary preparation of acid digestion. The chemical composition of FBC and FGD solid residues and their corresponding carbonation products are summarized in Table 1. The crystalline phases of the FBC solid residue was analyzed by XRD. Anhydrite ($CaSO_4$), quartz (SiO_2), periclase

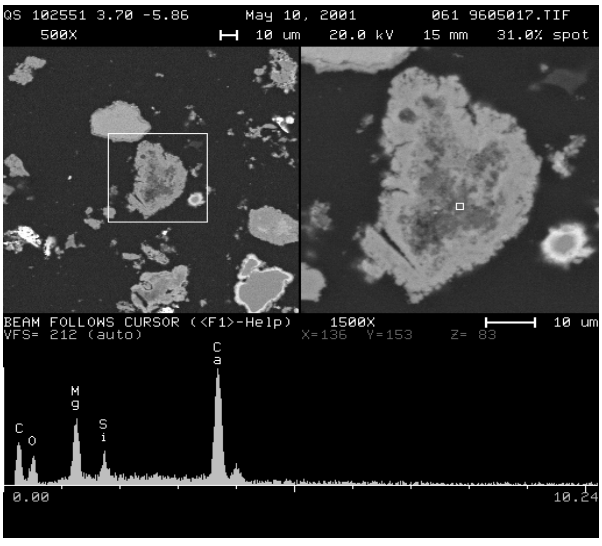

Figure 1. SEM image with EDS spectra of supercritical CO_2-treated FBC ash (Freeman United Coal Mining Co.)

(MgO), lime (CaO) and hematite (Fe_2O_3) were identified as minor phases for the FBC ash (Freeman United Coal Co.) feed sample. XRD confirmed a trace constituent; calcite ($CaCO_3$) was also present. Dolomite, $CaMg(CO_3)_2$ and calcite were determined as being the primary constituents in the supercritical CO_2-treated FBC solid product. Free CaO was identified as the primary constituent for the FGD spray dryer ash material obtained from Consol Energy. XRD analysis coupled with a relatively high CO_2 concentration of in FGD reaction product, confirmed $CaCO_3$ as the major element in the Consol Energy FGD carbonation product.

Table 1. Chemical composition of FBC and FGD solid residues

Oxide	FBC Residue	FBC Product	FGD Residue	FGD Product
Al_2O_3	5.9	6.1	15.9	12.7
CaO	27.1	22.7	31.9	23.1
FeO, Fe_2O_3	6.3	5.9	3.9	3.2
MgO	9.6	8.0	1.4	1.2
SiO_2	24.4	25.0	35.0	26.8
Na_2O	0.6	0.7	0.3	0.3
TiO_2	0.3	0.3	0.8	0.8
P_2O_5	0.1	0.1	0.1	0.1

Figure 1 shows a SEM photomicrograph with EDS spectra obtained for a supercritical CO_2-treated FBC ash (Freeman United Coal Co.). Although the EDS spectra are elemental, it is assumed that they are representative of the oxide species, unless otherwise noted. SEM with EDS spectra identified a number of large grains within the representative sample to contain relatively high concentrations of Ca, Mg, C, and O with trace amounts of silica. These particles dispersed throughout the mount were identified as dolomite by SEM-EDS. SEM-EDS analysis also showed the majority of the grains to contain high concentrations of silica. These particles could represent unreactive quartz (SiO_2).

Results obtained from tests investigating the mineral carbonation efficiency of FBC residues (Freeman United Coal Mining Co.) and FGD residues (Consol Energy) in an aqueous bicarbonate/NaCl solution are shown in Table 2. Extent of reaction achieved in tests conducted for one hour using the FBC solid residue was 50 and 51% stoichiometric, respectively. The main components of the FBC solid residue from coal combustion in fluidized beds, using limestone as a sorbent of SO_2 formed during the combustion process, are those arising from the reaction ($CaSO_4$), and by-products of reaction (CaO, $CaCO_3$). These reactants, including $CaSO_4$ react with the dissolved CO_2 to form the resulting mineral carbonate. Tests conducted with the latter feed (FGD residue) resulted in higher stiochiometric conversion to calcite. The concentration of free lime (CaO) was obvious much higher for the FGD residue than for the corresponding FBC solid residue.

The annual production rate of the FBC solid residue was estimated at approximately 400,000 t/year. Based on our preliminary results and the composition of the FBC solid residue, the order of magnitude of CO_2 sequestration is 15.8 wt % of the FBC residue. Therefore, 63,200 t CO_2/year or about 17,236 t C/year could be sequestered at the Farmerville, Illinois complex.

Conclusions

Preliminary results at NETL indicate direct aqueous mineral carbonation to be a viable technique for converting both FBC ashes and FGD materials into mineral carbonates. Although the sequestration potential of these materials are small, the ability to effectively process such a stream could lead to industrial interest in the development of a cost effective direct aqueous carbonation technology.

References

1. Freund, P.; Ormerod, W.G., *Energy Conversion Management*; No. 8:S199; 1997.
2. Seifritz, W. *Nature* 345, 486, 1990
3. Lackner, K.; Wendt, C.; Butt, D; Joyce Jr. E.; Sharp, D., *Energy* **20**, 1153-70, 1995
4. Walters, R.P.; Chen, Z.Y.; Goldberg, P.M.; Lackner, K.S.; McKelvy, M.J.; Ziock, H., *Mineral Carbonation: A Viable Method for CO_2 Sequestration*; Program Plan and Approach, National Energy Technology Laboratory, http://www.fetc.doe.gov/products/ggc, 1999
5. Dahlin, D.C.; O'Connor, W.K.; Nilsen, D.N.; Rush, G.E.; Walters, R.P.; Turner, P.C., *A Method for Permanent CO_2 Sequestration: Supercritical CO_2 Mineral Carbonation;* 17th Annual International Pittsburgh Coal Conference, Sept.2000
6. O'Connor, W.K.; Dahlin, D.C.; Nilsen, D.N.; Walters, R.P.; Turner, P.C., Proceedings of the 25th International Technical Conference on Coal Utilization & Fuel Systems, Clearwater, Florida, 153-64, Edited by B.A. Sakkestad, Coal Technology Association, Rockville, Md., 2000
7. Fauth, D.J.; Baltrus, J.P.; Knoer, J.P.; Soong, Y.; Howard, B.H.; Graham, W.J.; Maroto-Valer, M. M.; Andrésen, J.M.;; Prepr.Symp. *Am. Chem. Soc., Div. Fuel Chem.*, **2001**, 46 (1), 278.
8. Goff, F.; and Lackner, K.S.; *Environmental Geosciences*; **5**, 88-101
9. Maroto-Valer, M.M., Fauth, D.J.; Kuchta, M.E.; Zhang, Y.; Andrésen, J.M.; Soong, Y.; *Study of Magnesium Rich Minerals as Carbonation Feedstock Materials for CO_2 Sequestration;* 18th Annual International Pittsburgh Coal Conference, New South Wales, Australia, December, 2001
10. O'Connor, W.K.; Dahlin, D.C.; Nilsen, D.N.; Gerdemann, S.J.; Rush, G.E.; Walters, R.P.; Turner, P.C.; *Research Status on the Sequestration of Carbon Dioxide by Direct Aqueous Mineral Carbonation*; 18th Annual International Pittsburgh Coal Conference, New South Wales, Australia, December, 2001

Table 2. Summary of FBC and FGD Carbonation Experiments

Feed sample	Temp., °C	P_{CO2} , atm.	Time, hrs.	Carbonation solution	Pct. Stoich. Conv.
FBC - Freeman	185	75	1	0.5 M Na_2CO_3/0.5 M NaHCO3, 1 M NaCl	50
FBC - Freeman	155	75	1	0.5 M Na_2CO_3/0.5 M NaHCO3, 1 M NaCl	51
FGD - Consol	185	115	1	0.5 M Na_2CO_3/0.5 M NaHCO3, 1 M NaCl	72
FGD - Consol	155	115	1	0.5 M Na_2CO_3/0.5 M NaHCO3, 1 M NaCl	69

Characterization of Soil Organic Matter with Rapid Pyrolysis Molecular Beam Mass Spectrometry (py-MBMS)

K. A. Magrini, C. M. Hoover, R. J. Evans, M. Looker, and M. F. Davis

Chemistry for Bioenergy Systems Center
National Renewable Energy Laboratory
1617 Cole Blvd.
Golden, CO 80401

Introduction

Soil carbon is one of the most poorly understood global carbon pools. This is partly due to the difficulty and expense of current techniques available to measure soil organic matter (SOM) components and changes and partly due to spatial variability and the difficulty of obtaining representative samples. As a result, the uncertainty in SOM knowledge is so great that opposition exists to giving credit for soil carbon sequestration in international greenhouse gas negotiations. The perception is that it will be difficult, if not impossible, to verify claims that carbon is actually being absorbed and retained in soils, a problem that is compounded by the fact that the dynamics and chemistry of SOM are not well understood. The work described here begins to address the need to develop and demonstrate analytical techniques that can rapidly provide information on soil carbon concentration and chemistry, information that is crucial to verifying carbon uptake and storage in the largest terrestrial pool – soil.[1]

A primary component of soil organic matter comes from the decomposition of biomass-derived materials. The resulting humic substances vary greatly in their decomposition rates, and when accurately measured, provide a foundation for estimating the uptake of carbon in soils. Separating and measuring these components with classical techniques is both difficult and complex. Most soil analyses require mechanical preparation, extraction and one or more chemical analyses; processes which are time consuming and labor intensive. Moreover, some analyses may not be representative of the original material due to the harsh chemical separations used.

We have developed the py-MBMS technique for analyzing a wide range of large and complex biomolecules that include lignins, cellulosic materials, plastics, and polymers. Schulten[2] details the application of pyrolysis field ionization mass spectroscopy to identify SOM components. This work applies MBMS analyses to whole soils. The method consists of rapidly heating soil samples (0.1 g) in an inert, helium atmosphere at 500°C for pyrolysis analysis and to 800°C in a helium/oxygen mixture for combustion analysis. Both processes take place at ambient pressure in a quartz reactor, which is connected to the inlet of the MBMS. The generated pyrolysis or combustion products are sampled directly in real time by expanding through a sampling orifice with subsequent formation of the molecular beam, which provides rapid sample quenching and inhibits sample condensation.[3,4,5,6] The molecular beam method of sample generation is rapid (1-5 minutes) and provides sample throughputs of 100-200 samples per day depending on analytical conditions.

To demonstrate the feasibility of these techniques for SOM and total carbon and nitrogen analysis, we analyzed forest soil samples taken from three experimental sites in the Northeast and North Central regions of the country, and agricultural soils managed for switchgrass production (South Central) and hybrid poplar production (Northwest).

At each of the sites, only mineral soil was sampled and 5-cm cores were taken as a function of depth. Samples were dried and sieved through a 2-mm screen prior to MBMS analysis. Soil samples (~0.1 g) were weighed in quartz boats in triplicates and pyrolyzed or combusted in a reactor consisting of a 2.5 cm quartz tube with helium flowing through at 5 L/min (at STP). The reactor tube was oriented so that the sampling orifice of the molecular-beam mass spectrometer (Figure 1) was inside the end of the quartz reactor. We used a molecular beam system comprised of an ExtrelTM Model TQMS C50 mass spectrometer for both pyrolysis and combustion vapor analysis. The reactor was electrically heated and its temperature maintained at 500°C or 800°C. Total pyrolysis time was 5 minutes and combustion time 2 minutes. The residence time of the vapors in the reactor pyrolysis zone was estimated to be ~75 ms. This residence time is short enough that secondary cracking reactions in the quartz reactor are minimal. We used a soil reference material (Carlo Erba, Milan, Italy, PN 33840026) containing 3.55 wt% C and 0.37 wt% N to calibrate the m/z 44 (CO_2) and the m/z 30 (NO) mass spectral peaks.

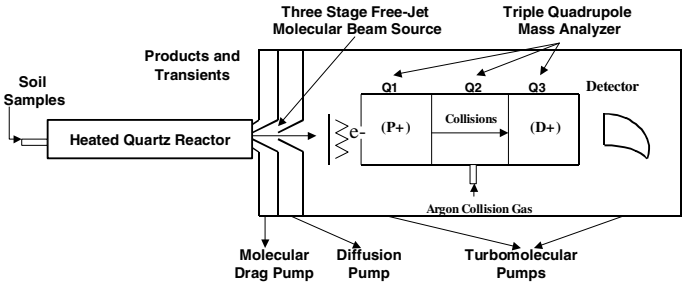

Figure 1. Schematic representation of the molecular beam sampling mass spectrometer (py-MBMS) system. The soil samples were introduced into the heated quartz reactor for pyrolysis and combustion analysis.

Mass spectral data from 15-350 amu were acquired on a Teknivent Vector 2™ data acquisition system using 22eV electron impact ionization. Data acquisition was continuous, through digitization of electron-multiplier signals from the arrival of positive ions and programmed storage in an IBM PC computer. Repetitive scans (typically one 300 amu scan/s) were recorded during the evolution of a pyrolysis or combustion wave from each soil sample. The stored spectra could be manipulated to give average spectra, subtracted spectra, or time evolution of different masses. Using this system, both light gases and heavy molecules are sampled simultaneously and in real time. We used multivariate data analysis (pattern recognition) to handle mass spectral data sets and identify trends to discover the underlying chemical changes that may not be obvious by comparison of such complex mass spectra.[7-8]

Results and Discussion

Figure 2 shows the weight percentages (wt%) of total carbon and nitrogen obtained from combustion-MBMS data from agricultural soils managed for hybrid poplar production. Hybrid poplars, which

grow rapidly, are biomass energy crops. Three sites were sampled in depth increments of 0-5, 5-10, and 10-20 cm. Total carbon (C) and nitrogen (N) contents are the average of two separate samples per site. Site 1 is fallow after one rotation of hybrid poplar, site 2 is currently in a second rotation of hybrid poplar, and site 3 is adjacent unmanaged sagebrush. All samples exhibited decreasing C and N contents with increasing depth. The fallow soil contained the least total carbon and nitrogen likely because of soil disturbance from harvesting the rotation. The soil in the second rotation of poplars contained about twice as much C and N as the fallow site and the amounts were approximately equal in the deeper increments. The unmanaged sagebrush contained the most C and N in the 0-5 cm increment and C and N contents in the 5-10 and 10-20 cm increments were about equal to those of the second rotation. The high C and N content in the 0-5 cm sagebrush increment may be attributed to the presence of dense fine roots from the sagebrush. These preliminary results show the utility of combustion-MBMS method for rapidly determining total C and N contents.

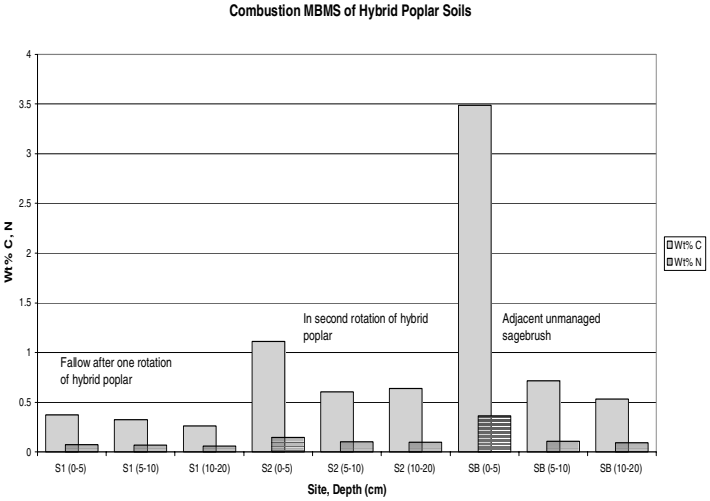

Figure 2. Total carbon and nitrogen contents of soils from a hybrid poplar plantation. Soil cores were taken in depth increments of 0-5, 5-10, and 10-20 cm. The first site (left 3 samples) was fallow after one rotation of poplar had been harvested, the middle 3 samples come from a site in a second rotation of poplar, and the 3 samples on the right are from adjacent unmanaged sagebrush.

Figure 3 shows mass spectra from the pyrolysis of soil samples taken from the Tionesta Scenic and Research Area in northwestern New York. These forest soils, which come from a site vegetated with 600-year old virgin beech hemlock, were chosen for maximum SOM carbon content. Figure 3a shows the pyrolysis mass spectrum for the 0-5 cm depth increment and Figure 3b the spectrum from the 15-30 cm increment. Comparison of the spectra shows that the shallow increment contains pyrolysis products characteristic of more recent biomass decomposition (carbohydrates, lignin) and the deep increment contains more degraded forms of biomass (phenolics, nitrogen-containing compounds).

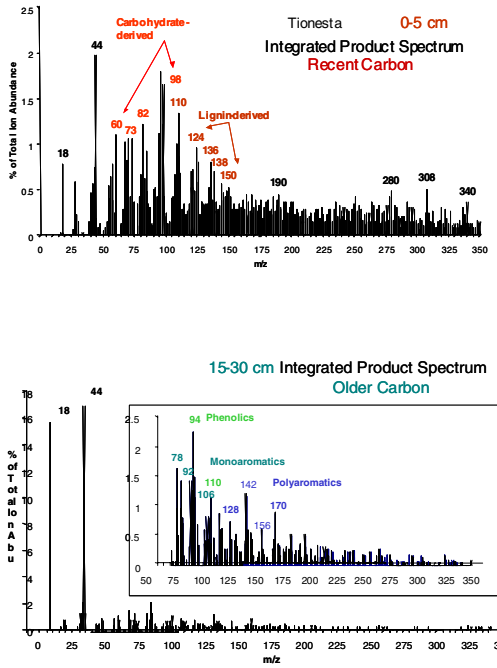

Figure 3: Integrated spectra for 0-5-cm (a) and 15-30-cm (b) samples from the py-MBMS analysis of the Tionesta forest soil. The mass spectra that occur over the pyrolysis wave for each sample are averaged. Higher mass ranges are shown in the inset of (b).

These preliminary results show that py-MBMS can distinguish the chemical changes that occur with depth. Recent biomass is characteristic of shallow samples and more aromatic species, representative of more degraded biomass, are found in the deeper samples. This technique can also distinguish among samples of different ecological sites. With continued development, this rapid analytical technique offers the opportunity to greatly increase our understanding of the role of SOM in carbon sequestration and carbon cycling, and to assess how forest and agricultural management practices can enhance that role.

References

(1) Rosenberg, N. J.; Izaurralde, R. C.; and Malone, E. L. (Eds.), *Carbon Sequestration in Soils: Science, Monitoring, and Beyond;* Battelle Memorial Press, Columbus, Ohio, **1998**; pp. 1-199.
(2) Schulten, H. R., In *Mass Spectrometry of Soils*; Boutton, T. W., Yamasaki, S.-H. Eds., Marcel Dekker, Inc., New York, **1996**, pp. 373-436.
(3) Evans, R. J. and Milne, T. A., *Energy and Fuels,* **1987,** *1*, 123-137.
(4) Evans, R. J.; Milne, T. A.; Soltys, M. N., *J. Anal. Appl. Pyrolysis*, 1986, *9*, 207-236.
(5) Evans, R. J.; Milne, T. A.; Soltys, M. N.; Schulten, H. R., *J. Anal. Appl. Pyrolysis*, **1984,** *6*, 273-283.

(6) Milne, T. A. and Soltys, M. N., *J. Anal. Appl. Pyrolysis*, **1983,** *5*, 93-131
(7) Windig, W.; McClennen, W.H.; Muezelaar, H.L.C., Che*mometrics & Intelligent Lab. Systems,* **1987,** *1*, 151-165.
(8) Agblevor, F. A.; Evans, R.J.; and Johnson, L.D., *J. Anal. Appl. Pyrol.,* **1994,** *30*, 125-144.

CO_2 ABSORPTION PERFORMANCE OF AQUEOUS ALKANOLAMINES IN PACKED COLUMNS

Amornvadee Veawab, Adisorn Aroonwilas, and Paitoon Tontiwachwuthikul

Faculty of Engineering, University of Regina
Regina, Saskatchewan, Canada S4S 0A2

Introduction

It is now scientifically evident that human activities have caused concentrations of greenhouse gases to rise significantly over the last two hundred years.[1] This causes a change in the atmosphere composition and the problem of global warming. The desire to alleviate the global warming problem has resulted in a serious environmental concern and a need to either reduce greenhouse gas emissions from industrial sources or put them into long term storage. Carbon dioxide (CO_2) is the largest contributor to the global warming problem, and is thus the major target for the reduction. Among the capture techniques, the flue gas scrubbing using absorption solvents is the most mature and readily applied technology for the reduction of CO_2 emissions from the stationary power plants.[2]

Aqueous solutions of alkanolamines are the chemical solvents that have been used extensively for the CO_2 capture.[3] Common alkanolamines are monoethanolamine (MEA), diglycolamine (DGA), diethanolamine (DEA), diisopropanolamine (DIPA) and methyldiethanolamine (MDEA). At present, formulated solutions containing a variety of alkanolamines are gaining popularity in the gas separation industry. These solutions often provide a greater absorption performance or meet unique needs when compared to the aqueous solutions of single alkanolamines.[4] The most common formulations consist of blends of MDEA and other alkanolamines to form MDEA-based solvents. The MDEA-based solvents can provide excellent absorption capacity, great energy efficiency and low corrosivity in comparison with the single alkanolamines.[5]

Research objective

The choice of the absorption solvents can be determined by a number of factors, such as absorption efficiency, energy consumption, corrosion, and solvent degradation. The absorption efficiency is an important factor since it measures the mass-transfer rate of acid gas into the absorption solvent that is required to achieve a removal target. In most cases, the efficiency is theoretically evaluated by using classical laboratory reactors, such as stirred cell and laminar jet absorber where the interfacial area for the mass-transfer is known and fixed. These reactors do not take into account the hydrodynamic features of the contacting devices, which may vary with type of absorption solvents during the plant operation. Therefore, it is necessary to use a column (packed or tray) as a gas-liquid contacting device for evaluating the absorption efficiency of any solvent of interest. This work evaluated and compared the CO_2 absorption efficiency of the aqueous solutions of single and blended alkanolamines in a packed column fitted with structured packing. Effects of two important operating conditions, including CO_2 loading of solution and liquid load (flow rate per cross sectional area), on the absorption efficiency were also examined. The test alkanolamines were MEA, DEA, DIPA, MDEA, and MEA-MDEA.

Experiments

The experiments were carried out in a bench-scale absorption unit of which the main component was the acrylic absorption column with an internal diameter of 20-mm and height of 2.0-m. The column was packed with stainless steel structured packing (Sulzer DX). A series of gas sampling points were installed for measuring the gas-phase CO_2 concentrations along the column. An IR gas analyzer (model 301D, Nova Analytical System Inc.) was used for measuring the CO_2 concentration with an accuracy of ±0.4%. The liquid samples taken from the bottom of the column were analyzed for their compositions using titration methods. The experimental results were presented as gas-phase CO_2 concentration profiles along the height of the absorption column. The CO_2 absorption or removal efficiency (η) was determined using the following equation:

$$\eta = \left[1 - \left(\frac{y_{out}}{1-y_{out}}\right) \times \left(\frac{1-y_{in}}{y_{in}}\right)\right] \times 100 \qquad (1)$$

where y_{in} and y_{out} denote mole fractions of CO_2 in gas-phase at the bottom and the top of the absorption column, respectively.

Results and discussion

CO_2 absorption performance of single alkanolamines. MEA and DEA were found to have a superior CO_2 absorption performance over DIPA and MDEA. As shown in Figure 1, 10% CO_2 in the feed gas was completely absorbed by the fresh (nil CO_2 loading) aqueous solutions of MEA and DEA within 2.0-m column height, while certain amounts of CO_2 in the treated gas (at the column top) were detected in cases of DIPA and MDEA.

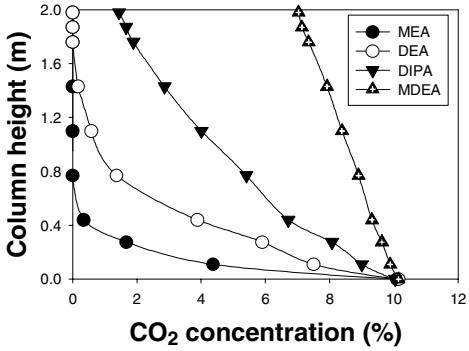

Figure 1. Gas-phase CO_2 concentration profile along the column for single alkanolamine solutions (3 kmol/m^3 solution concentration; 0.00 mol/mol CO_2 loading; 10.0 m^3/m^2-h liquid load).

Although both MEA and DEA were able to provide a complete removal of CO_2, their absorption performance can be distinguished by considering the column height required for the absorption. The CO_2 absorption into the MEA solution took place within only 0.8-m from the column bottom while the DEA required as high as 1.8-m to complete the same task. This illustrated the superior performance of MEA over the DEA solution. Consequently, the absorption performance of the test solutions was in the following order: MEA > DEA > DIPA > MDEA.

The absorption experiments were further conducted under different CO_2 loadings of the solution and different liquid loads in order to broaden the performance comparison. The CO_2 loading and the liquid load were found to have no impact on the order of the absorption efficiency (Figures 2 and 3). The order remained as it was under the fresh solution condition, i.e. MEA > DEA > DIPA > MDEA. However, the performance of the CO_2 absorption had an inverse relationship with the CO_2 loading of the feed solution, i.e. it decreases with the increasing CO_2 loading of the solution. The deterioration of the absorption efficiency was caused by a reduction of the available reactive alkanolamine concentration that provided a driving force during the mass transfer. The result also shows that increasing the liquid load caused a reduction in the CO_2 concentration

of gas phase, indicating a greater absorption efficiency. This was a result of two basic phenomena that take place in parallel. First, an increase in the liquid load led to a greater degree of the wetted packing surface (hydrodynamics) participating in the mass transfer process. Second, the liquid solution at a higher flow rate experienced a smaller change in its concentration, thus retaining the bulk of its absorption capacity throughout the column and maintaining the mass transfer driving force.

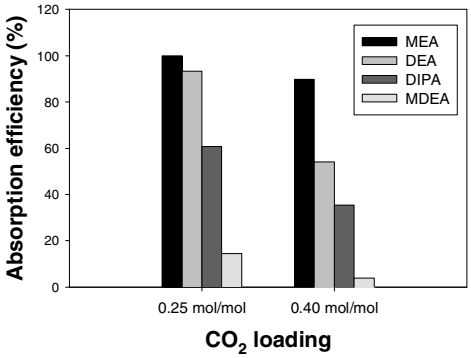

Figure 2. CO_2 absorption efficiency of single alkanolamine solutions (3 kmol/m^3 solution concentration; 10.0 m^3/m^2-h liquid load).

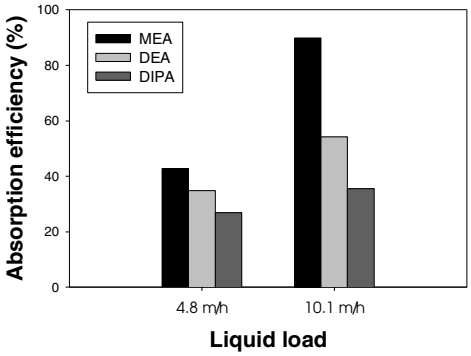

Figure 3. CO_2 absorption efficiency for single alkanolamine solutions (3 kmol/m^3; 0.00 CO_2 loading).

CO_2 absorption performance of blended alkanolamines. The CO_2 concentration profiles of the MEA-MDEA lie between those of the pure components (Figure 4), indicating a hybrid absorption behavior. The absorption also appeared to be influenced by the variations in CO_2 loading. As the CO_2 loading increased, the CO_2 concentration profile of the MEA-MDEA shifted upwards, resulting in a lower CO_2 absorption efficiency. It was noticed that the CO_2 concentration profile or absorption efficiency of the MEA-MDEA was close to that of the MEA in case of no or very small CO_2 loading. However, once the CO_2 loading was increased, the profile (efficiency) of MEA-MDEA moved towards in a direction of the MDEA profile. This behavior manifests a kinetic competition of the two components (MEA and MDEA) in the blended solution. It is likely that, under low CO_2 loading conditions, the MEA plays a dominant role in the CO_2 absorption since its reaction rate with CO_2 is much faster than the MDEA's. However, once the CO_2 loading increases to a certain value, the MEA will loose its competitive characteristic in absorbing the CO_2 due to the depleting active MEA. As a result, the MDEA will gain its role in absorption at high CO_2 loading. This behavior suggests that, the transfer of CO_2 from gas phase at the top portion of the column takes place primarily due to the pure solution with a faster reaction rate with CO_2 (MEA) while that at the bottom portion of the column takes place primarily due to the solution with a lower reaction (MDEA).

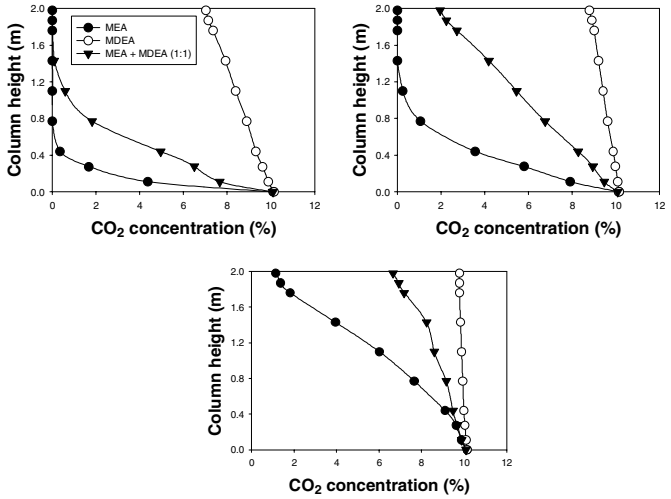

Figure 4. Gas-phase CO_2 concentration profile along the column for 3 kmol/m^3 MEA-MDEA (1:1) solution (0.00-top-left, 0.25-top-right and 0.40-bottom mol/mol CO_2 loading; 10.0 m^3/m^2-h liquid load).

Conclusions

The absorption efficiency of various alkanolamines was evaluated in a packed column where the hydrodynamic feature was taken into account. The absorption efficiency increased in the order of MEA > DEA > DIPA > MDEA. The absorption efficiency of MEA-MDEA solution was a combination of those of the pure components. A kinetic competition behavior was exhibited. At low CO_2 loading, the component with a faster CO_2 absorption rate was primarily attributable to the CO_2 removal whereas the component with a slower rate played a dominant role at high CO_2 loading.

Acknowledgment

Authors gratefully acknowledge the financial support received from the Natural Science and Engineering Research Council of Canada (NSERC) and the structured packing supplied by the Sulzer Chemtech, Switzerland.

References

1. Wilkinson, C. Negotiating the Climate: Canada and the International Politics of Global Warming- A Report on Key Issues at the Sixth Conference of the Parties (COP6) to the United Nations Framewaork Convention on Climate Change (UNFCCC), commissioned by The David Suzuki Foundation, BC, Canada, November 2000.
2. Wolsky, A. M.; Daniels, E. J.; Jody, B. J. *Environmental Progress* 1994, *13(3)*, 214-219.
3. Maddox, R. N. *Gas Conditioning and Processing, Vol.4: Gas and Liquid Sweetening*, 3rd ed.; Campbell Petroleum Series: Oklahoma, 1984.
4. White, L.; Street, D. E. Corrosion Control in Amine Treating Units. *Proceedings of Corrosion in the Oil Refining Industry Conference*, Phoenix, Sep. 17-18, 1998.
5. Ball, T.; Veldman, R. Improve Gas Treating. *Chemical Engineering Progress* 1991, *87(1)*, 67-72.

CO_2 CAPTURE UTILIZING SOLID SORBENTS

Ranjani Siriwardane, Ming Shen, Edward Fisher, and James Poston

U.S. Department of Energy
National Energy Technology Laboratory
3610 Collins Ferry Road, P.O. Box 880
Morgantown, WV 26507-0880
(rsiriw@netl.doe.gov; 304-285-4513, Fax: 304-285-4403)

Introduction

Fossil fuels supply more than 98 percent of the world's energy needs. However, the combustion of fossil fuels is one of the major sources of the greenhouse gas, CO_2. It is necessary to develop technologies that will allow us to utilize the fossil fuels while reducing the emissions of greenhouse gases. Commercial CO_2 capture technology that exists today is very expensive and energy intensive. Improved technologies for CO_2 capture are necessary to achieve low energy penalties. Pressure swing adsorption (PSA) is one of the potential techniques that could be applicable for removal of CO_2 from high-pressure gas streams, such as those encountered in integrated gasification combined-cycle (IGCC) systems.

PSA processes[1-4] are based on preferential adsorption of the desired gas (e.g., CO_2) on porous materials at a high pressure. When the pressure is decreased, the gas is desorbed from the porous sorbent and the sorbent can be reused for subsequent adsorption. PSA technology has gained interest due to low energy requirements and low capital investment costs. Development of regenerable sorbents that have high selectivity for CO_2 and high adsorption capacity for CO_2 is critical for the success of the PSA process.

The objective of this work is to understand the adsorption properties of CO_2 on both synthetic and natural molecular sieves[5] that can be utilized in PSA processes. In this work adsorption and desorption of CO_2 was studied on both synthetic and natural zeolites. Volumetric adsorption and desorption studies of CO_2, N_2, O_2, or H_2 with the sorbents were conducted at 25 °C up to a pressure of 300 psi (~2 x 10^6 Pa). Competitive gas adsorption studies were also conducted with CO_2-containing gas mixtures in the presence of water vapor.

Experimental

Adsorption and desorption isotherms at 25 °C of pure CO_2, N_2, O_2, and H_2 on molecular sieves Z10-08 and Z10-10 (proprietary zeolites from Sud Chemie) and three natural zeolites were measured up to an equilibrium pressure of about 300 psi (~2 x 10^6 Pa) utilizing a volumetric adsorption apparatus. Approximately 10 ml of the sorbent materials were placed in the sample chamber, which was evacuated to ~5 x 10^{-5} Torr (~6.75 x 10^{-3} Pa). The amount of CO_2 adsorbed was calculated utilizing the pressure measurements before and after the exposure of the sample chamber to CO_2. Desorption studies were conducted by gradually decreasing the pressure from 300 psi after the adsorption cycle. After each cycle the sorbent was evacuated overnight. Competitive gas adsorption studies were conducted in a lab-scale, fixed-bed reactor at 14.7 psi (~1.01 x 10^5 Pa) using a gas mixture with a composition of 15 percent CO_2, 82 percent N_2, 3 percent O_2 in the presence of water vapor at ambient temperature. The samples were heated at 100 °C for 1 hour and cooled down to ambient temperature before the introduction of the gas mixture.

Results and Discussion

Volumetric adsorption/desorption isotherms of CO_2, N_2, O_2, and H_2 on molecular sieve Z10-08 at 25 °C are shown in **Figure 1**. The CO_2 adsorption increased rapidly when the pressure was increased up to 50 psi but the CO_2 adsorption after 50 psi appeared to be gradual. At all pressures, adsorption isotherms of nitrogen were lower than those of CO_2, and adsorption isotherms of hydrogen were significantly lower than those of CO_2. Preferential adsorption of CO_2 indicates that this material can be used for separation of CO_2 from some gas mixtures. The adsorption and desorption isotherms were very similar indicating that the adsorption of CO_2 on Z10-08 is reversible. Thus, the adsorbed CO_2 can be recovered by lowering the pressure.

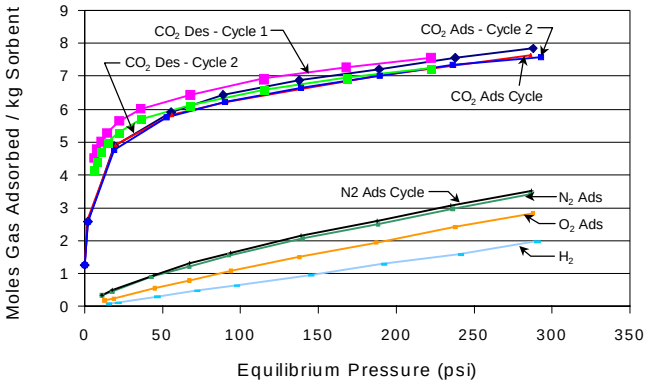

Figure 1. Adsorption and desorption isotherms of Z10-08.

The results of the competitive gas adsorption studies conducted utilizing a gas mixture of 15 percent CO_2, 82 percent N_2, 3 percent O_2, and water vapor on molecular sieve Z10-08 in the atmospheric micro reactor are shown in **Figure 2**. The gas mixture was introduced to 1 g of molecular sieve at a flow rate of 15 cc/min and at 25 °C. After the introduction of the gas mixture to the molecular sieve Z10-08, the CO_2 concentration decreased to almost zero until the breakthrough. This indicates that an excellent separation of CO_2 can be obtained from a gas

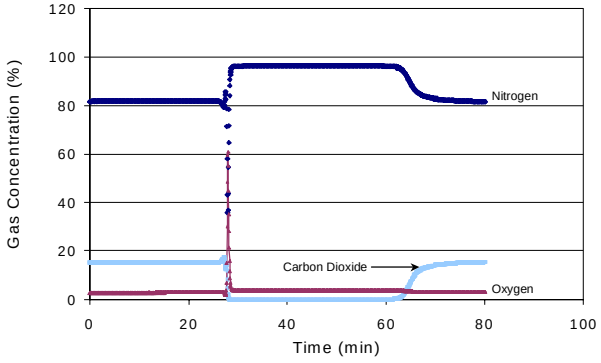

Figure 2. Competitive adsorption of CO_2, N_2, and O_2 on Z10-08 *(15% CO_2, 3% O_2, 82% N_2, and saturated with water vapor at 25 °C, 15 cc/min)*.

mixture of N_2, O_2, H_2O, and CO_2 with molecular sieve Z10-08. The total amount of CO_2 adsorbed at the breakthrough or saturation as calculated from the data was about 2.5-3 moles/kg of the sorbent. This value is very similar to the amount of CO_2 adsorbed at 1 atm from volumetric equilibrium adsorption studies, as shown in **Figure 1**. This indicates that the full capacity of the molecular sieve Z10-08 was utilized for CO_2 adsorption during competitive gas adsorption from a CO_2, N_2, O_2, and water vapor mixture. It is apparent that the water vapor does not affect the adsorption of CO_2 on molecular sieve Z10-08.

The results of both volumetric gas adsorption isotherm studies and competitive gas adsorption studies in the micro reactor of molecular sieve Z10-10 were very similar to that of Z10-08. However, the CO_2 adsorption capacity at high pressure (2×10^6 Pa) of Z10-08 was better than that of Z10-10.

The properties of three natural zeolites are shown in **Table 1**. The gas adsorption isotherms on the three natural zeolites indicated that there is preferential adsorption of CO_2 with all three zeolites. The adsorption capacities of both synthetic and natural zeolites are shown in **Table 2**. The natural zeolite with the highest sodium content and the highest surface area showed the highest CO_2 adsorption capacity at both low and high pressures.

Table 1. Natural Zeolites

Natural Zeolite	Chemical Composition (wt% Ratios)	Average Pore Diameter (A^0)	Surface Area (m^2/g)
Natural Herschelite-Sodium Chabazite	Sodium alumino silicate 1 Na_2O/K_2O - 7.4 SiO_2/Al_2O_3 = 3.7	4.3	520
Clinoptilolite	Sodium alumino silicate 2 Na_2O/K_2O - 1.1 SiO_2/Al_2O_3 = 6.3	4.3	40
Clinoptilolite	Potassium calcium sodium alumino silicate Na_2O/K_2O - 0.3 SiO_2/Al_2O_3 = 5.1 CaO/K_2O = 1	4.3	40

Table 2. Comparison of CO_2 Capture Capacities of Different Sorbents

Sorbents	Moles of CO_2/kg at 1 atm	Moles of CO_2/kg at 20 atm
Sythetic Zeolites		
Z10-08	2.5 - 3	7 - 8
Z10-10	2.5 - 3	6 - 8
Natural Zeolites		
Sodium Alumino Silicate 1	1 - 1.5	4 - 5
Sodium Alumino Silicate 2	0.5 - 1	2 - 2.5
Calcium Potassium Alumino Silicate	0.1 - 0.2	1 - 1.5

Conclusions

All molecular sieves showed preferential adsorption of CO_2 over nitrogen, oxygen, and hydrogen at all pressures up to 250 psi. The molecular sieve Z10-08 showed better CO_2 uptake than the other zeolites. Water vapor and oxygen did not affect the adsorption of CO_2 on synthetic molecular sieves during competitive gas adsorption studies.

References

(1) Skarstrom, C. W. U.S. Patent 2,944,627, **1960**.
(2) Guerrin de Montgareuil, P.; Domine, D. U.S. Patent 3,155,468, **1964**.
(3) Cheu, K.; Jong-Nam, K.; Yun-Jong, Y.; Soon-Haeng, C. Fundamentals of Adsorption, Proc. Int. Conf., D. LeVan (ed), Kluwer Academi Publishers, Boston, Massachusetts, 1996; pp. 203-210.
(4) Dong, F.; Lou, H.; Goto, M.; Hirose, T. Separation & Purification Technology, **1990**, *15*, 31-40.
(5) Siriwardane, R. V.; Shen, M.; Fisher, E.; Poston, J. Energy and Fuels, **2001**, *15*, 279-284.

CO_2 ELECTROCHEMICAL SEPARATION BY MOLTEN CARBONATE TECHNOLOGY

Hidekazu Kasai

Energy System Technology Department
Ishikawajima-Harima Heavy Industries, Co., Ltd.,
2-16,Toyosu 3-Chome, Koto-ku,
Tokyo, JAPAN

Introduction

Molten carbonate ($MxCO_3$) recognizes high activity and high electrical conductivity under high temperature. Then its have been used as electrolyte of MCFC•(molten carbonate fuel cell). In this cell CO_2 and O_2 translate between as carbonate ions. This method is expected to be applicable to CO_2 and O_2 recovery and production processes.

The concentration of CO_2 has been studied by Weaver[1] using MCFC. However, separation is also possible in other process using molten carbonate as the electrolyte. In this case, electrical energy is required for electrolysis. This system is shown schematically in Fig.1. Electrode reactions are as follows,

Cathode : $CO_2 + 1/2O_2 + 2e^- \rightarrow CO_3^{2-}$ (1)

Anode : $CO_3^{2-} \rightarrow CO_2 + 1/2O_2 + 2e^-$ (2)

This electrochemical process can apply CO_2 separation & concentration systems. We have investigated this mechanism and confirmed the CO_2 separation[2]. This system has high efficiency and can separate very low-level CO_2 gas. (Less than 0.5%). farther this system is very simple than other CO_2 separation system because its not needs mechanical pumping or pressurized system.

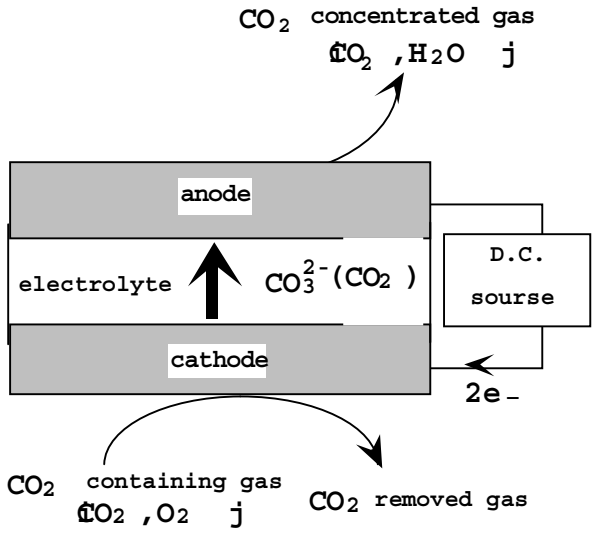

Fig.1 Schematic drawing of CO_2 separation using molten carbonate electrolytic cell.

The reaction (2) is the reverse of (1). Raw gas is introduced into the cathode and carbonate ions are formed. Carbonate ions move from the cathode to the anode. CO_2 and O_2 are produced by the decomposition of carbonate ions at the anode with a ratio of 2:1. Therefore the concentration of CO_2 at the outlet is 67 %. And 33 % O_2 is obtained theoretically, that means the concentration of O_2 is also increased in this process. The theoretical potential difference Ur for reactions (1) and (2) is expressed as follows,

$$Ur = (RT/2F)\ln(Pco_{2(a)}Po_{2(a)}^{0.5}/Pco_{2(c)}Po_{2(c)}^{0.5}) \quad (3)$$

Where (a) and (c) indicate the anode and cathode, respectively. When oxygen pressure is the same at the cathode and anode at 923 K. Only 0.09 V is required for 10 times concentration of CO_2. In this process, the over potential arising from electrode kinetics and resistance of the electrolytic cell are key factors for the practical application. Then we attempted to confirm the concentration of CO_2 in this study.

Experimental

Cell components of the electrolytic cell are shown in Fig. 2. SUS310S was used for housing material and the current collector was SUS316L. The electrolytic matrix was $LiAlO_2$ and the electrolyte is carbonate mixture.

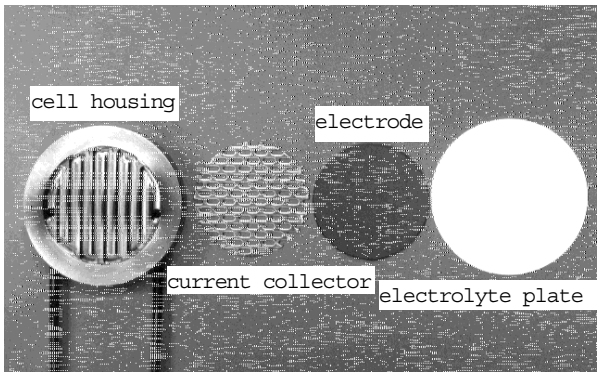

Fig.2 The example of small Cell Components.

The electrolyte plates and electrodes were formed by tapecasting. Both electrodes consist of porous NiO that oxidized and lithiated with carbonate. These components specifications are described in Table 1. We can make over $1m^2$ size of these parts. Cell operating conditions are indicated in Table 2.

Parts Material
Cathode NiO(porous)
Anode NiO(porous)
Electrolyte plate Li_2CO_3/K_2CO_3=70/30(electrolyte) LiAlO2(Matrix)

Table 1. Cell component specifications.

Result and Discussion

During electrolysis, the example of gas composition of anode outlet is shown in Table 3. The concentration of CO_2 in Cathode inlet is closed to the value of the exhaust gas from electric power station. Anode outlet gas was always maintained at CO_2 66.7 %, O_2 33.3 %. CO_2 concentration in the anode outlet gas was 130 times higher than that of cathode inlet gas in our cell test.

This composition is equal to the theoretical value determined based on the stoichiometric ratio of carbonate ion decomposition at the anode. Further more in this case, increase of O_2 concentration is also possible. The flow rate of anode outlet gas agreed with the theoretical flow rate calculated from the cell current. Therefore it was found that the current efficiency for CO_2 separation was almost 100 %. At 150 mA/cm^2 of current density, approximately 1 cm^3 CO_2 separates per 1cm^2 electrode area from the cathode to the anode.

Temperature	923 K
Pressure	0.1Mpa
Cathode gas flow rate (inlet)	300 cm^3/min
Anode gas flow rate (inlet)	0 cm^3/min
Current density	0～150 mA/cm^2

Table 2. Condition of cell test

Sampling position	O2(%)	N2(%)	CO2(%)
Cathode inlet	20.9	70.6	0.5
Anode outlet	33.3	0	66.7

Table 3. the example of gas composition of cell

The cell voltage, which actually decided the efficiency, significantly depended on current density during electrolysis. This relation is shown in Fig. 4 .

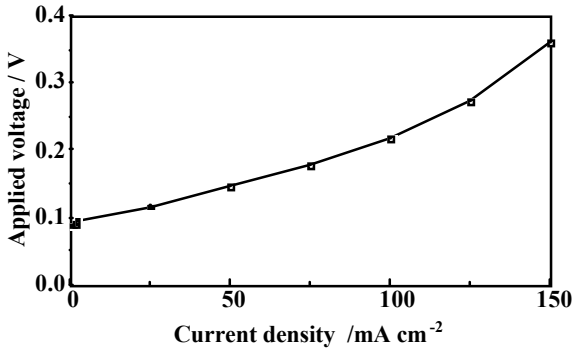

Fig.4 I-V curve of CO2 separation at 923K. The gas composition of Cathode is O2/N2/CO2=19/71/10

The cell voltage includes potential difference of both electrodes gases, over potential of the electrodes reactions and internal resistance of the cell (IR loss). IR loss of the cell was obtained by internal resistance and current. Therefore over voltage (Up) of reactions may be determined by subtracting potential difference (Ur) for CO_2 concentration from equation (3) and IR loss (U_{IR}) from total cell voltage (U) by the equation (4):

$$U_p = U - U_r - U_{IR} \qquad (4)$$

From equation (4), the sum of over voltage due to cathode and anode reactions was 200 mV. These result shown in Fig.5.

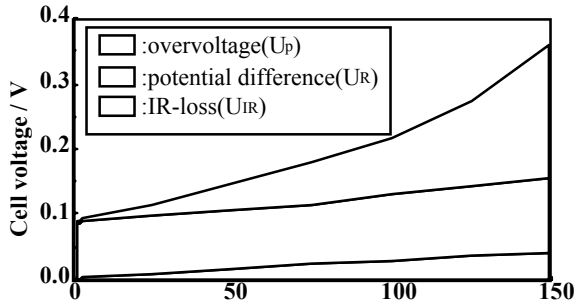

Fig. 5 Constitution of cell voltage for electrolytic CO2 separation at 923K. The gas composition of Cathode is O2/N2/CO2=19/71/10

Conclusion

CO_2 separation and concentration were confirmed to occur in a high temperature electrolysis cell using molten carbonate and NiO electrodes. Current efficiency was almost 100 % and stoichiometric gas composition at the anode outlet was obtained.

References

1. J.L.Weaver and J.Winnick, *J.Electrochem.Soc.*,**1983**, 130, 20.
2. H.Kasai, T.Matsuo, M,Hosaka, N.Motohira, N.Kamiya,K.Ota, DENKKI KAGAKU,**1998**,66,635-640

CO_2 SEQUESTRATION USING BRINES

Y. Soong, J. R. Jones, S. W. Hedges, D. K. Harrison, J. P. Knoer, J. P. Baltrus and R. L. Thompson*[1]

*U.S. Department of Energy, National Energy Technology Laboratory, P.O. Box 10940, Pittsburgh, PA 15236
[1]Parsons Project Services, Inc. P.O. Box 618, South Park, PA 15129

Introduction

Among various proposed sequestration options, injection of CO_2 into confined geologic formations-in particular, saline aquifers-is one of the most promising alternatives. In general, CO_2 can be stored by hydrodynamic trapping, which traps the CO_2 into flow systems for geological periods of time. The most important concern of hydrodynamic trapping is the potential for CO_2 leakage through imperfect confinement. In addition, mineral trapping, which involves a series of interactions between the formation mineralogy and CO_2-enriched formation waters, can convert CO_2 to an immobile and harmless carbonate mineral form that can be stored for millions of years.[1-2]

Various carbonates such as calcite, magnesite, dolomite, and siderite can be formed in the brine aquifer by mineral trapping. Conversion of CO_2 to stable carbonate minerals is expected to be slow. A computer simulation of the mineral trapping process (kinetic water-rock reaction model) was conducted under reservoir conditions by the Alberta Research Council, Canada.[2] These authors calculated times for precipitation of the various carbonates are on the order of hundreds of years. The extended long time required for mineral trapping is the major drawback of this process.

Several researchers[3-4] have conducted mineral trapping studies. Sass et al., [3] studied CO_2 and brine reactions over rocks for 7 days at a pressure of 800 psi and 110 °C. They found increased levels of calcium, magnesium, and carbonate in solution, which they interpreted as the dissolution of dolomite. They interpreted decreased brine concentration of calcium and sulfate as evidence for anhydrite precipitation. However, no extensive studies of the interaction between CO_2 and brine have been reported. The objective of this paper is to examine the feasibility of conducting mineral trapping of carbon dioxide with brine solution reactions in an autoclave reactor.

Experimental

Three different brine samples were used in this study. One was from a brine treatment facility located in Creekside, PA, which was a composite sample. A second sample was collected from the Oriskany formation in Indiana county, PA. In addition, brine obtained from Oklahoma was also used.

Brine carbonation experiments were carried out in a ½ liter autoclave (Hastelloy C-276) manufactured by Progressive Equipment Corp. In a representative experiment, 180 ml of brine was charged into the reactor. The reactor was sealed, and purged/evacuated with carbon dioxide three times. Finally, a predetermined amount of CO_2 was charged into the reactor to the desired testing pressure (450 or 650 psi). The brine/CO_2 mixture was agitated at 400 rpm during both heating to the desired temperature (155 °C) and testing to prevent any settling of precipitate. At the completion of each test, the remaining CO_2 was vented, and the slurry was removed from the reactor and filtered to separate solids from the aqueous solution. A digital pH meter was used to determine the pH values of pre- and post-product solutions. The brine was used either as received or its pH was adjusted before the reaction by adding KOH. The starting brines and brine products were prepared for analysis by filtration through a 0.45 µm membrane using a water aspirator. The collected solids were rinsed with deionized water on the membrane and dried in a nitrogen-purged oven at 110 °C. Metal concentrations were determined using inductively coupled plasma - atomic emission spectroscopy (ICP-AES) on a Perkin Elmer Optima 3000 ICP spectrometer.

Results and Discussion

Table 1. Carbonation Results for Brine Obtained from Creekside, PA

	units	Raw	Rxn 1	Rxn 2
Reaction Condition			155 °C, 950 psi CO_2, 400 rpm, 3 hrs	KOH was added to adjust the pH to 9. 155 °C, 690 psi CO_2, 400 rpm, 1 hr
Liquid	pH	3.2	-	3.8
Ba	mg/liter	663	556	534
Ca	mg/liter	16120	19120	15700
Mg	mg/liter	2098	2540	2210
K	mg/liter	177	212	7040
Na	mg/liter	53800	58240	53200
Fe	mg/liter	117	65	15800
Solid	g	none	0.38	0.0293
Ba	µg/g	N/A	117	57
Ca	µg/g	N/A	40000	2400
Mg	µg/g	N/A	13500	19500
K	µg/g	N/A	3790	1090
Na	µg/g	N/A	109000	N/A
Fe	µg/g	N/A	230000	331000

The scoping experiments on brine carbonation were conducted in two different ways. The reaction was conducted either with brine as received and CO_2 (Rxn 1) or after the pH of the brine was adjusted before reaction with CO_2 (Rxn 2). Results of the solids and solution analyses before and after reaction are shown in Tables 1, 2 and 3 for Creekside, PA; Indiana county, PA; and Oklahoma brines, respectively. The initial brine compositions are also shown for comparison with various reacted mixtures. In general, the changes of compositions in solution before and after the reaction were small. However, the amount of solid precipitated and the composition of solids varied with the reaction conditions utilized.

For the case of Creekside brine, the raw brine was very acidic with a pH value of 3.2 (Table 1). The reaction between the brine and CO_2 under the reaction conditions of Rxn 1 resulted in the precipitation of 0.38 gram of solids. Adjusting the pH of brine to 9 (Rxn 2) before reacting with CO_2 resulted in a lesser amount of solid precipitate (0.0293 g). The composition of the solids also varied with the reaction conditions. Under the conditions of Rxn 1, the precipitates were high in Na, Fe and Ca. However, under the reaction conditions of Rxn 2, the precipitation of Ca was significantly reduced by a factor of 10. Furthermore, the concentration of Fe in the precipitate increased from 230,000 to 331,000 µg/g in going from Rxn 1 to Rxn 2.

The results for brines collected from Indiana county, PA and the Oklahoma showed similar trends (Tables 2 and 3). More solids were precipitated when the pH of the brines was modified before reaction. The major elements present in the solids under reaction conditions Rxn 1 were Ca, Na, and Fe. However, after the pH was adjusted prior to reaction Rxn 2, the concentrations of Na and Fe in the precipitated solids were reduced by a factor of 100. Moreover, the concentration of Ca in the precipitated solid increased by a factor of 10.

About 53,300 µg/g of Barium were observed in the precipitated solid under the reaction conditions of Rxn 1 for the brine obtained from Indiana county, PA. The exact form of Ba is still under investigation. However, under the reaction conditions of Rxn 2, the concentration of Ba in the precipitate was significantly reduced from 53,300 to 1390 µg/g.

In general, the net increase in total solid precipitation could be attributed to the precipitation of mineral matter (primarily calcium, but may include carbonates, sodium and other minerals) during the reaction. It is important to note that values of alkalinity and pH in Tables 1, 2, and 3 might not be representative of actual conditions while the experiments were in progress.

Table 2 Carbonation Results for Brine Obtained from Indiana County, PA

	units	Raw	Rxn 1	Rxn 2
Reaction Condition			155 °C, 900 psi CO_2, 400 rpm, 1 hr	KOH added to adjust pH to 11, 155 °C, 670 psi CO_2, 400 rpm, 1 hr
Liquid	pH	3.9	3.6	3.9
Ba	mg/liter	1070	1060	1030
Ca	mg/liter	35000	34900	29500
Mg	mg/liter	2250	2250	2040
K	mg/liter	2600	2620	13800
Na	mg/liter	70400	70200	69100
Fe	mg/liter	234	188	1
Solid	g	0.02	0.048	2.069
Ba	µg/g	1570	53300	1390
Ca	µg/g	34900	49100	341000
Mg	µg/g	2010	3000	2710
K	µg/g	3250	2020	63
Na	µg/g	59900	47200	552
Fe	µg/g	311000	119000	16700

Significant amounts of sodium along with some aluminum (not shown in Tables) were found for all brine tested under the reaction conditions of Rxn 1. However, the concentration of sodium precipitated under the conditions of Rxn 2 was reduced by a factor of 1000 for all brine tested. It was speculated that the sodium precipitated might be related to the formation of dawsonite ($NaAlCO_3(OH)_2$).[5] In general, calcium, precipitated under the reaction conditions of Rxn 1 was probably in the form of calcium carbonate. The same general behavior was observed for brines obtained from Indiana county, PA and Oklahoma. The observation that significantly less calcium precipitated under the reaction conditions of Rxn 1 could be attributed to the pH of the brine solution remaining too low to stabilize a carbonate mineral. In subsequent experiments, a pH buffer (KOH) was added to control the pH. As a result of the pH increase, about 10 fold more calcium precipitated under the conditions of Rxn 2 than that of Rxn 1. However, an opposite behavior in Ca concentration was observed for the brine collected from Creekside, PA. Magnesium, precipitated during the reaction is probably in the form of magnesium carbonate. Its precipitation is not affected by the variation of pH. Siderite ($FeCO_3$) was observed in the precipitated solids. Significant siderite was found under the reaction conditions of Rxn 1 for the Oklahoma brine and brine obtained from Indiana county, PA. As the pH increased, siderite precipitation was drastically reduced. The opposite trend was found for the Creekside, PA brine. The pH of brine has a significant effect on the carbonation reaction. For the mineral trapping processes to occur, the following reactions have to proceed:

CO_2 (gas) -> CO_2 (aq); CO_2 (aq) + H_2O -> H_2CO_3;
H_2CO_3 -> $H^+ + HCO_3^-$; HCO_3- -> H+ + CO_3^{2-}
$Ca^{++} + CO_3^{2-}$ --> ($CaCO_3$); $Ca^{++} + Mg^{++} + CO_3^{2-}$ --->$CaMg(CO_3)_2$
$Fe^{++} + CO_3^{2-}$ ---> $FeCO_3$; $Mg^{++} + CO_3^{2-}$ --> $MgCO_3$

Table 3. Carbonation Results for Brine Obtained from OK

	units	Raw	Rxn 1	Rxn 2
Reaction Condition			155 °C, 900 psi CO_2, 400 rpm, 1 hr	KOH was added to adjust the pH to 9.2, 155 °C, 670 psi CO_2, 400 rpm, 1 hr
Liquid	pH	5.5	4.5	5
Ba	mg/liter	323	338	321
Ca	mg/liter	10700	11200	9525
Mg	mg/liter	1965	2050	1975
K	mg/liter	525	559	3475
Na	mg/liter	52400	54700	53100
Fe	mg/liter	3	3	1.5
Solid	g	0.0586	0.046	0.4846
Ba	µg/g	1410	1215	1630
Ca	µg/g	23300	33900	326000
Mg	µg/g	4150	6720	4690
K	µg/g	1165	1750	45
Na	µg/g	51000	150000	1440
Fe	µg/g	56200	677000	6130

The pH along with other factors have an impact on these reactions. At low pH, H_2CO_3 (carbonic acid) dominates; at mid pH, HCO_3- (bicarbonate) dominates; and at high pH. CO_3^{2-} (carbonate) dominates. Temperature and pressure also play an important role in determining the solubility of CO_2 in solution. Aqueous-phase equilibration with CO_2 (g) promotes carbonate precipitation, while acidic conditions favor carbonate dissolution. Therefore, increased pH favors carbonate precipitation. The actual effectiveness of brine carbonation probably depends on the initial concentration of carbonate forming cations within the brine and the pH of the brine.

Conclusions

A study of mineral trapping (under temperature and pressure) in an autoclave reactor with the brine solution has been initiated by NETL. Three different brines were tested in a 1/2-liter autoclave under various conditions. Preliminary results indicated that the mineral species and amounts of solid precipitated depend on the source and the pH of the brine.

References

1. DOE report, DOE/SC/FE-1, Carbon Sequestration Research and Development, December 1999.
2. Hitchon, B., Gunter, W. D., Gentzis, T and Bailey, R. T., *Ener. Conv. & Man.* 40 (1999) 825-843.
3. Sass, B. N., Gupta, J., Ickes, J., Eagelhard, M., Bergman, P., and Byaer, C., " Interaction of Rock Minerals with CO_2 and Brine: a hydrothermal Investigation", Conference CD, 1st National Conference on Carbon Sequestration, Washington, D.C., May 15-17,2001.
4. Lebro'n, I and Suarez, D. L., Geochim. Cosmochim. Acta 62 (1998) 405-416.
5. Johnson, J. W., Nitao, J. J., Steefel, C. I., and Knauss, K. G.., "Reactive transport modeling of geologic CO_2 sequestration in saline aquifers ":Conference CD, 1st National Carbon Sequestration meeting, May 12-15, 2001, Washington, DC.

COST ESTIMATION OF CO_2 RECOVERY TECHNOLOGY USING HYDRATES

Fumio Kiyono, Akihiro Yamazaki, and Keiichi Ogasawara

Institute for Environmental Management Technology
National Institute of Advanced Industrial Science and Technology
16-1, Onogawa, Tsukuba, Ibaraki, 305-8569, Japan

Introduction

Although the global warming problems may be one of the most crucial matters that will threat the future existence of human beings, the steps for solving are late. Main reason for the delay is said to lie in economical problems. For instance, if we recovered CO2 from a thermal electric power station and sequestrated it in an isolated place we would lose 40% of the total energy produced. Among many cost factors the separation cost accounts for main part. So far several methods, like the amine absorption method or the zeolite adsorption method, have been presented but in those methods we must use expensive chemicals.

Recently the separation technology using hydrates is attracting many concerns, where necessary chemicals for separation are mere water which exists everywhere and is obtained effortlessly. So the hydrate separation technology has a potential as an alternative method since its cost could be low if an appropriate process was developed. In this paper the results of cost estimation is presented when applying the hydrate separation technology to the case of CO2 separation at the thermal electric power station.

Separation mechanisms by hydrates

The basic phenomenon that explains the reason why hydrates can separate the specified constituent from mixed gases is demonstrated in **Figure 1**. The constituent is separated as the solid solutions.

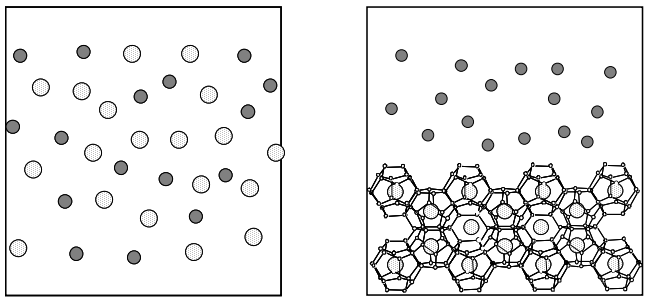

Figure 1. The separation mechanism of the specified constituent from mixed gases by hydrates.

If the mixed gases were compounded of the components that formed hydrates and the components that could not make hydrates, the former components would be captured in hydrates' cages and the latter components should be left in the mixed gases.

In addition intermolecular force between the gas molecule in the cage and water molecules that surrounding the gas molecule is different among gas components, so the specified constituent exists excessively in the hydrate phase.

The mole fraction of each component in hydrate phase depends basically upon the fugacity of each component in the gas phase and the intermolecular potential between the gas molecule and water molecules when they take the hydrate structure. The flue gases from the thermal electric power station contained mainly CO_2, N_2, O_2, and H_2O. Although these components all can make hydrates, but the intermolecular potential is different each other, that enables us to separate CO_2 from other components. The comparison of the intermolecular potential is indicated in **Figure 2**. The potential well depth of CO_2 is deeper than that of other components and it means that CO_2 makes hydrates in more moderate condition than others.

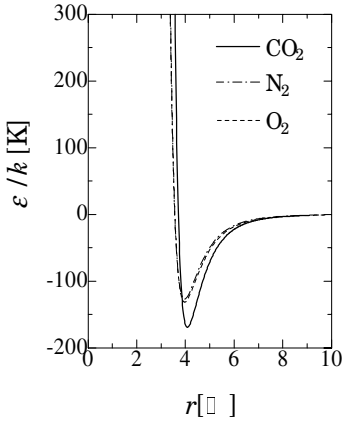

Figure 2. The intermolecular potentials of CO_2, N_2, and O_2.

Hydrate separation process

A simple outline of the hydrates separation process is demonstrated in **Figure 3**. Hydrates are generally formed in high pressure and low temperature conditions. At first the pressure of flue gases is increased up to 20 atm by the compressor. At the same time, the temperature rises up to almost 560°C owing to the work given. This extra heat is recovered at the heat exchanger and utilized to rotate turbine blades in the gas turbine. At the next stage, flue gases are cooled down to 4°C, and then conveyed to the hydrate formation chamber where flue gases make hydrates in contact with sprayed water. The formation heat of hydrates must be removed from the chamber. Then hydrates are carried to the separator and decomposed to water and gases again. The heat of decomposition is supplied from sea water.

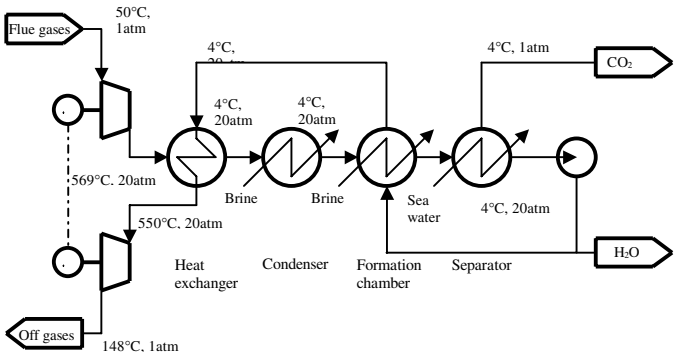

Figure 3. The outline of hydrates separation process.

Composition of flue gases. Main constituents of flue gases are CO_2, N_2, O_2, and water after eliminating NO_X and SO_X. The mole fraction of CO_2 differs according to the type of the electric power station. In case of a coal fired power station the mole fraction of CO_2 is almost 0.15. While in a natural gas fired power station this figure is relatively low. In this estimation the mole fraction of CO2 in flue gases is assumed to be 0.1. The composition of flue gases is

summarized in **Table 1**. The temperature of flue gases is set at 50. and pressure 1 atm. The flow rate of flue gases is guessed at 1 M Nm^3/h.

Table 1. The Composition of Flue Gases

	Mole Fraction	Molar Weight	Feed Rate		
			kmol/h	Nm^3/h	t/h
CO_2(g)	0.10	44.010	4,464	100,000	196
N_2(g)	0.79	28.010	35,268	790,000	988
O_2(g)	0.04	32.000	1,786	40,000	57
H_2O(g)	0.07	18.020	3,125	70,000	56
Flue Gases	1.00	29.070	44,643	1,000,000	1298

Compression of flue gases. The flue gases must be compressed to achieve the pressure sufficient to make hydrates. This pressure differs according to the temperature, the composition of flue gases, and whether hydrate promoters exist or not. In this estimation necessary pressure is assumed to be 20 atm.

The temperature of flue gases increases with compression. For simplicity adiabatic compression is adopted. The temperature of flue gases alters from 50°C to 569 °C.

The energy that needs to compress the flue gases can be calculated by the enthalpy difference after and before compression. Mole heat capacities of each component and the mean value of the flue gases are indicated in **Table 2** and results of enthalpy calculation are summarized in **Table 3**. Necessary energy for the compression is 681,637MJ/h.

Table 2. The Mole Heat Capacity of CO_2, N_2, O_2, H_2O, and Flue Gases

	Mole Fraction	Cp J/(K mol)		
		a	10^3b	10^6c
CO_2(g)	0.10	26.748	42.258	-14.247
N_2(g)	0.79	27.016	5.812	-0.289
O_2(g)	0.04	25.594	13.251	-4.205
H_2O(g)	0.07	30.204	9.933	1.117
Flue Gases	1.00	27.155	10.043	-1.743

Table 3. The Enthalpy Change of Flue Gases at the Compressor

		a	10^3b	10^6c	
		27.155	10.043	-1.743	
T_1 (K)	T_2 (K)	$a.\Delta T$	$b/2.\Delta T^2$	$c/3.\Delta T^3$	q , J/mol, h)
323	842	14,094	1,353	-81	15,365

Cooling of flue gases. The high temperature of flue gases due to compression must be decreased to the sufficient low temperature to make hydrates. Flue gases are cooled by two steps.

In the first stage the temperature is decreased to 40°C at the heat exchanger by utilizing the off gases (4°C, 20 atm) from the hydrate chamber. This recovered energy is utilized to rotate the gas turbine of the compressor. In the second stage the temperature of 40°C falls down to 4°C. Here brine is used as the coolant. The recovered energy at the heat exchanger is calculated as the difference of enthalpy of gases before cooling and after cooling. Necessary data for the enthalpy calculation and results are indicated in **Table 4**. The recovered energy is 575,000MJ/h.

The removed energy at the condenser is also estimated as the enthalpy difference of flue gases. Data used in the calculation and results are shown in **Table 5**. In this process the heat of condensation of water must be also considered. The enthalpy change due to condensation is 134400MJ/h and that due to cooling is 43400MJ/h, so total enthalpy change at the condenser is 177800MJ/h.

Table 4. The Enthalpy Change of Flue Gases at the Heat Exchanger

		a	10^3b	10^6c	
		27.155	10.043	-1.743	
T_1 (K)	T_2 (K)	$a.\Delta T$	$b/2.\Delta T^2$	$c/3.\Delta T^3$	q , J/mol, h)
842	313	-14,365	1,405	86	-12,874

Table 5. The Enthalpy Change of Flue Gases at the Condenser

		a	10^3b	10^6c	
		27.155	10.043	-1.743	
T_1 (K)	T_2 (K)	$a.\Delta T$	$b/2.\Delta T^2$	$c/3.\Delta T^3$	q , J/mol, h)
313	277	-978	7	0	-971

Formation of CO_2 hydrates. After compression and cooling, flue gases are transported to the hydrates formation chamber where flue gases contact with water and make hydrates. The mole fraction of CO_2 in the hydrate phase is higher than that in flue gases. The recovery rate of CO2 is assumed to be 3844kmole/h.

To continuously make hydrates the heat of formation must be removed from the hydrate chamber. For this purpose brine is utilized. If the heat of formation of hydrates is assumed to be 63kJ/mol, total heat that should be removed from the chamber is 242,200MJ/h.

Dissociation of CO_2 hydrates. After CO_2 is separated from flue gases as hydrates at the hydrate formation chamber, CO_2 hydrates are transported to the separator, where CO_2 hydrates are dissociated to water and gaseous CO_2 again. It is also possible to send CO_2 hydrates to the deep sea bottom without dissociation. The heat is 242,200MJ/h that needs to decompose hydrates.

Cost estimation

Results of the thermodynamic analysis of the process enable us to estimate capacities, sizes, abilities, and so on of necessary equipments like the compressor, the heat exchanger, the hydrate formation chamber, and so on. According to these specifications the cost of facilities can be decided. Also energy cost can be calculated. Final results of the cost estimation are summarized in **Table 6**. In this table the cost of the amine absorption method is also shown for comparison. It is concluded that the hydrates separation method has enough cost competitive position.

Table 6. Results of Cost Estimation

	Hydrates yen/kg-CO_2	Amine absorption yen/kg-CO_2
Depreciation cost	1.02	0.65
Repair & Supplies	0.27	0.17
Labor cost	0.09	0.09
Energy cost	4.18	5.03
Total cost	5.56	5.94

DEGRADATION OF MONOETHANOLAMINE USED IN CO_2 CAPTURE FROM FLUE GAS OF A COAL-FIRED ELECTRIC POWER GENERATING STATION

Brian R. Strazisar, Richard R. Anderson, and Curt M. White

U. S. Department of Energy, National Energy Technology Laboratory
P. O. Box 10940, Pittsburgh, PA 15236

Introduction

Increasing awareness of the possible influence of greenhouse gases on global climate change has led to recent efforts to develop strategies for the reduction of carbon dioxide (CO_2) emissions.[1,2] One such strategy that has received a great deal of attention involves the capture of CO_2 from large point sources (such as fossil fuel-fired power plants) and the long-term storage underground or in the ocean. The CO_2 capture step is expected to make up the majority (up to 75%) of the expense for a carbon sequestration process.[2]

Although there are several different methods that have been proposed for the capture and separation of CO_2, the only method that has been proven to work on an industrial scale is chemical absorption using monoethanolamine (MEA) as a solvent.[2] In this method, MEA absorbs CO_2 through chemical reaction in an absorber column. Since the reaction is reversible, the CO_2 can be driven off by heating the CO_2 rich amine in a separate stripper column. The MEA may be recycled through the process. For the low CO_2 partial pressure present in flue gas, alternative methods of CO_2 removal are less efficient and more expensive than chemical absorption.[2]

A major problem associated with chemical absorption using MEA is the degradation of the solvent through irreversible side reactions with CO_2 and other flue gas components.[3,4,5] This leads to numerous problems with the process. First, degradation of MEA results in solvent loss, requiring the replacement of up to 8 pounds of MEA per ton of CO_2 captured.[6] It is also known to lead to foaming, fouling, and increased viscosity of the amine. In existing CO_2 capture facilities, the degradation products are separated in an evaporative reclaimer and disposed of as hazardous chemical waste.

In the case of carbon sequestration, the most significant problem presented by MEA degradation is associated with increased corrosion caused by the degradation.[3] In order to keep machinery corrosion rates at an acceptable level, the concentration of MEA must be kept low (typically under 20% for coal boilers and ~30% for natural gas-derived flue gas and then only if corrosion inhibitors are employed). Low MEA concentration reduces the effectiveness of the solvent, necessitating large equipment sizes and faster circulation rates. In addition, more energy is required in the stripping column in order to regenerate the amine.[7] This increased "parasitic load" is of particular concern for carbon sequestration. In addition to being an additional cost, producing this extra energy leads to increased CO_2 emissions, which decreases the overall benefit of sequestration.[2] A sensitivity analysis indicates that increasing the concentration of MEA to 70% will cut the parasitic load on a power plant by more than half.[7]

The current study is aimed at developing an increased chemical understanding of MEA degradation processes. Increased insight into the mechanisms and chemical pathways associated with MEA degradation may result in decreasing or eliminating its negative effects. There have been several previous studies on reactions of alkanolamines with O_2,[5] CO_2,[3] COS,[8] or CS_2.[9] Most of these studies were aimed at understanding natural gas sweetening processes, and all were conducted under laboratory conditions. However, in flue gas from a fossil fuel-fired boiler, the process becomes much more complicated due to the presence of a mixture of CO_2, O_2, CO, SO_x, NO_x, fly ash, and other constituents. The degradation process in this case remains poorly understood, particularly under conditions that are common to power plants.[10]

Experimental

The IMC Chemicals Facility in Trona, California is a plant that has been performing CO_2 capture from flue gas since 1978. CO_2 is separated from flue gas of a coal-fired boiler, which is used to produce electricity. In this case, the captured CO_2 is used for carbonation of brine from Searles Lake, California for the commercial production of sodium carbonate. For the current study, MEA samples were obtained from this plant in order to identify the degradation products from the CO_2 separation process. Three samples were obtained: (1)virgin concentrated MEA, (2)"lean" MEA, taken before the CO_2 absorption step, and (3)reclaimer bottoms, which represents the still bottoms that remain after the amine is distilled to remove the degradation products.

In order to identify the volatile organic compounds in the samples, each mixture was separated and analyzed using combined gas chromatography-mass spectrometry (GC-MS) and combined gas chromatography-Fourier transform infrared absorption spectrophotometry (GC-FTIR). Two separate gas chromatographic columns were used for separation. The first was a 60 m × 0.32 mm i. d. fused silica column coated with a 0.25-µm film of 14%-(cyanopropyl-phenyl)-methylpolysiloxane (DB-1701 from J&W Scientific). This column was temperature programmed from 35 to 280°C at 1 C°/min. The second column, a 60 m × 0.25 mm i. d. column coated with 0.25-µm modified polyethylene glycol (Nukol™ from Supelco), was temperature programmed from 50 to 200°C at 5 C°/min. Helium carrier gas was used with initial linear velocities of 40 and 36 cm/s, respectively. In both cases, samples were introduced via a split injector held at 250°C. GC-MS experiments were performed using an HP 5973 mass selective detector (MSD) and GC-FTIR experiments employed an HP 5965A infrared detector (IRD).

In addition, precise molecular masses of the organic compounds were obtained using low voltage high-resolution mass spectrometry (LVHRMS). Mass spectra were acquired on a Kratos MS-50 high-resolution mass spectrometer. In this experiment, the samples were introduced to the ion source directly without prior separation.

Inorganic ionic species were identified using ion chromatography (IC) as well as combined inductively coupled plasma-atomic emission spectroscopy (ICP-AES). IC experiments were performed for anions using a Dionex DX-100 Ion Chromatograph equipped with a conductivity detector. The analytical column used was an IonPac CS14 (4 mm), and the guard column was an IonPac AG14 (4 mm). The eluent was 3.5 mM sodium carbonate/1 mM sodium bicarbonate, at a flow rate of 1.2 ml/min. A self-regenerating ASRS-Ultra (4 mm) suppressor was used. ICP-AES experiments were performed using a Perkin Elmer Optima 3000 to measure trace metal concentrations.

Also, analyses were performed to determine the total nitrosamine concentration in each sample by a technique described elsewhere.[11]

Results and Discussion

Since the focus of this study was on the MEA degradation products, the reclaimer bottoms sample, where these products were concentrated as a result of distillation provided the most important information. Organic compounds that were identified are listed in Table 1 along with the methods of identification. An "x" in the GC-MS or GC-FTIR column indicates a positive match from an electronic search of either MS or FTIR libraries. MS library searches were performed using the NIST/NIH/EPA Mass Spectral Library. FTIR searches were performed using the FTIRsearch.com service.

The LVHRMS column indicates whether a match within 0.003 amu of the mass of the indicated molecule was present in the mass spectrum of the entire sample. Also included in Table 1 is an indication of the column used for the experiment in which each compound was detected. The % of total area refers to the integrated peak area from the total ion chromatogram as a percentage of the total signal intensity for each chromatogram. Other than the MEA, none of the peaks identified in Table 1 were present in identical experiments performed on the virgin MEA.

Table 1. Identified organic compounds from MEA reclaimer bottoms

		method of identification			GC column		%of total area	
peak	compound	GC-MS	GC-FTIR	LVHRMS	DB-1701	Nukol	DB-1701	Nukol
1	N-acetylethanolamine ($C_4H_9NO_2$)	x		x	x	x	8.86	6.28
2	N-glycylglycine ($C_4H_8N_2O_3$)	x		x	x		<0.01	
3	N-(hydroxyethyl)-succinimide ($C_6H_9NO_3$)	x		x	x	x	0.16	*
4	N-(2-hydroxyethyl)-lactamide ($C_5H_{11}NO_3$)	x	x	x	x		0.07	
5	1-(2-hydroxyethyl)-2-imidazolidinone ($C_5H_{10}N_2O_2$)	x	x		x		0.24	
6	N,N-diacetylethanolamine ($C_6H_{11}NO_3$)		x	x	x		21.83	
7	ammonia (NH_3)	x				x		0.10
8	acetic acid ($C_2H_4O_2$)	x		x		x		2.02
9	propionic acid ($C_3H_6O_2$)	x				x		0.30
10	*n*-butyric acid ($C_4H_8O_2$)	x		x		x		0.01
11	monoethanolamine (C_2H_7NO)	x	x	x	x	x	*	35.18
12	2,6-dimethyl-4-pyridinamine ($C_7H_{10}N_2$)	x		x		x		0.05
13	2-imidazolecarboxaldehyde ($C_4H_4N_2O$)	x		x		x		0.05
14	1-methyl-2-imidazolecarboxaldehyde ($C_5H_6N_2O$)	x		x		x		0.17
15	2-oxazolidone ($C_3H_5NO_2$)	x		x		x		0.80

* Area percentage not calculated due to overlap with other peaks

Peaks 5 and 15 are known degradation products of MEA resulting from reaction with CO_2,[3] but are relatively minor components. Carboxylic acids (peaks 8,9, and 10) have been previously identified as products of oxygen induced MEA degradation.[5] The acetylated MEA components (peaks 1 and 6) are the most abundant degradation products, and are believed to be the result of reaction between acetic acid and MEA.

The results of the ICP-AES and IC analyses are shown in Table 2. ICP-AES measurements were made for 23 different metal cations. Shown are seven metals that were present at no less than 0.2 ppm concentration in either of the two samples. Most prominent is the sodium concentration, mostly due to the sodium carbonate added to the reclaimer in order to regenerate MEA that has been converted to its protonated (acidic) form. Other metals are believed to originate in large part from the coal. In addition, mercury was found to be present in the reclaimer bottoms at 1.0 ppb and was not detectable in the lean MEA (<0.02 ppb).

Anion concentrations are all relatively higher, with chloride being the most significant at 4.9% (wt.). The halogens present in the samples are thought to be present as a result of simple acid/base chemistry between mineral acids (HX where X is any halogen) present in the flue gas with MEA to form "heat stable salts". HX is the combustion product of halogens present in the feed coal. Also, note that, with one exception, the concentration of various anions is greater in the reclaimer bottoms than in the lean MEA. This is what would be expected, since the purpose of the reclaimer is to remove contaminants from MEA and concentrate them in the bottoms. The exception is the sulfate, which is an order of magnitude more concentrated in the lean MEA than in the reclaimer bottoms. It is thought that the concentration of sulfate in the reclaimer bottoms is limited by solubility factors.

Nitrosamines are known carcinogens that are formed by a reaction between an amine with a nitrogen oxide. Nitrosamines were found to be present at a concentration of 580 ppm in the lean MEA. This is believed to be due to reaction between MEA and nitrogen oxides from the flue gas. There was not a detectable amount of Nitrosamines in the reclaimer bottoms, likely due to their low boiling point.

Table 2. Ion Concentrations in ppm

	Lean MEA	Reclaimer Bottoms
Cations		
Sodium	80	821
Potassium	2.2	18
Calcium	1.1	1.3
Iron	1.4	1.1
Copper	0.2	0.1
Zinc	0.3	0.2
Aluminum	not detectable	0.4
Selenium	not detectable	17.4
Arsenic	not detectable	1.7
Anions		
Fluoride	300	1500
Chloride	1600	49000
Bromide	0.9	80
Sulfate	2200	250
Nitrate	290	3100
Nitrite	130	**
Phosphate	7.8	230

** not quantified due to overlap with chloride peak

Acknowledgements

Some work was performed while B.R.S. held a National Research Council Research Associateship Award at the National Energy Technology Laboratory. GC-IR spectra were obtained at the Mass Spectrometry Facility, Department of Chemistry and Chemical Biology, Cornell University. Nitrosamine measurements were performed by Delbert Eatough of Brigham Young University. The authors wish to thank Leroy Williams of IMC Chemicals Inc. for providing the samples and information about the process.

References

1. *Carbon Sequestration Research and Development*, U. S. Dept. of Energy Report, (December 1999).
2. Herzog, H., "An Introduction to CO_2 Separation and Capture Technologies," Energy Laboratory Working Paper, Massachusetts Institute of Technology (August 1999).
3. Polderman, L. D.; Dillon, C. P.; Steele, A. B. *Oil & Gas Journal* **1955**, *54(2)*, 180-183.
4. Chi, S. and Rochelle, G. T., "Oxidative Degradation of Monoethanolamine", Presented at the First National Conference on Carbon Sequestration, Washington, D. C. **2001**.
5. Rooney, P. C.; DuPart, M. S.; Bacon, T. R. *Hydrocarbon Processing*, July **1998**, 109-113.
6. Arnold, D. S.; Barret, D. A.; Isom, R. H. *Oil and Gas Journal* 1982, *80**(47)***, 130-136.
7. Leci, C. L. *Energy Convers. Mgmt*. **1997**, **38**, S45-S50.
8. Dawodu, O. F; Meisen, A. *Ind. Eng. Chem. Res*. **1994,** *33*, 480-487.
9. Dawodu, O. F.; Meisen, A. *Gas. Sep. Purif*. **1996**, *10*, 1-11.
10. Meisen, A.; Shuai, X. *Energy Convers. Mgmt*. **1997**, *38*, S37-S42.
11. Ding, Y.; Lee, M. L.; Eatough, D. J. *Int. J. Envir. Anal. Chem.* **1998**, *69*, 243-255.

DEVELOPMENT OF A GENERAL METHODOLOGY FOR EVALUATION OF CARBON SEQUESTRATION ACTIVITIES

K. Thomas Klasson and Brian H. Davison

Life Sciences Division
Oak Ridge National Laboratory
Oak Ridge, Tennessee 37831-6226

Introduction

The United States may soon be focusing national attention on processes and activities that mitigate the release of CO_2 to the atmosphere and, in some cases, may remove CO_2 from the atmosphere. As we invest national resources to these ends, it is important to evaluate options and invest wisely. How can we apply consistent standards to evaluate and compare various CO_2 sequestration technologies? A standard methodology that considers all the carbon impacts is needed. This would be useful for policy makers to understand the range of options and for technology developers and investors to guide investment decisions. It would also serve as a source of information for calculations or estimations of carbon credits in a future credit trading system.

The performance objective for a sequestration technology is not necessarily zero emission of CO_2 but rather a reduction compared with the baseline of current practice. To make sure that all carbon aspects are considered, care must be taken to ensure that there are no hidden emissions when making an alteration from the baseline. The fundamental question underlying an analysis of merit of a process or alteration of a process is as follows:

How much CO_2 is generated as a result of the sequestration process, and what is the sequestered carbon's ultimate fate?

Both inputs and outputs must be considered to obtain a total picture. When we speak of carbon sequestration in this manuscript, we refer to all greenhouse gas sequestration measured in carbon dioxide or carbon equivalence (CE). The carbon dioxide equivalence is also called the Global Warming Potential (GWP). A complete list of GWP values has been prepared by IPCC.[1]

To address our objective, we have developed and elaborated on the following concepts:

- All resources used in a sequestration activity should be reviewed by estimating the amount of greenhouse gas emissions for which they historically are responsible. We have done this by introducing a quantifier we term *Full-Cycle Carbon Emissions* (FCCE), which is tied to the resource or product.[2]
- The future fate of sequestered carbon should be included in technology evaluations. We have addressed this by introducing a variable called *Time-Adjusted Value of Carbon Sequestration* (TVCS) to weigh potential future releases of carbon, escaping the sequestered form.
- The *Figure of Merit* of a sequestration technology should address the entire life cycle of an activity. The figures of merit we have developed relate the investment made (carbon release during the construction phase) to the lifetime sequestration capacity of the activity.[2] To account for carbon flows that occur during different times of an activity, we incorporate the *Time Value of Carbon Flows*.

In this short preprint we limit ourselves to discussing the development of TVCS and how it relates to FCCE.

Results

Future carbon emissions occurring from sequestered carbon should be considered when evaluating different sequestration approaches. To determine the FCCEs for streams that will cause carbon emissions in the future, we introduce the Time-Adjusted Value of Carbon Sequestration (TVCS). One way to estimate this value is to employ our global climate models to predict changes in atmospheric CO_2 levels as a result of sequestration and future release from sequestered carbon. This would be a labor-intensive task. Moreover, if an individual sequestration effort is moderate, it will be considered merely as noise in existing global models. We propose another approach—to start by defining a sequestration duration goal that will serve as a metric for future reference. For example, we may chose to use 200 years as our goal for sequestration. In this scenario, if we sequester 2 megatons of carbon (2 MtC = 7.4 Mt of CO_2) today and are able to keep it sequestered for at least 200 years, we should receive full value (100%) for the activity. If we have partial or full release in less than 200 years, we are not doing as well and the value is less. The question is this: how do we evaluate different carbon release profiles and determine their proper values?

Consider the graphs in Figure 1a–1d, in which several value curves have been constructed based on the instantaneous release of 2 Mt of sequestered carbon sometime in the future. We will later consider partial release over time. Figure 1a shows a scenario that does not give any value (or credit) to a sequestration of less than 200 years. Figure 1b takes a more gradual approach by applying a straight-line model. Here, if we instantaneously release all the carbon at any time before 200 years (e.g., 150 years), we would get fractional credit (e.g., 150/200×2=1.5 MtC). To give proportionally more credit to longer sequestration periods, we can construct a curve as in Figure 1c. Here we emphasize that there is increasingly more value in focusing on technologies that will keep the carbon sequestered longer, thus discouraging activities with potential quick release. It is clear that this third approach is very sensitive to prior knowledge about the future release, especially for the years close to year 200. To counter this, we may choose to use a fourth approach (Figure 1d) which suggests that we should consider short-term solutions favorably while recognizing that future predictions are hard to make. In all the cases, we have chosen to give full credit, or value, to sequestration past 200 years (or whatever metric we select as a goal).

It should be pointed out that all the curves drawn in Figure 1 were constructed using the same basic equation, namely (for $y \le Y$)

$$Value = (Amount\ of\ Carbon\ Released) \times \left[\frac{(1+i)^y - 1}{(1+i)^Y - 1} \right] , \qquad (1)$$

where i is the penalty interest rate, y is the number of years sequestered, and Y is the sequestration goal (expressed in years). This equation is of the same type as interest rate functions but has been normalized by the expression in the denominator so that the function takes a value of 1 (one) when $y = Y$. The different curve shapes constructed in Figure 1 were obtained by changing the penalty interest rate from 500% to 0.01% to 3% to –3% for Figure 1a, 1b, 1c, and 1d, respectively. We propose the following abbreviated expression for the modifier:

$$V = R \times TVCS(i, y, Y) , \qquad (2)$$

where V is the value of carbon sequestration and R is the amount of carbon released.

The preceding example showed how to penalize (or discount) the maximum sequestration value for discrete releases of the sequestered carbon; however, it is more likely that future carbon release from an activity is predicted via a mathematical expression (e.g., a half-life constant). In this case, Equation 2 is modified to yield the time-integrated value,

$$V = S_C - \int_0^Y R(y) \times (1 - TVCS(i, y, Y))\, dy , \qquad (3)$$

where S_C is the net amount of carbon initially sequestered and $R(y)$ is the release profile. The carbon release profile could, for example, be from the use of slowly decomposing ammonium carbonate fertilizer.

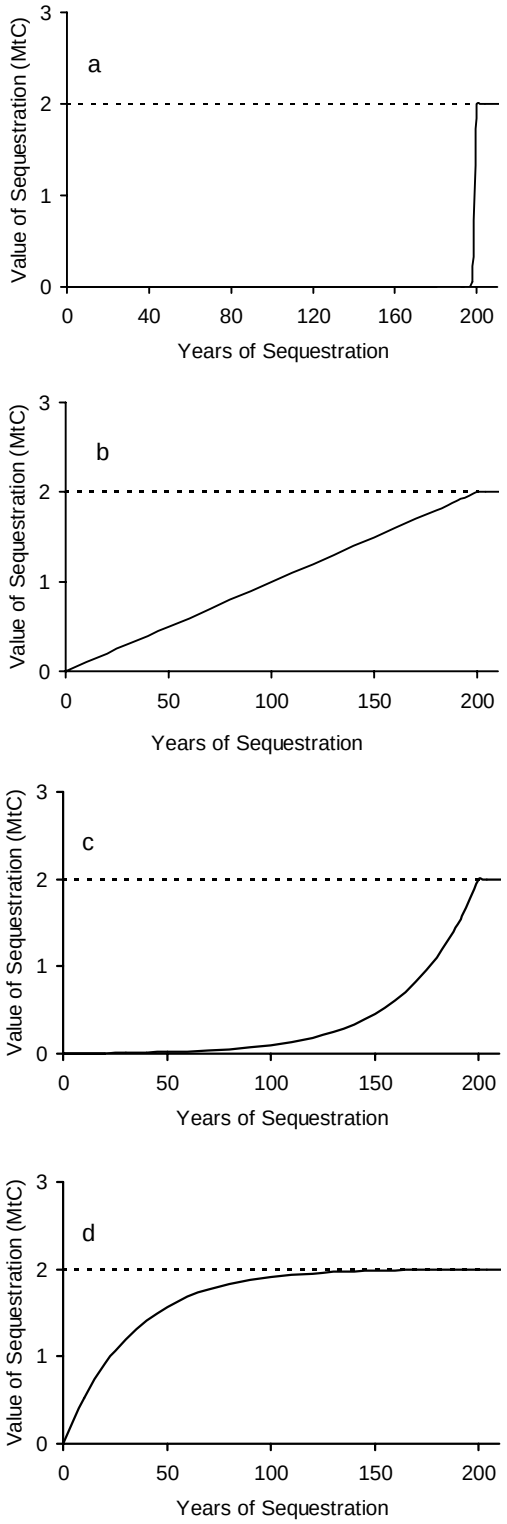

Figure 1. Several potential profiles for calculation of the time value of carbon sequestration.

We have discussed the future release of carbon from a sequestration activity. We should also consider that energy and materials might be needed in the future for "maintenance" to retain the carbon in its sequestered form. Intuitively, we can say that the use of energy and materials in the future should be limited. Because we expect that their use generate CO_2, we need to incorporate this knowledge in the value of sequestration. To keep with the approach that we have taken concerning TVCS, we would value delayed use of energy more than early use. The easiest way to visualize this it to realize that any maintenance in the future will generate CO_2, and this amount must be added to that potentially released from the sequestered carbon. Thus, R in Equations 2 and 3 represent the total CO_2 (or CE) released in the future, whether from captured CO_2 itself or from any CO_2-generating activity associated with the captured carbon. Incorporating maintenance activities into the projected scenario creates a situation that would cause some sequestration technologies to have a negative value, indicating a poor carbon management strategy.

The FCCE of the sequestered carbon stream is the amount of carbon equivalents of future emissions related to this stream. In introducing the TVCS, we have acknowledged that emissions may occur in the future from the sequestered carbon and we have also incorporated a projected value to address future releases. Thus, the time-adjusted FCCE is the right-hand part of the expression in Equation 3,

$$FCCE = \int_0^Y R(y) \times \left(1 - TVCS(i, y_j, Y)\right) dy \,. \qquad (4)$$

Conclusions

Our objective was to develop a general methodology for evaluation of carbon sequestration technologies. We wanted to provide a method that was quantitative but also structured to give robust qualitative comparisons despite changes in detailed method parameters—that is, it does not matter what "grade" a sequestration technology gets, but a "better" technology should always achieve a higher score. We think that the methodology we have begun to develop provides this capability.

- This is a methodology that will assist in evaluation and comparison of well-defined sequestration activities.
- This is a methodology that should be used to address long-term merit prior to engaging in an activity.
- This is a methodology that treats a sequestration activity as an engineering process of which we have knowledge and control.
- This is a methodology that addresses carbon sequestration in life-cycle terms.

Acknowledgement. This work was supported by the U.S. Department of Energy's Office of Fossil Energy Advanced Research Program.

References

(1) *Climate Change 1995—The Science of Climate Change*, Houton, J. T.; Meira Filho, L. G.; Callander, B. A.; Harris, N.; Kattenberg, A.; Maskell, K., Eds.; Cambridge University Press: Cambridge, MA, 1996; pp. 21–22.

(2) Klasson, K. T.; Davison, B. H. *A General Methodology for Evaluation of Carbon Dioxide Sequestration Activities*. Presented at the First National Conference on Carbon Sequestration, May 14–17, 2001, Washington, DC.

EFFECT OF $CaCO_3$ PARTICLES ON THE FORMATION PROCESS OF CO_2 HYDRATE AND DISPOSAL PROCESS IN THE OCEAN

*Satoko Takano, Minoru Fujii, Yukio Yanagisawa, and Akihiro Yamasaki**

School of Frontier Sciences, The University fo Tokyo
7-3-1 Hongo, Bunkyo-ku, Tokyo, JAPAN

*Institute of Environmental Management
National Institute of Advance Industrial Science and Technology
16-1 Onogawa, Tsukuba, JAPAN

Introduction

Ocean disposal scenario of anthropogenic CO_2 in the form of clathrate hydrate have been proposed for mitigation of global warming[1]. The disposal process of CO_2 hydrate has advantages over direct discharge of gaseous or liquid CO_2 from the environmental impact. Since the density of CO_2 hydrate is larger than that of seawater, the disposed hydrate particles has negative buoyancy in the seawater and descend to the ocean bottom. On the other hand, the density of liquid or gaseous CO_2 is smaller than that of seawater at the dept shallower than 3000 m, the discharged CO_2 would ascend to the ocean surface, and some part might be release to the atmosphere when the dissolution is not completed. The hydrate particles disposed in the ocean have a dissociation fate because they are unstable when the ambient seawater is unsaturated with CO_2. The dissociation of CO_2 hydrate would release CO_2, and cause an impact on the marine environment. However, the impact would depend on the rates of descending and dissociation of CO_2 hydrate particles in the ocean. Since these rates depend primarily on the particle size, the environmental impact could be controllable through a proper design of the formation process of the hydrate particle.

The hydrate particle growth process should depend on various factors. In this study, effect of calcium carbonate particles was studied from the following viewpoints.

- The addition of calcium carbonate would increase the CO_2 solubility in water, which is favorable for the hydrate formation. In addition, the $CaCO_3$ particles would provide a crystallization center for the CO_2 hydrate. Consequently, the hydrate formation could be promoted by $CaCO_3$ addition.
- After formation of the CO_2 hydrate, the remained $CaCO_3$ could be disposed of with the hydrate particles in the form of slurry. Since the $CaCO_3$ has a buffering effect for the pH change caused by the dissolution of CO_2 released from the hydrate particles, the disposal process could be more environmentally benign.

Effect of $CaCO_3$ addition on the CO_2 hydrate formation process has been investigated experimentally in a laboratory scale setup. Also numerical simulations of the buffering effect of $CaCO_3$ on the pH change caused by a disposal process of CO_2 hydrate have been conducted.

Experimental Apparatus and Procedure

Figure 1 shows a schematic drawing for the experimental system for the hydrate formation. The batch-type high-pressure reactor was composed of a transparent polycarbonate tube that can bear pressure up to 200 bar. A Pyrex glass tube (inner volume was about 740 cm^3) was inserted in the polycarbonate tube to avoid the direct contact of liquid CO_2 with polycarbonate tube, which could cause a severe damage to the material. The absolute pressure in the Pyrex tube was controlled by a piston-type pressure controller in the range of 1 to 100 bar with an accuracy of 0.1 bar. Pressure between the Pyrex glass tube and the polycarbonate tube was equilibrated by a pressure equilibrator to avoid the excess pressure difference on the Pyrex tube (maximum bearing pressure 20 bar). The reaction contents could be stirred by a 3-wing propeller type agitator with the speed range of 0 to 750 rpm. The temperature was controlled by immersing the reactor in a constant-temperature bath of which the temperature was controlled with an accuracy of 0.1 K through a constant-temperature cooling unit.

A known amount of ion-exchanged water was first introduced to the reactor with or without a given amount of $CaCO_3$ particle at the atmospheric pressure. Then liquid CO_2 was supplied to the system through a high-pressure pump after pre-cooling. After reaching the experimental pressure, the supply of CO_2 was stopped, and the agitation was started. Formation process of hydrate was directly observed and recorded by a digital video camera through the reactor.

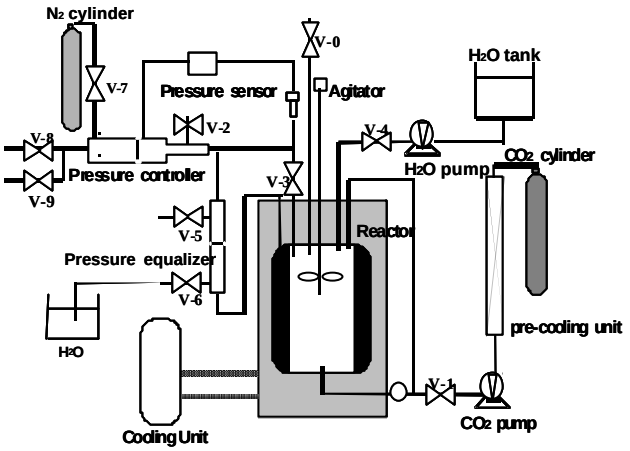

Figure 1. Schematic drawing for the experimental apparatus

Results and Discussion

Observation of hydrate formation process

Without agitation or with agitation at low speed (< 200 rpm), the liquid CO_2 phase and the water phase was separated with a thin hydrate film at the interface. With an increasing in the agitation rate, the hydrate film collapsed at 200 rpm, and liquid CO_2 drops and hydrate particles (about several mm diameter) were dispersed into water phase. When the agitation stopped, the hydrate particles coagulated to form a cluster, but the cluster was easily broken into smaller hydrate particles by a slight agitation (Figure 2) for the cases without $CaCO_3$. For the cases with $CaCO_3$, on the other hand, a large lump of CO_2 hydrate (about 7~10 cm diameter) formation was observed after agitation at 750 rpm as shown in Figure 3. The effect of $CaCO_3$ found to depend on various conditions such as the agitation rate, temperature, and $CaCO_3$ content. No clear effect of the $CaCO_3$ addition on the hydrate formation rate was noticed because the

hydrate formation took place immediately after the agitation even without $CaCO_3$. Thus, the addition of $CaCO_3$ may help the formation of large CO_2 hydrate particle.

Simulation of pH change caused by the CO_2 hydrate particle disposed in the ocean

Numerical simulation of pH change in the seawater by the ocean disposal process of CO_2 was conducted based on the following assumption. In the process, CO_2 was captured and separated from the flue gas of an LNG-fired thermal power plant of 3000 MW. The emission rate of CO_2 is 370 kg/s; this amount of CO_2 will be converted into hydrate particles with $CaCO_3$ addition in a submerged hydrate reactor at 500 m depth. Then hydrate particles will be disposed of in the ocean with an excess amount of $CaCO_3$ slurry. The hydrate particles disposed will descend in the ocean with $CaCO_3$ slurry, and will be dissociated to release CO_2 into the ambient sweater during the descending process. In the meantime, the hydrate particles will be transported horizontally by the eddy diffusion and the ocean current. The following assumption was made for the calculation of pH change caused by the dissolution of CO_2 in the seawater. The following ionic equilibrium relations are always established in the ambient seawater.

$$[H_2CO_3] / P_{CO2} = 10^{-1.5} \quad (1)$$

$$[H^+]\,[HCO^{3-}] / [H_2CO_3] = 10^{-6.3} \quad (2)$$

$$[H^+]\,[CO_3^{2-}] / [HCO^{3-}] = 10^{-10.3} \quad (3)$$

$$[H^+]\,[OH^-] = 10^{-14} \quad (4)$$

$$[Ca^{2+}]\,[CO_3^{2-}] = 10^{-8.4} \quad (5)$$

- The charge is conserved.

$$[H^+]+2[Ca^{2+}] = [OH^-]+[HCO^{3-}]+2[CO_3^{2-}], \text{ with } CaCO_3 \quad (6)$$

$$[H^+] = [OH^-]+[HCO^{3-}]+2[CO_3^{2-}], \text{ without } CaCO_3 \quad (7)$$

- Emission rate of CO_2 by the dissociation of CO_2 hydrate particles was given by the following mass transfer equation.

$$-C_h^* \frac{d}{dt}\left(\frac{4\pi r^3}{3}\right) = 4\pi r^2 k (C_L - C_W) \quad (8)$$

where C_h* is the concentration of CO_2 in the hydrate, C_L is the solubility of CO_2 in the seawater, and C_w is the CO_2 concentration in the ambient seawater. r is the radius of CO_2 hydrate, and k is the overall mass transfer coefficient. The value of mass transfer coefficient is constant at 10^{-7} m/s.

- The descending rate of hydrate particles in the sweater is the terminal velocity in seawater; the drag coefficient, C_D, was given by the following equations depending on the diameter-based Reynolds number (Re).

$$C_D = \begin{cases} 24 / \mathrm{Re} & (\mathrm{Re} < 2) \\ 24/\mathrm{Re}^{1/2} & (2 < \mathrm{Re} < 500) \\ 0.44 & (\mathrm{Re} > 500) \end{cases} \quad (9)$$

where

$$\mathrm{Re} = \rho\, v\, d / \mu \quad (10)$$

ρ and μ are the density and the viscosity of the seawater, respectively, and v and d are the terminal velocity and the diameter of the hydrate particle, respectively. All the properties used for the calculation were those for the seawater at 283 K, and temperature or pressure dependency was neglected.

- The horizontal eddy diffusion coefficient in the ocean is 30 m^2/s (y-direction), and that for vertical direction was negligible. The average ocean current was 0.1 m/s (x-direction) horizontally. The vertical mass transfer of CO_2 takes place mainly by the descending (z-direction) process of hydrate particle in the seawater.

Based on the above assumptions, the pH change caused by the continuous disposal of CO_2 hydrate particles were simulated numerically. Figure 4 shows a steady state pH profile of the seawater at the depth of z = 1300 m as a function of the (y-direction) horizontal distance at x = 1000 m. The initial diameter of CO_2 hydrate particles was also shown in the figure. The pH change was significantly reduced by the addition of $CaCO_3$; the minimum pH in this point was larger than 6 when 0.1 m hydrate particle was disposed at 500 m. With an increase in the hydrate particle size, the low pH region was spread horizontally at this depth. This is so because the larger the initial size, the deeper the hydrate particles could reach.

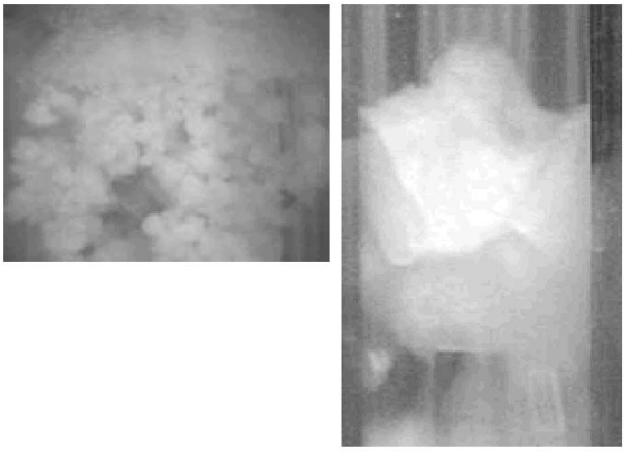

Figure 2. Formation of CO_2 hydrate; (a) hydrate particles cluster formed without $CaCO_3$, (b) hydrate lump formed with $CaCO_3$

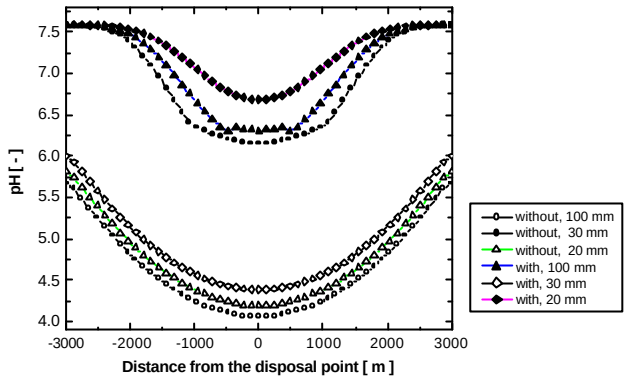

Figure 3. pH change simulation result at the depth of 1300 m and 1000 m away from the disposal point for various initial diameter of the CO_2 hydrate particles. The disposal depth was 500 m.

Conclusions

$CaCO_3$ addition was effective both for the size control of the hydrate particle size in the formation process and for the buffering of pH change by the dissociation of CO_2 hydrate in the ocean.

References

(1) Yamasaki, A.; Wakatsuki, M.; Teng, H.; Yanagisawa, Y.; and Yamada, K. *Energy*, **2000**, 25, 85.

EFFECT OF SWELLING ON THE ADSORPTION ISOTHERM OF CARBON DIOXIDE ON COAL

Ekrem Ozdemir[1,2], Karl Schroeder[2], and Badie I. Morsi[1]

[1] Chemical and Petroleum Engineering Department, University of Pittsburgh, 1249 Benedum Hall, Pittsburgh, PA 15261
[2] U.S. Department of Energy (DOE) - National Energy Technology Laboratory (NETL), P.O.Box 10940, Pittsburgh, PA 15236

Introduction

Although the study of the adsorption of carbon dioxide (CO_2) on coals has a long history, most of these measurements have been conducted at low pressures (below atmospheric) and low temperatures (-78 °C to 25 °C)[1] in order to estimate coal surface areas.[2] Isotherms obtained at high pressures have been reported to poorly fit the conventional adsorption models including monolayer (Langmuir), multi-layer (BET), and pore filling (Dubinin-Radushkevich (DR) and Dubinin-Astakhov (DA)) models.[3,4]

The purpose of this study was to determine the effect that swelling might have on the equations used to develop the adsorption/desorption isotherms of CO_2 on coal and to apply the newly derived equation to the interpretation of the isotherm data, particularly at pressures greater than one atmosphere.

Experimental

Adsorption apparatus. Gaseous CO_2 adsorption isotherms were obtained using the manometric gas adsorption apparatus as shown schematically in **Figure 1**. The manometric apparatus consists of a reference cell of approximately 13 ml and a sample cell of about 6 ml; both contained within a temperature-controlled bath (±0.1 °C). The cell volumes were estimated by the helium expansion method. The pressure within each of the cells was monitored using a pressure transducer (Omega PX300-5KGV), accurate to ± 0.25% full scale

Measurement Methods. Because the volume of each cell can be calculated, the temperature of the system is constant, and the pressure within each cell is measured, the number of gas-phase moles of any adsorbate in each cell can be calculated from Eq 1 where *z*, the compressibility factor, corrects for real gases.

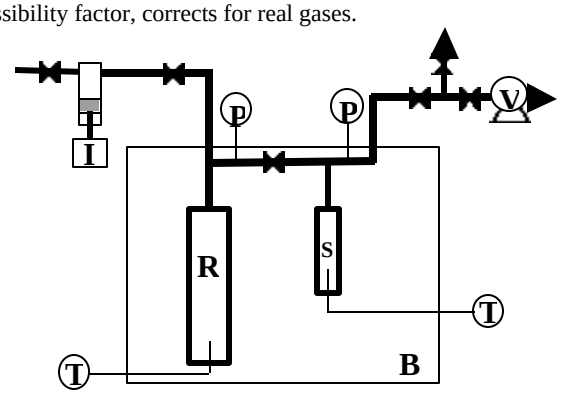

Figure 1. Manometric gas adsorption apparatus: **R**: reference cell, **S**: sample cell, **P**: pressure transducer, **I**: ISCO syringe pump, **V**: vacuum pump **T**: thermocouples **B**: constant temperature bath.

$$n = \frac{PV}{zRT} \qquad (1)$$

The following procedure was used to estimate the amount of CO_2 adsorbed on a coal. (1) Initially, the reference and sample cells contained n_{R1} moles of gas at a pressure of P_{R1} and n_{S1} moles of gas at a pressure of P_{S1}, respectively. (2) The reference cell was charged with n moles of CO_2. At this point, the moles of gas in the reference cell became $(n_{R1}+n)$ at a pressure of P_{R2}. (3) A portion of the gas, Δn_{R1} moles, was transferred from the reference to the sample cell and both cells were allowed to equilibrate. During this period both temperature and pressure were monitored to ensure both thermal and adsorptive equilibrium. At equilibrium, the reference and the sample cells contained $(n_{R1}+n-\Delta n_{R1})$ moles of gas at a pressure of P_{R3} and $(n_{S1}+\Delta n_{S1})$ moles of gas in the gas phase at the pressure of P_{S3}, respectively. If no adsorption were to occur Δn_{S1} would equal Δn_{R1}. Normally, however, the gas phase moles transferred from the reference cell did not equal the gas phase moles found in the sample cell and the missing gas was accounted to CO_2 adsorption on the coal.

The amount of adsorbed CO_2 was calculated from the mass balance in the form of measurable quantities according to

$$\Delta n_{ads} = \frac{1}{w}\left[\left(\frac{P_{R_2}}{z_{R_2}} - \frac{P_{R_3}}{z_{R_3}}\right)\frac{V_R}{RT} - \left(\frac{P_{S_3}}{z_{S_3}} - \frac{P_{S_1}}{z_{S_1}}\right)\frac{V_0}{RT}\right] \qquad (2)$$

where w is the weight of the sample, V_R is the reference volume, and V_0 is the void volume of the sample cell, which is not occupied by the adsorbent (coal) and which was estimated by the helium expansion method prior to the original introduction of CO_2 into the sample cell.

The above procedure was repeated for incrementally increasing pressures of CO_2. Finally, the estimate of the total amount of gas adsorbed, n_{ads}, at the end of the i^{th} step was determined from

$$n_{ads} = \Delta n_{ads_1} + \Delta n_{ads_2} + \Delta n_{ads_3} + ... + \Delta n_{ads_i} \qquad (3)$$

The procedure to this point is typical for the measurement of adsorption isotherms and is applicable to rigid solids. However, we believe it to be inadequate for the description of porous materials that swell in the presence of the adsorbate.

Results and Discussion

Eq 2 is valid only when the void volume in the sample cell (V_0) is constant. However, for coals, it is likely that changes in the available volume in the sample cell occur due to the swelling of the coal, which results from the sorption of CO_2. For example, some micropores are closed to helium and may be accessed by CO_2[5] as shown schematically in **Figure 2**. It can be argued that the void volume measured by helium is not the same as the void volume when these adsorbing gases and vapors are presented to the sample. Thus, an extra accessible volume within the sample cell would be created and should be taken into consideration.

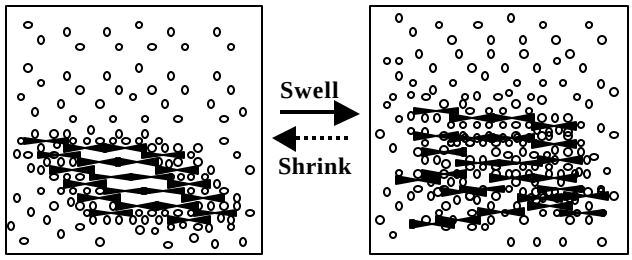

Figure 2. Depiction of the change in the void volume in the sample cell due to pore opening upon the sorption of swelling gases.

In the presence of a volume change, Eq 2 can be written as

$$\Delta n_{ads} = \left(\frac{P_{R_2}}{z_{R_2}} - \frac{P_{R_3}}{z_{R_3}}\right)\frac{V_R}{wRT} - \left(\frac{P_{S_3}}{z_{S_3}}\frac{V_1}{wRT} - \frac{P_{S_1}}{z_{S_1}}\frac{V_0}{wRT}\right) \qquad (4)$$

where V_1 is the void volume accessible for gas compression after the

introduction of CO_2 has swollen the coal and V_0 is the void volume of sample cell as initially measured by the traditional helium expansion method. In this interpretation, the volume inaccessible to the helium and represented by the hollow areas, or bubbles, on the left side of **Figure 2** becomes available for the gas phase compression of CO_2 in the swollen coal. This can be generalized by defining the change in the accessible volume as

$$\alpha_i = \frac{V_i - V_{i-1}}{V_{i-1}} \qquad (5)$$

where α_i is the pore opening coefficient which is dependent on the change in volume at each step (shown as indices i) compared to the previous volume during the adsorption/desorption process. The actual amount adsorbed can be calculated from Eqs 4 and 5 to give Eq 6.

$$\Delta n_{ads} = \underbrace{\left(\frac{P_{R_2}}{z_{R_2}} - \frac{P_{R_3}}{z_{R_3}}\right)\frac{V_R}{wRT} - \left(\frac{P_{S_3}}{z_{S_3}} - \frac{P_{S_1}}{z_{S_1}}\right)\frac{V_0}{wRT}}_{PART\,II} - \underbrace{\frac{P_{S_3}}{z_{S_3}}\frac{\alpha_1 V_0}{wRT}}_{PART\,III} \qquad (6)$$

As shown in Eq.6, the adsorbed amount has two parts. The first part (PART I) is the experimentally determined amount of adsorbed gas (n_{exp}), in which there is no change in the volume in the sample cell and it remains constant at the value estimated by helium expansion. The second part (PART II) is the amount of gas occupied by the nascent cell volume, which was created as a result of the change in the accessible pore volume that occurred when the adsorbent became swollen or shrunken upon the adsorption or desorption of the gas, respectively. A general form of the adsorption equation can be obtained by combining Eqs 3, 5, and 6 to give:

$$n_{\exp} = n_{ads} + k\left(\frac{P}{z}\right) \qquad (7)$$

where n_{exp} is the same as n_{ads} in Eq 3, above, and represents the experimentally calculated total amount of adsorbed gas when the void volume of the sample cell (V_o) is constant, n_{ads} is the actual amount of adsorbed gas on the coal sample, and k is a constant expressed as

$$k = \frac{(\Delta V/w)}{RT} = \frac{(\Delta V/V_0)}{\rho_0 RT} \qquad (8)$$

where $\Delta V/w$ is the change in the accessible pore volume per gram of sample, $\Delta V/V_o$ is the ratio of the change in accessible pore volume of sample per the initial volume, and ρ_o is the helium-density of the sample.

In Eq.7, the only unknowns are the n_{ads} and k. Several equations can be used for the gas adsorption term (n_{ads}) including the Langmuir, DR, and DA equations. When a particular adsorption model is used to fit the experimental adsorption isotherm data, information about coal-CO_2 interactions, such as the monolayer adsorption capacity, the micropore volume, the equilibrium (Langmuir) constant, and/or the characteristic heat of adsorption, can be estimated along with the change in the accessible pore volume in the coal.

The adsorption isotherms of CO_2 at 22°C on the Argonne Pocahontas No.3 and Beulah-Zap coals are shown in **Figure 3**. The lines represent the best-fit values over the entire range of adsorption data. The Langmuir and DA are shown as examples of models that may be used. In practice, we found no significant difference among the three adsorption models investigated once the effect of the swelling was taken into account. As shown in **Figure 3**, the measured adsorption isotherms can be divided into two contributing parts. One is the actual, physical adsorption of CO_2 (Langmuir or DA in the Figure), and the other is the effect of swelling on the accessible pore volume. At low-pressures, the effect of the swelling on the adsorption isotherm is small when compared with the amount actually adsorbed. At high pressures, however, the amount of gas in the additional void volume is considerably higher due to the compressibility of CO_2. Thus, the derived equation is especially important at higher pressures when coal swelling cannot be ignored.

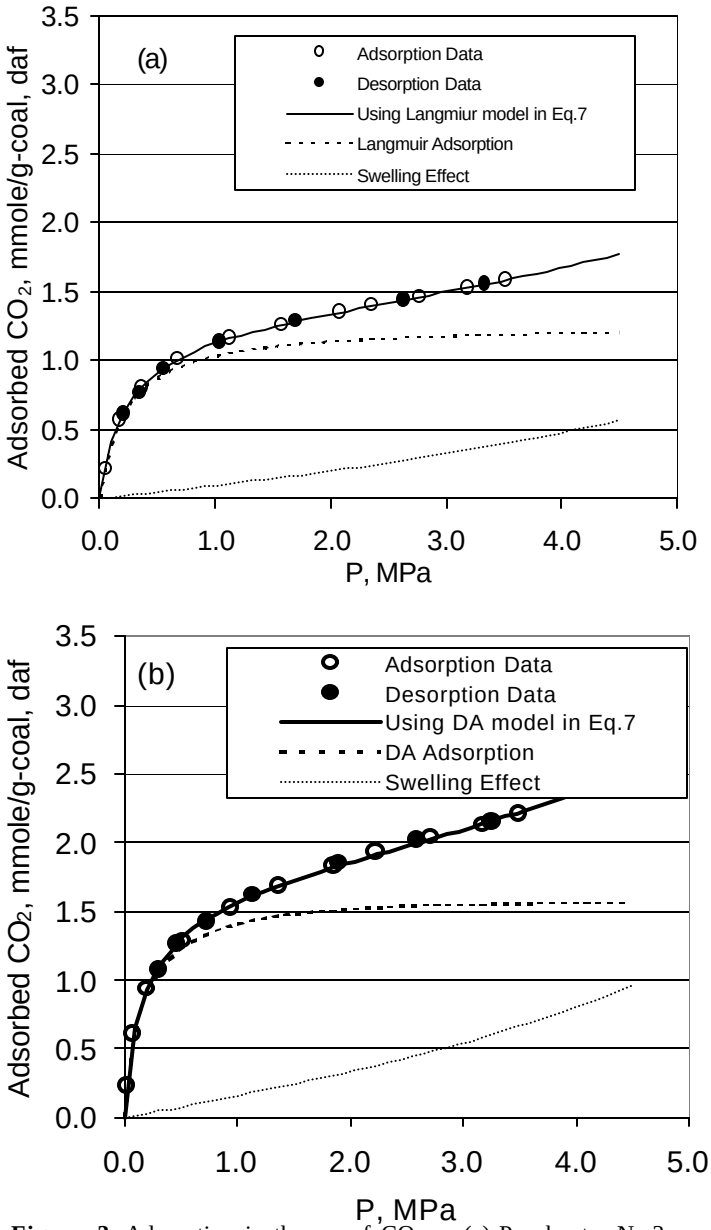

Figure 3. Adsorption isotherms of CO_2 on (a) Pocahontas No.3 - modified Langmuir Eq. (b) Beulah-Zap - modified DA Eq.

References

[1] Walker, Jr., P.L. and Kini, K.A. *Fuel*, **1965**, 44, 453.
[2] Ettinger, I.; Chaplinsky, A.; Lamba, E.; and Adamov, V. *Fuel*, **1965**, 351-356
[3] Clarkson, C.R.; Bustin, R.M.; and Levy, J.H. *Carbon*, **1997**, 35 (12), 1689-1705
[4] Duda, J.M.; Duda, J.; Nodzenski, A.; and Lakatos, J. *Langmuir*, **2000**, 16, 5458-5466
[5] Toda, Y. *Fuel*, **1972**, 44, 108

ELECTROCHEMICAL REDUCTION OF CO_2 TO METHANE IN METHANOL AT LOW TEMPERATURE

S. Kaneco,[1] M. Yabuuchi,[1] H. Katsumata,[1] T. Suzuki,[2] and K. Ohta[1]

[1]Department of Chemistry for Materials,
Faculty of Engineering,
Mie University, Tsu, Mie 514-8507, Japan
kaneco@chem.mie-u.ac.jp

[2]Environmental Preservation Center,
Mie University, Tsu, Mie 514-8507, Japan

Introduction

In the past 60 years, the amount of anthropogenic carbon dioxide (CO_2) emitted to the atmosphere, primarily because of expanding use of fossil fuels for energy, has risen from preindustrial levels of 280 parts per million (ppm) to present levels of over 365 ppm. Consequently, the dire warning of severe weather perturbations and globally rising temperatures have been given. Although scientists, engineers, policy makers, and others are looking for ways to reduce the growing threat of climate change, there is no single answer. Therefore, the development of carbon capture and sequestration technologies, which has accelerated greatly in the last decade, may play a significant role in addressing this issue. Carbon sequestration can be defined as the capture and secure storage of carbon that would otherwise be emitted to or remain in the atmosphere. In order that CO_2 can be economically transported and sequestered, carbon capture prefers a relatively pure stream of the gas. Pathways for carbon capture come from potential sources such as several industrial processes which produce highly concentrated streams of CO_2 as a byproduct, power plants which emit more than one-third of CO_2 emissions worldwide and the production method of hydrogen fuels from carbon-rich feedstocks. CO_2 can be removed from the gas streams by physical and chemical absorption. Recently, the chemical absorption using amines represents the most widely deployed commercial technology for capture. However, in other commercial applications, the typical solvents for physically absorbing CO_2 include glycol-based compounds and cold methanol.

Methanol is a better solvent of CO_2 than water, particular at low temperature, because the solubility of CO_2 in methanol is approximately five times that in water at ambient temperature and eight to fifteen times that in water at temperatures below 273 K.[1] Therefore, methanol has been industrially used as the physical absorbent of CO_2 in Rectisol method at low temperature.[1] Currently, over 70 large-scale plants apply the Rectisol process.

On the other hand, for the CO_2 sequestration technologies, the chemical conversion of CO_2 by radiochemical, chemical, thermochemical, photochemical, electrochemical and biochemical procedures has been of significant interest from the practical viewpoints. The electrochemical method appears to be a very suitable method for the conversion and reduction of CO_2. Since the present conversion efficiencies of single crystal, polycrystalline and amorphous silicon solar cells attainable in laboratory experiments are at the respective levels of about 20 %, 15 % and 12%, respectively, one possible system to industrially convert CO_2 to useful products may be a hybrid method of the solar cell and the CO_2 electrochemical reduction cell. Therefore, a combination technology of the Rectisol CO_2 absorption process and the electrochemical CO_2 conversion method will be able to apply the large scale plant.

Recently, many investigators have actively studied the electrochemical reduction of CO_2 using various metal electrodes in organic solvents, because organic aprotic solvents dissolve much more CO_2 than water.[2-4] It has been described that low reduced products containing carbon monoxide, oxalic acid and formic acid were produced by the electroreduction of CO_2 in dimethly sulfoxide, *N,N*-dimethyl formamide, propylene carbonate and acetonitrile. However, even at a cupper electrode, few hydrocarbons have been obtained in these organic solvents. Therefore, we tried to the electrochemical reduction of CO_2 at Cu electrode in methanol-based electrolyte.[5-7] In the electrochemical CO_2 reduction system using methanol, hydrocarbons were formed with relatively high Faradaic efficiencies and their Faradaic efficiencies increased with decreasing temperature.

Since the electrochemical reduction of CO_2 in organic solvents except for methanol was investigated only at ambient temperature,[2-4] there is little information on the effect of low temperature on the electrochemical CO_2 reduction in organic solvents. Therefore, in the present paper, the electrochemical reduction of CO_2 on copper electrode at 273 K are studied in a variety of organic solvents containing dimethly sulfoxide, *N,N*-dimethyl formamide, propylene carbonate, acetonitrile, ethanol, and methanol. The product distribution in the electrochemical reduction of CO_2 on copper electrode in methanol at 273 K is compared with those obtained in the residual organic solvents.

Experimental

The apparatus and experimental conditions for the electrochemical reduction of CO_2 are shown in **Table 1**. The electrochemical reduction of CO_2 was performed in a home-made, divided H-type cell. An Aldrich Nafion 117-type ion exchange membrane (0.18 mm thickness) was used as the diaphragm. The cathode potential was measured with respect to a silver rod quasi-reference electrode (QRE).

Dimethly sulfoxide, *N,N*-dimethyl formamide, propylene carbonate, acetonitrile, ethanol, and methanol was used as the catholyte. 300 mmol-dm^{-3} lithium perchlorate (Nacalai Tesque, Inc.) was used as the ionophore in the catholyte. Mechanical processing of the Cu and Pt electrodes required polishing each surface with successively finer grades of alumina powder (Baikalox emulsion, manufactured by Baikowski International Co.) down to 0.05 . m, followed by the removal of grease with acetone. Both electrodes were activated electrochemically at 500 mA, for 100 s, in 14.7 mol-dm^{-3} phosphoric acid. Following the above treatment, the electrodes were rinsed with both water and ethanol.

A discontinuous electroreduction procedure was used: first, CO_2 gas was bubbled into the catholyte for 1 h at a rate of 30 ml-min^{-1},

Table 1. Apparatus and experimental conditions

Electrochemical reduction	
Cell	H-type cell
Potentiostat/ galvanostat	Hokuto HA-105
Coulometer	Integrator 1109 (Fusou Seisakujyo, Inc., Japan)
Potential sweep	Hokuto HB-111 function generator
XY recorder	Graphtec WX1100
Thermostat	EYELA, Tokyo Rikakikai CO., LTD., CA-1500
Working electrode	Cu foil (30 mm × 20 mm, 0.1 mm thickness, 99.98 % purity)
Counter electrode	Pt foil (30 mm × 20 mm, 0.1 mm thickness, 99.98 % purity)
Reference electrode	Silver rod quasi-reference electrode
Electrolyte	
Catholyte	300 mmol-dm^{-3} $LiClO_4$ in dimethly sulfoxide, N,N-dimethyl formamide, propylene carbonate, acetonitrile, ethanol, and methanol
Anolyte	300 mmol-dm^{-3} KOH in methanol
Carbon dioxide	99.9999 % purity
Potential	-2.0 to -5.5 V vs. Ag/AgCl sat. KCl
Temperature	273 ± 0.5 K
Product analysis	
Gas products	Gas-chromatography TCD (GL Science GC-320, Molecular Sieve 5A; 13X-S, Ar and He carrier gas) FID (Shimadzu GC-14B, Porapak Q, N_2 and H_2 carrier gas)
Liquid products	HPLC with UV detector (Hitachi L4000) TCD and FID gas-chromatography

then the CO_2-saturated solution was reduced electrolytically at cathodic polarizations in the range from -2.0 to -5.5 V vs. Ag QRE. The electrolysis was performed at 273 K. The catholyte was stirred magnetically. The Faradaic efficiency of the main products was calculated assuming that a total of 50 coulombs of charge passed through the cell. Gaseous products obtained during electroreduction were collected in a gas collector and were analyzed by GC. Products soluble in the catholyte were analyzed by using HPLC and GC.

Results and Discussion

Hori et al. found that copper was an excellent electrode for the formation of hydrocarbons.[8] Therefore, copper was used as a cathode in this study. A suitable supporting salt was explored in order to compare the product distributions in the electrochemical reduction of CO_2 on Cu in various organic solvents. Since lithium perchlorate rapidly dissolved in all organic solvents tested, it was selected as the ionophore in the present work.

Product Faradaic efficiency

In the electrochemical reduction of CO_2 at Cu electrode in dimethly sulfoxide, when the temperature decreased to 273 K, the current density at –3.0 V was very low. Therefore, in order to obtain the current density enough to evaluate the product Faradaic efficiency, the electrolysis was performed at –5.0 V. In the electrolysis, dimethly sulfoxide was not stable and decomposed. Because the current efficiency of this decomposition could not be negligible, the electrochemical reduction of CO_2 on Cu electrode in dimethly sulfoxide at low temperature seems to be not an effective technology.

In the CO_2 electrochemical reduction on Cu in *N,N*-dimethyl formamide and propylene carbonate at low temperature, the current densities even at relatively negative potential were extremely low. Therefore, the CO_2 electrochemical reduction method using *N,N*-dimethyl formamide and propylene carbonate at 273 K appears to be able to apply the practical system.

The results dealing with the effect of the potential on the current efficiencies for the products by electrochemical reduction of CO_2 on Cu in $LiClO_4$/ethanol at 273 K are illustrated in **Figure 1**. Methane was detected as reduction product from CO_2. However, the formation efficiency was less than 2 %. The current efficiency for hydrogen was approximately 100 %. Hence, the applied energy was wasted on hydrogen evolution instead of being used for the reduction of CO_2. Although the electrochemical reduction of CO_2 was studied at relatively positive potential, the current density was < 1 mA-cm^{-2} and the product formation efficiency with low current density could not be evaluated in the view point of practical value. The product distribution obtained in the electrochemical reduction of CO_2 with

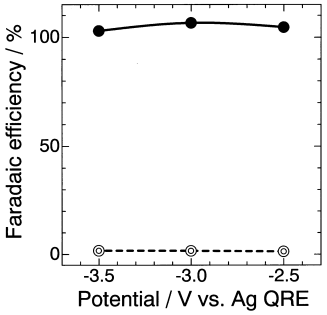

Figure 1. Effect of potential on Faradaic efficiencies for the products by electrochemical reduction of CO_2 at Cu electrode in ethanol at 273 K. CH_4 ; double circle, H_2 ; solid circle.

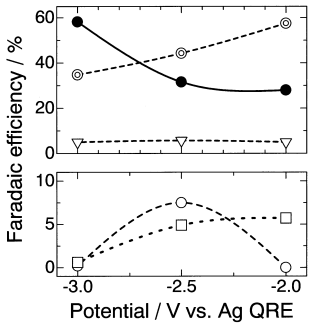

Figure 2. Effect of potential on Faradaic efficiencies for the products by electrochemical reduction of CO_2 at Cu electrode in methanol at 273 K. CH_4 ; double circle, C_2H_4 ; open triangle, CO ; open circle, HCOOH ; open square, H_2 ; solid circle.

copper electrode in acetonitrile was similar to those in ethanol. In the acetonitrile-based electrolyte, the reduction product from CO_2 was only methane and its Faradaic efficiency was < 2 %. On the contrary, the Faradaic efficiency of hydrogen was very large (about 100%).

Figure 2 shows the effect of potential on current efficiencies for the products by electrochemical reduction of CO_2 with Cu electrode in methanol at 273 K. The main products from CO_2 were methane, ethylene, carbon monoxide, and formic acid. The Faradaic efficiency for methane increased to 58 % with decreasing potential. In contrast, hydrogen formation at 273 K decreased to 28 %. A GC-MS study with deuterated methanol catholyte demonstrated that no reduction product was produced from methanol.[5] When the electrolysis was conducted under nitrogen atmosphere, electrolysis yielded exclusively hydrogen. Consequently, the targeted products were produced by the electrochemical reduction of CO_2.

Conclusions

The electrochemical reduction of CO_2 on copper electrode at 273 K was investigated in various organic solvents containing dimethly sulfoxide, *N,N*-dimethyl formamide, propylene carbonate, acetonitrile, ethanol, and methanol. Only in the methanol-based electrolyte, high formation efficiency of methane was observed at low temperature.

Acknowledgement. The present research was partly supported by a Grant-in-Aid for Scientific Research No.12750729 from the Ministry of Education, Science, Sports and Culture of Japan, as well as Industrial Technology Research Grant Program in '00 (No. 00B66010c) from the New Energy and Industrial Technology Development Organization (NEDO).

References

(1) Hochgesand, G. *Ind. Eng. Chem.*, **1970**, 62, 37.
(2) Ito, K.; Ikeda, S.; Iida, T.; Nomura, A. *Denki Kagaku*, **1982**, 50, 463.
(3) Ito, K.; Ikeda, S.; Yamauti, N.; Iida, T.; Takagi, T. *Bull. Chem. Soc. Jpn.*, **1985**, 58, 3027.
(4) Ikeda, S.; Takagi, T.; Ito, K. *Bull. Chem. Soc. Jpn.*, **1985**, 60, 2517.
(5) Naitoh, A.; Ohta, K.; Mizuno, T.; Yoshida, H.; Sakai, M.; Noda, H. *Electrochim. Acta*, **1993**, 38, 2177.
(6) Kaneco, S.; Iiba, K.; Ohta, K.; Mizuno, T. *Int. J. Energy Envion. Econ.*, **1998**, 7, 153
(7) Kaneco, S.; Iiba, K.; Suzuki, S.; Ohta, K.; Mizuno, T. *J. Phys. Chem. B*, **1999**, 103, 7456.
(8) Hori, Y.; Kikuchi, K.; Suzuki, S. *Chem. Lett.*, **1985**, 1695.

ENZYMATICALLY CATALYZED CO_2 SEQUESTRATION

[1]Gillian M. Bond, [2]Brian McPherson, [3]John Stringer, [2]Tristan Wellman, [2]Aaron Abel, and [1]Margaret-Gail Medina

[1] Dept Materials & Met. Eng, New Mexico Tech, Socorro, NM 87801; [2] Dept Earth & Environmental Science, New Mexico Tech, Socorro, NM 87801; [3] EPRI, Palo Alto, CA 94304

Introduction

Long-term sequestration of anthropogenic CO_2 is one suggested approach to the reduction of greenhouse gases in response to concerns over global warming. The most easily addressable source of CO_2 is that from the generation of electric power, and particularly that from the coal-burning stations, since they comprise a relatively small number of very large stationary sources. Coal-fired power plants currently account for a little more than half the total electricity generation. It is unlikely that there will be a dramatic change in this situation in the next twenty years, not least because there is a considerable quantity of coal-burning electricity-generating plant in place that is still operational, and its retirement and replacement would present a considerable economic penalty. In each of the last three years, the coal consumed by the electric utilities in the U.S. has been close to 900,000,000 tonnes. It is therefore essential that CO_2 sequestration is part of any carbon management strategy.

Geologic sequestration of CO_2 is the subject of many ongoing research studies, the majority of which are aimed at injection of supercritical CO_2 into underground formations, particularly deep saline aquifers. It should be noted that CO_2 represents about 18% by weight of the exhaust gas, or 15% by volume, and hence is relatively dilute. There are significant cost penalties associated with the concentration of CO_2 from the flue gas, compression to supercritical form, and subsequent transportation. Several environmental issues associated with the sequestration of supercritical CO_2 also cause concern. These include the risks associated with leaks in the transport lines (since, unlike natural gas, released CO_2 will concentrate in low-lying regions adjacent to the leak, and is not easy to detect), and the possibility of seeps of CO_2 from the subsurface, potentially causing air quality (suffocation) hazards within the vicinity of the seep. Characterization of the "cap rock" or upper confining units of the host formation must be completed to avoid areas in the basin where seeps may form. The possibility of unintended displacement of brines as a result of continued injection of supercritical CO_2 must also be considered.

Conversion of CO_2 to solid carbonates offers the possibility of a safe, stable product for long-term carbon sequestration. Naturally occurring carbonate minerals already comprise a massive carbon reservoir that has existed for millions of years. Large quantities of these carbonate minerals are of biogenic origin. Calcium carbonate can be precipitated from aqueous solution, given a suitable supersaturation of calcium and carbonate ions, and so the issue becomes one of how to produce carbonate ions rapidly from CO_2 and H_2O (1), a process which first requires the formation of bicarbonate ions. One important parameter to be considered is pH, because of its strong effect on the proportions of the carbonic species present (2), and because, at low pH, carbonates will tend to dissolve rather than precipitate. Although carbonate could be formed rapidly at high pH, this would pose both economic and environmental concerns, and hence a process that operates at very mildly basic pH values would be desirable. The rate-controlling step in the fixation of gaseous CO_2 into carbonate ions (Table 1) is the hydration of CO_2 (except at high pH). Thus, if a viable means to accelerate this reaction can be found, it should be feasible to fix large quantities of CO_2 into calcium carbonate at moderate pH. The solution to this problem in fact already exists in biological systems, in the form of a biological catalyst, the enzyme carbonic anhydrase. We have, in fact, demonstrated proof of principle for a novel biomimetic approach to carbon sequestration, which uses carbonic anhydrase to accelerate the formation of bicarbonate ions in aqueous solution (4). In the presence of suitable cations, this can then be precipitated out in carbonate form.

Table 1. Basic carbonate aqueous chemistry reactions.
Equilibrium constants from Langmuir (3).
(1) $CO_2\,(g) = CO_2\,(aqueous)$
(2) $CO_2\,(aqueous) + H_2O = H_2CO_3$
(3) $CO_2\,(g) + H_2O = H_2CO_3$ $K = K_{CO2} = 10^{-1.47}$
(4) $H_2CO_3 = H^+ + HCO_3^-$ $K_1 = 10^{-6.35}$
(5) $HCO_3^- = H^+ + CO_3^{2-}$ $K_2 = 10^{-10.33}$

Cation Sources: Brines

One of the issues we are now addressing is the selection of suitable sources of cations. Along with seawater, and waste brines from desalination operations, brines from deep saline aquifers offer an attractive possibility. In this context, it is important to understand the effects of brine flow on geologic media, both during brine extraction and during possible reinjection of bicarbonate-enriched brines. A preliminary numerical analysis of a sedimentary basin, the Powder River Basin of Wyoming, has been performed. The numerical model includes multiphase flow of CO_2, groundwater and brine, allowing evaluation of residence times in possible aquifer storage sites, and migration patterns and rates away from such sites in the Powder River Basin of Wyoming. The model has also been used to simulate CO_2 flow through fractures, to evaluate partitioning of CO_2 between the fracture network and rock matrix. These simulations provide insight regarding the ultimate propensity of permeability reduction versus permeability enhancement in the fracture zone associated with carbonate reactions.

A two-dimensional finite-volume model of the Powder River Basin cross-section SW-NE was used for all the simulation analyses. The model domain is 230 km horizontal by 5 km vertical, consisting of 5000 grid-blocks (100 horizontal by 50 vertical), each 2300 m by 100 m. The TOUGH2 code (5), which couples flow of heat, groundwater, and brine, was used for these simulations.

Results (Figure 1) suggest that sustained injection of CO_2 may incur wide-scale brine displacement out of adjacent sealing layers, depending on the injection history, initial brine composition, and hydrologic properties of both aquifers and seals. While the results presented here are unique to the simplified model of the Powder River Basin used in this analysis, they may have more general implications for other basins of interest for CO_2 sequestration.

We are also using numerical simulations to evaluate and compare the effects of supercritical CO_2 flow to the effects of bicarbonate solution flow on geologic media. Specifically, we are examining diagenetic changes and time-scales of these changes associated with flow of the two different fluids. For these simulations we are using a reactive transport model that includes coupled groundwater flow, heat flow, and relevant geochemical reactions. The model simulates mass and energy flow and subsequent chemical reactions induced by carbon dioxide and bicarbonate solution injection in the subsurface. Chemical reactions and solute transport are evaluated by TRANS, a simulator developed by Peter Lichtner at Los Alamos National Laboratory (6). Fluid and heat flow are evaluated

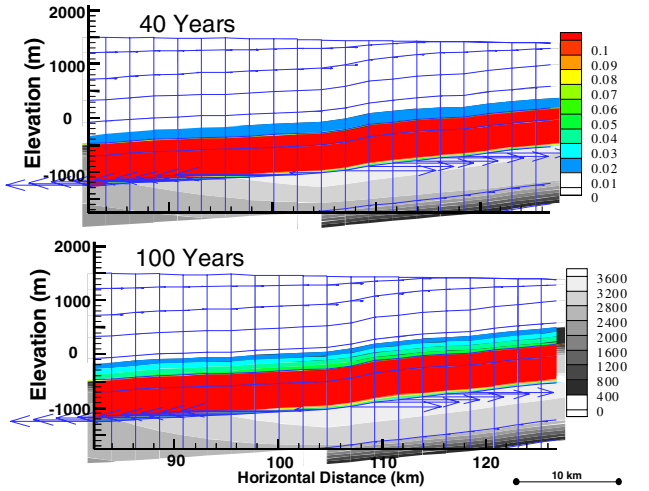

Figure 1. Simulation results illustrating displacement of brine out of a shale sealing layer as a consequence of CO_2 injection in aquifer below. Color contours are brine saturation in the sealing layer and aquifer above, grayscale contours are equivalent hydraulic head in the aquifer below. Arrows are flow vectors illustrating flow away from the injection well.

using TOUGH2, a geothermal simulator developed by Pruess at the Lawrence Berkeley National Laboratory (5). A driver program for coupling the two codes was recently completed by co-author Wellman, for this study. These simulations are being conducted for laboratory-scale models, with the intention that these results will be used for calibration of and upscaling to larger-scale hydrogeologic models.

Catalyst Response in Presence of Toxic Metal Ions

The concentration ranges of various monovalent and divalent ions in seawater, brackish water and saline reservoir waters vary widely. The levels of toxic metal ions that are emitted in flue gases are very carefully limited, and are extremely low (7). Nevertheless, they will not be zero. In a system based on a biological catalyst, it is important that the catalyst still function in the presence of representative levels of these ions. Satisfactory performance in solutions both representing, and more concentrated than, seawater has already been demonstrated (4).

Recent data provide information relating to the performance of solutions containing either purified bovine carbonic anhydrase (BCA) or live cells (modified bacteria, E. coli, expressing human carbonic anhydrase II (HCA II)), in the presence of a range of concentrations of these ions. It is found that the amounts of arsenic, mercury or lead that inhibit enzyme activity are considerably higher than the amounts (10 or 15 µg/ton (7, 8)) that may be present in volumes of air. Thus it appears that neither the live-cell nor the purified-enzyme activities would be significantly affected by the small traces of arsenic, mercury and lead that might be present in flue gases. For both the live cells and the purified enzyme, activity can be seen to decrease strongly, however, at concentrations of these cations in the mg/ton (parts per billion) range. Figure 2, for example, illustrates the activity of both enzyme sources when exposed to increasing concentrations of arsenic ions. Arsenic may attack cell function, leading to large-scale loss of enzyme activity from whole cells at 29 mg/ton, whereas the purified enzyme shows loss of activity at 290 mg/ton.

The purified enzyme performs better than the live-cell enzyme in all experimental conditions. The cost of pure enzyme may prove prohibitive, however, for industrial application, and the difference in activity may not seem so stark when the low cost of live cell production is taken into account. Purified bovine carbonic anhydrase is available commercially for about US$300/gram, whereas E. coli cells expressing HCAII may be produced for about US$0.001/gram (9).

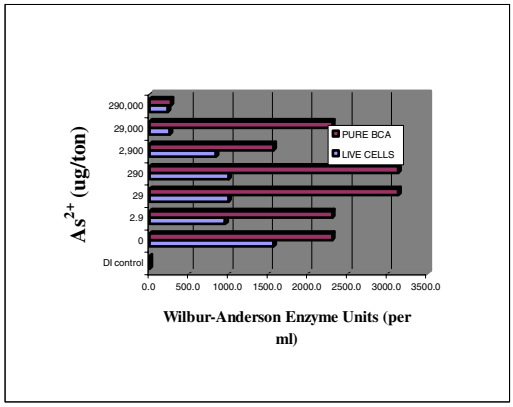

Figure 2. Activity of live E. coli cells versus purified BCA in the presence of arsenic ions.

Acknowledgement. Support for this research from EPRI (WO9000-26) is gratefully acknowledged.

References

(1) Wilbur, K.M. and Simkiss K., *Comparative Biochemistry* **1968,** *26A,* 229.
(2) Loewenthal, R.E. and Marais, G.v.R. *Carbonate Chemistry of Aquatic Systems: Theory and Application, volume 1,* chapter 3, Ann Arbor Science: Ann Arbor (second printing, 1978).
(3) Langmuir, D., *Aqueous Environmental Geochemistry,* Prentice-Hall: New Jersey, 1997.
(4) Bond, G.M., Stringer, J., Brandvold, D.K., Simsek, F.A., Medina, M-G., and Egeland, G. *Energy & Fuels,* **2001,** *15,* 309.
(5) Pruess, K., TOUGH2: A general-purpose numerical simulator for multiphase fluid and heat flow, *Rep. LBL - 29400*, Lawrence Berkeley Lab., September 1991.
(6) Lichtner, P. C., FLOTRAN User's Manual, Los Alamos Laboratory Report, **2000**.
(7) Johnson, J., *Chemical & Engineering News* **2001,** 79(1), 18.
(8) www.atsdr.cdc.gov/tfacts13.html
(9) Belfort, G. *Biotechnology and Bioengineering,* **1989,** *33,* 1047.

EXTRACTION OF CARBON DIOXIDE FROM THE ATMOSPHERE THROUGH ENGINEERED CHEMICAL SINKAGE

M. K. Dubey, H. Ziock, G. Rueff, S. Elliott and W. S. Smith

Earth and Environmental Sciences Division
MS D462, Los Alamos National Laboratory, Los Alamos, NM 87545

K. S. Lackner
H. Krumb School of Mines
Columbia University, New York, NY 10027-4711

N. A. Johnston
Division of Natural Sciences
Lewis-Clark State College, Lewiston, Idaho 83501

Introduction

The 2001 Third Annual Report of the Intergovernmental Panel on Climate Change projects that atmospheric carbon dioxide (CO_2) can approach 1000 ppm in 2100.[1] In addition it concludes that the observed warming over the last 50 years is likely to have been due to the increase in greenhouse gas concentrations, particularly the 30% rise in atmospheric CO_2 caused by man. Fossil fuel use will be limited by our ability to mitigate their environmental effects since they are abundant and cost effective. Future concerns are underscored by the long lifetime of CO_2 in the atmosphere, the accelerating rate of fossil-fuel consumption, and our non-linear climate system that can migrate to a different state in response radiative forcing on decadal time-scales. Consequently technologies for reduction of the world's CO_2 emissions are being explored aggressively. Current emphasis is on fixing CO_2 at large sources such as centralized power plants by emission free conversion of fossil fuels to electricity and hydrogen.[2] However, more than half of the total emissions is from the transportation sector and small distributed sources such as home heating and small industry. Most solutions for dealing with these sources explicitly or implicitly imply a complete overhaul of the existing infrastructure. To surmount this problem Los Alamos National Laboratory has conceived a novel concept of extracting CO_2 directly from the atmosphere by engineering a chemical sink.[3,4]

Direct CO_2 extraction converts the dilute CO_2 (370 ppm) in the atmosphere (from all sources) to a pure CO_2 stream ideal for permanent sequestration. For dealing with the world's total fossil fuel related CO_2 emission rate, extracting CO_2 from the air involves processing of on the order of up to 1% of the earth's atmosphere (containing ~750 Gt CO_2) each year. The fast time scales of atmospheric mixing make this approach feasible. It is a massive undertaking with offsetting advantages:

- Preserves our existing energy use and fuel distribution network that represents a huge investment,
- Captures CO_2 from a myriad of small, distributed, and mobile sources that otherwise are not accessible to sequestration,
- Allows atmospheric CO_2 levels to be restored to their pre-industrial age value,
- Provides free transport of CO_2 to suitable sequestration sites by using the natural atmospheric circulation, and
- Is relatively compact and therefore inexpensive approach when compared to renewable concepts.

This method compensates for all CO_2 sources, can be scaled to yield a net zero or negative emissions, and harnesses the atmosphere as a free CO_2 transportation network.

Our CO_2 extraction from air concept is summarized here and developed it in more detail later. By equating an amount of CO_2 with the energy released in a combustion process, one can associate an energy density with CO_2 in air. By this measure, the energy associated with atmospheric CO_2 is a factor of approximately 100 times more concentrated than wind energy, which is harnessed routinely. Building on this premise our concept harnesses atmospheric circulation to extract CO_2 from air (where it is present at 370 ppm) and binds it to an adsorbent. The saturated absorbent is subsequently heated to release the bound CO_2 thereby generating a pure CO_2 stream for disposal and adsorbent ready for reuse. Low cost chemical extraction reagents such as calcium hydroxide (a prime ingredient in mortar) readily extract CO_2 and demonstrate the feasibility. The reagents would be continuously recycled with the captured CO_2 being recovered and sent to a permanent disposal process such as the mineral carbonation of serpentine deposits that permanently sequester the CO_2 as solid, harmless, and inert mineral carbonates,[5] or direct injection in underground reservoirs or in the deep ocean.

Case for CO_2 Extraction from Air

Concept. To determine the viability of CO_2 extraction from air we compare it to renewable energy options, examining the relative size and therefore likely cost and environmental impact. We also examine the energy requirements of one specific approach to CO_2 capture, which although far from ideal demonstrates feasibility. Our estimates are meant to establish orders of magnitude rather than precise values. The yardstick we employ is the primary energy per unit area and unit time available. We start by examining wind power, which is routinely harvested, albeit on a modest scale. The power per unit area is given by $1/2\ \rho v^3$, where ρ is the density of air and v is its wind velocity. At 10 m/s the wind power contained in the airflow is 0.6 kW/m^2. The time averaged power flux from sunlight on the ground is less, amounting to 0.2 kW/m^2 in the US. The equivalent power collected by biomass represents no more than 0.003 kW/m^2 of heat of combustion amounting to 50t of dry mass hectare^{-1} year^{-1}.

For the extraction of CO_2 from the atmosphere, we consider the same airflow as for wind power. The 10 m^3 of air that flows through the 1 m^2 aperture in one second contain 0.15 moles of CO_2. There is of course no energy in this CO_2. However, if we were to remove all CO_2 from the 10 m^3 of air, we would then be able to burn a certain amount of carbon based fuel without increasing the net CO_2 content of the air. For gasoline we would generate 100 kJ of heat energy per second, less for coal and more for natural gas. Thus in the above example, a combined CO_2 extraction unit/gasoline motor would be able to produce 100 kW/m^2 of primary energy without any impact on the atmospheric level of CO_2. In contrast, a windmill of the same area would only draw on 0.6 kW/m^2 of raw power, a factor of over 100 less. Comparison with other renewable resources is even more dramatic.

Process Description. The low CO_2 concentration in air limits the choice of collection methods. Chemical or physical absorption from an essentially free flow atmospheric air stream appears to be the only viable option. For absorption, the primary energy demand lies in absorbent recycling. The free energy of mixing sets a lower bound on energy expenditure. It is given by $RT \log(P/P_0)$. P_0 is the ambient CO_2 partial pressure, P the desired output pressure, R is the gas constant, and T, the absolute temperature. Separating CO_2 from air at ambient conditions and delivering the output at 1 bar requires 20 kJ/mole. This is only 3% of the energy released in the combustion of gasoline. However, practical implementations will require more energy for rapid CO_2 absorption and concentration.

As air moves over an absorber surface, CO_2 is stripped out. The rate of extraction depends on the efficiency of the absorber, but even the best absorber is limited by the transport of CO_2 through air. The molecular diffusion coefficient of CO_2 in air at ambient temperature is $D = 1.39 \times 10^{-5}$ m^2/s. The mass flux to an absorbing surface is given by $\mathbf{N} = D\ \mathbf{grad}\ \rho_{CO_2}$, ρ_{CO_2} being the local density of CO_2 in the air. For a good absorber, the partial pressure of CO_2 at the absorption surface nearly vanishes, and the mass flux, N_0, to a boundary is given approximately by $N_0 = D\ \rho_{CO_2}/\ L$. Here, L is the transport distance; *i.e.* the typical distance to the nearest surface or for an open system the thickness of a boundary layer. As a specific example, consider air flowing at 10 m/s through a set of parallel tubes, 2.5 mm in diameter. Empirical formulae suggest an effective $L = R/1.8$, where R is the radius of the tube. Comparing the CO_2 flux to the wall with the CO_2 flux through the tubes suggests that most of the CO_2 will be removed after ~ 30 cm. The distance over which the CO_2 is absorbed is proportional to the flow velocity. With a typical velocity of 3 m/s the length of the tube is reduced to less than 10 cm.

In passing over an absorber that removes a portion of the CO_2 from the air-stream, a similar fraction of the air's momentum will be removed, as these two molecular diffusion processes operate similarly. Thus, for a system designed to extract most of the CO_2, the pressure drop is roughly the kinetic energy density in the gas or about 0.06 kPa at 10 m/s. Thus, maintaining the airflow requires an energy input of 0.06 kJ/m^3, which is less than 1% of the energy released in producing that CO_2. Quite likely, a practical implementation would utilize natural convection or wind for this task.

CO_2 Adsorption Collection. Can CO_2 be collected? The common reagent $Ca(OH)_2$ provides a proof of principle. An aqueous solution of $Ca(OH)_2$ is very efficient in collecting CO_2 from air. Simply bubbling air through a few centimeters of $Ca(OH)_2$ solution removes the bulk of the CO_2. The overall resistance to mass transfer is not substantially larger than the transfer resistance in the gas phase. The high degree of extraction that is achieved with $Ca(OH)_2$ is obtained at the price of a substantial binding energy. The reaction can be summarized as follows: $Ca(OH)_2 + CO_2 \rightarrow CaCO_3 + H_2O +$ 114 kJ of energy release. The return calcination reaction $CaCO_3 \rightarrow CaO + CO_2$ requires 179 kJ/mole, which is the energy penalty for recovering CO_2. While this is a non-negligible fraction of the energy from burning gasoline (~650 kJ/mole CO_2), it is still a manageable amount.

System Design. Based on these observations, an idealized process plant would have a number of units, presumably wind or convection driven, that form $CaCO_3$ from an aqueous $Ca(OH)_2$ solution. The $CaCO_3$ precipitate is dried and calcined, which requires energy. The energy for drying could be provided by the heat of hydration when CaO is transformed back into $Ca(OH)_2$. However, calcination would require additional energy, which can come from a number of sources. To be specific, we assume that it is provided by the combustion of coal. The amount of CO_2 generated in the combustion is about 40% of what is stored on the sorbent. Since the process operates on a large scale and is obviously located at a disposal site, the CO_2 from the coal would be directly captured and disposed of.

Cost and Economics. To estimate costs we assume that the cost per unit area of airflow is the same for a windmill and a CO_2 absorption unit. This assumption is justified, since lightweight structures covered with a film of calcium hydroxide solution would be sufficient. Windmills cost about \$700/m^2 of swept area. A CO_2 collection unit of 1 m^2 sweep area, with an extraction efficiency of 50%, and seeing an average wind velocity of 3 m/s would collect 3.6 kg of CO_2 per hour. Assuming a total annual cost for capital investment, operation, and maintenance of 30% of the cost of the machine, the collection cost is \$6.70 per tonne of CO_2. At this point, the collected CO_2 is in the form of $CaCO_3$. Freeing the CO_2 again requires energy. Without accounting for inefficiencies, one would need ~0.15 t coal/t of CO_2. At a price of \$20/t, the cost of this coal would add \$3.00 to the tonne of CO_2. A rough estimate of the annual cost of the calcination plant is determined by multiplying the fuel cost by a factor of four. This is approximately the situation for a power plant. With these assumptions, the calcination process would add \$12/t of CO_2 to the cost of the capture process. This cost would be tolerable compared to the cost of today's energy as well as compared to other sequestration efforts. For example, the cost of pipelining CO_2 a distance of 1,000 km has been estimated at ~\$10/t of CO_2. For a coal-fired power plant at 33% conversion efficiency, \$10/t of CO_2 translates into a little less than 1¢/kWh of electricity. Based on the relative carbon contents of coal and gasoline, the calcination required to collect the CO_2 from one liter of gasoline consumes about 0.7¢ worth of coal. Using the calculations performed above, the price of the complete process should be less than 5¢ per liter of gasoline, well within the range of recent price changes.

Land Requirements. Finally the size of the facilities to collect CO_2 or the required land area is considered. Imagine small collection units of some extent normal to the airflow, but of a height that is negligible on the horizontal scale of the system. On the large scale, one may consider the surface of the horizontal area to be a good CO_2 absorber reducing the CO_2 density from an ambient value of ρ_{CO_2} to $(1 - \varepsilon)\rho_{CO_2}$, where ε is the CO_2 removal efficiency. CO_2 is transported horizontally over the area by a wind velocity v, and it is transported vertically through eddy diffusion. The collection units near the surface remove CO_2 providing a gradient for vertical eddy diffusion transport. The observed eddy diffusion coefficient of the lower atmosphere is 10 m^2/s. The vertical rate of mass transport is roughly $\varepsilon\rho_{CO_2}(D_e v/L)^{1/2}$, where L is the dimension of the collection area in the wind direction. Thus for an area of size L×W, the total rate of CO_2 removal is given by $\varepsilon\rho_{CO_2}W(D_e L v)^{1/2}$. Assuming that L=W, ε=0.5 and v=3 m/s, the land area required for collecting all CO_2 from a residential vehicle fleet of a city of 2 million is about 2.8 km on the side. A square, 530 km on the side, is sufficient to collect the CO_2 from all current anthropogenic sources. Since the rate of collection is proportional to $L^{1/2}$ rather than L, collection from several separate smaller areas would be more efficient than a single large area. If combined into a single area, these units will interfere with each other, with downwind units extracting CO_2 from already depleted air. *If one were to limit the size of a collection unit to a square of 100 m on the side, then the world output of CO_2 would require 380,000 units, which is 1.4% of the area of a single collection system*. Each of the hectare units could consist of five vertical units, each 19 m tall by 19 m wide. Intuitive estimates indicate that the individual collection areas need to be spread over a total area as calculated above. Further spreading is not effective.

Results and Discussion

We are performing global and high resolution atmospheric modeling and laboratory uptake experiments to further examine, quantify and develop CO_2 extraction from air as an advanced greenhouse gas separation and capture technology.

Global Scale Modeling. We have conducted large scale global simulations and sensitivity studies at 4^o x 5^o latitude/longitude resolution where a single grid-point land-based flat CO_2 sink is placed at various locations and with various deposition velocities (v)

in the UC Irvine Chemical Transport Model (CTM).[6] The CTM contains nine vertical layers centered at 975, 909, 800, 645, 478, 328, 206, 112 and 40 mbar. The vertical resolution of the bottom layer is of order 1 km. This off-line code accepts wind fields from general circulation models and advects chemically interacting tracers and has been validated for many tropospheric applications. It allows us to assess the efficacy of global scale CO_2 extraction and identify locations that minimize impacts on downwind ecosystems that will experience reduced CO_2 levels and enhanced alkaline aerosols.

Figure-1 below shows the CTM's sensitivity of the calculated amount of CO_2 extracted from the entire atmosphere as a function of time for a range of deposition velocities (v) at a single grid point surface sink centered in Nevada, USA. Observed deposition velocities for gases that react rapidly at terrestrial surfaces like SO_2 and HNO_3 are 1 and 4 cm/sec respectively.[7] Our simulations indicate that extraction of the order of 10 Gtonnes-C/year is possible, even with a simple flat sink. These simulations also reveal the magnitude and extent of CO_2 depletion downwind of the sink that will be valuable to identify locations that minimize impact on terrestrial ecosystems. Saturation effects at high deposition velocities are caused by inability of mixing to replenish the sink box with more CO_2 from the rest of the atmosphere in this coarse CTM model.

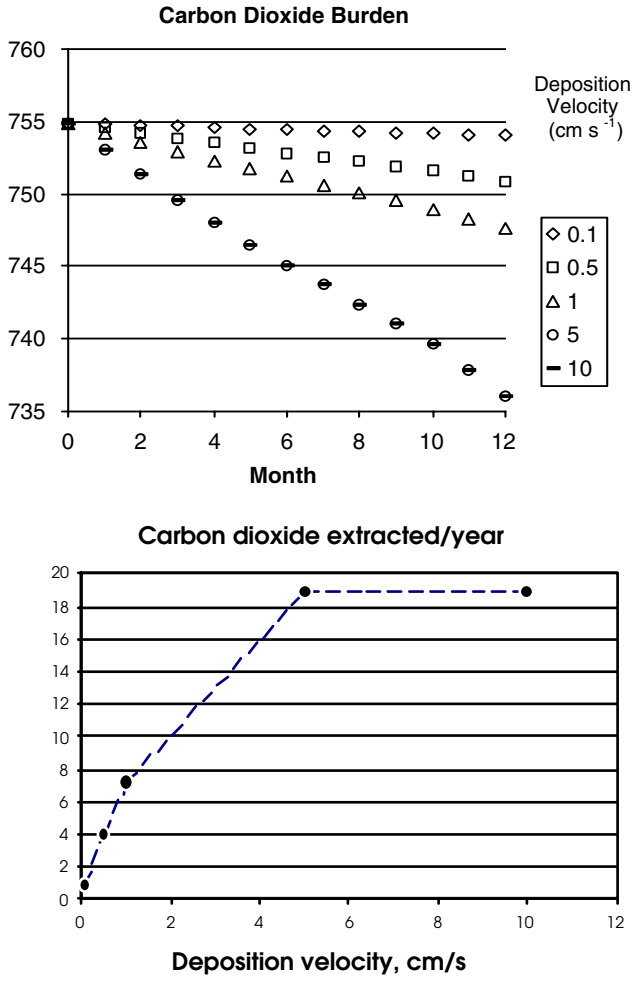

Figure 1 Top panel: total atmospheric CO_2 burden (Gton C) as a function of time for 4^o x 5^o sink centered in Nevada box for various deposition velocities. Bottom panel: The amount of CO_2 extracted from air in a year as a function of deposition velocity.

High Resolution Modeling. The coarse global scale CTM modeling results presented above provide a lower limit to the CO_2 uptake flux per unit land area, as we illustrated earlier using scaling arguments in our land requirements section. Clearly we can improve our collection efficiency per unit of active land area by orders of magnitude by using smaller units with optimal spacing and designing structures that enhance turbulent mixing. We are using LANL's *high resolution and strong gradient* (HIGRAD) code to quantitatively examine the detailed effects of mixing and turbulence on CO_2 collection.[8,9] The code operates on a grid-point, finite-difference, compressible, and non-hydrostatic platform in terrain following coordinates with adaptive mesh capabilities. It uses a forward-in-time integration scheme that preserves local extremes and signs of transported properties. The parallel architecture allows it to harness our high-performance supercomputing platforms.

We are performing high-resolution simulations of air extraction of CO_2 using HIGRAD. The 2-Dimensional computations presented here have a horizontal resolution of 200 m and 63 vertical boxes with vertical grid being stretched gradually from 23 m at the surface to ~200 m at the top layer at 1.2 km. The velocity was set to 4 m/sec, and temperature of 300 K in an atmosphere with neutral buoyancy. The simulation used a steady stream of air with 370 ppm of CO_2 as its initial condition. The CO_2 concentrations were set to zero at the surface boundary to mimic an ideal flat sink that covers the entire horizontal domain. A parametric relation between the aerodynamic roughness and the friction velocity over water and similarity theory were used to treat the sub-grid fluxes and the vertical logarithmic wind profile above the surface.[10]

The results shown below in Figure 2, clearly reveal that CO_2 loss is observed hundreds of meters above the surface layer. Vertical mixing by turbulence is an effective source for CO_2 to the surface layer in a neutral atmosphere. Because we start with a uniform velocity profile, the turbulent velocity takes some time to get established as evident below. After this is achieved the real turbulent eddy structures become apparent for the conditions of our simulation.

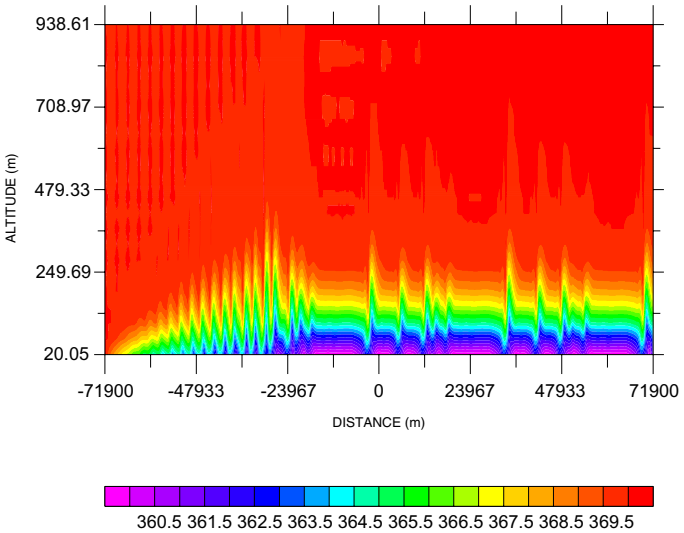

Figure-2: Carbon dioxide concentration in ppm over a perfect aqueous sink simulated using HIGRAD. The distances are in meters above the surface and horizontally about a center of the domain.

Laboratory Experiments. We are performing controlled experiments of CO_2 uptake by saturated $Ca(OH)_2$ solutions in the laboratory. Ambient air is bubbled through a saturated $Ca(OH)_2$

solution with excess solid in an impinger. Care is taken to avoid evaporation by humidifying the input air stream. A metering pump is used to maintain stable slow flow that generates individual bubbles of a few mm in size that rise and remain intact in the solution. The amount of $CaCO_3$ formed at the end of a run (ranging from 15 minutes to 8 hours) is measured by titrating the mixture with acid and monitoring the pH. The inflection points of the pH curve yield the hydroxide, carbonate and bicarbonate fractions. The titration is done slowly and with rapid-stirring to ensure prompt dissolution of the fine $Ca(OH)_2$ particles. A LICOR CO_2 sensor is also being used to provide a continuous measure of the CO_2 extracted from the air by bubbling.

The results from several CO_2 uptake experiments are summarized in Figure 3. There is close to a linear increase in $CaCO_3$ formed and CO_2 uptake with the volume of air processed. The contact time of the bubbles with the solution was varied by changing the height of the solution column. From the slopes of the above $CaCO_3$ formation data for 11 experiments we derive a the mean CO_2 collection efficiency of 53 ± 5% from air by a saturated $Ca(OH)_2$ solution. The collection efficiency could be limited by kinetic factors such as CO_2 diffusion in the bubble and local in-homogeneity in the $Ca(OH)_2$ concentrations and pH of the solution in the vicinity of the bubble which will strongly influence the CO_2 uptake.[11] However, an

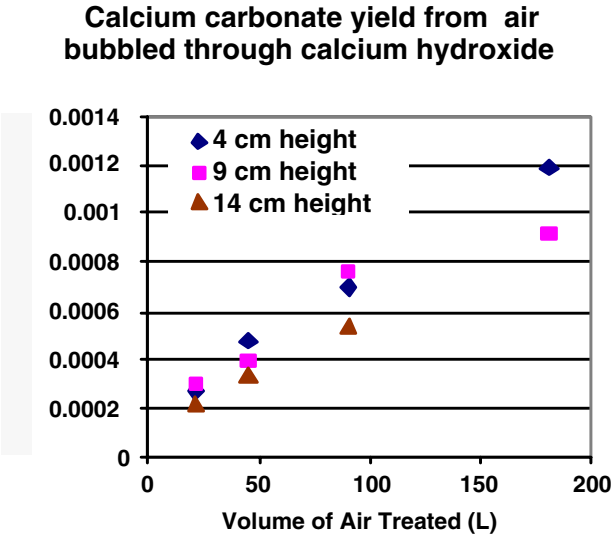

Figure 3. Measurements of $CaCO_3$ formed as a function of the volume of ambient air (~370 ppm CO_2) bubbled through a saturated $Ca(OH)_2$ solution under controlled laboratory conditions.

efficiency of this size should be sufficient to effectively extract CO_2 from air.

Conclusions and Directions

Our economics and scaling arguments, atmospheric simulations, and laboratory experiments make a strong case to explore carbon-dioxide extraction from air as an advanced CO_2 capture and sequestration technology. By all measures we applied, this process compares very favorably against renewable sources such as solar, wind, or biomass. This scheme is attractive because; it allows CO_2 sequestration without a costly change in the existing infrastructure; it collects the CO_2 from the transportation and other distributed power sources; it retains carbon-based energy, which continues to be highly cost-effective, and it has the potential of restoring atmospheric CO_2 to pre-industrial levels providing us insurance against any large and rapid climate change events in the future. We are aggressively pursuing research on active and passive collection schemes, feasibility of CO_2 adsorbents like zeolites, silicates, amines, and $Mg(OH)_2$ with lower binding energy than $CaCO_3$, and identify locations that maximize collection, facilitate disposal, and minimize environmental impact. Our goal is to optimize the scale of the processes in order to design, construct, and develop a small prototype CO_2 extraction plant for field studies.

Acknowledgment

This work is supported by the Laboratory Directed Research and Development (LDRD) Program at Los Alamos National Laboratory, Los Alamos NM 87545.

References

1. http://www.ipcc.ch for *Climate Change 2000* and *Climate Change 1995,* Cambridge University Press, 1996.
2. http://www.zeca.org, Zero Emissions Coal Alliance.
3. Lackner, K. S.; Grimes, P.; Ziock, H., *Proceedings of the 24th Annual Technical Conference on Coal Utilization And Fuel Systems,* March 8–11**, 1999**. Clearwater, Florida. Available as Los Alamos National Laboratory Report LA-UR-99-583.
4. Elliott, S.; Lackner, K.; Ziock, H.; Dubey, M. K.; Hanson, H. P.; Barr, S.; Ciszkowski, N. A.; Blake, D. R., *Geophys. Res. Lett.*, **2001,** *28,* 1235-1238.
5. Lackner, K. S.; Butt, D. P.; Wendt, C. H., *Energy Convers. and Mgmt.*, **1997**, 38, Suppl, S259-S264, Elsevier Science Ltd.
6. Johnston, N. A. C.; Blake, D. R.; Rowland, F. S.; Elliott, S.; Lackner, K.; Ziock, H. J.; Dubey, M. K.; Hanson, H. P.; Barr, S., Submitted to *Energy Convers. and Mgmt.,* **2001.**
7. Sienfeld, J. H.; Pandis, S.N., Atmospheric Chemistry and Physics: From air Pollution to Climate Change, John Wiley and Sons: New York, 1998.
8. Smith, W. S.; Reisner, J. M.; Kao, C.Y.J., Atmos. Env., **2001**, *35*, 3811-3821.
9. Reisner, J.; Wynne, S.; Margolin, L.; Linn, R., *Monthly Weather Rev.,* **2000**, *128*, 3683-3691.
10. Pielke, R. A., Mesoscale Meteorological Modeling, Academic Press: London, 1984.
11. Boniface, J.; Shi, Q.; Li, Q.; Cheung, J.L.; Rattigan, O.V.; Davidovits, P.; Worsnop, D. R.; Jayne, J. T., Kolb, C. E., *J. Phys. Chem. A,* **2000,** *104*, 7502-7510.

FUNDAMENTAL ELEMENTS OF GEOLOGIC CO_2 SEQUESTRATION IN SALINE AQUIFERS

James W. Johnson, John J. Nitao, and Carl I. Steefel

Geosciences and Environmental Technologies Division
Lawrence Livermore National Laboratory
Livermore, CA 94550

Introduction

Geologic sequestration represents a promising strategy for isolating CO_2 waste streams from the atmosphere. Successful implementation of this approach hinges on our ability to predict the relative effectiveness of subsurface CO_2 migration and sequestration as a function of key target-formation and cap-rock properties, which will enable us to identify optimal sites and evaluate their long-term isolation performance. Quantifying this functional relationship requires a modeling capability that explicitly couples multiphase flow and kinetically controlled geochemical processes.

We have developed a unique computational package that meets these criteria, and used it to model CO_2 injection at Statoil's North-Sea Sleipner facility, the world's first saline-aquifer storage site. The package integrates a state-of-the-art reactive transport simulator (NUFT[1]) with supporting geochemical software and databases (SUPCRT92[2]). In our Sleipner study[3], we have quantified—for the first time—the influence of intra-aquifer shales and aquifer/cap-rock composition on migration/sequestration balance, sequestration partitioning among hydrodynamic, solubility, and mineral trapping mechanisms, and the isolation performance of shale cap rocks.

Here, we review the fundamental elements of geologic CO_2 sequestration in saline aquifers as revealed from model XSH of our Sleipner study[3]; this model, unlike CSH[3] and DSH[3], does not address the complicating (yet advantageous) presence of intra-aquifer shales.

Reactive Transport Modeling of CO_2 Injection at Sleipner

In the Sleipner field, CO_2-rich natural gas is produced from 3500 m below the seabed. Excess CO_2 is removed from the production stream by amine absorption on the platform, then stripped from the amine and injected—at the rate of one million tons per year since 1996—into a saline aquifer (the Utsira) 2500 m above the hydrocarbon reservoir.[4] The 200-m-thick Utsira is a highly permeable, fluid-saturated sandstone, which is capped by the Nordland Shale. Hydrologic and compositional properties of the Utsira are relatively well constrained, while those of the Nordland Shale are virtually unknown, and must therefore be estimated.[3]

Our reactive transport simulations of CO_2 injection at Sleipner focus on the near-field sequestration environment. The adopted spatial domain extends 600 m horizontally and 250 m vertically; it contains a 200-m-thick saline aquifer (35% porosity, 3-darcy permeability), 25-m-thick shale cap rock (5% porosity, 3-microdarcy permeability), and an overlying 25-m-thick saline aquifer.[3] Pure CO_2 is injected at the rate of 10,000 tons/yr into the basal center of this domain (37°C, 111 bars), which corresponds to a 1-m-thick cross-section though the actual 100-m screen length at Sleipner.[3,4]

Compositionally, the saline aquifers are represented as impure quartz sand (80% quartz, 10% K-feldspar, 5% plag-ab_{80}, 3% muscovite, 2% phlogopite), while the shale cap rock is represented as 60% clay minerals (50% muscovite, 10% Mg-chlorite), 35% quartz, and 5% K-feldspar.[3] Mg end-member components (phlogopite, Mg-chlorite) are used to represent Fe/Mg solid solutions because *in situ* oxidation states are unknown.[3] The saline aquifers and shale are all saturated with an aqueous phase of near-seawater composition.[3,4]

The simulations are carried out for 20 years, with equal-duration prograde (active-injection) and retrograde (post-injection) phases.

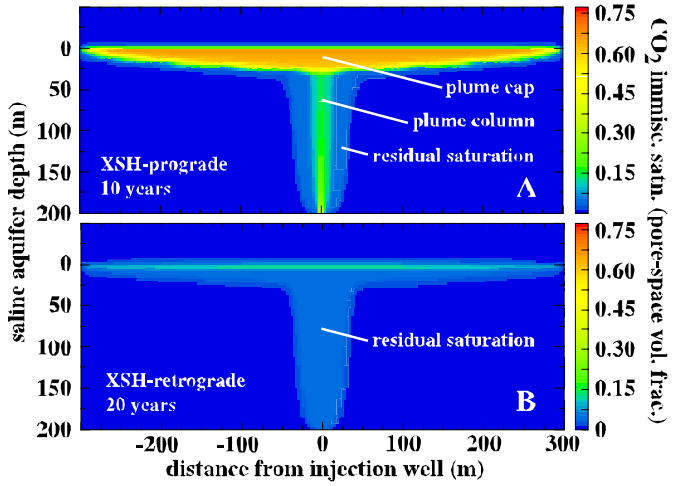

Figure 1. Steady-state configuration of the immiscible CO_2 plume during (A) the prograde phase after 10 years of continuous injection, and (B) the retrograde phase 10 years after injection has ceased.

Modeling Results and Discussion

CO_2 migration/sequestration balance is most conveniently evaluated in terms of contributions from three interdependent yet conceptually distinct processes: CO_2 migration as an immiscible fluid phase, direct interaction of the immiscible plume with formation waters, and indirect plume interaction with formation minerals through the aqueous wetting phase. The first process is directly linked to hydrodynamic trapping, the second to solubility trapping and pH evolution, and the third to mineral trapping.

CO_2 immiscible migration and hydrodynamic trapping. Steady-state configuration of the immiscible CO_2 plume during the prograde phase is realized within one year. In the narrow, sharply delineated plume cap zone, CO_2 immiscible saturation increases from 0.55 at this time to 0.65 at 10 years (Figure 1A). The plume column represents the main conduit of immiscible CO_2 migration, while the residual saturation zone (where immiscible CO_2 is no longer a contiguous migrating phase) marks the wake of initial plume ascent.

In the near-field environment, roughly 85% of injected CO_2 remains and migrates as an immiscible fluid phase ultimately subject to hydrodynamic trapping beneath the cap rock—a very effective seal in this model (Figure 1). The immiscible plume establishes and defines the spatial framework of prograde solubility and mineral trapping. During the retrograde phase, residual CO_2 immiscible saturation (Figure 1B) effectively maintains the prograde extent of solubility trapping and continually enhances that of mineral trapping.

Solubility trapping and pH evolution. As the immiscible plume interacts and equilibrates with saline formation waters, intra-plume aqueous CO_2 concentration (primarily as CO_2(aq) and HCO3-) rapidly achieves the solubility limit, while pH decreases:

$$CO_2(f) + H_2O \leftrightarrow CO_2(aq) + H_2O \leftrightarrow HCO_3^- + H^+ \ .$$

For the present chemical system and P-T conditions, equilibrium aqueous CO_2 solubility is 1.1-1.2 molal (Figure 2A), accounting for about 15% of injected CO_2. Owing to residual saturation of immiscible CO_2 (Figure 1B), this degree of solubility trapping is virtually constant throughout the prograde and retrograde phases.

The initial pH drop caused by prograde solubility trapping—from 7.1 to 4.5—catalyzes silicate dissolution, which after 20 years has increased pH from 4.5 to 5.3 (Figure 2B). This dissolution hydrolyzes potential carbonate-forming cations (here, primarily Na,

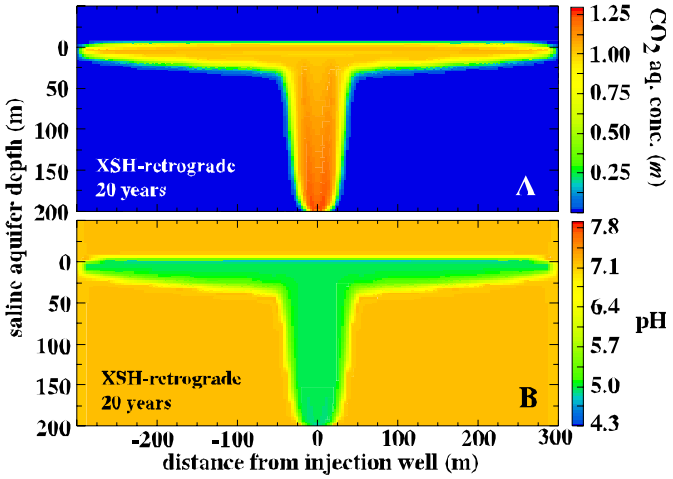

Figure 2. (A) Solubility trapping and (B) pH after 20 years.

Al, and Mg) within the immiscible-plume source region, and thus represents the critical forerunner of all mineral trapping mechanisms.

Mineral trapping. There are four distinct mechanisms whereby CO_2 precipitates as carbonate minerals.

Intra-plume dawsonite cementation (Figure 3A) is catalyzed by high ambient Na^+ concentration, plume-induced CO_2 aqueous solubility, and acid-induced K-feldspar dissolution:

$$\underset{\text{K-feldspar}}{KAlSi_3O_8} + Na^+ + CO_2(aq) + H_2O \leftrightarrows \underset{\text{dawsonite}}{NaAlCO_3(OH)_2} + 3\ \underset{\text{qtz+chal+crist}}{SiO_2} + K^+$$

This kinetic reaction proceeds to the right with an increase in solid-phase volume of 17%; hence, it leads to a slight (0.02%) decrease in intra-plume aquifer porosity over 20 years.[3] Pervasive dawsonite cementation will likely be characteristic of saline aquifer storage in any feldspathic sandstone. In fact, there is a natural analog for this process: widespread dawsonite cement in the Bowen-Gunnedah-Sydney basin of Eastern Australia, which has been interpreted to reflect magmatic CO_2 seepage on a continental scale.[5]

Magnesite rind forms along lateral and upper plume boundaries; genetically distinct, these two processes can be described by:

$$\underset{\text{(magnesite)}}{MgCO_3} + 2\ H^+ \leftrightarrows Mg^{+2} + CO_2(aq) + H_2O\ .$$

As intra-plume formation waters, progressively enriched in Mg^{+2} from phlogopite dissolution, migrate outward across lateral plume boundaries, they traverse steep gradients in CO_2(aq) and pH; the net effect strongly promotes magnesite precipitation (Figure 3B). In the plume cap zone, CO_2(aq) concentration and pH are nearly constant, but aqueous Mg^{+2} concentration increases most rapidly here because formation-water saturation is minimized; this leads to magnesite cementation from the cap-rock interface downward (Figure 3B).

However, magnesite precipitation is most extensive from this interface *upwards* (cf. Figures 3B-C), owing to the relatively high concentration of Mg in clay-rich shales. The coupled reaction is:

$$\underset{\text{K-feldspar}}{KAlSi_3O_8} + 2.5\ \underset{\text{Mg-chlorite}}{Mg_5Al_2Si_3O_{10}(OH)_8} + 12.5\ CO_2(aq) \leftrightarrows \underset{\text{muscovite}}{KAl_3Si_3O_{10}(OH)_2} + 1.5\ \underset{\text{kaolinite}}{Al_2Si_2O_5(OH)_4} + 12.5\ \underset{\text{magnesite}}{MgCO_3} + 4.5\ \underset{\text{qtz+chal}}{SiO_2} + 6\ H_2O.$$

This kinetic reaction proceeds to the right with an increase in solid-phase volume of 18.5% (magnesite accounting for 47 vol.% of the

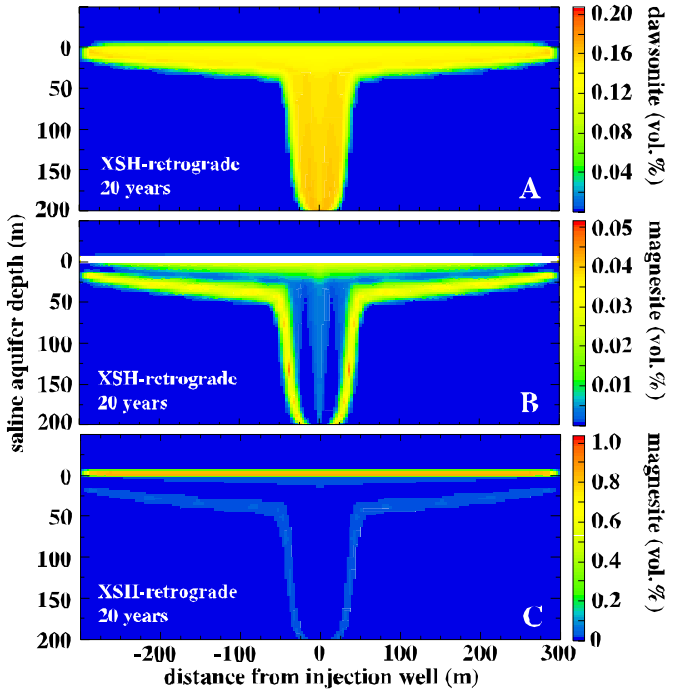

Figure 3. Mineral trapping mechanisms: (A) intra-plume dawsonite cementation, (B) magnesite precipitation—lateral and upper plume boundaries, and (C) magnesite precipitation—shale cap rock.

product assemblage), which after 20 years has reduced porosity and permeability of the 5-m-thick cap-rock base by 8% and 22%.[3]

Conclusions

Geologic CO_2 sequestration in saline aquifers can be subdivided into three fundamental elements: prograde migration of the immiscible plume, direct interaction of the plume with formation waters, and its indirect interaction with formation/cap-rock minerals through the aqueous wetting phase. In the near-field environment of Sleipner-like settings, relative effectiveness of the associated trapping mechanisms on a mass basis is hydrodynamic (85%) >> solubility (15%) >> mineral (<1%).[3]

Although seemingly negligible, mineral trapping has enormous strategic significance: it improves cap-rock integrity and thereby improves containment of the voluminous immiscible plume. Moreover, the prograde extent of mineral trapping is continuously enhanced during the retrograde phase—which spans geologic time scales—by the presence of residual CO_2 immiscible saturation in the aquifer and hydrodynamically-trapped CO_2 beneath the cap rock.[3]

Intra-aquifer shales, solid solutions, and other refinements do not modify the set of fundamental elements reviewed above; they do impose key variations on the style and interaction of these elements.[3]

References

(1) Nitao, J.J., 1998, UCRL-MA-130651, LLNL, 55 p.
(2) Johnson, J.W., Oelkers, E.H., and Helgeson, H.C., 1992: *Comp. Geosci.*, 18(7), 899-947.
(3) Johnson, J.W., Nitao, J.J., Steefel, C.I., and Knauss, K.G., *Proceedings, First Natl. Conf. Carbon Sequestration*, 2001, 60 p., www.netl.doe.gov/publications/proceedings/01/carbon_seq/P28.pdf
(4) Final Technical Report "SACS"—Saline Aquifer CO_2 Storage, 34 p., and other documents available at www.ieagreen.org.uk/sacshome.htm
(5) Baker, J.C., Bai, G.P., Hamilton, P.J., Golding, S.D., and Keene, J.B., *J. Sed. Res., Sec. A – Sed. Petrol. Processes*, 1995, 65(3): p. 522-530.

HIGH EFFICIENCY CAPTURE OF CO_2 FROM MIXED GAS STREAMS

Jijun Ge, Yinjie Qin, Robert M. Cowan, and Michael C. Trachtenberg

Sapient's Institute, 20 Ag Extension Way, Cook College/Rutgers University, New Brunswick, NJ 08901, and Carbozyme, Inc., 1200 Florence-Columbus Rd., Bordentown, NJ 08505

Introduction

The economic capture of CO_2 from mixed gas streams for purification and/or use in CO_2 sequestration remains a substantial hurdle to the widespread application of greenhouse gas remediation. We have developed technologies to help address this need. Our technology development program devised reactors for the efficient removal of CO_2 from Human Space Flight crew environments (e.g. space shuttle, space station, and spacesuit). More recently it has involved the study of CO_2 removal from natural gas, and as described here the CO_2 capture from a wide variety of sources. We have generated an enzyme based contained liquid membrane (EBCLM) reactor as the technological basis for a family of CO_2 removal and capture devices.

The EBCLM works as follows: CO_2 in a mixed gas stream diffuses across a microporous hydrophobic membrane to contact an aqueous buffered enzyme solution. The enzyme, carbonic anhydrase (CA – EC 4.2.1.1), greatly increases solvation via catalytic hydration of CO_2 resulting in the formation of bicarbonate. Bicarbonate diffuses across the liquid membrane. At the permeate side gas-liquid interface CA catalyzes the dehydration reaction and CO_2 is released to the sweep gas stream having diffused through a second microporous hydrophobic polymer membrane.

Experimental

Materials and methods

Bovine carbonic anhydrase (BCA2 - Sigma Chemical Co.) was used as the enzyme catalyst. The buffer was made from monobasic anhydrous potassium phosphate (99.0% purity - Sigma) and dibasic anhydrous sodium phosphate (99.5% purity - Fisher Scientific). Microporous polypropylene (Celgard PP-2400 - Celanese) was used to contain the enzyme/buffer solution. The Celgard PP-2400 membrane is 25.4 μm thick, with a porosity of 35%, a nominal pore size of 41 nm x 120 nm with a tortuosity value of 5 [1]. The thickness of the liquid membrane was controlled by the use of polyester mesh (Small Parts Inc., CMY-200) spacers cut in the form of flattened O-rings. Gases, purchased from Matheson, included ultra-zero air, ultra high purity argon and high purity CO_2. Air and argon were purged of residual CO_2 by a purification column (OMI-4, Supelco) before being used.

Bioreactor configuration and test stand setup

The membrane reactor is constructed by sandwiching a CA containing phosphate buffered solution between two polypropylene membranes. Perforated metal screens (Millipore) retain the polymer membranes. The total liquid membrane area is 380.1 mm^2. The thickness of the aqueous phase was 330 μm. The liquid membrane volume was maintained by means of a fluid reservoir. The feed gas stream delivered via an Environics mass flow controller (Environics, Series 2020 – NIST-traceable calibration). The composition of gas was measured by mass spectrometer (Questor IV, ABB Extrel) The separation performance includes selectivity ($\alpha=Q_i/Q_j$) and permeance ($Q= J/\Delta P$) where J is the flux through the membrane and ΔP is the partial pressure difference across the membrane. The unit of Q is mol m^{-2} Pa^{-1} s^{-1}, i, and j are permeance for species i and j, respectively.

Results and Discussion

Table 1 contains examples of selectivity and permeance values that have been obtained using the EBCLM. Along with these values Table 1 provides information regarding the feed stream CO_2 concentration, the concentration of CA and buffer in the liquid membrane, and the sweep stream condition (pressure and composition). Figure 1 provides a different view of these results in a plot of selectivity versus permeance. This plot also contains information obtained from the literature detailing the performance of competing membrane technologies.

Table 1. Examples of Selectivity and Permeance for CO_2 Separation from Air, Oxygen, and Methane

Sweep pressure	$[CO_2]$ in feed	[CA]	[Buffer]	Selectivity	Permeance	Other Gas(es
kPa	(%)	(mg/ml)	(mM)		(mol/m^2-Pa-s)	
101.3	0.23%	5.0	75	1401	1.44E-7	N_2 & O_2
-70.0	0.50	5.0	75	269.0	8.0E-09	O_2
-70.0	0.50	20.0	800	335.7	8.3E-09	O_2
101.3	2.44	5.0	75	187.4	7.4E-09	CH_4

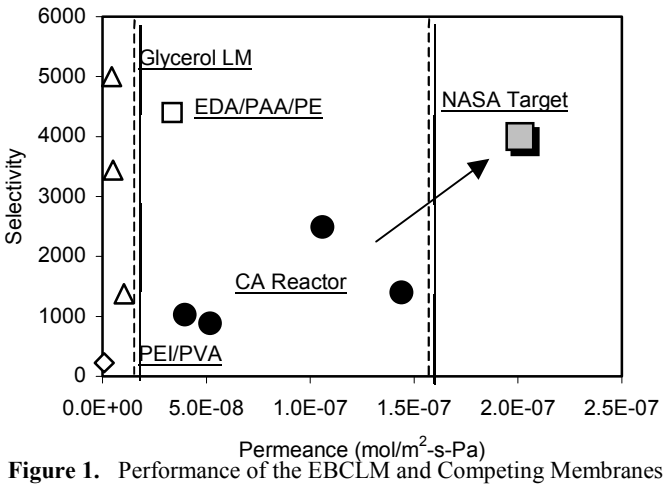

Figure 1. Performance of the EBCLM and Competing Membranes - CO_2 Removal from Air and Other Low Concentration Sources

As seen from Figure 1 the use of traditional nonporous polymer membranes (*e.g.*, PEI/PVA) for CO_2 separation from air provides very low permeance and selectivity [2]. With the use of the glycerol LMs reported by Sirkar and colleagues [1] and the EDA/PAA/PE gel filled membranes of Matsuyama et al. [2] it is possible to obtain high selectivity versus N_2, but the permeance values are at best moderate. While these high selectivity membranes can provide good CO_2 enrichment, the low permeance means large membrane area is needed. This will increase the volume, weight and cost of the membrane device. The data given in Figure 1 for our CLM (closed circles) shows the evolution of its performance [3-8] and the NASA target. Our EBCLM both high permeance and high selectivity are possible, making this CA based EBCLM desirable for use in the capture of CO_2 from very low concentration sources.

Understanding EBCLM Performance

Because the configuration of EBCLM is complicated space and time restrictions prevent full coverage of the topic. The focus here is on a few select influences on EBCLM performance. These include CA chemistry and the influence of environmental factors on CA activity; physical and chemical configuration of the EBCLM (e.g., LM thickness, buffer composition and buffer concentration), and operational factors which influence optimization of the EBCLM design for use in a particular application (e.g., effects of feed and sweep gas composition and pressure).

CA Chemistry

CA is a naturally occurring enzyme that increases the rates of hydration of CO_2 to form H_2CO_3, and the dehydration of H_2CO_3 to form CO_2. As expected from the importance of CO_2 to living organisms CA is present in all animals, most plants, and many fungi, archaea, and bacteria. CA provides a means of making a set of reactions that occur quickly at extremes of pH occur quickly at more neutral pH. Figure 2 illustrates, as a function of pH, the rates of CO_2 hydration and dehydration for both the uncatalyzed and the CA (HCA II) catalyzed conditions. From Figure 2 it is clear that without CA low values of pH favor the dehydration of H_2CO_3; high pH favors hydration of CO_2; and over the range of pH shown (5 to 10) both rates are quite slow. When CA is present there is an approximately 100 to 1000 times increase in the rate of the hydration and dehydration reactions over this entire pH range.

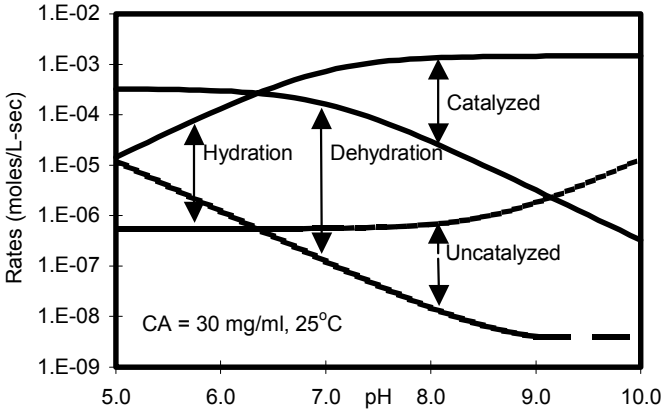

Figure 2. Effect of pH on the Rates of CO_2 Hydration and H_2CO_3 Dehydration

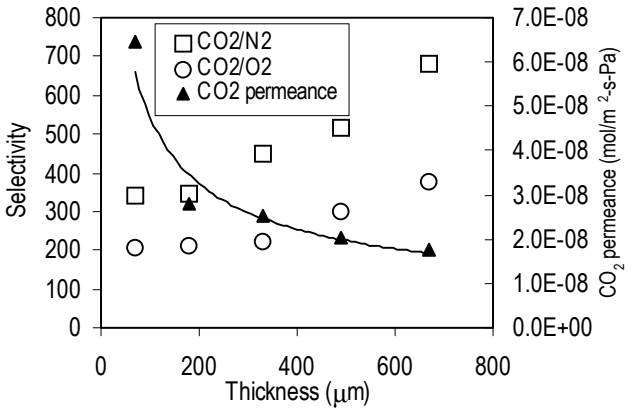

Figure 3. Effect of Thickness on separation performance

Other influences on CA activity include temperature, ionic strength, the concentrations of carbonate and bicarbonate, and the concentration of specific inhibitors of the enzyme such as halides. The particulars of these influences depend on which CA isozyme is in use

EBCLM Configuration – Liquid Membrane Thickness

Figure 3 illustrates the way in which liquid membrane thickness influences the selectivity and permeance of the EBCLM. The results show that as thickness increase, selectivity increases but permeance decreases.

Conclusions

The creation of a CA-based EBCLM accomplishes the following: the generation of a highly selective, high permeance CO_2 capture membrane capable of removing CO_2 from a variety of gas mixtures over a range of temperatures and pressures. The CO_2 can be removed when very dilute (<0.1%) to moderate concentrations (~20%). In current form this system is capable of operating to at least 45°C but may be modified to temperatures possibly as high as 75°C. The system operates independent of relative humidity in the feed or sweep streams and can use a wide variety of gases in the sweep. The design relies on CA to convert a solution-limited process to a diffusion-limited process. Finally, the various parameters controlling the design can be identified, analyzed, modeled and independently manipulated. The performance characteristics, if maintained on scaling and with long-term stability support the idea of a dramatic improvement in CO_2 capture efficiency and consequent decrease in cost, a key to industrial and environmental application.

Acknowledgement.

This work was supported by NASA grants NAG 9-1021, NAG 9-1923, NAG 9–1383 and DOE grant DE-FG02-01ER86129. Additional support was provided by Cook College and the NJ EcoComplex both of Rutgers University, and by M. Toro and M.E. Opper.

References

1. Chen H., Kovvali A.S., Majumdar S. and Sirkar K.K., *Ind. Eng. Chem. Res.*, 38(9) (1999) 3489-3498; Chen, H.; Obuskovic, G.; Majumdar, S.; Sirkar, K. K., *J. Membr. Sci.* 183 (2001) 75-88.
2. Matsuyama H., Terada A., Nakagawara T., Hitamura Y., Teramoto M., *J. Membr. Sci*., 163 (1999) 221-227; Matsuyama H., Teramoto M., Iwai K., *J. Membr. Sci.* 93 (1994) 237-244.
3. J.-J. Ge, R. M. Cowan, C.-K. Tu, M. L. McGregor, M. C. Trachtenberg, Life Support & Biosphere Science, submitted.;
4. Ge J.-J., Trachtenberg M. C., McGregor M. L., Cowan R. M., 31st International Conference on Environmental Systems (ICES), Orlando, Florida, July, 9-12, 2001;
5. Trachtenberg M. C., Tu C.K., Landers R. A., Willson R. C., McGregor M. L., Laipis P.J., Kennedy J. F., Paterson M., Silverman D.N., Thomas D., Smith R.L., and Rudolph F.B., Life Support & Biosphere Science, 6 (1999) 293-302;
6. Trachtenberg M.C., Ge J.-J., Cowan, R. M., McGregor M.L., NAMS, May 15-20, 2001, Lexington, Kentucky;
7. Trachtenberg M.C., Cowan R .M., Ge, J. J., and McGregor M. L., International Conference of Life Support & Biosphere Science, LSBS'2000, Aug.6-9, 2000;
8. Trachtenberg M.C., Ge J. J., Cowan R .M., and McGregor M. L., Bioastronautics Investigators' Workshop, January 17-19, 2001, Galveston, TX, 218-219.

HIGH EFFICIENCY DIRECT CARBON FUEL CELL FOR CO_2 EMISSION AND SEQUESTRATION

Meyer Steinberg

Energy Resources Division
Brookhaven National Laboratory
Upton, NY 11973-5000

John F. Cooper

Lawrence Livermore National Laboratory
Livermore, CA 94551

Introduction

Hydrogen fuel cells have been under advanced development for a number of years and are now nearing commercial applications. Direct carbon fuel cells have, heretofore, not reached practical development because of difficulties in fuel and electrolyte configuration. The carbon/air fuel cell has the advantage of near zero entropy change allowing 100% theoretical thermodynamic efficiency at temperatures to 1000°C. The activities of the C fuel and CO2 product are invariant allowing constant EMF and full utilization of fuel in a single pass mode of operation. The hydrogen fuel cell has a theoretical thermodynamic efficiency of only 70% at 1000°C and the activity of the H_2 fuel and H_2O product limit utilization to 80% in a single pass (Table 1). A direct carbon fuel cell is currently being developed which utilizes clean reactive carbon particulate in a molten carbonate salt slurry. Concentrated CO_2 is evolved at the anode and oxygen from air is utilized at the cathode (Fig. 1).[1,2] At temperatures of 750°C to 850°C, a voltage efficiency of 80% has been achieved at a power density of 1Kw/sqM (Fig. 2).[1,2] The clean carbon and hydrogen fuel is produced from (1) natural gas, by thermal decomposition (Fig. 3), (2) petroleum, by pyrolysis coking (Fig. 4), (3) coal, by sequential hydrogasification and thermal pyrolysis (Fig. 5), and (4) biomass, by sequential hydro- and thermal-pyrolysis (Fig. 6), and are integrated with C and H_2, fuel cells for power cycle estimates.[3] Thermal to electric efficiencies indicate 80% (HHV), 85% (LHV) for petroleum, 75.5% (HHV), 83.4% (LHV) for natural gas and 68.3% (HHV), 70.8% (LHV) for lignite coal (Table 2). The benefits of integrated combined carbon and hydrogen fuel cell power generation cycles include, (1) more than twice the efficiency of conventional fossil fuel steam plants, (2) reduced power generation cost, especially for increasing fossil fuel cost, (3) reduced CO_2 emission by over a factor of 2 or more, and (4) capability for direct sequestration or utilization of the concentrated CO_2 from the carbon fuel cell effluent.

References

References should use ACS style. References may be inserted and numbered manually, or automatically by using the endnote/footnote function of the word processor. For manual insertion, format the references as follows:

(1) Cooper, J. F..; Cherepy, N.; Upadhye, R.; Pasternak, A.; and Steinberg, M. Direct Carbon Conversion, Report No. UCRL ID 141818. Lawrence Livermore National Laboratory, Livermore, CA, **2000**.

(2) (2) Turning Carbon Directly into Electricity, *Science and Technology Review*, **2001**, pp. 4-12, Lawrence Livermore National Laboratory, Livermore, CA.

(3) Steinberg, M; Technologies and Economics for Production of Electrochemical Fuels from Fossil Fuel Resources for use in High Efficiency Integrated Fuel Cell Combined Cycle Power Generation Plants, Consultant Report to Lawrence Livermore National Laboratory, Livermore, CA, 2001.

Table 1. Comparison of Efficiencies of Fuel Cells Using Synthetic or Refined Fuels Operating Temp. 750°C - 850°C

Fuels	Thermal Efficiency 100%ΔG/ΔH %	Fuel Utilization Factor	Voltage Efficiency	Net Efficiency
C	100.3	1.0	0.8 - 0.9	0.80 - 0.90
H_2	70.0	0.75 - 0.85	0.8	0.42 - 0.48
CH_4*	89.0	0.75 - 0.85	0.8	0.53 - 0.60

*Assumes efficient internal steam reforming reaction. Direct electrochemical reaction of methane at a catalyst surface does not occur at practical rates.

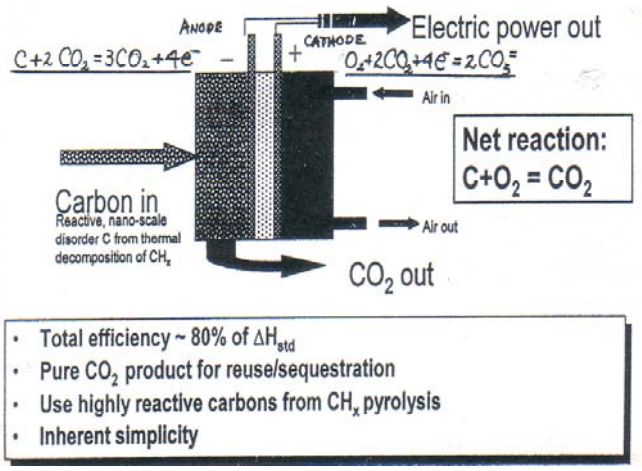

Figure 1. Direct Carbon Conversion (DCC): electric power from electrochemical reaction of C and O_2.

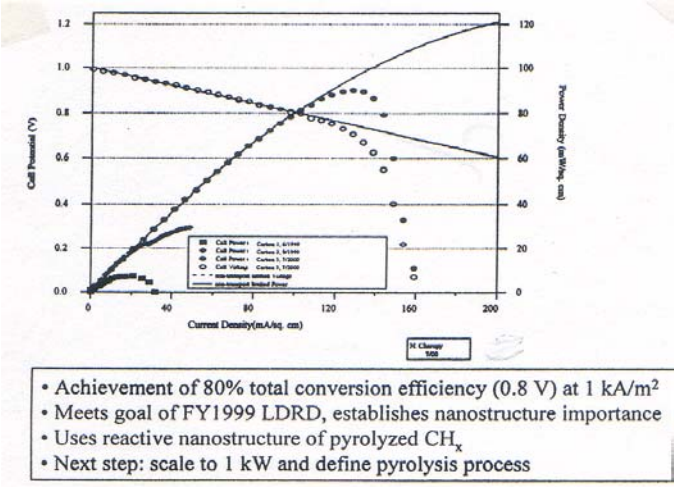

Figure 2. Carbon/air cells operate at sufficiently high power density for base-load power applications.

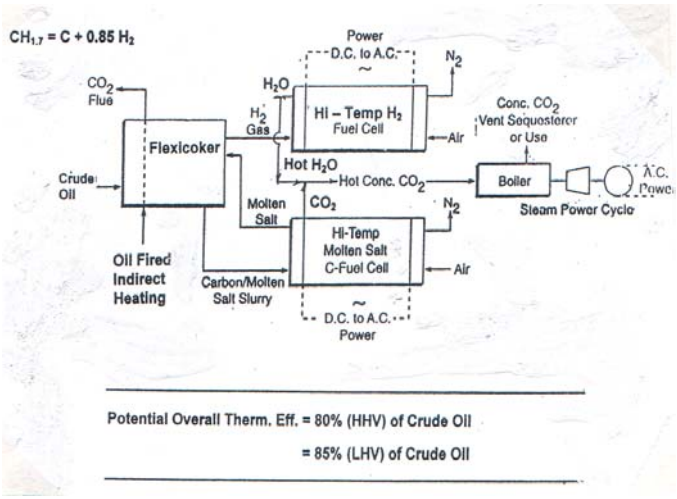

Figure 4. Crude oil fired integrated combined fuel cell power cycle hi-efficiency.

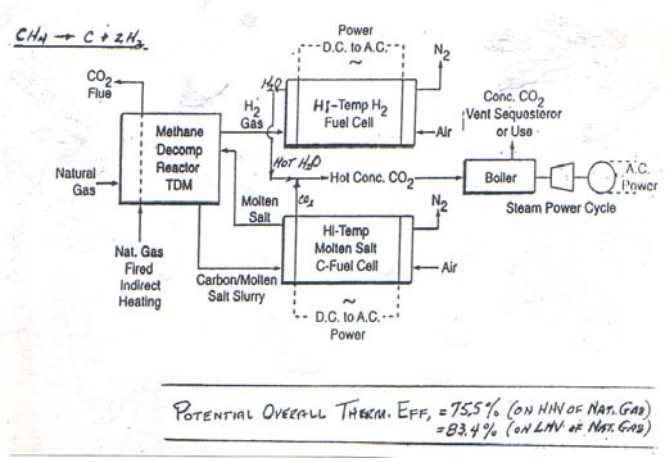

Figure 3. Natural gas combined fuel cell power cycle hi-efficiency.

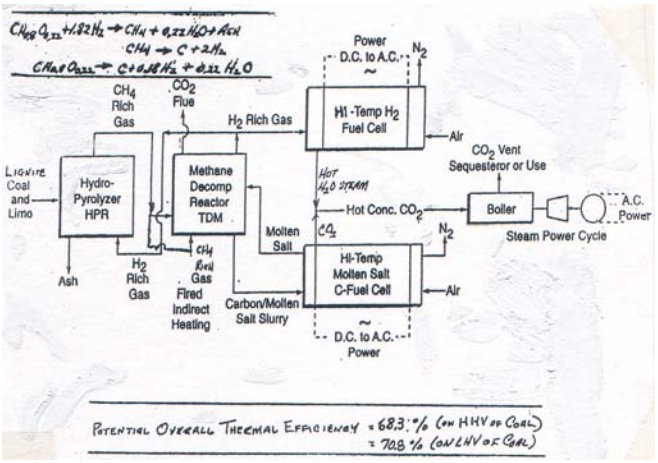

Figure 5. Coal fueled reversible hydrocarb combined fuel cell power cycle.

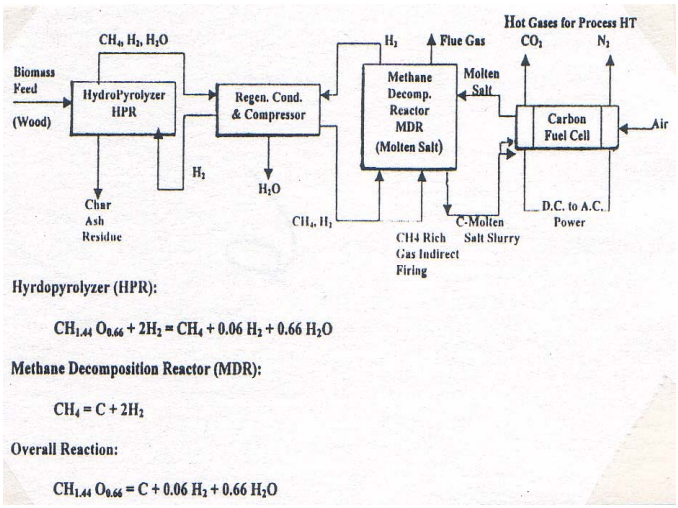

Figure 6. Biomass fueled carbon fuel cell power plant.

HIGH-PRESSURE WATER TUNNEL FACILITY FOR OCEAN CO_2 STORAGE EXPERIMENTATION

Robert P. Warzinski and Ronald J. Lynn
U.S. Department of Energy, National Energy Technology Center
P.O. Box 10940, Pittsburgh, PA 15236-0940

Anne M. Robertson and Igor V. Haljasmaa
University of Pittsburgh, Department of Mechanical Engineering
648 Benedum Hall, Pittsburgh, PA 15260

Introduction

In recent years, considerable effort has been devoted to investigating non-atmospheric storage of anthropogenic CO_2 emissions [1,2]. Deep ocean disposal (>500 m depth) is being considered as one option for long-term storage of large quantities of CO_2. The capacity of the Earth's oceans for CO_2 sequestration has the potential to exceed that of all other alternatives [2].

Such a serious action as large-scale CO_2 sequestration requires extensive and thorough investigation of all aspects of the process, including CO_2 fluid particle behavior after injection. Predicting the behavior of liquid CO_2 injected into the ocean at depths greater than 500 m is complicated by formation of crystalline CO_2 clathrate hydrate. Hydrate can form as discrete particles or as shells on CO_2 drops and significantly affects mechanical and chemical particle behavior (buoyancy, dissolution rates, etc.) [3]. Experiments in the ocean are very expensive and difficult to perform. It would be preferable to use laboratory facilities designed to simulate the deep ocean.

A previous publication [3] described the initial efforts of the National Energy Technology Laboratory (NETL) of the U.S. Department of Energy to develop experimental units intended to model direct ocean sequestration. We discussed some aspects of the development of a High-Pressure Water Tunnel Facility (HWTF) and outlined steps for design optimization. Assembly of the HWTF is now complete, and experiments with CO_2 droplets will soon be initiated. This paper describes recent design optimization efforts.

The HWTF

The water tunnel associated with the HWTF is depicted in Figure 1. It consists of a test section integrated into a closed flow loop with a centrifugal variable-speed pump and control valves for precise water circulation control; a syringe pump to generate and control high pressure in the system; and a chiller for cooling the system to deep-ocean temperatures. The pressurized components are located in a securely-isolated and structurally-reinforced room. Observations and control of all the system components are performed from a control room computer by means of programs developed using Labview software from National Instruments.

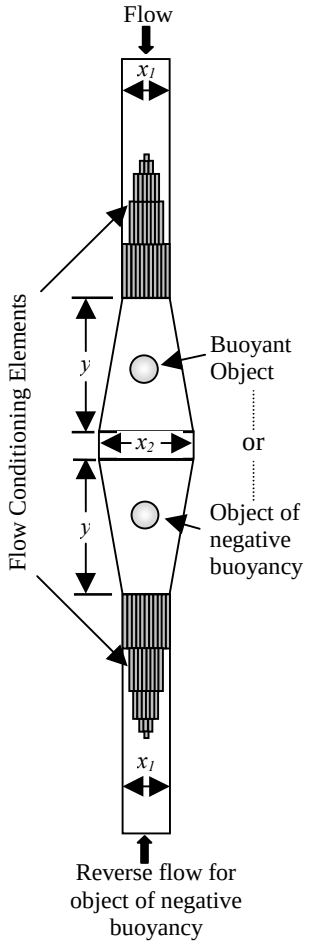

Figure 1. Water tunnel schematic.

Two conical test sections allow stabilization of either a rising or sinking fluid particle by countercurrent flow. Several ports on different levels of the test section serve for fluid/gas injection into the system. For direct observation of fluid particle behavior, as well as for automatic control of the particle motion, both conical sections have two pairs of windows. The HWTF can operate under pressures up to 350 bars and temperatures down to the freezing point of the circulating fluid.

Experiments in the HWTF will be more cost effective than direct experiments in the ocean; however, there are legitimate concerns about being able to adequately simulate fluid particle behavior in such an experimental facility. Therefore, it is important that the design and operation of the unit minimizes any unnatural chemical or physical behavior.

The parameters most easily set to real ocean conditions include water salinity and alkalinity, pressure and temperature. For salinity and alkalinity, natural or artificially constituted ocean water can be used. The pressure and temperature in the system can be varied during the experiment to simulate that experienced by a particle rising or sinking in the ocean. It is more challenging to simulate the level of dissolved CO_2. Finally, the most significant concern is the dynamic behavior of a particle in a relatively small pipe (ID=51-75mm); that can be strikingly different from its free ocean counterpart. This last issue is discussed below.

Discussion

Reference 3 describes a Low-Pressure Water Tunnel Facility (LWTF) designed and operated at NETL. The LWTF serves as a benchmark system to test fluid particle behavior for various test section designs and flow conditions. It is also used to develop and evaluate theoretical models of the system. The section below describes some experimental results on the LWTF unit and their applicability to the HWTF.

Flow conditioning elements are used to provide a desired velocity profile for lateral stabilization of a fluid particle in the test section. They are composed of a bundle of small (from 1/9 to 1/15 of pipe ID) straws of different length located in the straight pipe above and below the test section. The central part of the conditioner typically has longer straws, causing a local velocity minimum in the center of the pipe (for more details see Reference 3). An automated traversing Pitot tube system was used to determine the velocity profiles in the test section.

Figure 2 displays the development of a representative velocity profile downstream of the flow conditioner. The length of the region adjacent to the conditioner outlet where the influence of individual jets from the straws is pronounced depends on the flow rate and straw diameter. This zone of active mixing and high shear rates should be avoided by the fluid particles. For example, in the experiment depicted in Figure 2, a particle should be kept at a distance of at least 2 pipe ID's ($D = x_1$) from the conditioner. However, a problem will also arise if the particle is too far away from the conditioner outlet and the desired profile is lost. Fortunately, the development length for a single straw (order of centimeters) is much less than the development length for the whole pipe (order of a meter). Therefore, these data show that the desired velocity profile can be achieved and the high-shear region avoided.

In the process of this research, concepts on the shape of the optimal velocity profile underwent significant evolution. Early flow conditioners were designed to stabilize an air bubble. The properties

of air (negligible density compared to water) required a design with a deep, narrow well in the velocity profile at the center of the pipe. Though these conditioners managed to keep the bubble relatively stable near the pipe axis, they did not provide a good simulation of particle behavior in the oceanic environment. The narrow velocity well restricts natural lateral motion of a particle, which often occurs as a particle rises in water in geometries with negligible wall effects [4]. In addition, the high velocity gradients of the narrow velocity well, can alter flow patterns around the particle compared with flow in the open ocean. These altered flow patterns can cause unrealistic heat and mass transfer and material shaving from the particle. They may also affect hydrate formation and dissolution kinetics.

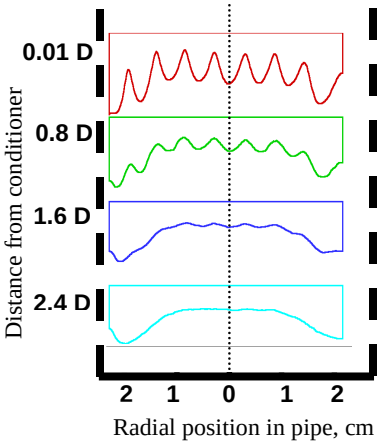

Figure 2. Velocity profile development in the LWTF.

The purpose of more recent flow conditioners was to provide a wide velocity well with relatively low-velocity gradients near the center. Such a profile would keep a particle away from the wall and at the same time allow some freedom of lateral motion. The maximum velocity gradient in the profile should also be kept as small as possible to minimize deviation from natural heat and mass transfer. Figure 3 depicts velocity profiles for 3 similar conditioner designs. They were obtained by progressive shortening (from conditioner 1 to 3) of the central section of straws. In light of the above factors, conditioner 3, with the flattest central part and lowest velocity gradient, would be the most preferable.

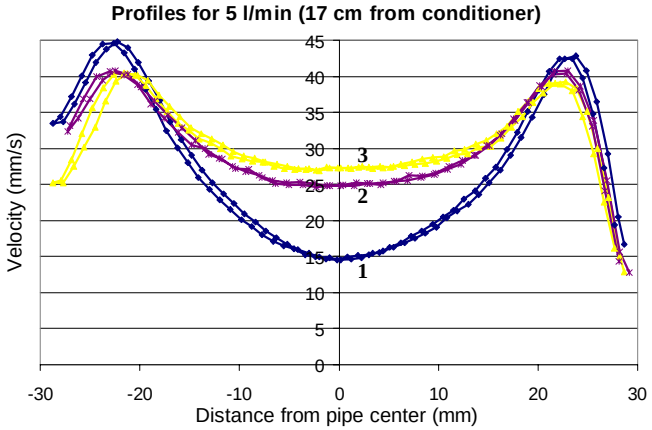

Figure 3. Effect of conditioner size on velocity profiles.

These conditioners were used to stabilize a particle of vegetable oil (Specific Gravity ≈ 0.91). Oil particles with an equivalent diameter in the range of 0.3 cm to 1 cm were successfully kept in the test section for several hours (equivalent diameter of a non-spherical particle is defined as the diameter of a spherical particle with the same volume).

Under certain assumptions, the behavior of a liquid particle in a fluid flow may be uniquely defined by two dimensionless parameters, the Eotvos and Morton numbers [3]:

$$Eo = \Delta\rho g D_e^2 / \gamma \quad \text{and} \quad Mo = \Delta\rho g \mu^4 / (\rho\gamma^3),$$

where ρ and μ – fluid density and viscosity, $\Delta\rho$ – particle-fluid density difference, γ – interfacial surface tension on particle liquid boundary, D_e – equivalent particle diameter. These two parameters for an oil particle in LWTF are relatively close to the values for a CO_2 particle at the depth of approximately 1000 m. For example, for a particle with an equivalent diameter of 4 mm, the dimensionless numbers for both cases fall into the range: $Eo \approx 0.6 - 0.75$ and $Mo \approx 0.5 - 1.5 \times 10^{-10}$. The full range of these parameters for physical systems is $Eo \approx 0.01 - 1000$ and $Mo \approx 10^{-12} - 10^{5}$, and rising velocity dependence from these parameters is rather monotonic. Hence, we expect that behavior of both particles will be very similar. Therefore, model experiments with vegetable oil in the LWTF are used to mimic the behavior of CO_2 drop in the HWTF.

For proper simulation, the size of a fluid particle must not only be significantly smaller than the pipe diameter, but also the width of the 'velocity well'. In particular:

$$D_e << D_{pipe}, \qquad (\partial u / \partial y) D_e << u_{av},$$

where u and $\partial u / \partial y$ are the axial velocity and its gradient at the position of the particle. This will help to minimize the wall effects, as well as lateral particle migration caused by velocity profile gradients. Since the lift force is proportional to some powers of particle size and velocity gradient, even low gradients can cause significant lift on relatively large particles. Based on the profile shapes from Figure 3 and noting that the pipe diameter in the stabilization area is about 6 cm, we expect that a suitable size for the particle would be about 0.5 cm (particle cross section area / pipe cross section area < 1%).

In the LWTF with the velocity profiles shown in Figure 3, we also noticed differences in the behavior of solid and liquid particles of the same volume. An oil particle with an effective diameter of about 1-1.5 cm successfully remained in the central part of the pipe, close to the location of the local velocity minimum. Solid particles of the same diameter tended to stabilize away from the pipe center.

Unfortunately, there have been no systematic experimental studies devoted to buoyant solid or liquid particle behavior in vertical pipe or channel flows. Thus, systematization of such a behavior and attempts to reveal its mechanisms are interesting and challenging theoretical and experimental studies. An additional complication is possible if a thin hydrate shell forms on a CO_2 particle. Such an encased particle is intermediate between a solid or liquid particle and its behavior will likely differ from both.

References

1. Carbon Sequestration Research and Development, U.S. Department of Energy Report, DOE/SC/FE-1, 1999, available NTIS.
2. Herzog, H.; Eliasson, B.; Kaarstad, O. *Scientific American*, Feb., 2000, 72-79.
3. Warzinski, R.P.; Lynn, R.J.; Robertson, A.M.; Haljasmaa, I.V.; *Prepr. Pap., Amer. Chem. Soc., Div. Fuel Chem.,* 2000, **45**(4), 809-813.
4. Ellingsen K.; Risso, F., *J. Fluid Mech.,* 2001, **440**, 235-268.

Hybrid Mesoporous Materials for Carbon Dioxide Separation

Seamus W Delaney, Gregory P Knowles, Alan L Chaffee

School of Chemistry, PO Box 23, Monash University, Victoria 3800, Australia

Introduction

Gas separation processes are becoming increasingly important in a world changing the way it looks at energy production and its emissions. Increased energy demand has led to an increase of fossil fuel burning, releasing large amounts of gases such as CO_2 into the atmosphere. This is the major cause of several environmental phenomena, including the 'greenhouse effect'[1].

Methods for long-term sequestration of CO_2 have been proposed. Long term storage in used oil wells and deep ocean waters is being considered as an alternative to releasing CO_2 into the atmosphere.[2] There are also proposals to re-use CO_2 produced from one process in another process such as dry reforming of natural gas.[3] However, such applications would require CO_2 to be 'captured' in concentrated form.

One common method for CO_2 separation from mixed gas streams is by absorption in aqueous solutions of alkanolamines[4], for example monoethanolamine (MEA) or diethanolamine (DEA). It is widely accepted that CO_2 becomes absorbed via the formation of both carbamates and bicarbonates.

However, some of the problems associated with this absorption approach include: (a) the corrosive nature of the scrubbing solutions leading to the build up of corrosion by products; (b) vapourisation losses due to relatively high volatility of alkanolamines; and (c) energy intensive regeneration of the absorbent solutions, due to high heats of dissolution[4].

A recent report by Leal et al[5,6] indicated that CO_2 reversibly adsorbs on silica gel (Davidson grade 62) modified by the addition of 3-aminopropyl groups bonded to the surface. In this solid phase analogue of the liquid phase process the amine functional groups behave as active sites for CO_2 chemisorption. Adsorption capacities of approximately 10 STP cm3 dry CO_2 per gram of adsorbent (or 1.8% by weight) were achieved at room temperature and the CO_2 could be desorbed at temperatures below 100ºC. The mechanism of adsorption appears to involve the formation of surface bound carbamates (see Figure 1). In dry CO_2, this limits the adsorption capacity to 1 mole of CO_2 for every 2 moles of surface bound amino groups. In the presence of water, however, the capacity for CO_2 adsorption doubles since the possibility for proton transfer allows the carbon dioxide adsorption capacity to be doubled by the transformation of surface bound carbamate into bicarbonate.

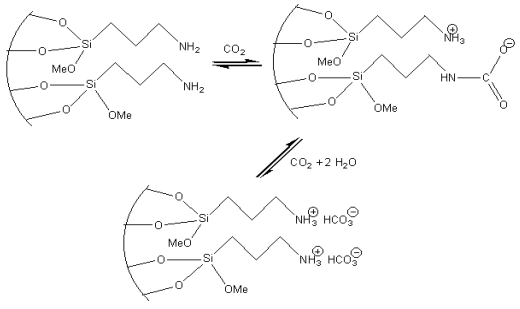

Figure 1. Scheme of the surface reaction of carbon dioxide with modified HMS materials

The silica gel used by Leal et al has a substantial surface area (380 m^2/g), but we reasoned that much improved CO_2 adsorption capacities could be achieved with (a) the use of higher surface area support materials and/or (b) the use of surface modifying groups that contain more amine functional groups.

In this study, solid phase hexagonal mesoporous silicas (HMS) of known porosity (pore diameter) were modified using aminopropyl-trimethoxysilane and related compounds to provide very high surface area materials with varied concentrations of surface bound amine and hydroxyl functional groups (see Figures 2 and 3).

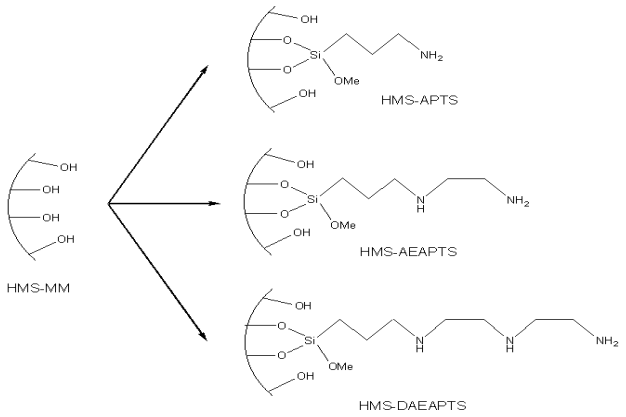

Figure 2. Modified HMS materials with increasing amine content employed in the present study.

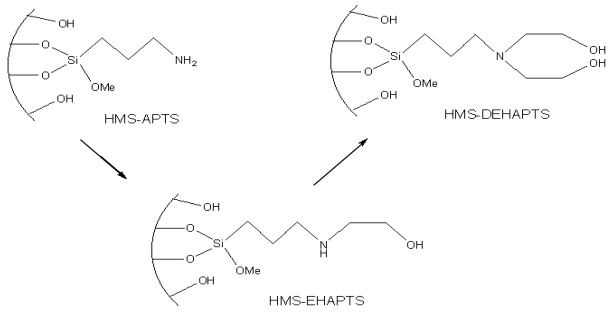

Figure 3. Modified HMS materials with increasing hydroxyl group content employed in the present study.

Experimental

Preparation of HMS. HMS materials were prepared by the neutral template method[7] using dodecylamine (DDA). The reaction involved the addition of tetraethyl-orthosilicate to the amine template in a water and ethanol solution, which was left to age at ambient temperature for 24 hours. The solvent was then removed from the crude "template filled" silica formed via evaporation under gentle air-flow at ambient temperature. The template was subsequently extracted from the crude silica into hot ethanol. The remaining solids were then collected over filter, washed with hot EtOH and finally dried under vacuum at 150ºC to form an HMS product with a total pore volume of 0.53 mL/g.

Preparation of Hybrid HMS. Five modified HMS materials were prepared as illustrated by Figures 2 and 3. Aminopropyl-trimethoxysilane (APTS), aminoethyl-aminopropyl-trimethoxysilane (AEAPTS) and N-[3-(Trimethoxysilyl)propyl)diethylenetriamine (DAEAPTS) modified HMS were prepared in toluene solution (room temperature, 2h) using a published alkylsilylation procedure[8].

Ethylhydroxyl-aminopropyl-trimethoxysilane (EHAPTS) and diethylhydroxyl-aminopropyl-trimethoxysilane (DEHAPTS) modified HMS were prepared by N-alkylation of the APTS HMS using bromoethanol in ethanol solution (room temperature, 2h). The modified silica was then filtered and dried under vacuum at 150ºC.

Characterization of Materials. N_2 adsorption/desorption experiments were conducted at –196°C using a Micromeritics ASAP 2010 instrument. BET surface areas (SA) were determined from the adsorption isotherms over the partial pressure range 0.05 - 0.22. BJH pore size distributions were determined from the desorption isotherms. Mass % elemental N compositions were determined by CMAS P/L, Belmont Vic.

Carbon Dioxide Adsorption. CO_2 adsorption and desorption experiments were conducted on a Setaram Thermogravimetric analyzer (TGA). In a typical experiment, the adsorbent sample was heated to 150ºC (held 40 min) under flowing Ar (60 mL/min) to remove residual water. The sample was cooled to 20ºC before the gas flow was switched to CO_2. CO_2 adsorption capacities were determined from the weight increase observed after 75 minutes CO_2 exposure. After 75 minutes, the gas flow was reverted to Ar so as to monitor the CO_2 desorption. Approximately 90% of the adsorbed CO_2 was desorbed immediately. The remaining CO_2 was removed by heating the adsorbent to 65ºC. High purity CO_2 (99.95%) was used with a manufacturer specified moisture content of <100 ppm. In some experiments, a molecular sieve trap was placed on the feed gas line to ensure the complete exclusion of water from the gas feed stream.

Results and Discussion

Table 1 reports the properties determined from nitrogen isotherm characterization of the HMS materials prepared in this study. It can be seen that the unmodified HMS material has an average pore diameter and surface area of 24.1Å and 1425m^2/g, respectively. Both these figures are substantially higher than the corresponding figures (14.0Å and 340m^2/g, respectively) reported for silica gel described in references 5 and 6. In addition, it can also be seen that the pore diameters and surface areas are both reduced as the length of the modifier used or the extent of substitution at the N atom increases.

Table 1. N_2 Isotherm Results for Modified HMS Materials

Sample	BET SA (± 10m^2/g)	BJH Av. Pore Dia. (± 0.2Å)
HMS	1425	24.1
HMS-APTS	1268	20.1
HMS-AEAPTS	1047	19.6
HMS-DAEAPTS	869	18.6
HMS-EHAPTS	1186	19.3
HMS-DEHAPTS	1108	19.0

Table 2 reports the carbon dioxide adsorption capacities that were observed for these materials. The unmodified HMS material itself has the capacity to adsorb 2.0% CO_2 by mass. This is already higher than the 1.8% reported for APTS modified silica gel. However, the CO_2 adsorption capacity is substantially further improved through modification with N-containing tethers. HMS-APTS adsorbs 3.8% CO_2 by weight and the incorporation of more N atoms and/or hydroxyl groups into the tether increased CO_2 adsorption still further. In all cases the, adsorbed CO_2 was completely desorbed at temperatures below 100ºC.

It is interesting to note that for HMS-APTS, HMS-AEAPTS and HMS-DEAPTS the ratio of carbon dioxide molecules adsorbed per available N atom is approximately 0.5. This is consistent with the carbamate formation mechanism postulated for silica gel (Figure 1).

Table 2. CO_2 Adsorption Results for Modified HMS Materials

Sample	Weight % N incorporated in sample (± 0.1)	CO_2 adsorption capacity Weight % (±0.1)	mole CO_2 adsorbed / mole N incorporated
HMS	0	2.0	-
HMS-APTS	2.3	3.8	0.54
HMS-AEAPTS	5.1	7.5	0.46
HMS-DAEAPTS	6.4	8.2	0.41
HMS-EHAPTS	2.1	5.0	0.74
HMS-DEHAPTS	1.5	5.1	0.98

With HMS-DEHAPTS the ratio is approximately 1. Tertiary amines cannot form stable carbamates so that another mechanism must be invoked to explain the substantial enhancement of adsorption capacity (and changed stoichiometry) that is observed in the presence of hydroxyl groups. Currently it is thought that the hydroxyl groups may serve to stabilise carbamate type zwitterions in a manner depicted by Figure 3. The CO_2 adsorption behaviour of HMS-EHAPTS can then be understood as a mixture of the two mechanisms (some carbamate formation and some zwitterion stabilization).

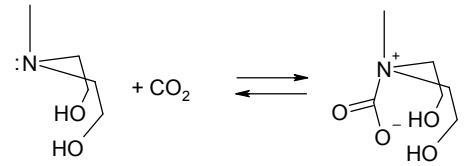

Figure 3. Proposed scheme of the surface reaction of carbon dioxide with HMS-DEHAPTS.

Conclusions

Modified HMS materials have been shown to reversibly adsorb substantially more CO_2 than previously observed for modified silica gel. There is substantial scope to further tailor the surface of HMS materials to achieve higher adsorption capacities and more selective adsorption behaviour. On a stoichiometric basis the same adsorption capacities are observed as for the liquid phase absorption process. Thus the development of a solid phase adsorption analogue of the current liquid phase absorption process may offer technical benefits.

Acknowledgement. The authors acknowledge support from the Monash University Research Fund.

References

(1) Socolow, R. (Ed.). R & D paper, C*arbon Sequestration: State of the Science;* US DoE - Office of Science (Fossil Energy): Washington, DC, 1999; pp. 21-28.
(2) Adams, E.; Golomb, D.; Zhang, X.; Herzog, H. *Direct ocean disposal of carbon dioxide*; Washington, DC, 1995; pp. 153-164.
(3) Herzog, H.; Drake, E.; Tester, J.; Rosenthal, R. A*ssessment for the capture, utilisation and disposal of carbon dioxide*; US DoE - Office of Science (Fossil Energy): Washington, DC, 1993; 13.
(4) Kohl, A.; Nielsen, R. *Gas Purification*, Gulf Publishing Company: Houston, Texas, 1997; pp.41-52.
(5) Leal, O.; et al. *Inorganica Chimica Acta.***1995**, *240*, pp. 183-189.
(6) Leal, O.; et al. US Patent, **1991**, no. 5,087,597.
(7) Beck, J. S.; et al. *J. Am. Chem. Soc.* **1992**, *114*, pp. 10834-10843.
(8) Vrancken, K.; et al. *J. Coll. Interfac. Sci* **1995**, *170*, pp. 71-77.

Molecular Basis for Carbon Dioxide Sequestration in Coal

Thomas J. Dick, Orlando Acevedo, Pranav Dalal, Jeffry D. Madura, Jeffrey D. Evanseck, and Jonathan P. Mathews[#]

Center of Computational Sciences, and Department of Chemistry and Biochemistry, Duquesne University, 600 Forbes Avenue, Pittsburgh, PA 15226;
The Energy Institute & Department of Energy & Go-Environmental Engineering, 151 Hosler Building, The Pennsylvania State University, University Park, PA 16802

Introduction

Sequestration of CO_2 within coal seams that are either too deep, thin, or uneconomic has been suggested to mitigate climate change. Additionally, if there is methane present within the coal it can be replaced with the carbon dioxide, apparently at a 2:1 ratio (1) thus releasing CH_4 to help offset the sequestration cost. We have utilized computational molecular modeling to investigate the forces involved between bituminous coal structure (or idealized pores) and the molecular species CH_4 and CO_2. The molecular computations and simulations provide useful information on accessible pore volumes, energy of interactions between host and guest molecules, self-diffusion coefficients, identification of likely sorption sites, impact of carbon dioxide sorption/methane exchange upon the coal matrix (expansion/contraction), and competitive adsorption isotherms.

Experimental

Density functional theory, second-order Moller-Plesset theory, and classical molecular dynamics were utilized to investigate three chemical models of coal. In order of increasing model sophistication, small molecules (CH_4, CO_2, and N_2) were complexed with (a) anthracene, (b) nanotube(s), and (c) model of bituminous coal structure. Our goal is to uncover the fundamental physical interactions between small molecules and simple aromatic structures, and use the computed information to enhance the sequestration of CO_2 in more complex coal structures.

Anthracene Model. All density functional theory calculations were carried out with the Gaussian 98 program (2), using a 16-node SP IBM RS/6000 super computer. The Becke three parameter exchange functional and the nonlocal correlation functional of Lee, Yang, and Parr (B3LYP) with 6-31G(d) basis set was employed. All energy optimizations and frequency analyses were performed using the B3LYP/6-31G(d) level of theory, which has been shown to produce realistic structures and energies for weak nonbonding interactions between aromatics and small organic molecules. Vibrational frequency calculations at the same level of theory were used to confirm all stationary points as either minima or transition structures, and provide thermodynamic and zero-point energy corrections. The energy profile for CH_4, CO_2, and N_2 traversing across anthracene, see Figure 1, are investigated to determine the structure and energy of interaction as the small molecules passes over the aromatic structure.

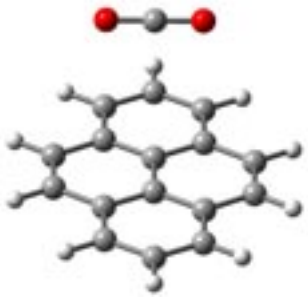

Figure 1. Oblique View of CO_2 Interacting with Anthracene.

Nanotube Model. Insight II was used to plot the energy profile of the gases within idealized pores, here treated as buckeytubes and buckyballs. In our first case, a nanotube was constructed, as shown in Figure 2. Dummy atoms set along the centerline of the "pore" was used to define a pathway for the molecules. A strong harmonic "pushed" the guest molecule along the defined pathway and the structure allowed to minimize. To save computational expense the "pore" was rigid and did not relax or strain with the passage of the molecule. Step size along the centerline was 0.2 Å. The dummy atoms were placed several rings within the tube to reduce "end effects". The energy of interaction between the host and guess molecule were followed. Similar techniques have been used in Zeolite simulations (3) and are well discussed there.

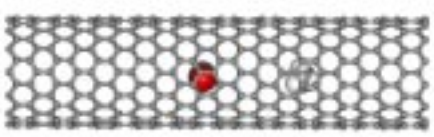

Figure 2. 3D Representation of a nanotube with CH_4 and CO_2 inserted in its cavity.

Classical molecular dynamics calculations were performed to compute the potential of mean force of each solute through the nanotube model. Self-diffusion coefficients were also computed using molecular dynamics simulations.

Bituminous Coal Model. Recent experimental and computational advances have the potential to produce a first-time reasonable constitutional model (chemical and physical structure) and enable its use. First, structural diversity may be incorporated through the combination of high-resolution transmission electron microscopy (HRTEM) and laser desorption mass spectroscopy, which has not been previously included into a three-dimensional structural model of coal (4). Secondly, methodological advances in molecular simulations that have been successfully applied to biomolecular systems and new engineering materials coupled with available high capacity and high speed parallel super computers make the modeling of CO_2 sequestration by coal realistic and practical. A relatively simplistic three-dimensional model of bituminous coal structure (5) is given in Figure 3.

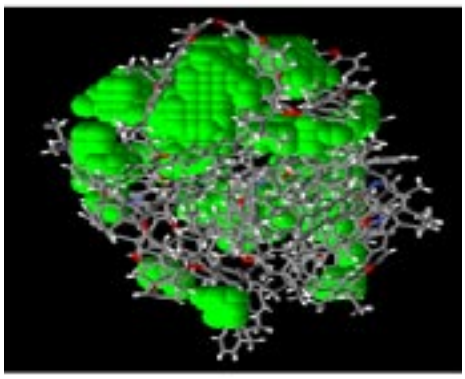

Figure 3. Porosity (green spheres) of a Bituminous Vitrinite Coal Model

The CHARMM (6,7) force-field was used in our simulation work (many more will be evaluated). Constant pressure molecular dynamics have been carried out using periodic boundary conditions. Physical aspects such as porosity will be compared to experimental values to ensure a reasonable representation of our proposed large-scale coal model simulation (> 50,000 atoms). The time-scale used will be consistent with the diffusion times of the slowest diffusion rates.

Results & Discussion

Figure 4 shows the relative size and shape of the three gasses: nitrogen, methane, and carbon dioxide. The sizes appear similar to the naked eye although significant differences in size are present (when in appropriately sized pores), although methane is bulkier. The quadrupole and octapole from the higher-level quantum mechanical computations are also used to better understand the sorption of the small molecules to aromatic surfaces.

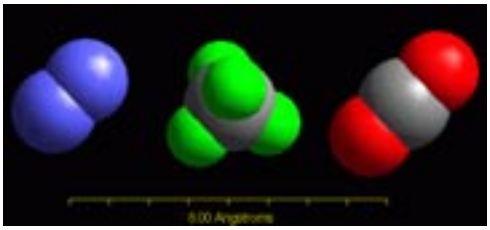

Figure 4. Relative Size and Shape of N_2, CH_4 and CO_2

To test the molecular interactions, a low level of molecular modeling was first utilized. The results of this basic simulation are shown in Figure 5. Nitrogen as expected had the "easiest" transition through the "pore". The shape of the molecule permitted the long axis to lie perpendicular to the "pore" axis and low energetic strain indicated only slight conformational changes where required. Methane being a bulkier molecule has to undergo conformational changes to "squeeze" through the pore. An oblique view of both CO_2 and CH_4 inside of the nanotube is given in Figure 6. Greater peaks and valleys in the plot (Figure 5) indicate conformational changes to accommodate the passage. These conformational changes can be treated as an apparent activation energy. This low apparent activation energy indicates the molecule will pass though the pore with little retention. Carbon dioxide however has a very different profile and a much higher apparent activation energy to the passage within the pore. Several local energy minima and global energy minima are present. These are sites where the interaction energy between the host and guest molecule would require significant conformational rearrangement to proceed through the pore, possibly becoming "trapped" within the pore.

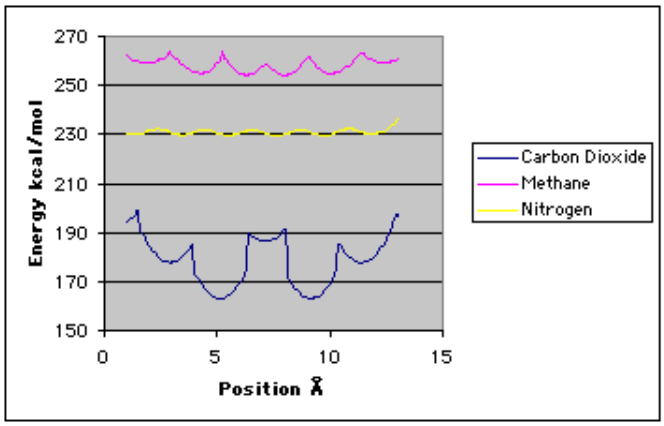

Figure 5. Energy Profile of CO_2, CH_4 and N_2 within a Nanotube

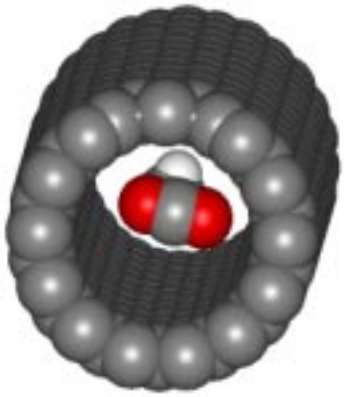

Figure 6. CPK representation of CO_2 (front) and CH_4 (back) inside the nanotube.

Conclusions

We aim to use accurately computed atomic-level structural and dynamical information to aid in the creation of technology for optimal geological sequestration of CO_2. Our strategy is to generate a realistic and testable three-dimensional state-of-the-art molecular model of Pocahontas No. 3 coal by incorporating new structural diversity information based upon HRTEM and laser desorption data (rather than average values), while maintaining traditional analytical information (i.e., H/C aromaticity) and physical parameters (i.e., density and pore volume). Large-scale molecular dynamics simulations (> 50,000 atoms) will be carried out on this model to follow its structural changes during addition of CO_2 and removal of CH_4. The simulation work will also be used to determine the differences in sorption characteristics and diffusion rates between CO_2, H_2O, N_2 and CH_4. This significance of the proposal is that new opportunities in the optimization and gaseous management necessary for low-cost forms of CO_2 sequestration will result from this novel procedure.

Acknowledgement. The authors thank support from the University Coal Research Program at American Universities for funding for this research.

References

1. Gentzis, T., *International Journal of Coal Geology*, 2000, **43**, (1-4), 287.
2. Frisch MJ, Trucks GW, Schlegel HB, Scuseria GE, Robb MA, Cheeseman JR, Zakrzewski VG, Montgomery JA Jr., Stratmann RE, Burant JC, Dapprich S, Millam JM, Daniels AD, Kudin KN, Strain MC, Farkas O, Tomasi J, Barone V, Cossi M, Cammi R, Mennucci B, Pomelli C, Adamo C, Clifford S, Ochterski J, Petersson GA, Ayala PY, Cui Q, Morokuma K, Malick DK, Rabuck AD, Raghavachari K, Foresman JB, Cioslowski J, Ortiz JV, Stefanov BB, Liu G, Liashenko A, Piskorz P, Komaromi I, Gomperts R, Martin RL, Fox DJ, Keith T, Al-Laham MA, Peng CY, Nanayakkara A, Gonzalez C, Challacombe M, Gill PMW, Johnson B, Chen W, Wong MW, Andres JL, Gonzalez C, Head-Gordon M, Replogle ES, Pople JA. Gaussian, Inc., Pittsburgh PA, 1998; *Gaussian 98*, Revision A.5.
3. Horsley, J. A., Fellmann, J. D., Derouane, E. G. and Freeman, C. M., *J. of Catalysis*, 1994, **147**, 231.
4. Mathews, J. P., Jones, A. D., Pappano, P. J., Hurt, R. and Schobert, H. H., New insights into coal structure from the combination of HRTEM and laser desorption ionization mass spectrometry, 11th Int. Conf. on Coal Science, 2001, San Fransico, CA
5. Mathews, J. P., Hatcher, P. G. and Scaroni, A. W., Proposed Model Structures for Upper Freeport and Lewiston-Stockton Vitrinites, Energy & Fuels, 2001, 15, (4).
6. MacKerell, A. D Jr.; Bashford, D.; Bellott, M.; Dunbrack, R. L.; Evanseck, J. D.; Field, M. J.; Gao, J.; Guo, H.; Ha, S.; Joseph, D.; Kuchnir, L.; Kuczera, K.; Lau, F. T. K.; Mattos, C.; Michnick, S.; Ngo, T.; Nguyen, D. T.; Prodhom, B.; Reiher, W. E.; Roux, B.; Schlenkrich, M.; Smith, J.; Stote, R.; Straub, J.; Watanabe, M.; Wiorkiewicz–Kuczera, J.; Yin, D.; Karplus, M. *J. Phys. Chem. B* **1998**, *102*, 3586.
7. B. R. Brooks, R. E. Bruccoleri, B. D. Olafson, D. J. States, S. Swaminathan and M. Karplus, *J. Comput. Chem.*, 1983, **4**, 187-217.

NETWORK MODELING OF BRINEFIELD CO_2 SEQUESTRATION: DISPLACEMENT EFFICIENCIES AND FUNDAMENTAL LIMITATIONS ON CO_2 STORAGE VOLUMES

M. Ferer, Grant S. Bromhal, Duane H. Smith

National Energy Technology Laboratory, 3610 Collins Ferry Rd., Morgantown, WV 26505-0880, duane.smith@netl.doe.gov, W: 304-285-4069, F: 304-285-4403

The sequestration of liquid carbon dioxide in deep brine-saturated formations has been cited as an important potential component in an overall carbon dioxide sequestration strategy. Brinefield sequestration of CO_2 is a commercially-proven technology; however, the effective saturation of carbon dioxide in brine-saturated formations is very low, on the order of a percent of available void space. It is known that fluid viscosity, fluid density, and interfacial tension are significant factors in determining the efficiency of displacement in two-phase fluid flow.

We have developed a pore-level numerical model of the immiscible injection of one fluid (CO_2) into a porous medium saturated with another fluid (brine). The model incorporates a distribution of throat radii, fluid viscosities, and fluid densities to mechanistically represent the flow. This model has previously been used to study the relationship between saturation and important dimensionless numbers, such as the Bond number (ratio of gravitational to capillary forces) and the capillary number (ratio of viscous to capillary forces). The model is now being used to calculate the displacement efficiency for a variety of capillary and Bond numbers.

I. Introduction

Flow in porous media is a subject of scientific and engineering interest for a number of reasons. Flow in porous media has long been modeled as a compact (i.e., Euclidean) process whereby the interface advances linearly with the total amount of the fluid as predicted by a Darcy's law treatment using saturation-dependent relative permeability.[1]-[5] In the last fifteen years, it has been appreciated that flow in porous media is fractal in certain well-defined limits.[6]-[9] The flow is known to be described by self-similar diffusion-limited-aggregation (DLA) fractals in the limit of zero viscosity ratio, $M = \mu_I / \mu_D = 0$. [6]-[8],[10]-[12] The flow is known to be described by self-similar invasion percolation (IP) fractals in the limit of zero capillary number (see Eq. 6a), where viscous drag forces (viscosity of the displaced fluid times average fluid velocity) are zero, while the capillary forces (proportional to interfacial tension, times cosine of the contact angle) are finite.

Recently, we have shown that our model produces results which agree with both DLA (large viscosity ratio limit) and with IP with trapping (IPwt) (small capillary number limit).[13] Having demonstrated the validity of our model in these two very different limits, with the physicality of the model and the excellent consistency with fluid conservation, we are confident in extending our study to the physically relevant intermediate regime, where the limiting models (DLA and IPwt) are not valid.

II. Description of the Model

The pore-level model is intended to realistically incorporate both the capillary pressure that tends to block the invasion of narrow throats and the viscous pressure drop in a flowing fluid. The two-dimensional model porous medium is a diamond lattice, which consists of pore bodies of volume ℓ^3 at the lattice sites and throats connecting the pore bodies, which are of length ℓ and have a randomly chosen cylindrical cross-sectional area between 0 and ℓ^2. Compared to several models reported in the recent literature, we believe that our model should be both more general and more flexible, in part because both the throats and the pore bodies have finite volume in comparison first with refs. [6] and [14], where the throats contain zero volume of fluid, and secondly with refs. [15]-[17], where the pore bodies have zero volume. Furthermore, in our model, the volumes of both the pore bodies and throats can be set as desired. In this sense the work of Periera is closer to our model but focuses on three-phase flows at constant pressure.[18] Of course all of these models include the essential features of random capillary pressures blocking the narrowest throats and a random conductivity depending on a given viscosity ratio.

Capillary pressure determines the pressure drop needed to move a meniscus through a throat. The radius of curvature, R, of the meniscus is fixed by contact angle, θ, and the radius of the pore throat, r, so that the pressure drop across the meniscus is fixed at the capillary pressure,

$$P_{cap} = \frac{2\sigma \cos\theta}{r}, \qquad (1)$$

where σ is the interfacial tension. Following refs. [15]-[17], we modify Eq. (1) to remedy problems arising from blockages at throat entries, giving

$$P_{cap} = \frac{2\sigma \cos\theta}{r} \sin(\pi x), \qquad (2)$$

where $x\ell$ is the distance along the throat from 0 to ℓ. This sine dependence solves problems encountered in adjusting throat blockages and in maintaining a constant velocity condition and can be assumed to result from variations in contact angle.

The pressure difference due to buoyancy across a throat and its connecting pores also is calculated for each throat. The invading fluid is assumed to be a ball in the center of the spherical pore, while the defending (wetting) fluid surrounds it and stays next to the pore wall, so the pressure gradient along the pore is

$$P_G = \rho_{nw} g \left(\frac{3a}{4\pi}\right)^{1/3} \sin\psi + \rho_w g \left[\left(\frac{3}{4\pi}\right)^{1/3} - \left(\frac{3a}{4\pi}\right)^{1/3}\right] \sin\psi, \qquad (3)$$

where ρ_{nw} and ρ_w are the non-wetting and wetting fluid densities, respectively, g is the acceleration due to gravity, ψ is the angle that the throat makes with respect to the horizontal, and a is the volume fraction of invading fluid in the pore. Thus (see Fig. 1) the flow velocity is given by the throat conductance times the total pressure drop across the throat:

$$q = g_{throat} (P_{nw} - P_w - P_{cap} + P_G), \qquad (4a)$$

where g_{throat} is the conductance of a throat from Poiseuille's law, and P_{nw} and P_w are the pressures of the non-wetting and wetting fluids in their respective pores. In the model, the transmissibility (conductance) of the throat is given by

$$g_{throat} = g^* \frac{\left(A_{throat}^2 / \ell^4\right)}{\ell\left[x + (1-x)M\right]}, \qquad (4b)$$

where A_{throat} is the throat cross-sectional area, x is the fraction of the throat of length ℓ which is filled with defending fluid, and M is the ratio of the non-wetting, invading fluid's viscosity to that of the wetting, defending fluid, $M = \mu_{nw}/\mu_w$.

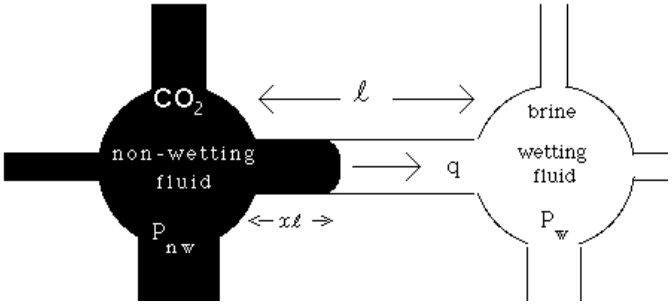

Figure 1 shows the CO_2 displacing the brine with volume flow velocity $q_{throat} = g_{throat}(P_{nw} - P_w - P_{cap})$. Of course, if $P_{nw} - P_w < P_{cap}$, the CO_2 retreats and the brine re-occupies the throat.

The quantity, g^*, carries all the dimensionality of g_{throat}, $g^* = \ell^3/(8B\,\mu w)$. From Eq. (4a), the non-wetting fluid advances if the pressure difference between the pore filled with CO_2 (non-wetting fluid) and the pore filled with brine exceeds the capillary pressure. Otherwise the CO_2 will retreat.

The pressures in the pore bodies cane be determined from the volume conservation of the incompressible fluid, dictates that the net volume flow q out of any pore body must be zero. Let us consider use of the above rules for the situation in Fig 2. In Fig. 2, the flow velocities, as directed out of the (i,j) pore body through the throats are

$$\begin{aligned} q_{i-2,j-1} &= g_{i-2,j-1}\left(P_{i,j} - P_{i-2,j-2}\right) \\ q_{i,j+1} &= g_{i,j+1}\left(P_{i,j} - P_{i+2,j+2} - P_{cap,i,j+1}\right) \\ q_{i-1,j} &= g_{i-1,j}\left(P_{i,j} - P_{i-2,j} - P_{cap,i-1,j}\right) \\ q_{i+1,j} &= g_{i+1,j}\left(P_{i,j} - P_{i+2,j} - P_{cap,i+1,j}\right). \end{aligned} \qquad (5)$$

Once the location of the interface is known, the numerical value of the capillary pressure in each throat is determined. Then the program iterates (Eq. 5), determining the pressure field until pressure balance is achieved. In one of the typical sets of five runs presented in this paper, after an average of 77,000 time steps there was an average difference of less than 1% between the total volume of fluid injected into the medium and the total volume of fluid expelled from the medium.

To maintain a constant volume flow q_o, the flow velocity was determined for two estimates of the inlet pressure. The linear relationship between flow velocity and inlet pressure (Eq. 4) predicts an inlet pressure, P_o, producing the desired volume flow, q_o.[17] With a good choice of initial estimates, this procedure is very accurate, with error less than of 0.007%.

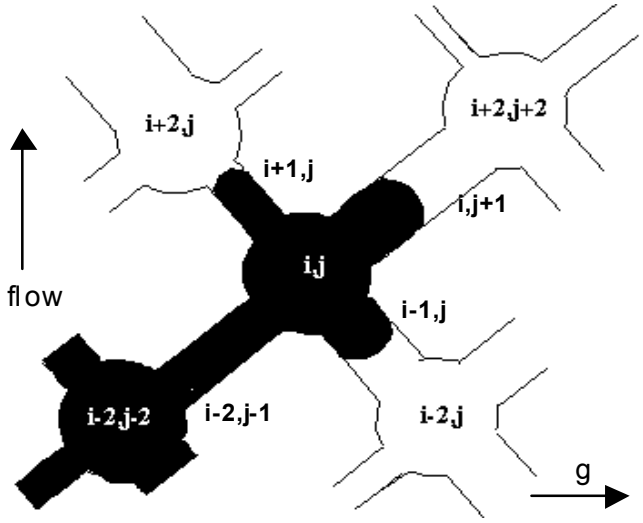

Figure 2 shows a possible occupation of adjacent pore-bodies. For this occupation, the flow velocities are given by Eq. (4) and the pressure in the (i,j) pore body can be calculated from Eq. (5).

Once the pressure field has been determined, the flow rules determine the interface advance through a time interval Δt. A throat is on the interface, if the pore body at one end contains some wetting fluid (it may be filled with wetting fluid) and if the pore body at the other end is fully invaded by non-wetting fluid (or was fully invaded and is not yet fully re-invaded by wetting fluid due to backflow). As discussed earlier, a time interval, Δt, needs to be chosen which is small enough that spurious local oscillations in the flow are avoided but not so small that the program run-time is unnecessarily long. For the cases discussed here, with large surface tension, the following prescription seems adequate. For all interfacial throats where the non-wetting fluid has yet to reach the midpoint of that throat, so that the capillary pressure is still increasing, the time interval is chosen so that the non-wetting fluid advances no more than 3.5% into any such throat. For all throats where the non-wetting fluid has advanced past the midpoint, so that the capillary pressure is decreasing, the time step allows the interface to advance no further than 33% into any such throat.

Flow increases the amount of CO_2 within the pore throat (Fig. 3a) or through the pore throat into the pore body (Fig. 3b). Similarly, backflow causes the interface to retreat within the pore throat or through the pore throat into the pore body. If either type of fluid over-fills a pore body, the outflow throats share the excess.

We have attempted to make the flow-rules as non-restrictive and physical as possible: i) all parts of the porous medium have a volume which can be occupied by either type of fluid; ii) locally, back-flow and forward flow are allowed if ordained by the local pressure drops; iii) complications, such as over-filled pore bodies, are treated as physically as possible; iv) unphysical aspects, such as isolated 'blobs' of wetting fluids residing in pore-bodies, are tracked and have been found to be insignificant; and v) most importantly, the flow rules accurately account for all of the non-wetting fluid injected into the porous medium.

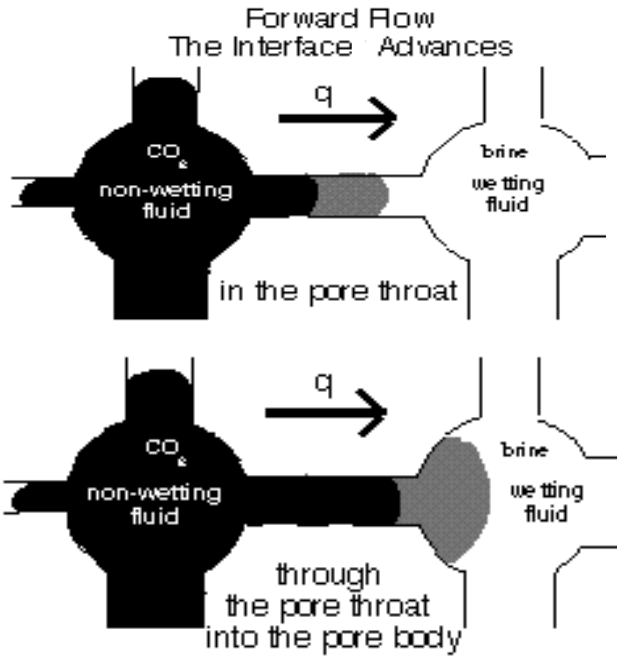

Figure 3. The CO_2 can advance in a throat (upper fig., 3a) or through a throat into the pore body (lower fig., 3b).

III. Simulations and Results

The model was run for 16 simulations of sizes 60x30 pore networks for a range of capillary and Bond numbers:

$$Ca = \nu\mu_w / \sigma\cos\theta, \qquad (6a)$$

$$B = \Delta\rho g d L / \sigma, \qquad (6b)$$

where v is the average velocity of the total fluid system, σ is the interfacial tension between the two fluids, $\Delta\rho = \rho_{nw} - \rho_w$, L is number of pores in the direction of flow, and d is the average throat diameter. The capillary number, Ca, is a ratio of viscous to capillary forces, and the Bond number, B, is the ratio of buoyancy to capillary forces. These dimensionless numbers have been shown to be related to residual saturation.[20],[21] All simulations use a viscosity ratio, M, of 0.05 to correspond to carbon dioxide infiltrating brine.

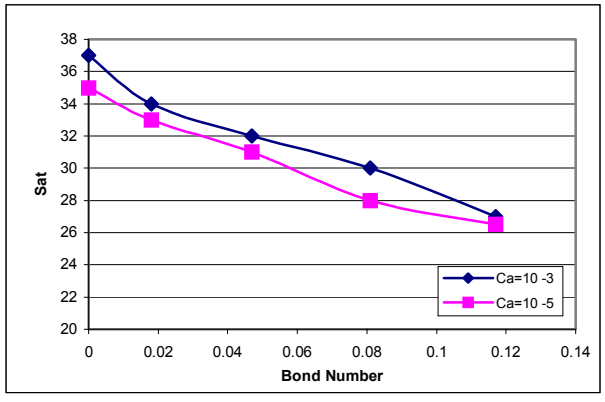

Figure 4. Plot of breakthrough saturation vs. Bond number on a 60x30 network at M=0.05.

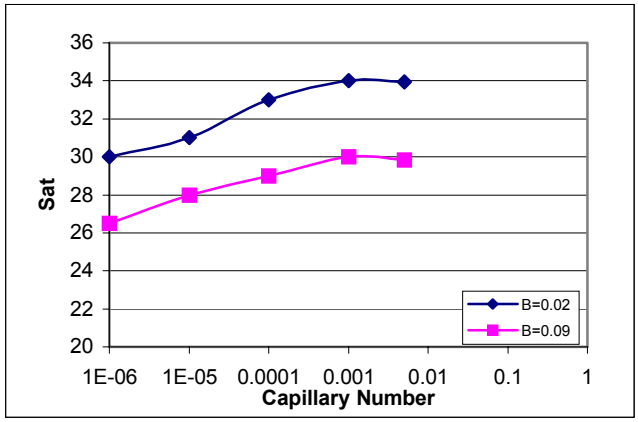

Figure 5. Breakthrough saturation vs. capillary number on a 60x30 network at M=0.05.

The results from these simulations are presented in Figures 4 and 5. These initial results show relationships between saturation and Bond number and capillary number similar to what others have found.[20],[21] They show that saturation decreases with decreasing capillary number, though this dependence is not as strong as seen in water flooding experiments, most likely because of the low viscosity ratio between CO_2 and brine. Saturation also decreases with increasing Bond number, and at a more rapid rate than with capillary number.

IV. Discussion

The results presented here are preliminary, both in the size of the networks and in the number of simulations. However, they do support what is already known about the relationships between the capillary and Bond numbers and the saturation of the invading fluid. The results also suggest that there is a fundamental limitation on the storage capacity of a homogeneous aquifer (perhaps different for heterogeneous aquifers [22]) for CO_2, and it is less than 50% of the available void space.

Acknowledgement. This work was performed while Grant Bromhal held a National Research Council Research Associateship.

References

1. Blackwell, R. J., J. R. Rayne and W. M. Terry, Trans. AIME, **216**, 1-8, (1959).
2. Collins, R. E., "Flow of Fluids through Porous Materials," 1961 Reinhold Publishing Corporation, New York.
3. Bear, J., "Hydraulics of Ground Water," 1979 McGraw-Hill Publ. Co., New York.
4. Dullien, F.A.L. "Porous Media: Fluid Transport and Pore Structure," 2nd ed., Academic Press, New York, (1992).
5. Rhee, H.-K., R. Aris and N. R. Amundson, "1st-Order Partial Differential Equations: Vol. I (Theory and Applications of Single Equations," 1986 Prentice Hall, Englewood Cliffs, New Jersey.
6. Lenormand, R., E. Touboul and C. Zarcone, J. Fluid Mech., **189**, 165-187, (1988).
7. Feder, J., "Fractals," 1988 Plenum Press, New York.
8. Vicsek, T., "Fractal Growth Phenomena," 1989 World Scientific, Singapore.
9. Meakin, P., "Fractals, scaling, and growth far from equilibrium," 1998 Cambridge University Press, Cambridge.

10. Chen, J.-D. and D. Wilkinson, Phys. Rev. Lett., **55**, 1892-1895, (1985).
11. Nittmann, J., G. Daccord and H. E. Stanley, Nature, **314**, 141-144, (1985).
12. Daccord, G., J. Nittmann and H. E. Stanley, Phys. Rev. Lett., **56**, 336, (1986).
13. Ferer, M., G. S. Bromhal and D. H. Smith, Groundwater, to be sumbitted, (2001).
14. van der Marck, S. C., T. Matsuura and J. Glas, Phys. Rev. E, **56**, 5675-5687, (1997).
15. Aker, E. et al, Transport in Porous Media, **32**, 163-186, (1998).
16. Aker, E., K. Jorgen-Maloy and A. Hansen, Phys. Rev. E, **58**, 2217-2226, (1998).
17. Aker, E., K. Jorgen-Maloy and A. Hansen, Phys. Rev. E, **61**, 2936-2946, (2000).
18. Pereira, G., Phys. Rev. E, **59**, 4229-4242, (1999).
19. Akers, E., A Simulation for Two-Phase Flow in Porous Media, Thesis, Univ. of Oslo, (1996).
20. Morrow, N.R. and B.Songkren, "Surface Phenomenon in EOR," ed. D.O. Shah, 1981 Plenum Press, New York.
21. Pennell, K.D., G.A. Pope, and L.M. Abriola. ES&T, **30**, 4, 1328-1335, (1996).
21. Benson, Sally Proceedings of the First National Conference on Carbon Sequestration, May 14-17, (2001).

OPTIMAL CHOICE OF IMMOBILIZED, SUPPORTED AMINES FOR CO_2 REMOVAL

Thomas Filburn
University of Hartford
West Hartford, CT 06117

R. A. Weiss, Joseph Helble, Samuel Huang
University of Connecticut
Storrs, CT 06296

William Papale
Hamilton Sundstrand Space Systems International
Windsor Locks, CT 06096

Introduction

Aqueous solutions of amines have long been used by industry as absorbents for acid gas (CO_2, H_2S) removal, and in fact provide a large percentage of the natural gas sweetening operations[1]. While these chemical solutions have found a dominant position in the natural gas and refinery gas treatment, they have several shortcomings that can be greatly mitigated by immobilizing them into a solid polymeric support, an approach that has been used by NASA to provide regenerative CO_2 removal on long-term space shuttle orbiter missions[1].

Recent research in our group has produced a new solid amine CO_2 sorbent that has displayed approximately a twofold increase in cyclic CO_2 removal capacity over the material presently operated on board the space shuttle. This boost in capacity has been achieved through the application of a stable secondary amine onto a solid non-ionic polymeric support. This new sorbent may have applicability in the global search for methods to reduce greenhouse gas emissions. When combining these solid amine sorbents with a sequestration mechanism, long term, lower energy CO_2 sequestration systems may be achieved.

The first and foremost shortcoming presented by aqueous liquid amine systems comes from their corrosive effects on the metal piping systems used to contain them. The combination of acid gases and high pH sorbents can greatly accelerate the corrosive action on many mild steel components (valves, piping and pipe fittings). Numerous additives are frequently added to the aqueous liquid amine systems to minimize foaming, prevent corrosion, and promote the acid gas/ amine reaction. Our solid amine system greatly diminishes the corrosion concern and eliminates the need for many additives like foam depressants.

When applied as a fixed sorbent bed the solid amine system has the potential to simplify the present scrubbing system. Incorporating a solid amine system has the potential for eliminating several of the phase separation steps, as well as requiring a smaller absorbing and desorbing column. The smaller columns come from the higher amine/gas contact efficiency and increased amine density possible with the solid support pellets versus the packed trays typically used in the liquid systems. Finally, eliminating the aqueous carrier liquid offers the potential of lower regeneration energy. The liquid amine systems consistently keep amine concentrations below 30%, chiefly for corrosion concerns, however this reduced concentration raises both the fluid circulation rate and the regeneration energy costs.

Experimental

Amine Types.

Figure 1 shows the three amine types for the ethanolamine molecules investigated, monoethanolamine (MEA, primary), diethanolamine (DEA, secondary), and triethanolamine (TEA, tertiary).

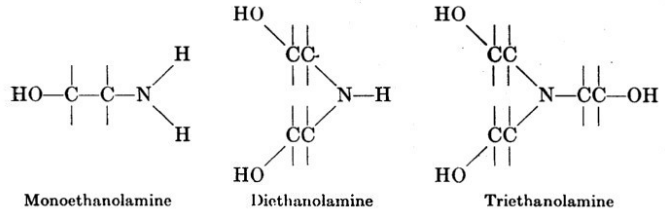

Figure 1. Amine Types MEA, DEA, TEA.

These amine types were immobilized into the pores of HP2MG, a poly(methylmethacrylate) support manufactured by Mitsubishi Chemical. This non-ionic polymeric support provided a high surface area (475 m^2/gm), large pore volume (1.2 ml/gm) to retain the amine and produced a pseudo-solid acid gas removal bead.

TEPAN a reaction product of TEPA (tetraethylenepentamine) and acrylonitrile, Figure 2, was also investigated for its CO_2 removal capacity while loaded onto the same PMMA support. Unlike the MEA, DEA and TEA, this amine, TEPAN, is not an alkanolamine.

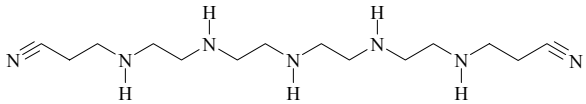

Figure 2. Schematic of TEPAN Molecule

Sorbent Manufacture.

Solvent evaporation with a rotary evaporator was used to immobilize the amine within the pores of the support. In this process we mixed the amine to be impregnated with an equal volume of methanol. The alcohol allowed the amine mixture to diffuse into the bead pore volume much more rapidly. The alcohol also allowed the support to become easily wetted by the amine/alcohol solution, as well as reduced the viscosity of the mixture. We heated the solution and porous beads to 100 °C while under a slight vacuum (~4-8 psia). This step allowed us to evaporate the alcohol from the support while leaving the amine within the pores. After the bulk of the alcohol had been removed as vapor we removed the beads from the flask and tested their capacity for CO_2 removal.

Capacity Measurements

We used a 110 cc aluminum reactor to retain the solid amine beads while testing their capacity for CO_2 removal. This reactor used a fine mesh screen at the inlet and outlet face to hold the beads within the reactor volume. An open cell aluminum foam (10% density) was also brazed into the reactor cavity. This foam coupled with the aluminum of the reactor housing provided an essentially isothermal test for both the absorb and desorb cycles. The testing used a fixed inlet concentration of 1 kPa of CO_2 with the balance being N_2 and water vapor at a total pressure of 1 atmosphere. An IR CO_2 analyzer monitored the outlet CO_2 concentration during the fixed absorption time period (25 minutes). After the absorb period an equal time (25 minutes) of vacuum desorption allowed the sorbent beads to partially regenerate. The data reported represents the steady state working capacity of the various sorbents. The amines can remove CO_2 more effectively with moisture, so the inlet gas stream was maintained at a 7 °C Dew point for all the tests.

Results and Discussion

Figure 3 shows the comparison between the three amine types. A nearly 50% increase in the amine cyclic utilization was achieved for the secondary amine (DEA) compared with the primary amine (MEA). The slight variation in amine loading was (0.22M vs. 0.26M) removed by normalizing the capacity data based on the total amount of amine present. The low capacity shown by the tertiary amine is not surprising at these low CO_2 concentrations. The weak bond formed between the tertiary amine and the CO_2 molecule does not provide a ready means for removing the acid CO_2 molecule from our gas stream.

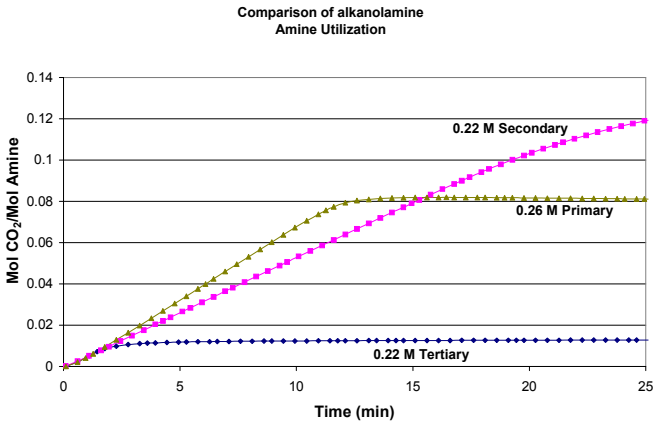

Figure 3. Normalized CO_2 Removal capacity for Primary (MEA), Secondary (DEA) and Tertiary (TEA) amine.

Figure 4 below shows the effect of amine loading within the support on its utilization in removing the CO_2 gas. The 4X (0.114 M – 0.515 M) range in amine loading within the support did not appreciably change the utilization of the amine on the support. This indicates that any surface interaction between the support and the amine did not diminish the activity of the amine for CO_2 removal. If interaction between the amine and the support had occurred, we would expect a difference in the amine utilization curves especially at the lower loadings. The shallower slope and lower utilization limit shown by the higher amine loadings in Figure 4 simply are an artifact of the fixed cycle time used. If the cycle had been extended for the higher loading case a similar utilization limit, as shown by the lower loadings, would have been reached.

Table 1 below shows a comparison of the physical/chemical properties of the 4 amines reported in this preprint. All four of the amines show a similar range of pH values. The large range in viscosity values do not provide any indication in the CO_2 removal capacity. TEPAN had the highest viscosity and the largest CO_2 removal capacity, TEA had the 2nd highest viscosity and showed no capacity for CO_2 removal.

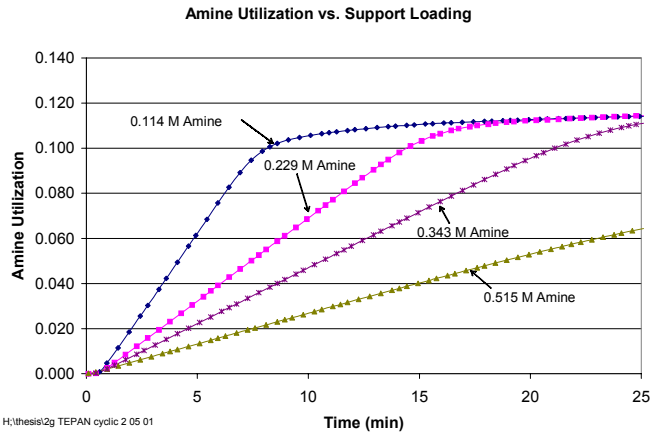

Figure 4. Normalized CO_2 Removal Capacity for variable loading of TEPAN amine within HP2MG support.

Amine	pH	Viscosity cp	BP °C	MW
MEA	11.66	18.9	171	61
DEA	11.32	352	269	105
TEA	10.55	614	340	149
TEPAN	10.98	750		311

Table 1. Physical/Chemical Property Data of amine types

Conclusions

The results of the alkanolamine CO_2 removal testing clearly show the higher working capacity displayed by secondary amines. The primary amines also show some effective affinity, but are clearly eclipsed by the secondary amines. The tertiary amines display a very weak capacity for CO_2 at the low levels (1 kPa) tested here.

All of the TEPAN amine results shown in Figure 4 display a similar asymptotic limit in CO_2 capacity, normalized for the amount of amine present on support. These curves show that the amine and support do not interact, at least in a manner that renders the functional site on the amine molecule unavailable for CO_2 removal. The lower amine loadings did not display any reduction in amine utilization as would be expected if surface/amine interaction affected the amine functional group.

Acknowledgment

Tom Filburn and Bill Papale are grateful for the support of Hamilton Sundstrand Space Systems International.

References

1. Ouellette, F., Winkler, E., Smith, G.," The Extended Duration Orbiter Regenerable CO_2 Removal System", SAE 901292, presented at 20th ICES, July 1990
2. Kohl, A., Nielsen, "**Gas Purification"**, 5th Ed. Gulf Publishing, Houston TX,1997

PREPARATION OF NOVEL CO_2 "MOLECULAR BASKET" OF POLYMER MODIFIED MCM-41

Xiaochun Xu, John M. Andresen, Chunshan Song, Bruce G. Miller, and Alan W. Scaroni*

Clean Fuels and Catalysis Program, The Energy Institute, and Department of Energy & Geo-Environmental Engineering, The Pennsylvania State University, 209 Academic Projects Building, University Park, PA 16802, USA

* Corresponding author. E-mail: csong@psu.edu; Tel: 814-863-4466; Fax: 814-865-3248

Introduction

Fossil fuels will remain the mainstay of energy production well into the 21st century. The availability of these fuels to provide clean, affordable energy is essential for prosperity and security in the world. However, an increase in the concentration of CO_2 in the atmosphere due to carbon emissions is expected to occur unless energy systems incorporate carbon emission reduction concepts. Carbon sequestration, along with reduced carbon content of fuels and improved efficiency of energy production and use are considered to be viable ways to stabilize and ultimately reduce the concentration of this greenhouse gas.[1] For carbon sequestration, the costs of separation and capture are generally estimated to make up about three quarters of the total costs of ocean or geologic sequestration.[2] Novel technologies to decrease the cost of CO_2 separation have great social and commercial value.

Adsorption is one of the promising methods that could be applicable for separating CO_2 from gas mixtures. Generally, molecular sieves and activated carbons yield relatively high adsorption capacity.[3-4] However, these adsorption capacities rapidly decline with incremental increase in temperature and separation factors are low. For practical use, many of the separations require operation at relatively high temperature, e.g., ~150 ^oC for flue gas. Developing an adsorbent with high CO_2 selectivity and high CO_2 adsorption capacity, which can also be operated at relatively high temperature, is critical for the success of this method.

Recently, we developed a new kind of high-capacity, highly selective CO_2 adsorbent, which is a CO_2 "molecular basket".[5] By loading the sterically branched polymer polyethylenimine (PEI), which has branched chains with numerous CO_2-capturing sites such as amino groups, into the large pore volume of MCM-41, its adsorption capacity was significantly increased. In this paper, the preparation approaches to further improve the CO_2 adsorption performance of the novel "molecular basket" are reported. The synergetic effect of the MCM-41 on the adsorption of CO_2 by the PEI is discussed.

Experimental

Mesoporous molecular sieve of MCM-41 with different Si/Al ratios was synthesized as reported in a previous publication.[6] The PEI modified MCM-41 (MCM-41-PEI) was prepared by the wet impregnation method. In a typical preparation, the desired amount of PEI was dissolved in 20 g methanol under stirring for about 15 min, after which 5 g of calcined MCM-41 was added to the mixture solution. The resultant slurry was continuously stirred for about 30 min and dried at 70 ^oC for 16 h under vacuum. The preparation conditions, such as PEI loadings, preparation methods, Si/Al ratio of the MCM-41, and third component of PEG were investigated.

The mesoporous molecular sieves of MCM-41 before and after modification were characterized by X-ray diffraction (XRD, Rigaku Geigerflex), N_2 adsorption/desorption (Quantachrome Autosorb 1) and thermalgravimetric analysis (TGA, PE-TGA 7).

The adsorption and desorption performances of the adsorbents were measured in a flow system under pure CO_2 atomosphere at 75 ^oC. A PE-TGA 7 thermalgravimeter was used to track the weight change of the adsorbent in the experiments. Adsorption capacity in mg of adsorbate/g of adsorbent and desorption capacity in percentage were used to evaluate the adsorbent and were calculated from the weight change of the sample in the adsorption/desorption process. The desorption capacity in percentage was defined as the ratio of the amount of the gas desorbed to the amount of gas adsorbed.

Results and Discussions

1 Preparation and characterization of MCM-41-PEI

The MCM-41-PEI with different PEI loadings was prepared and characterized by XRD, N_2 adsorption/desorption and TGA. After loading the PEI, the structure of the MCM-41 was preserved. However, the intensity of the diffraction patterns of the MCM-41 decreased. Meanwhile, the Bragg diffraction angle of the 100 plane of MCM-41 slightly shifted to a higher degree, which indicated that the PEI was loaded into the channels of the MCM-41.[6] N_2 adsorption/desorption showed that the pore size, surface area and pore volume decreased after loading the PEI, which confirmed that the PEI was loaded into the channels of the MCM-41. When the PEI loading was 50 wt%, the mesopores were completely filled with PEI.

TGA results showed that there was no weight loss for MCM-41 until 600 ^oC. The PEI lost 3.8% of its original mass at 100 ^oC, and began to decompose above 150 ^oC. A sharp weight loss happened at 205 ^oC. At 600 ^oC, the PEI was completely decomposed and removed as volatiles. After the PEI was loaded into the channels of the MCM-41, a sharp weight loss takes place at a lower temperature, e.g., 125 ^oC for MCM-41-PEI with PEI loading of 50 wt%, which indicated that the decomposition temperature of PEI had decreased. The weight loss also took place in a narrower temperature range than that of the pure PEI. These phenomena can be ascribed to the uniform dispersion of the PEI throughout the nanopores, since the melt or decomposition temperature will decrease when the particle size of the substance decreases.[7]

2 Adsorption performance of MCM-41-PEI

2.1 The influence of preparation method

Two methods, i.e., wet impregnation and mechanical mixing, were employed for the preparation of the MCM-41-PEI adsorbent. The PEI loading was 50 wt%. The adsorption capacity was 99 mg/g adsorbent for the adsorbent prepared by the mechanical mixing method and 112 mg/g for the adsorbent prepared by the wet impregnation method. The high adsorption capacity of the wet impregnation method can be ascribed to the uniform dispersion of the PEI into the channels of the MCM-41. For the mechanical mixing method, only part of the PEI was loaded into the channels of the MCM-41. The remaining PEI may coat the outer surfaces of the particles as a thick layer, which may block CO_2 adsorption sites and impede CO_2 from accessing the channels of the molecular sieve.

2.2 The influence of PEI loading

The influence of PEI loading on the CO_2 adsorption performance of MCM-41-PEI was investigated and the results are shown in Figure 1. Before the PEI was loaded, the bare MCM-41 showed a CO_2 adsorption capacity of 8.6 mg/g adsorbent. After loading the PEI, the adsorption capacity increased. The adsorption capacities were 112 mg/g adsorbent and 133 mg/g adsorbent for PEI loadings of 50 wt% and 75 wt%, respectively, both of which are higher than that of the pure PEI of 109 mg/g adsorbent. The MCM-41

showed synergism for the adsorption of CO_2 by PEI. The desorption was complete for all the MCM-41-PEI adsorbents as well as the MCM-41 support. However, desorption for the pure PEI was slow and was not complete for the same desoption time. The fast desorption of CO_2 from MCM-41-PEI can be explained by the high dispersion of PEI into the MCM-41 channels, which was indicated by the N_2 adsorption/desorption and the TGA data.

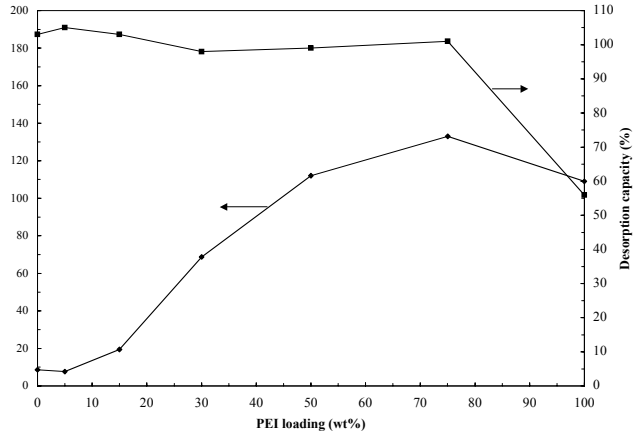

Figure 1 The influence of PEI loading on the adsorption and desorption performance of MCM-41-PEI

2.3 The influence of the Si/Al ratio of the MCM-41

A change in the Si/Al ratio of the MCM-41 will not only change the physical properties of the support (e.g., pore size, pore volume and surface area), but also change the interaction between the support and PEI. Figure 2 shows the adsorption capacity of MCM-41 and MCM-41-PEI with different Si/Al ratios. The adsorption capacity was nearly identical for the MCM-41 support with different Si/Al ratios. However, the Si/Al ratio of the MCM-41 influenced the adsorption capacity of MCM-41-PEI. The higher the Si/Al ratio, the higher the adsorption capacity. The adsorption capacity of MCM-41-PEI with a Si/Al ratio of 100 was 12 % higher than that of MCM-41-PEI with pure silica.

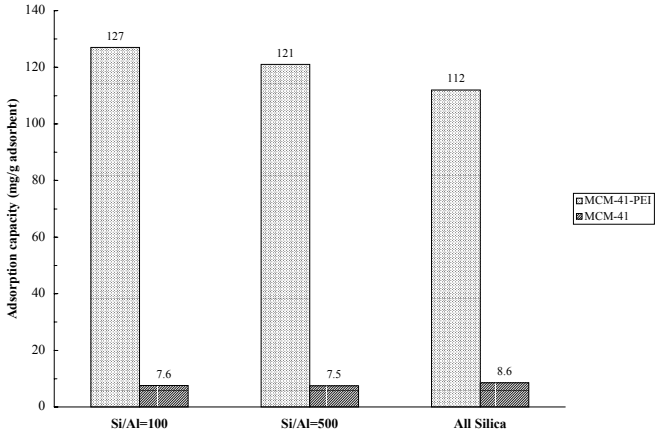

Figure 2 The influence of Si/Al ratio on the adsorption performance of the MCM-41-PEI (PEI loading: 50wt%)

2.4 The influence of third component of PEG

The influence of the third component of PEG on the adsorption/desorption performance of the MCM-41-PEI was investigated. Figure 3 compares the adsorption and desorption performance of the adsorbent with and without the addition of PEG. The adsorption and desorption rates of the MCM-41-PEI-PEG were faster than those of the MCM-41-PEI. In addition, the adsorption capacity of the MCM-41-PEI-PEG was higher than that of MCM-41-PEI.

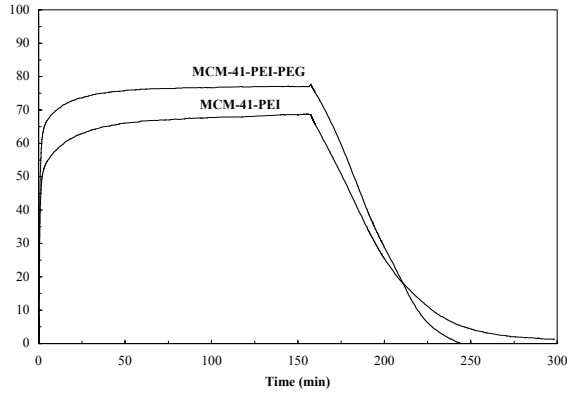

Figure 3 The effect of PEG on the CO_2 adsorption/desorption performance of MCM-41-PEI. (PEI loading: 30 wt%, PEG loading: 20 wt%)

Conclusion

A novel CO_2 "molecular basket" based on PEI modified mesoporous molecular sieve of MCM-41 (MCM-41-PEI) has been successfully developed. The MCM-41 had a synergetic effect on the adsorption of CO_2 by PEI. By loading substances with affinities for different gases to the mesoporous molecular sieve, this concept can be used to develop different types of highly selective, high adsorption capacity "molecular baskets".

Acknowledgments

Funding for the work was provided by the U.S. Department of Defense (via an interagency agreement with the U.S. Department of Energy) and the Commonwealth of Pennsylvania under Cooperative Agreement No. DE-FC22-92PC92162.

Reference

1. DOE Fossil Energy-Carbon Sequestration, **2001**, http://fossil.energy.gov/coal_power/sequestration/index.shtml
2. DOE, Carbon sequestration research and development, Chapter 2-Separation and capture of carbon dioxide. **1999**
3. Ishibashi, M.; Ota, H.; Akutsu, N.; Umeda, S.; Tajika, M.; Izumi, J.; Yasutake, A.; Kabata, T.; Kageyama, Y. *Energy Conv. Manag.*, **1996**, *37*, 929-933.
4. Foeth, F.; Bosch, H.; Sjostrand, A.; Aly, G.; Reith, T. *Sep. Sci. Tech.*, **1996**, *31*, 21-38.
5. Xu, X.C.; Andresen, J.M., Song, C.S., Miller, B.G., Scaroni, A.W. *Energy & Fuels*, in preparation
6. Reddy, K.M.; Song, C. *Catal. Lett*., **1996**, *36*, 103-109.
7. Zeng, P., Zajac, S., Clapp, P.C., Rifkin, J.A. *Mat. Sci. Eng. A-Struct.,* **1998**, *252*, 301-306.

Producing Negatively Buoyant CO_2 Streams at Intermediate Ocean Depths

Olivia R. West, Costas Tsouris, Liyuan Liang, Sangyong Lee

Oak Ridge National Laboratory
Oak Ridge, TN 37831

Introduction

Direct injection of CO_2 into the ocean has been proposed as a means for carbon sequestration because the ocean has a large storage capacity for carbon (Herzog, 1998; Audus, 1997, Brewer et al., 1999). A fraction of the CO_2 injected into the ocean will eventually repartition back into the atmosphere. However, depending on the depth of injection as well as the subsequent interaction of CO_2 with seawater, CO_2 residence time in the ocean can be on the order of several hundred years leading to significantly reduced peak levels of atmospheric CO2 (Herzog et al., 1997).

One of the proposed methods for direct ocean injection is to release liquid CO_2 at intermediate ocean depths between 800 and 1500 m, forming a rising plume of CO_2 droplets. To prolong the residence time of the injected CO_2, the injection depth for the droplet plume must be sufficiently great to allow for complete dissolution of the CO_2 into the surrounding seawater before the droplets reach depths of ~0.5km where pressures are low enough for the CO_2 to gasify and more rapidly partition back into the atmosphere. Another approach is to perform injections at depths greater than 3000 m where CO_2 is denser than seawater. CO_2 released at these depths will sink through the water column resulting in increased residence time and improvement in the overall efficiency of ocean carbon sequestration by direct CO_2 injections. However, this improved efficiency comes with implementation costs and energy requirements that increase significantly with injection depth.

The objective of the research described here is to develop a new technique for direct ocean CO_2 injection in which CO_2 can be disposed at ocean depths of 1000 to 1300 m in the form of a water/ CO_2/hydrate composite stream. Produced by intense in-line mixing of CO_2 and water, this composite stream can be negatively buoyant, prolonging the residence of injected CO_2 in the ocean and improving the overall efficiency of ocean carbon sequestration by direct CO_2 injection.

Experimental Methods

Experiments were conducted to test the concept of promoting CO_2 hydrate formation by mixing water with CO_2 in a discharge pipeline. A co-flow injector was designed and set up in the ORNL Seafloor Process Simulator (SPS), a 70-L, temperature controlled, high-pressure vessel designed for simulating conditions at intermediate ocean depths (Fig. 1; Phelps et al., 2001). The injector (Fig. 2) consists of an internal capillary tube located at the center of an outer tube, where the inner and outer tubes are for water and CO_2, respectively. The mixing zone, as shown in Fig. 2, is the space between the ends of the inner and outer tubes. In a typical experiment, the SPS was filled with water, pressurized up to a predetermined level (10 to 13 MPa, corresponding to ~1 to 1.3 km depth) then cooled in a temperature-controlled room down to the experimental temperature. (4-7ºC). Liquid CO_2 and water were then delivered through the injector using syringe pumps at predetermined flow rates ranging from 15-25 mL/min and 4-20 mL/min, respectively. Vessel pressure increased slightly (less than 0.5 MPa) during the injection experiments, or was kept constant using a backpressure regulator. The stream issuing from the injector was then observed and recorded by a video camera through one of the 5-cm diameter sapphire windows on the SPS.

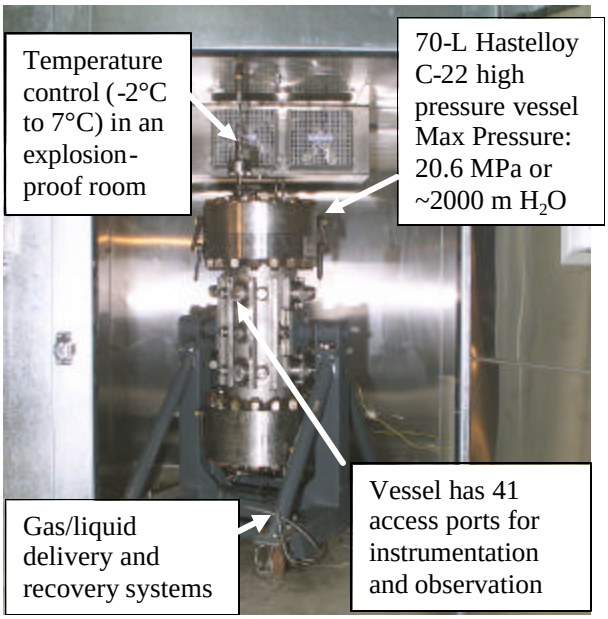

Figure 1. The ORNL Seafloor Process Simulator (SPS).

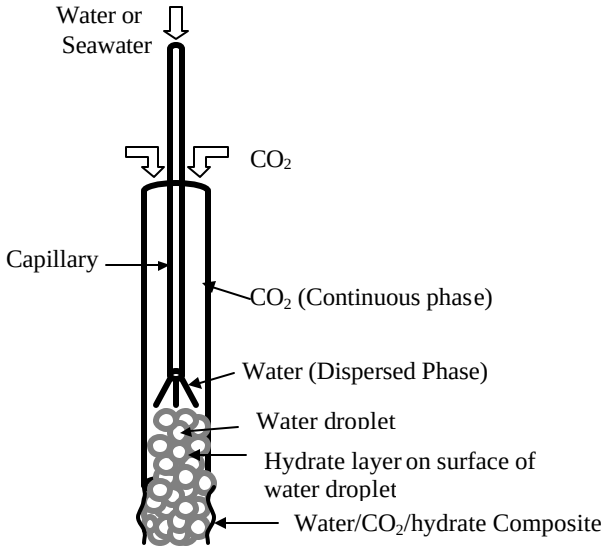

Figure 2. Schematic of the co-flow injector for producing a water/CO2/hydrate composite stream.

Results and Discussion

Using the co-flow injector at varying flow-rate ratios of water and CO_2, we obtained a paste-like stream (Fig. 3) under conditions typical of intermediate ocean depths (1-1.3 km). The produced stream maintained its cylindrical shape and remained fairly intact when released from the injector, occasionally breaking up into cylindrical sections. For a given ambient pressure, the stream was negatively buoyant at certain flow rate ratios between water and CO_2. To eliminate the effects of jet flow that may be pushing the stream down in a vertically oriented injector, experiments were also conducted with the injector mounted horizontally in the SPS. Negative buoyancy in this case was indicated by a stream that bent downward as it was released from the injector (Fig. 4). Experiments using both distilled and seawater showed that a negatively buoyant stream can be produced at pressures as low as 10.3 MPa, corresponding to an ocean depth of ~1 km.

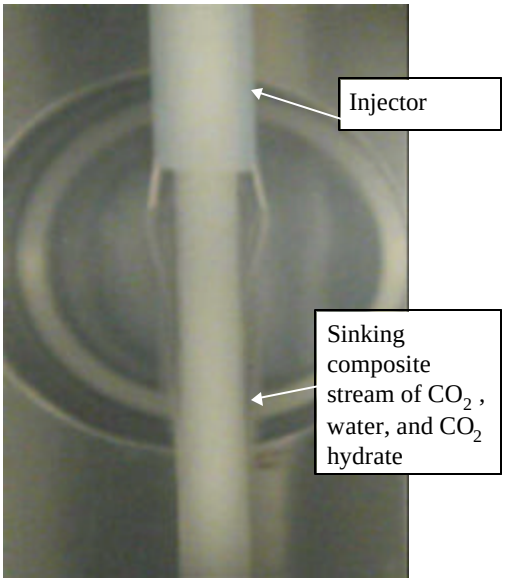

Figure 3. Negatively buoyant stream produced by CO_2 injector oriented vertically in the SPS.

The stream produced by our injector probably consists of a composite of liquid CO_2, water, and CO_2 hydrate where the solid hydrate serves as a cementing phase for the other stream components. Presence of water in the stream was inferred from the flow rate ratios between water and CO_2 used to produce the stream, which exceeded what was required for complete conversion of CO_2 to CO_2 hydrate. It was also observed that some streams that were initially positively buoyant would sink some time after being released from the injector, or when vessel pressure was increased. These observations indicate the presence of liquid CO_2 trapped in the produced stream, where it either continues to convert to CO_2 hydrate with time or becomes denser with increasing pressure.

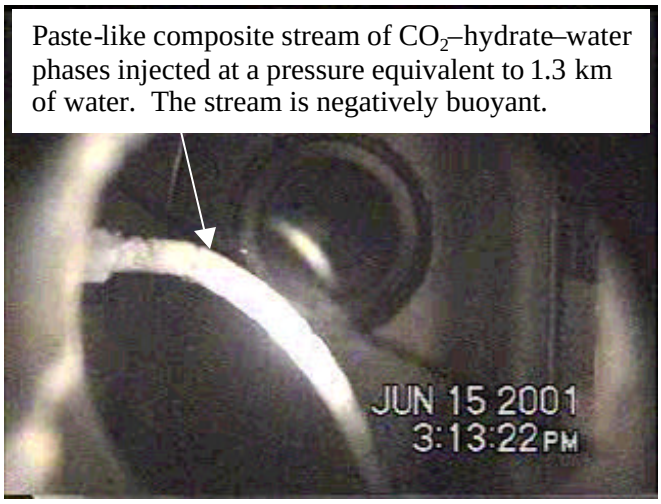

Figure 4. Negatively buoyant stream produced by CO_2 injector oriented horizontally in the SPS.

Conclusions

A negatively buoyant composite stream containing CO_2 hydrate, liquid CO_2, and water at conditions simulating intermediate ocean depths (~1-1.3 km) was produced using a novel concept of premixing seawater into a CO_2 stream before injection. Such a development is significant because it generates a sinking stream at depths <1.5 km, which will prolong the residence of CO_2 injected into the ocean and improve the overall efficiency of direct CO_2 injections for ocean carbon sequestration. Because implementation costs increase significantly with injection depth, this approach allows CO_2 injections to be performed not only with a lower risk of leakage to the atmosphere, but also without significant increase in operating cost when compared with other proposed injection methods. Additionally, because of its low surface-to-volume ratio, the produced composite stream is expected to have a slower dissolution rate than that of a similar volume of liquid CO_2 in the form of a droplet plume. The deeper the CO_2 hydrate stream sinks after injection, the more stable it becomes internally, the deeper it is dissolved, and the more dispersed is the resulting CO_2 plume. This slower rate will reduce the potential for low-pH conditions surrounding the injector, thereby minimizing the negative impact of direct CO2 injections on the ocean environment.

Acknowledgment. This research was funded by the Ocean Carbon Sequestration Program, Biological and Environmental Research (BER), U.S. Department of Energy (Grant #KP120203), and by the Oak Ridge National Laboratory's Seed Money Program. We would also like to thank Scott McCallum and David Riestenberg for their assistance with the laboratory experiments. Oak Ridge National Laboratory is managed by UT-Battelle, LLC, for the U.S. Department of Energy under Contract No. DE-AC05-00OR22725.

References

(1) Herzog, H. J. Ocean Sequestration of CO2—An Overview. in *Fourth International Conference on Greenhouse Gas Control Technologies,* **1998** (Interlaken, Switzerland).

(2) Audus, H. *Energy*, **1997**, *22*, 217.
(3) Brewer, P. G.; Friederich, G.; Peltzer, E. T.; Orr, F. *Science*, **1999**, *284*, 943.
(4) Herzog, H.; Drake, E.; Adams, E. *CO2 Capture, Reuse and Storage Technologies for Mitigating Global Climate Change*. **1997**, MIT Energy Laboratory, Cambridge, MA.

PROPOSAL OF SLURRY TYPE CO_2 SENDING SYSTEM TO THE OCEAN FLOOR, NEW COSMOS

Izuo Aya[1], *Kenji Yamane*[1], *Koki Shiozaki*[2], *Peter G. Brewer*[3], *and Edward Peltzer*[3]

1) Osaka Branch, National Maritime Research Inst. (NMRI)
3-5-10 Amanogahara, Katano, Osaka 576-0034, Japan
2) Power and Energy Div, NMRI
3) Monterey Bay Aquarium Research Inst. (MBARI)

Introduction

The idea to store CO_2, recovered from power plants, in the deep ocean[1] has been a promising measure to mitigate the global warming especially after the Third Conference of the Parties (COP 3) held in Kyoto, December 1997, because the achievement of Kyoto Protocol was thought difficult only by conventional measures such as the energy saving and the forestation. This CO_2 ocean sequestration can be divided into two categories, that is, the dissolution (or dilution) method and the storage method.

In the former method, CO_2 droplets are released in mid depth of 1000 to 2000 meters where CO_2 is lighter than seawater, and they completely dissolve before reaching phase change boundary of about 400 meters depth. The sequestration term is expected to be the order of hundred years, which depends on the release point and the depth.[2]

On the other hand, in the latter method, CO_2 is stored in a depression on the ocean floor deeper than 3500 meters where liquid CO_2 is heavier than CO_2 saturated seawater. Its sequestration term is expected to be longer than a few thousand years equivalent to the vertical circulation term of the ocean.[3] It is a shortcoming of this method, however, to send CO_2 deeper than the former method.

The Maritime Research Institute (NMRI, the former name of the Ship Research Institute) had investigated the various aspects of the latter method in the last decade.[4-15] And in 1998, the authors proposed a system to overcome the above mentioned shortcoming of the storage method.[16,17] This system called as COSMOS, CO_2 Sending Method for Ocean Storage, is characterized as cold release of large CO_2 droplets with about 1 meter diameter into rather shallow waters such as 500 meters depth, where CO_2 colder than -30 Celsius is heavier than the ambient seawater and sinks to the ocean floor although being warmed up by the heat transfer from seawater.

In order to get the basic data prior to the development of the real COSMOS, an international joint research with University of Bergen supported by the NEDO (New Energy and Industrial Technology Development Organization) was started in 1999.[18] And parallel with this research, two *in situ* experiments with the Monterey Bay Aquarium Research Institute (MBARI) were also conducted in 1999 and 2000 to confirm the performance of manufactured trial cold CO_2 release nozzle.[19] Through the process of the joint research with University of Bergen, it was found that Taylor type instability[20] on the interface were too strong for a large cold CO_2 droplet to keep its shape, although ice and hydrate layers covering cold CO_2 droplet had been expected to support its shape.[21] From the latest *in situ* experiment with the MBARI, CO_2 slurry, that is, mixture of solid CO_2 (dry ice) and cold CO_2 of -55 Celsius, showed its capability to prevent from breaking up during sinking process.

Then the authors proposed a new COSMOS[22] modified from the original one, in which CO_2 is released as slurry balls into much shallower depth such as 200 meters. The New COSMOS, which is much easier to be realized because the limit droplet size is about 40 % of the original COSMOS, has another advantage that it can be applied to the dissolution type as well as the storage type. Moreover, the cost is also expected to be drastically reduced due to shallower release depth that requires a shorter pipeline equivalent to the length of CO_2 carrier, which means no troublesome connecting works on the ocean.

Concept of COSMOS

CO_2 carriers are required when we apply the storage method because the potential sites deeper than 3500 meters are too far for a pipeline to be laid down from the land. And liquid CO_2 transported by a carrier should be cooled down to -55 Celsius to reduce the tank pressure as much as possible (The triple point of CO_2 is -56.6 Celsius). Such cold CO_2 is heavier than the seawater even in rather shallow sea. If a CO_2 droplet released into 500 meters depth is lager than a certain diameter, which depend on the temperature of CO_2, it sinks to the storage site beyond 2700 meters depth where the density of CO_2 in thermally equilibrium (the same temperature) is the same as that of the seawater. Paying attention to this nature of cold CO_2, the NMRI proposed an innovative CO_2 sending method, COSMOS, and got a Japanese patent in March 1999. **Figure 1** shows the conceptual drawing of COSMOS, which was expected to solve the above-mentioned shortcoming of the storage method.

The temperature of liquid CO_2 released into the shallow sea is -45 to -30 Celsius that depends on the thermal insulation of riser tube from the CO_2 carrier. When such cold CO_2 is released into the seawater, a CO_2 droplet will soon be covered with ice layer and CO_2 hydrate membrane. These were expected to prevent the break up of a large droplet into small droplets but they will make difficult to release smoothly and steadily large CO_2 droplets from the nozzle. Therefore, the technical breakthrough to realize the COSMOS was thought as the development of CO_2 release nozzle.

Then in 1999, the NMRI started an international joint research with the University of Bergen to get the basic data to develop the release nozzle for cold CO_2, under the auspice of the New Energy and Industrial Technology Development Organization (NEDO).[18]

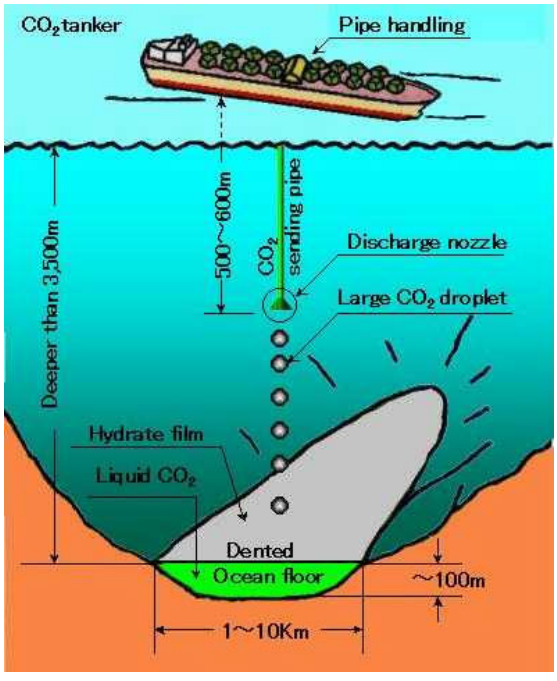

Figure 1. Concept of COSMOS proposed in 1998.

Figure 2. Original trial CO_2 release nozzle.

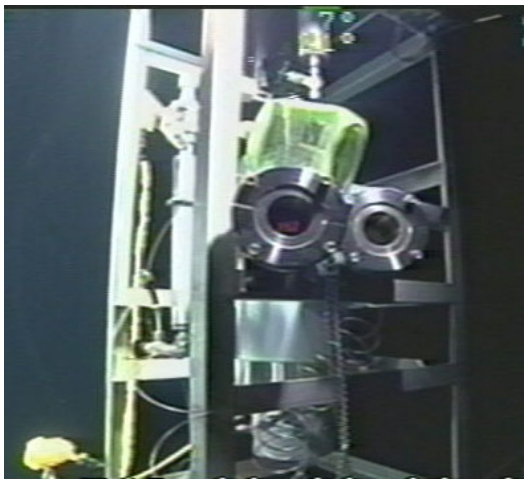

Figure 3. Temperature and pressure monitors mounted on the second trial nozzle.

In 1999 and 2000, the NMRI and the MBARI also conducted two joint *in situ* experiments to confirm the function of trial CO_2 release system.

Land Experiments

To ensure the success of *in situ* experiments with the MBARI, some land-based experiments with a mock liquid and cold CO_2 were conducted for original and second trial nozzles.

Trial CO_2 release nozzles. **Figure 2** shows the original trial CO_2 release nozzle used for the performance test at the *in situ* experiment in 1999. And **Figure 3** shows the second trial nozzle used to release CO_2 slurry ball at the *in situ* experiment in the fall of

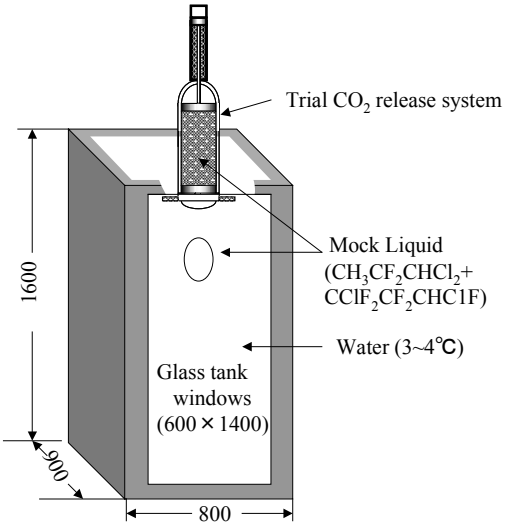

Figure 4. Layout of atmospheric simulation experiment.

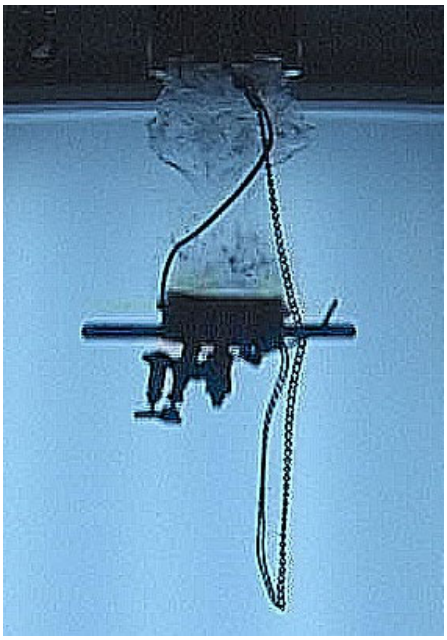

Figure 5. Cold mock liquid just flowed out from the chamber.

2000. The original nozzle was designed to release CO_2 in 500 meters depth through simple two actions that the ROV pilot can easily manipulate through the robot arm. The volume and the diameter of chamber to hold CO_2 or mock liquid were 2.16 liters and 10 cm, respectively. The total weight including frames was about 60 kg, which was smaller than the weight limit of the ROV, 113 kg (= 250 lbs).

The second nozzle, of which specifications were almost the same as the original one, was not only improved in its thermal insulation to keep CO_2 cool enough until its release but also the temperature and pressure monitoring devices were installed.

Mock liquid experiment. Because the saturation pressure of CO_2 at room temperature (≒20 Celsius) is 5.8 MPa, an appropriate mock liquid was required to check the performance of the manufactured CO_2 release nozzle at atmospheric pressure. Then

Figure 6. Large test tank for trial CO_2 release nozzles.

considering the properties of density, specific heat, boiling and solidification points, surface tension and noxiousness, *Asahi-Kurin AK-225* (mixture of $CH_3CF_2CHCl_2$ and $CClF_2CF_2CHClF$) was selected as the mock liquid for simulation experiment (specific density: 1.55, specific heat: 1.00 J/(gr·K), boiling point: 54 Celsius, solidification point: -131 Celsius, surface tension: 16.2 mN/m, weak noxious). **Figure 4** shows the layout of atmospheric simulation experiment. And **Figure 5** shows the scene that the cold mock liquid just flowed down from the opening of the chamber. As shown in this figure, the mock liquid was pushed out as one mass following the sinking lid of the chamber but not covered with ice layer although it was initially cooled down to about -60 Celsius. And the liquid mass broke up into small droplets in a several seconds. Its small specific heat (about a half of CO_2, about a quarter of water) was thought to be not enough to form thick ice layer so fast that the shape of large droplet was kept one mass.

Tank experiment with CO_2. A large tank made of stainless steel, of which main specifications are 5 MPa, 1.0 meter diameter and 3.0 meters height, was manufactured to confirm the perform-ance of CO_2 release nozzles, prior to shipping it to the MBARI. **Figure 6** shows the large tank fixed at the pit. The tank and the foothold for the experiment were enclosed with thermal-insulated room of which temperature was controlled from 5 to 20 Celsius by an air-conditioning system.

Figure 7 shows the scene that the cold CO_2 melted from dry ice was pushed down from the original release nozzle. It was seen that some liquid CO_2 was drown by the falling lid and other CO_2 followed it. Comparing Figs 5 and 7, the ratio of drown liquid in case of CO_2 seems larger than the case of mock liquid. **Figure 8** shows a lot of ascending small CO_2 droplets that might have been broken up from heated CO_2 mass once fell down to the bottom of tank. Figure 8 also shows an ice horn (hollowed icicle) appearing after almost CO_2 was discharged, which implies that cold CO_2 has enough cold heat capacity to make hard ice layer around CO_2 mass.

The results of simulation tests with the mock liquid and CO_2 suggested that the heat transfer rate to form ice layer on the cold CO_2 might not be fast enough to form strong ice layer to keep the shape of a large CO_2 mass against Taylor type interface instability, although the heat capacity of cold CO_2 is enough to form thick ice.

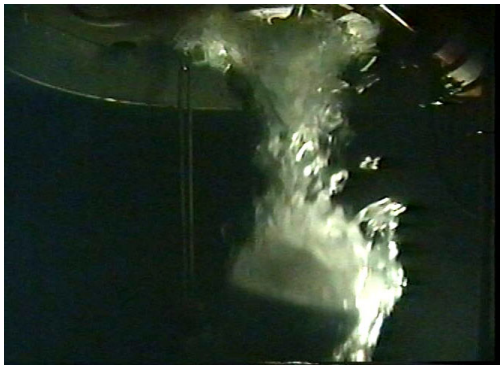

Figure 7. Cold CO_2 pushed down from the release nozzle.

Figure 8. Ascending small CO_2 droplets broken up from heated CO_2 mass and hollowed icicle.

***In Situ* Experiments**

Experiment with original release nozzle. On October 12, 1999, using the original release nozzle shown by Fig. 2, an *in situ* CO_2 release test was conducted in Monterey Bay as the 2nd joint experiment with the MBARI.[23] **Figure 9** shows the original CO_2 release nozzle mounted on the ROV, Ventana. It took about one hour to charge CO_2 into the chamber and to bring it down to the release point by the ROV. The thermal insulation of the release nozzle, which was tested before shipping the nozzle to the MBARI, was not enough for cold CO_2 release. So the temperature of CO_2 in the chamber increased to the same level of the ambient seawater when reached the release depth of 450 meters.

Figure 10 shows that CO_2 was released as one mass from the nozzle, but as shown in **Figure 11**, CO_2 mass was broken up in a few seconds to a lot of small CO_2 droplets which might be covered with hydrate membrane and ascended around CO_2 release nozzle.

The basic performances required to a cold CO_2 release nozzle, that is, two simple actions for the initiation of CO_2 release, were well demonstrated at the *in situ* experiment with the original release nozzle, but the capability to release cold CO_2 mass, which was expected to be covered with thick ice layer, was not achieved.

Experiment with improved release nozzle. The second CO_2 release nozzle was manufactured, considering the defects found in

Figure 9. CO_2 release nozzle mounted on the ROV, Ventana.

Figure 10. CO_2 mass just released from the nozzle.

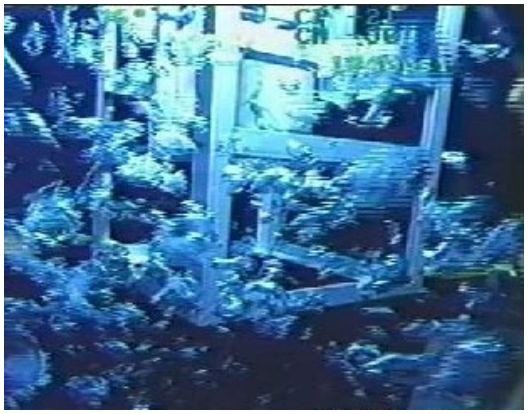

Figure 11. Ascending CO_2 droplets covered with hydrate.

the above-mentioned *in situ* experiment. That is, the thermal insulation was improved by covering it thick with air-containing cast plastic and monitoring devices for the temperature and pressure in the chamber were attached.

On October 5 and 6, 2000, two cold CO_2 release trials were conducted at the same water as before. **Figure 12** shows the improved release nozzle mounted on the ROV. After checking carefully the valves and devices of the nozzle with 2 kg of dry ice,

Figure 12. Improved release nozzle mounted on the ROV.

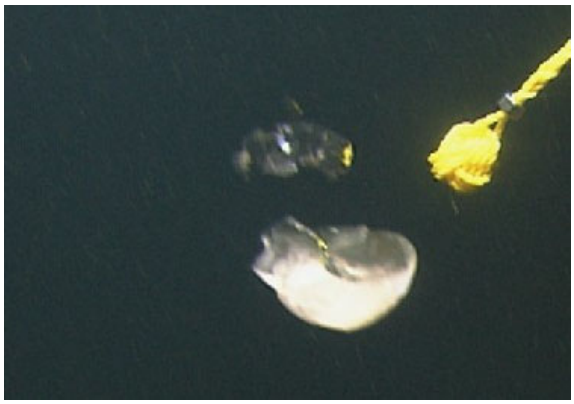

Figure 13. A CO_2 slurry mass（8 cm）sinking at 0.3 m/s.

the ROV sank to 500 meters depth in about 15 minutes, which was almost two times faster than the usual sinking rate. This time, the thermal insulation was improved so much that almost CO_2 was kept as dry ice when arriving at the release point of 500 meters depth.

At the first trial on October 5, being thought worth to observe the behavior of released dry ice mass, cold CO_2 almost consisting of dry ice was released by the simple two actions of robot arm explained above. The dry ice ball with about 10 cm diameter sank so fast that the ROV could not catch up with it. Only the release and very first sinking scene was recorded.

At the second trial on the next day, after two-hours wait at the releasing depth for warming up of CO_2, 2 kg of cold CO_2 including some dry ice was released as the same manner as before. And melted and warmed CO_2, which occupied in the upper space of the chamber, followed the cold CO_2 and broke up into small droplets ascending in the ocean. The content of dry ice in the cold CO_2 mass was estimated about 50 % from the sinking rate that the ROV could catch up with. **Figure 13** shows the scene that a CO_2 slurry mass with 8 cm diameter sank in around 530 meters depth at the rate of 0.3 meters per second. As shown in Fig. 13, CO_2 slurry was coated with thick ice layer. From the video image during sinking process of this slurry mass for about four minutes while the ROV could follow, it was confirmed that this ice layer had enough strength to prevent from breaking up to small slurries. Thin hydrate layer should also form between CO_2 slurry and ice layer, but it was not observed due to its thinness and transparency. It was observed that some part of melt CO_2 due to heating up by ambient seawater leaked upward

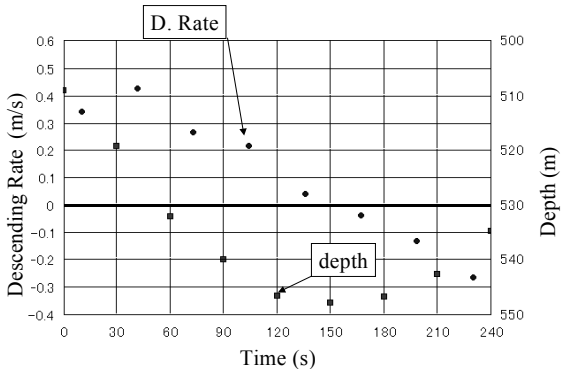

Figure 14. Depth and velocity of a sinking slurry ball.

(a) Just before breaking

(a) Just after breaking

Figure15. Deformed and breaking CO_2 mass covered with hydrate film.

from the slurry. This volume increase came from the fact that the density of dry ice is about 1.4 times larger than cold liquid CO_2.

Figure 14 shows how the depth and velocity of the slurry mass observed in the second trial change with lapse of time. It was shown that the slurry once reached 548 meters depth at 150 seconds but it began to ascend, which means the slurry mass was heated up during 150 seconds descent and lost its negative buoyancy. During ascent, the ice layer continued to shrink and at 240 seconds it broke up to small CO_2 droplets covered with hydrate membrane. Just before breaking up, curious movement of CO_2 mass due to changes of surface tension was seen. **Figure 15** shows its deformed shape during such unique movement. The size of broken up droplets is 2 to 3 cm, which can dissolves in the ascent less than 1000 meters.

Proposal of New COSMOS

Results of land-based and *in situ* experiments. Through several land-based experiments and two *in situ* experiments the following results were obtained:

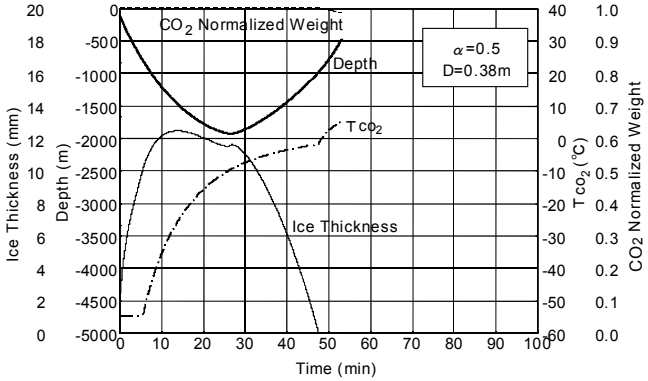

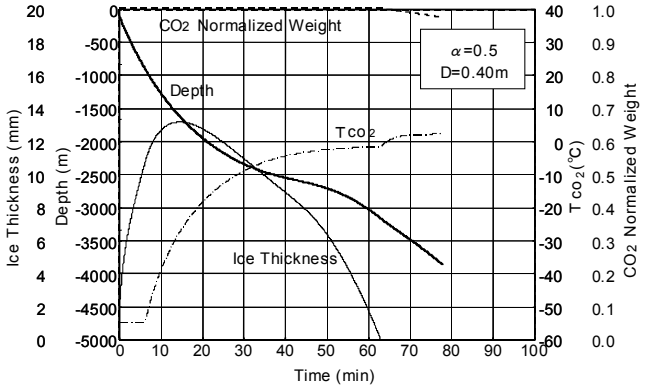

Figure16. Behavior of a CO_2 slurry ball released into 100 meters depth

(1) The basic skill to release small amount of cold CO_2 (2kg) to 500 meters depth was established.
(2) Simulation of cold CO_2 release using a mock liquid was difficult because no liquid having the same properties as those of CO_2.
(3) The heat capacity of cold CO_2 is enough to form thick ice layer to protect a cold CO_2 droplet.
(4) But the surface instability of a cold CO_2 (Taylor type instability) was so large that thick ice layer was difficult to form before released CO_2 mass broke up.
(5) Only CO_2 slurry (mixture of dry ice and cold CO_2) can sink in the ocean without breaking up.
(6) It might be possible to realize the original COSMOS proposed in 1998, but it should be much easier to release CO_2 as slurry balls.

Motion of CO_2 slurry ball in the ocean. Considering above results, the authors would like to propose another CO_2 Sending Method for Ocean Storage, new COSMOS, in which CO_2 will be released as slurry balls instead of cold CO_2 droplets. In case of slurry release, the required depth is 100 to 200 meters, much shallower than 500 meters the original COSMOS requires, because cold heat capacity of a slurry ball is larger than a cold CO_2 droplet and melt CO_2 is expected not to be heated up before reaching the phase change boundary, about 400 meters depth.

Figure 16 is an example of numerical simulation to show how a CO_2 slurry ball released into 100 meters depth behaves.[22] The dry ice ratio, α, was chosen as 0.5 in this simulation. In case of 0.38 meter, the slurry ball reaches 1950 meters then ascends, but in case of 0.4 meter, it sinks to the ocean floor through 2700 meters of density equilibrium depth. In both cases, the temperature of slurry ball is kept -55 Celsius, melting point of CO_2, until it reaches 800 to 900 meters

depth, far deeper than the phase change boundary, which means the cold heat capacity of a slurry ball is enough. At this depth, a slurry ball becomes a cold CO_2 droplet covered with thick ice layer. Then a CO_2 droplet is gradually heated up as shown in Fig. 16. When the temperature becomes -1.9 Celsius, the ice layer completely melts and the dissolution of CO_2 starts (the normalized weight starts to decrease). Heating up rate increases when ice layer disappears. The maximum thickness of ice layer reaches 12.5 and 13 cm for D = 0.38 meter and 0.40 meter, respectively.

Figure 17 shows the simulation result as the relation of the depth and temperature of a slurry ball ($\alpha = 0.5$, release depth = 100 meters). From this figure, the limit size that can sink to the ocean floor is between 0.38 meter and 0.40 meter as mentioned above. This size is less than 40 % of original COSMOS (cold liquid CO_2 release). The similar results like Figs. 16 and 17 were obtained by B. Kvamme, a member of the international joint research team.[24]

Advantages of New COSMOS. Figure 18 shows the concept of new COSMOS to be applied for a Japanese patent. The only additional component required by new COSMOS is a refrigerator to change cold CO_2 of -55 Celsius to CO_2 slurry. When the main engine of 200 thousand tons CO_2 carrier is used for the compressor of the refrigerator, it will take two days to make all CO_2 slurry. This treating rate is almost equivalent to the amount of CO_2 released from five power plants of 1000 MW. Since the volume of dry ice is 1.4 times smaller than cold CO_2, the choking of pipe while making slurry might be avoided.

The new COSMOS has the following advantages:

(1) Easy to realize. The basic techniques to release a CO_2 slurry mass into the ocean have accumulated through *in situ* experiments with the MBARI. And it was confirmed that a CO_2 slurry ball does not break up until the ice layer covering it almost completely melts. Therefore it can be said that the most important phenomenological aspects of new COSMOS has been elucidated.

On the other hand, it may not be so easy to keep a large CO_2 droplet as one mass, the most important requirement of original COSMOS, because the Taylor type interface instability is so strong for ice layer to cover the droplet before breaking, although the heat capacity of cold CO_2 droplet is large enough.

(2) Low initial cost. As shown in Fig. 17, the CO_2 slurry size to be sent to the ocean floor is around 0.4 meter, although it depends on dry ice ratio, α. This size is 0.4 times smaller than the original COSMOS. And the required pipe length is also 0.4 times (200/500 = 0.4). Such smaller sizes will result in drastic cost reduction.

(3) Low running cost. The theoretically required pipe length is less than 100 meter, but 200 meters pipe is recommended in the new COSMOS for the safety. This 200 meters pipe can be put on the deck of 200 thousand tons of CO_2 carrier. Therefore, troublesome works to connect a lot of pipes on the deck, which original COSMOS and other CO_2 ocean sequestration methods require, can be avoided.

(4) Applicable to the dissolution method. Considering the facts that a CO_2 droplet breaks up to small ones just before complete melting of the ice layer which covers the droplet and broken up droplets are so small that they can dissolve before reaching the phase boundary depth of about 400 meters, the new COSMOS can be applied to the dissolution method as well as the storage method. That is, if the dry ice content, α, and the slurry size are well controlled, we can optionally choose the depth that the CO_2 slurry released in 200 meters depth turns back. Moreover, if we set the turn-back depth to a little bit shallower and deeper than the neutral depth of around 2700 meter, the full depth from the ocean floor to the phase boundary can be used for the CO_2 dissolution field, which makes the maximum CO_2 concentration the lowest. Figure 17 also suggests that the application to the dissolution method is not difficult.

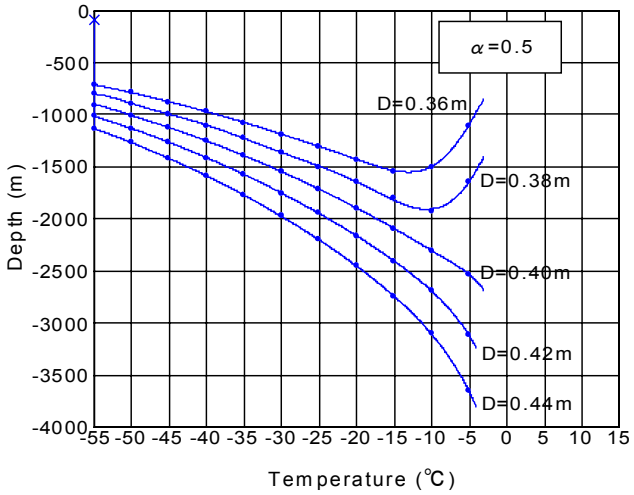

Figure17. Relation of the depth and temperature of a slurry ball ($\alpha = 0.5$, release depth = 100 m).

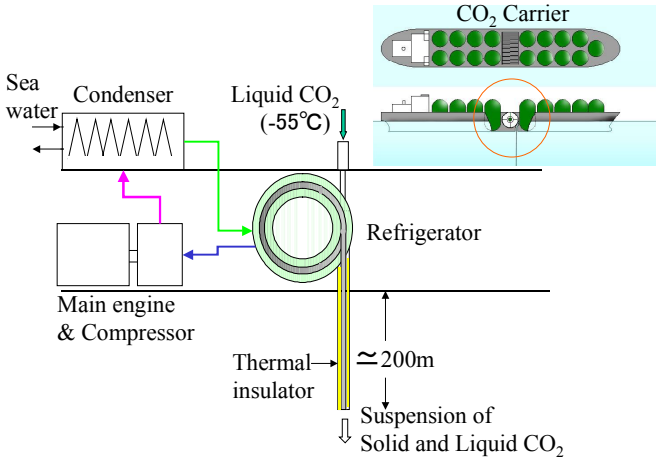

Figure18. Concept of new COSMOS, in which CO_2 is released as slurry balls.

Conclusions

Through various types of land-based and *in situ* experiments with the MBARI, it was found that the development of a cold CO_2 release nozzle, which was thought to be a breakthrough technology to realize the COSMOS proposed in 1998, was not necessarily easy. Moreover, the last *in situ* experiment and the numerical simulation for a CO_2 slurry mass release suggest that the release of CO_2 as slurry mass was much easier than cold liquid CO_2 release. Then the authors proposed a new COSMOS in which CO_2 transported by a CO_2 carrier is released as slurry masses into 200 meters depth.

The new COSMOS has several advantages compared to the original COSMOS and other CO_2 ocean sequestration methods proposed so far. That is, the new COSMOS is easy to realize and requires low initial and running costs. And when applying the new COSMOS to the dissolution method, the full depth from the ocean floor to the phase change boundary can be utilized for the dissolution field, which results in the lowest CO_2 concentration.

Acknowledgement

This work was done as a part of COSMOS Project supported by an International Research Grant from the NEDO (New Energy and Industrial Technology Development Organization). The authors wish

to express their sincere gratitude to Drs. P. G. Brewer and E. T. Peltzer of the MBARI for the successful joint *in situ* experiments and three COSMOS project members, Profs. B. Kvamme, T. Johannessen and P. M. Haugan of University of Bergen for their useful comments on the design of new CO_2 release nozzle.

References

1. Machetti, C., *Climate Change*, 1977, p.59-68.
2. NEDO Report, NEDO-GET-9407 (in Japanese), 1995, p.200.
3. Ohsumi, T., *Institute of Applied Energy*, **19- 4**, 1997, p.45-54.
4. Aya, I.; Yamane, K., 17th Mtg. of UJNR/MFP, 1991, p.273-279.
5. Aya, I.; Yamane, K.; Yamada, N., 1st Int. Conf. on Offshore and Polar Engineering (ISOPE-91), 1991, p.427-432.
6. Aya, I.; Yamane, K.; Yamada, N., ASME 1992 Winter Annual Mtg., HTD-Vol.215, Fundamentals of Phase Change: Freezing, Melting and Sublimation, 1992, p.17-22.
7. Aya, I., 2nd Int. Workshop on Interaction between CO_2 and Ocean, 1993, p.233-238.
8. Aya, I.; Yamane, K.; Yamada, N., Int. Symposium on CO_2 Fixation and Efficient Utilization of Energy, 1993, p.351-360.
9. Aya, I.; Yamane, K.; Yamada, N., *Energy Convers. Mgmt.* **36**, 6-9, 1995, p.485-488.
10. Aya, I.; Yamane, K.; Nariai, H., *Energy-Int. Journal*, 22, 2/3, 1997, p.263-271.
11. Yamane, K.; Aya, I.; Nariai, H., 2nd ISOPE Mining Symposium, 1997, p.154-158.
12. Yamane, K.; Aya, I.; Namie, S.; Nariai, H., Greenhouse Gas Control Tech., Pergamon, Proc. of GHGT-4, 1998, p.1069-1071.
13. Yamane, K.; Aya, I.; Namie, S.; Nariai, H., *Annals of New York Academy of Science*, 2000, p.254-260.
14. Aya, I.; Yamane, K.; Kojima, R, Greenhouse Gas Control Tech., GHGT-5, CISRO, 2001, p.423-428.
15. Aya, I.; Yamane, K.; Kojima, R.; Nariai, H., *ditto*, p.492-498.
16. Aya, I.; Yamane, K.; Shiozaki, K., Greenhouse Gas Control Tech., Pergamon, Proc. of GHGT-4, 1998, p.269-274.
17. Aya, I.; Yamane, K.; Shiozaki, K., 22nd Mtg. of UJNR /MFP, 1998, p.152-157.
18. Kvamme, B.; Aya, I.; Johannessen, T.; Haugan, P. M., NEDO Int. Joint Res. Grant, Ind. Tech. Dep., NEDO, 2000, p.119-120.
19. Aya, I.; Yamane, K.; Kojima, R.; Brewer, P. G.; Peltzer, E. T., 23rd UJNR/MFP, 2, 2000.
20. Schlichting, H., Boundary Layer Theory, McGraw Hill, 1955, p.439.
21. Kvamme, B., Greenhouse Gas Control Tech., GHGT-5, CISRO 2001, p.435-439.
22. Yamane, K.; Aya, I.; Kojima, R.; K. Shiozaki, K., 1st Mtg. of Maritime Res. Inst., 39, 2001, p.177-180.
23. Aya, I.; Yamane, K., *Techno Marine*, **846** (in Japanese), 1999, p.890-894.
24. Kvamme, B., Proc. of 11th Int. Offshore and Polar Eng. Conf. (ISOPE-2001), 1, 2001, p.498-505.

A PROTOCOL FOR DETECTION OF SURFACE LEAKAGE FROM A CO_2 INJECTION PROJECT

Ronald W. Klusman

Dept. of Chemistry and Geochemistry
Colorado School of Mines
Golden, CO 80401

Introduction

The success of CO_2 sequestration by deep injection in geologic formations is dependent on the seals and aquitards being able to confine the large amount of fluid injected under overpressured conditions. The possibility for relatively rapid vertical transport of a buoyant phase increases with overpressuring of a reservoir during the injection process. The Rangely, Colorado field has been undergoing large-scale CO_2 injection since 1986 for purposes of enhanced oil recovery (EOR). Cumulative CO_2 injection has been 27.4 billion cubic meters (BCM), of which 11.3 BCM is new, the remainder being recycled gas from production wells.

This report is on methods to detect diffuse surface leakage of gases at the surface. A protocol for the detection of a deep source of gases in the presence of a large amount of surface and near-surface biological production of gases requires a thorough understanding of the noise being generated in the shallow parts of the system and processes influencing soil gas exchange with the atmosphere.

Experimental

Measurements of CO_2, CH_4 and light alkanes at 30-, 60-, and 100 cm in soil gas, and as fluxes into the atmosphere were made in the winter of 2000-01 and summer of 2001, and will continue in the winter of 2001-02. The measurements were at 67 locations over the Rangely field, a background area, and a major fault adjacent to the field. The measurements of CO_2 concentrations for flux calculations were made at each location by field infrared spectroscopy on circulating air from under three closed 1.00 m^2 flux chambers set 10 m apart. Methane from under the flux chambers and soil gas CH_4, CO_2, and light alkanes were analyzed by laboratory gas chromatography. Stable carbon isotope ratios were measured in CO_2 from soil gas and flux chamber samples by isotope ratio mass spectrometry.

Additional measurements were made of soil moisture and temperature, air temperature and barometric pressure, gas permeability of soils and subsoils, stable carbon isotope ratios of various solid and gaseous samples. Five "deep" holes were augered for nested sampling of gases at depths of 1-, 2-, 3-, 5-, and total depth, which ranged from seven to nine meters.

Results and Discussion

The summer fluxes of CO_2 from the soil to the atmosphere had a median of 3.8 g CO_2 m^{-2} day^{-1} and CH_4 fluxes had a median of 0.46 mg m^{-2} day^{-1}, with soil microbiological production/consumption dominating as indicated by stable isotopes. The preliminary winter measurements in 2000/2001 averaged 0.2 g CO_2 m^{-2} day^{-1} and 0.1 mg CH_4 m^{-2} day^{-1}, respectively. These data are summarized in Table 1 where means are shown, and also medians for highly skewed data.

Seasonal variation in both CO_2 and CH_4 fluxes, and in shallow soil gas samples was the largest source of variation. Summer CO_2 fluxes were at least a factor of ten greater than winter fluxes at Rangely, due to rise and fall of root respiration and soil microbiological activity. Methane fluxes were largely influenced by rise and fall of methanotrophic activity, which can consume CH_4 from a subsurface source, and/or from the atmosphere, which then results in negative (downward) fluxes.

Soil gas CO_2 concentrations vary by about a factor of three from summer to winter. Soil gas CH_4 showed little variation from atmospheric concentration, except in a few locations. The stable carbon isotopic data exhibited slight negative values during the winter, suggesting a small, but dominating biological influence on soil CO_2. The atmospheric influence was reduced in the winter of 2000/01 because the soils had some snow cover, and were frozen to at least 30 cm depth. The summer stable carbon isotope data were very close to atmospheric ratios, suggesting an effective exchange with the atmosphere through dry, porous soils.

Two of three "deep" holes over the Rangely field had high CH_4 and alkane concentrations suggesting a deep source of these gases. One of the holes over the field, the single hole over background and the single hole over the Mellen Hill Fault indicated methanotrophic activity consuming atmospheric CH_4.

Short-term noise related to precipitation events, time-of-day measurements, and barometric variation also occurred. In a dry climate, a precipitation event will cause a burst in soil microbiological activity, increasing flux, and shifting stable carbon and oxygen isotopic ratios to more negative values. Barometric gradients exert a significant influence on flux magnitude, resulting in an increased upward flux with falling pressure.

Table 2 illustrates parameters where significant differences were found among the on-field, background, and fault locations for the summer of 2001.

Conclusions

Some evidence of a small magnitude deep source was indicated at Rangely by stable isotopes, and supported by the presence of light alkanes in shallow soil gas over the field, and their absence in a background area of similar surface geology, soils, and climate. Detection of a low intensity, deep diffuse signal requires special care in selection of the parameters to be measured. Faults may serve as conduits for leakage and should also be monitored. The best time for making flux and soil gas measurements will be under winter conditions, when soil respiration and microbiological activity is at a minimum, possibly allowing a deep-source signal to be detected.

Acknowledgement. Financial support provided by Department of Energy, under the "Climate Change Technology Initiative," Grant DE-FG03-00ER15090 to the Colorado School of Mines.

Table 1. Summary of Seasonal Variations in Key Parameters.

	Winter 2000/01 Mean (Median)	Summer 2001 Mean (Median)
CO_2 Flux (g $m^{-2}day^{-1}$)	0.23 (0.19)	3.80 (3.02)
CH_4 Flux (mg $m^{-2}day^{-1}$)	0.10 (-0.18)	3.59 (0.46)
30 cm CO_2 (ppmv)	518.	1091.
60 cm CO_2 (ppmv)	621.	2043.
100 cm CO_2 (ppmv)	836.	2751.
30 cm CH_4 (ppmv)	1.98	32.1(2.39)
60 cm CH_4 (ppmv)	2.03	404.(2.49)
100 cm CH_4 (ppmv)	2.29.	1925.(2.61)
Chamber $\delta^{13}C_{CO2}$-Atm. $\delta^{13}C_{CO2}$(‰)	-0.67	-0.03
30 cm $\delta^{13}C_{CO2}$-Atm. $\delta^{13}C_{CO2}$(‰)	-1.92	+0.02
60 cm $\delta^{13}C_{CO2}$-Atm. $\delta^{13}C_{CO2}$(‰)	-1.58	+0.26
100 cm $\delta^{13}C_{CO2}$-Atm. $\delta^{13}C_{CO2}$(‰)	-1.78	+0.23

Table 2. Non-Parametric Two Group Median Test.

	Background Area	Mellen Hill Fault
CO_2 Flux	-	NA
CH_4 Flux	-	NA
30 cm CO_2	*	*
60 cm CO_2	-	-
100 cm CO_2	-	-
30 cm $\delta^{13}C_{CO2}$	-	* Fault
60 cm $\delta^{13}C_{CO2}$	-	** More
100 cm $\delta^{13}C_{CO2}$	*	* Negative
30 cm CH_4	** On-Field	-
60 cm CH_4	** Highest	-
100 cm CH_4	*	-

NA - Only two flux measurements on Mellen Hill Fault
- Not significant
* Significant at α=0.05
** Significant at α=0.01

Recent advances in deep-sea CO_2 sequestration experiments.

Edward T. Peltzer, Peter G. Brewer, Rachel M. Dunk, Jon Erickson, Gregor Rehder and Peter Walz.

Monterey Bay Aquarium Research Institute
7700 Sandholdt Road,
Moss Landing, CA 95039-9644.

Introduction

Over the last five years, we have developed and refined techniques for the precise and controlled release of small quantities (0.5-7L) of liquid CO_2 in the deep ocean using MBARI's advanced remotely operated vehicle (ROV) technology. We have used this technology to pursue fundamental chemical, physical, and biological studies associated with ocean CO_2 sequestration. This technology was designed to allow us to conduct experiments mimicking some of the many ocean CO_2 sequestration processes which have been proposed, such as those summarized by Hanisch[1]. Notably, we wanted to observe and test ideas concerning CO_2 behavior during releases in the mid-water (400m to 2000m), to mimic plumes of CO_2 that might arise from CO_2 released from shallow pipelines or pipes towed from tankers, and in the deep-sea (>3000m), where liquid CO_2 is denser than the surrounding seawater and the experiments are gravitationally stable. We report here the development of a 56L accumulator system, capable of delivering 42-46L of liquid CO_2 at 3600m depth, constructed of carbon fiber composite, for meso-scale studies. This represents the size and weight limit possible with current MBARI ROV technology.

Subsequently, we have completed a series of experiments in Monterey Bay using this technology. We have used this system for new observations of the fate of liquid CO_2 on the sea floor at depths >3000m. We have used a time lapse camera to image the fate of ~16L of liquid CO_2 in a 50cm diameter corral at 3600m depth; where dissolution was complete in 14 days. We have observed *in situ* the pH of a pocket formed in the liquid CO_2 surface film, and migration of CO_2 saturated water into the sediments with massive hydrate formation following.

Experimental

Technology Development. Our initial device consisted of two hydraulic cylinders mechanically connected in tandem. One cylinder was controlled using the hydraulic system on the ROV. When this device was activated, its ram would move the piston in the other cylinder and expel the liquid CO_2 contained therein. Although the capacity was small (0.5L), use of this device did allow us to conduct our earliest experiments and to gather needed experience with handling, transferring and deploying liquid CO_2 in the ocean from an ROV[2]. However, the small capacity of this system quickly proved to be limiting on both the size and duration of the experiments we could undertake, so we developed a larger CO_2 delivery system that employed a steel, 9L piston accumulator as the liquid CO_2 reservoir. A tandem cylinder pump was used to force seawater into one side of the piston accumulator. This pumping action served to drive the internal piston and expel liquid CO_2 from the other end. The use of these pumps freed us from the volume restrictions imposed by the size of the ROV hydraulic system reservoir and also served to provide us with a precise volume measurement of the amount of liquid CO_2 dispensed. This device served us well for both our first benthic CO_2 release study[3], and subsequent droplet experiments at mid-water depths[4].

The desire to conduct experiments with volumes several times larger than the 9L capacity of our steel accumulator system, yet wanting to avoid wasting valuable ROV dive-time ferrying liquid CO_2 to the sea-floor, led us to develop a larger system limited only by the ROV payload capacity in terms of weight and size. This system consists of a carbon-fiber composite piston accumulator of 56L internal capacity constructed by Hydratech, Fresno, CA. At 23 cm outside diameter and 194 cm length, it is close to the largest object the ROV can contain within the tool-sled. Yet the use of a carbon-fiber reinforced fiberglass composite for construction of the accumulator barrel provided sufficient strength (3000 psig rating) at a fraction of the weight of a steel cylinder of comparable size.

Tandem cylinder pumps were used to actuate the 56L CO_2 accumulator as was done previously. In order to have both fine control of small volumes of liquid CO_2 dispensed, and the capacity to deliver larger volumes relatively quickly, we choose to use two tandem cylinder pumps: one of 128mL capacity and a second of 970mL capacity. The two pumps also provide a level of redundancy to successfully complete a CO_2 deployment should either of the tandem cylinder pumps fail to function during a dive.

Deep-sea Releases. We have now completed several release experiments using the 56L piston accumulator at depths of 3000m and deeper. Our initial attempt using this system was at a site 153km west of Moss Landing, CA, at a water depth of 3604m. We made several deployments of 10-20L aliquots of liquid CO_2 into plastic "corrals" made of 50cm, pipe cut to 12cm lengths (Figure 1). One of these corrals occupied the field of view of our deep-sea time-lapsed video camera so "continuous" observations could be made for several weeks. In addition, we repeated the beaker experiment[3] at this site. All told six delivery dives were made successfully.

Figure 1. A "corral" filled with liquid CO_2 at 3604m water depth and 1.55ºC. Notice that the strong surface tension precludes the liquid CO_2 from completely covering the bottom of the corral.

Our second series of CO_2 releases using the 56L accumulator system occurred at a site 100km southwest of Moss Landing, CA, with a water depth of 3322m. This time, 30cm deep corrals were used and the time-lapse video camera was deployed to make long-term observations. Additionally, an attempt to measure the surface strength of the hydrate skin was made. Only two delivery dives were made at this site. Both were successful and on the last we delivered the maximum theoretical volume of liquid CO_2 that could be contained within the CO_2 piston accumulator.

In all of these experiments, pH measurements were made near the liquid CO_2 seawater interface both inside the CO_2 containers (beakers and corrals) as well as outside the containers in ambient

seawater using a Sea-Bird SBE-18 pH probe (Figure 2). These pH measurements were made inside the containers by moving the pH probe with the ROV manipulator arm as well as several meters up-stream or down-stream of the corrals by relocating the ROV.

Figure 2. Sea-Bird pH probe (SBE-18) measuring ambient pH within a few cm of a pool of liquid CO_2 at 3604m depth.

Results

Unlike the smaller steel cylinder reservoirs which were easily filled with liquid CO_2, the carbon fiber composite cylinder required a different protocol to completely fill it with liquid CO_2. The steel cylinders can be easily cooled, either with flowing water or packed in ice, to facilitate the transfer of heat from the cylinder and condensation of liquid CO_2 inside. However, the carbon fiber composite does not allow this easy removal of heat, so the CO_2 has to be transferred as a cooled liquid and kept under pressure at all times. This required a delicate balancing of the CO_2 delivery into one side of the piston accumulator along with the venting of water from the other side. If the piston was allowed to move too quickly, or if the internal pressure of the system dropped below the vapor pressure of the liquid CO_2, then a gas pocket formed inside the accumulator and incomplete filling resulted.

Because of the compressibility of liquid CO_2, the volume of CO_2 delivered at-depth is dependent upon both the ambient PT conditions at-depth and the temperature and pressure of the liquid CO_2 at the time the accumulator is filled. The colder the liquid CO_2 is during the filling operation, the greater volume that will be available for release at depth. Theoretical delivery volumes for the 56L accumulator at two release depths are given in Table 1.

Table 1. Theoretical Delivery Volumes (L) for 56L Cylinder

Fill T (ºC) at 900 psig	3200m, 1.60ºC	3600m, 1.55ºC
12	46.7	46.1
16	45.0	44.4
20	42.8	42.2

Behavior of the liquid CO_2 released at depth varied from experiment to experiment and even between different corrals during the same experiment. The spontaneous over-flow of liquid CO_2 from a 4L beaker due to the rapid formation of CO_2-hydrate observed in our initial CO_2 deployment[3] during 1998 was not observed. However, other dramatic behavior was observed. At the 3604m site, CO_2 hydrate formed overnight within the sediment at one of the corrals creating a massive "frost-heave" (Figure 3), yet a similar corral nearby, showed no such behavior. The reason(s) for this stochastic behavior elude us, however it does suggest that minor changes in the conditions of deployment leads to different outcomes.

Figure 3. CO_2-hydrate frost heave that formed overnight.

The dissolution rate of the liquid CO_2 was measured in two separate experiments. In one, we observed the slow decrease in the level of the liquid CO_2 pool inside a corral using the time-lapse video camera system. From this change in volume across a fixed surface area a crude approximation of the CO_2 dissolution rate of 0.2 $\mu mol/cm^2/sec$ was made. In the second experiment, a pH probe was inserted about 10 cm into a pool of liquid CO_2. Because of the strong tensile strength of the CO_2 hydrate skin, the liquid CO_2 did not flood the trapped volume, but instead a well containing ambient seawater was formed. From the observed change in pH as a function of time a dissolution rate of 1.8 $\mu mol/cm^2/sec$ was calculated. There are obvious uncertainties in both of these determinations, but as first-approximations they may prove useful to guide future work on deep ocean CO_2 sequestration.

Conclusions

It is now possible to deploy up to 46L of liquid CO_2 from a single ROV dive to depths of 3000-4000m. From initial dissolution rate measurements, we can expect that small pools (50cm dia., 10-20cm depth) of liquid CO_2 will have lifetimes on the order of a few weeks. This lifetime is sufficient to meet the needs of various benthic biology and geochemistry experiments.

Acknowledgement. This work was supported by a grant to MBARI from the David and Lucille Packard foundation and a grant from the Department of Energy, DE-FC26-00NT40929.

References

(1) Hanisch, C. *Environ. Sci. Tech.*, **1998**, *32* (1), 20A-24A.
(2) Brewer, P. G., Orr, F. M., Friederich, G., Kvenvolden, K. A., Orange, D. A. *Energy Fuels*, **1998**, *12*, 183-188.
(3) Brewer, P. G., Friederich, G., Peltzer, E. T., Orr, F. M. *Science*, **1999**, *284*, 943-945.
(4) Peltzer, E. T., Brewer, P. G., Friederich, G., Rehder, G. Prepr. Pap. - *Am. Chem. Soc., Div. Fuel Chem.*, **2000**, *45* (4), 794-798.

RECOVERY AND RECYCLING OF CO_2 IN AN ENZYMATIC REACTOR

Anne Tremblay and Frédéric Dutil

CO_2 Solution inc.
1091 Pie-XI blvd.
Val-Bélair, Quebec, Canada G3K 1J9

Introduction

The carbon dioxide greenhouse question has led many researchers involved in a variety of fields to study the phenomenon. Kyoto Protocol, which will be ratified by most of developed country this year, is a mechanism that will reduce global GHG emissions by 5.2 % in 2012 compared to 1990 level.

In response to that issue, CO_2 Solution has developed a system that involved the use of a biological process for the transformation of CO_2 into harmless compound, bicarbonate. This transformation of CO_2, also called ionisation, is catalyzed in presence of an enzyme.

The challenges associated with the bioreactor operation were to optimize gas to liquid flow ratio, packing height, concentration of gas at inlet, and pH of the liquid phase. Those operational parameters were set for the highest enzyme activity. Furthermore, one of our main objectives was to determine the best way to recycle bicarbonate ions. Studies were oriented toward precipitation in the form of metal carbonate such as calcite, magnesite, etc.

Over the past several years, the concept of employing an enzyme-based reactor to reduce CO_2 levels in many environments was successfully demonstrated. Results on CO_2 removal and beneficial reuse are presented in this document.

Experimental

Bioreactor system. The bioreactor is a packed column with enzyme immobilized onto the packing material. A packed column design was adopted since it enables an optimal contact area between gas, liquid and solid (the packing material with immobilized enzymes) phases. In this bioreactor, a gas containing CO_2 will enter the bioreactor and contact the liquid phase that will absorb the CO_2 stream. Immobilized enzyme will transform aqueous CO_2 into H^+ and HCO_3^-. A schematic representation of the bioreactor is presented in **Figure 1**.

Experimental conditions. Different operating conditions were tested with the bioreactor. When the notation "with enzyme" is used, the packing used has active enzyme bonded and immobilized to its surface. A packing "without enzyme" is one with all of the treatment for immobilisation but no enzyme on its surface.

All tests were conducted with an inlet gas concentration of approximately 5000 ppm CO_2, a Tris solution adjusted to a pH of 8.3 with H_2SO_4, a packing height of 15 cm and a gas flow of 0.064 kg/h. The effect of the variation of some of these parameters on the reaction rate of ionisation were studied: liquid/gas flow ratio, packing height and concentration of gas at inlet.

Precipitation of bicarbonate. Ions produced in the chemical reactions were concentrated with an anionic resin. Bicarbonate ions were then precipitated by the addition of dissolved cations. pH was varied by adding NaOH 2N. Solids were recovered by centrifugation or filtration through 0.4 µm filters and dried at 90°C. Solutions of 0.1 M $CaCl_2$ and $BaCl_2$ and dissolved synthetic sea salt (38 g/l) were used to precipitate bicarbonate ions. Glassware were used to limit solids adsorption. Essays were done in batch with 0.1 M $NaHCO_3$ to simulate bicarbonate concentration coming from an anion resin regenerating phase (after the bioreactor).

Analysis. Mineral identification was performed on few samples by electronic microscopy, X-rays diffraction and fluorescence. Metal concentration analysis were obtained by atomic absorption.

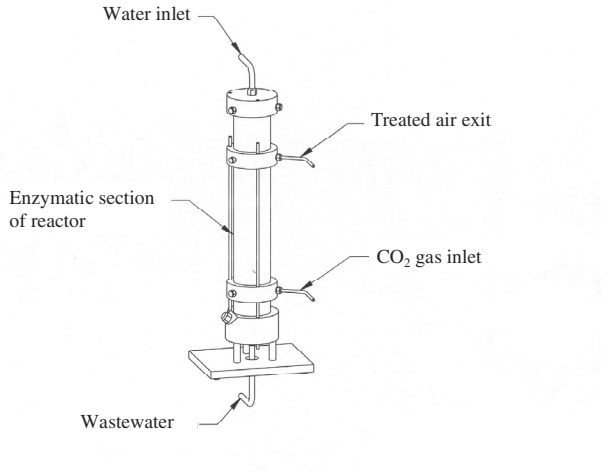

Figure 1. Schematic representation of the laboratory scale bioreactor.

Results and Discussion

Bioreactor optimization. Optimization of inherent parameters of the bioreactor allowed the determination of optimal operational conditions.

CO_2 ionisation rate in relation to packing (with or without enzyme) and liquid loading rate is presented in **Figure 2.** It shows that transformation rate rises when liquid to gas flow ratio (L/V) is increased. The major drawback of amplifying L/V is a higher liquid consumption and, thus, energy need. When calculating the improvement, in percentage, of the transformation rate when using enzyme compared to no enzyme, a lower L/V is better. For example, at a liquid loading rate of 6,500 kg/h.m^2 the improvement is 51 % compared to 39 % at 26,000 kg/h.m^2. A low L/V presents, hence, the best flow condition for a optimized operation.

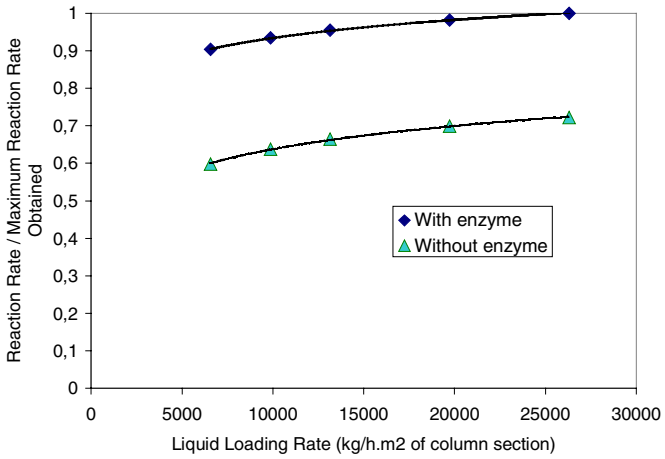

Figure 2. CO_2 ionisation rate in relation to packing (with or without enzyme) and liquid loading rate.

An increase in packing height shows a proportional rise in CO_2 transformation rate, the packing with enzyme being higher. Increasing CO_2 gas concentrations inlet from 1,000 ppm to 10,000 ppm has little influence on the reactor efficiency.

Finally, varying pH of the liquid media increased the CO_2 transformation in bicarbonate and subsequently in carbonate ions. A

few essays have demonstrated that fact (pH 6.5 to 10 increased slightly the global CO_2 removal efficiency). A numerical model predicted that pH over 11 will maximize CO_2 removal. But, to maintain a so high pH you must add chemicals and you may lose enzyme efficiency.

Globally, in the conditions tested, packing efficiency is 52 % more efficient than a packing without enzyme.

Precipitation of bicarbonate. Our first essays to precipitate calcite have demonstrated that mixing a source of carbonate and calcium ions ($CaCl_2$ + $NaHCO_3$ + NaOH) results in the formation of orthorhombic calcite crystals (diameter of about 5 µm; **Figure 3**).

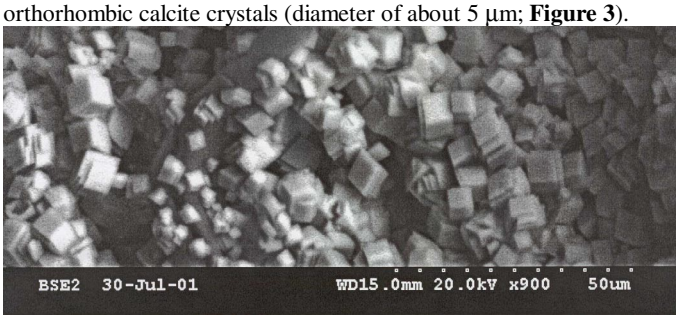

Figure 3. Electronic microscopy picture of calcite crystals.

Other essays have being done to study pH variation effect. **Figure 4** shows that the maximum weight that can precipitate is achieved at a pH as low as 8.

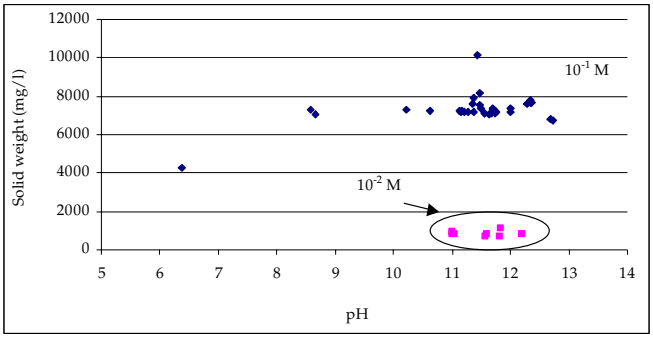

Figure 4. Relationship with calcite precipitation and pH (10^{-1} M and 10^{-2} M).

A chemical equilibrium model also predicted that calcite formation is optimal at pH 7 to 8 at operating conditions (**Figure 5**).

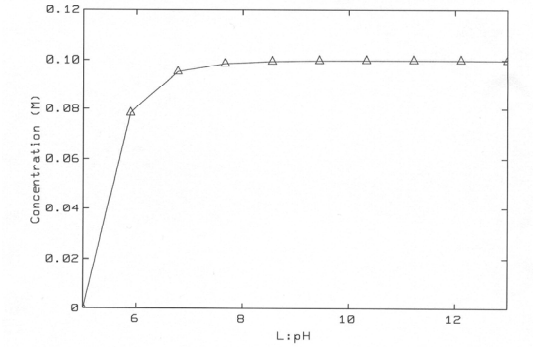

Figure 5. Relationship between calcite precipitation and pH.

However, a difference between theory (9.2 g/l of calcite attended) and experimental results (7.7 g/l ± 0.09) of 16 % is still remaining. One hypothesis to this difference is that a constant equilibrium is happening between the sample surface and atmosphere. Each time we shake the bottle to homogenize the sample, effervescence occurred, so CO_2 must be stripping in air. A mass balance study could confirm this hypothesis and will be realized on other essays.

A few experiments were done to precipitate witherite ($BaCO_3$), presented in **Figure 6**. Solid weight was about 18 g/l, either at pH 8 and 12, at an initial concentration of 0.1 M of both Ba and carbonate. There was no such significant difference with theory (19 g/l). Witherite is probably more stable than calcite (solubility product of 2.58E-9 and 3.36E-9 respectively).

Precipitation of bicarbonate ions with diluted synthetic sea salt was experimented in laboratory. For one sample, an electronic microscopy analysis has detected no crystals except an amorphous matrix. For another sample, in which we add $CaCl_2$ and sea salt to promote calcite precipitation, aragonite, a lesser stable form of calcium carbonate, and halite were detected.

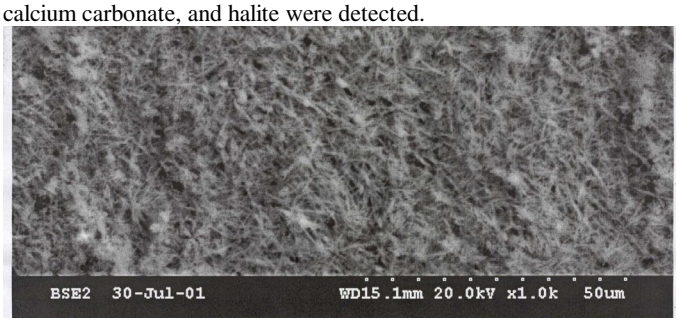

Figure 6. Electronic microscopy picture of whiterite crystals

Different pH (from 8 to 11) were tested for the precipitation of bicarbonate ions with sea salt. The results showed that at pH lower than 9.5 nothing really precipitate, and global solid weight increased with pH up to 11. The model predicted that calcite should mainly precipitate at pH higher than 11. Below that, dolomite ($CaMgCO_3$), $CaSO_{4(aq)}$ and Ca^{2+} are dominating species. More experiments will be done at pH 12 to verify this assumption.

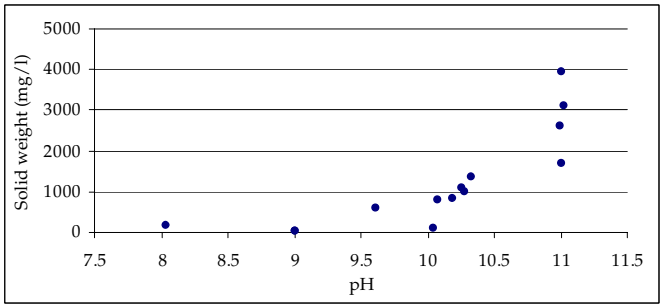

Figure 7. Relationship between precipitate weight and pH (sea salt).

Conclusions

CO_2 gas transformation in bicarbonate was realized in an enzymatic bioreactor. Bicarbonate ions are concentrated on an anionic resin, and subsequently precipitated with Ca - calcite, Ba – witherite and sea salt. Experiments have shown that precipitate weights are optimal at pH 8 for calcite and witherite minerals. On the opposite, solid weight of precipitates obtained with diluted sea salt is increasing with pH.

References

1. Khalifah, R.G. The Carbon Dioxide Hydration Activity of Carbonic Anhydrase. *J. Biol. Chem*. **1971** *(246)* 2561.
2. Steiner, H., B.-H. Jonsson and S. Lindskog. The Catalytic Mechanism of Carbonic Anhydrase. *Eur. J. Biochem*. **1975** (*59)* 253.

REDUCTION OF CO_2 TO C_1 PRODUCTS AND FUEL

Theodore Mill
SRI
Menlo Park, CA 94025

David Ross
U.S Geological Survey
Menlo Park, Ca 94025

Introduction

The combustion-based production of CO_2 has led to a major international environmental challenge to deal with global climate warming produced by atmospheric CO_2[1]. Global warming is projected to lead to disastrous consequences for most of the low-lying areas of the world[2]. The 1997 Kyoto Treaty to curtail CO_2 emissions includes collection and storage of a significant fraction of the 24 billion tons of CO_2 produced worldwide each year using depleted oil/gas reservoirs, deep saline aquifers, coal beds, and the deep ocean[3].

Sequestering CO_2 is a rational solution to reducing emissions , but a potentially more rewarding route to CO_2 reduction is to use chemical energy available from sunlight-driven semiconductors or from thermally promoted reduction with Fe(II) minerals to convert CO_2 back to C_1 products and fuel; in both cases, water serves as the hydrogen source.

Photoreduction of CO_2

Reduction of CO_2 to a variety of C_1 products using ZnO and $TiO_2$was reported in the early 1980s, but efficiencies generally were low (<5%)[4]. Reduction of CO_2 is effected by a photo-promoted electron with concomitant oxidation of water (Reactions [1] and [2]) by the valence band hole[5]. Generally, reduction efficiencies using bulk semiconductor particles are low. However, Q-ZnS nanoparticles in isopropyl alcohol, gave reduction efficiencies of over 20%[6].

$$CO_2 + 2e^- + 2H \longrightarrow HCO_2H \text{ (conduct band)} \quad (1)$$

$$2H_2O \longrightarrow 4H^+ + O_2 + 2\,e^- \text{ (hole)} \quad (2)$$

Reduction of CO_2 by several other materials, including GaP, WO_3, CdS, $LiNbO_3$, and several doped TiO_2 semiconductors has also been reported[7-12]. The band gap of TiO_2 of ~3.7 eV means that onset of UV absorption is near 360 nm, thus excluding the major fraction of energetic solar photons.

Hematite (Fe_2O_3) has a band gap of about 2.2 eV, thus extending the spectral range of sunlight that can be captured to about 550 nm[13]. The oxidation/reduction potentials are sufficient for Reactions (1) and (2), but electron hole recombination is fast and the reported efficiency of hematite for oxidation of water is low[14]. Nanometer particle films of hematite gave improved efficiency[15].

Ohta and coworkers[16] effected reduction of CO_2 to formate by solar irradiation of rocks containing hematite. Reduction of CO_2 using $CaFe_2O_4$ to methanol and formaldehyde is reported[17].

A variety of C_1 and C_2 products form on reduction of CO_2 depending on the semiconductor, wavelength, solvent polarity, and perhaps other factors[4]. In one case, the product changes from CO in water to formate in dichloromethane with isopropyl alcohol as the reducing agent. In propylene carbonate solvent, CO_2 reduction gave mostly methanol[18].

Thermal Reduction of CO_2

McCollom and coworkers[19-20] found that reaction of dissolved CO_2 with olivine in hydrothermal media, immediately gave formate at 300°C and 350 bar. Some experiments were conducted with no headspace possibly inhibiting further reduction to alkanes, a thermodynamically favored process.

When reduction was conducted with headspace, aqueous formate gave a broad array of Fischer-Tropsch-like products in the alkanes, alkenes, and oxygenated products, at 175°C. When headspace is available, further reduction of formate takes place in the gas phase through the molecular acid, probably on the reactor surfaces. Although no elemental balances were provided in the report, it is likely that the conversions proceeded through a series of highly exoergic formic acid disproportionations, like that in Reaction (3) for the formation of alkanes:

$$(3n+1)HCO_2H \longrightarrow (2n+1)CO_2 + C_nH_{2n+2} + 2n\,H_2O$$

Summary

Photochemical semiconductor processes readily reduce CO_2 to a broad range of C_1 products. However the intrinsic and solar efficiencies for the processes are low. Improved quantum efficiencies can be achieved using quantum-sized particles, but at the expense of using less of the visible solar spectrum. Conversely, semiconductors with small bandgaps utilize more of the visible solar spectrum at the expense of quantum efficiency.

Thermal reduction of CO_2 with Fe(II) is thermodynamically favored for forming many kinds of organic compounds and occurs readily with olivine and other Fe(II) minerals above 200° C to form higher alkanes and alkenes. No added hydrogen is required.

References

1. Stevens, W. K.. Seas and Soils Emerge as Keys to Climate, New York Times, May 16, 2000.
2. Revkin, A. Warming effects to be widespread. New York Times, June 12, 2000.
3. Noserale, D. News release, U.S. Geological Survey, October 22, 1999.
4. Yoneyama, H. Cat. Today **1997**, 39:169.
5. Hagfeldt, A. and Gratzel, M, Chem. Res. **1995**, 95**:**49.
6. Inoue, H., Torimoto, T. Sakata, T. Mori, H. and Yoneyama, H. Chem. Lett. **199**,1483.
7. Inoue, T., Fujishima, A. Konishi, S. and Honda. K. Nature **1979**, 277:637.
8. Aliwi, S. M., Al-Daghasteni. I. J. Solar Energy Res. **1989**, 7:49.
9. Ulman, M., Aurian-Bajeni, B. and Halmann, M. Isr. J. Chem. **1982**, 22:177.
10. Solymasi, F.,. Tombacy, I. Catal. Lett. **1994**, 27:61.

11. Goren, Z., Willner, I.. Nelson, A. J and. Frank, A. J J. Phys. Chem. **1990,** 94:3784.

12. Hoffman, M., Martin, S. T. Choi, W. and. Bahnemann, D. W Chem. Res. **1995**, 95:69.

13. Dare-Edwards, M. P., Goodenough, J. B. Hamnett, A. and Trevelick, P. R. J. Chem. Soc. Faraday Trans. 1 **1983**, 79:2027.

14. Kennedy, J. H., Frese, Jr., K. W. J. Electrochemical Soc. **1978**, 125:109.

15. Bjorksten, V., Moser, J. Gratzel, Chem. Mater. **1994,** 6:858.

16. Ohta, K., Ogawa, H. and Mizuno, T. Applied Geochemistry **2000,** 15:91.

17.Matsumoto, Y., Ohta, M. and Hombo, J. J. Phys. Chem. **1994**, 98:2950.

18. Liu, B.-J., Torimoto, T.. Matsumoto, H and Yoneyama, Y. Photochem. Photobiol. A **1997**,108:187.

19. McCollom, T. M. Presentation at First Astrobiology Science Conference, Ames Research Center, Mountain View, California, April 2-5, 2000.

20. McCollom, T. M., Ritter, G. and. Simoneit, B.R.T . Origins of Life and Evol. of the Biosphere **1999**, 29:153.

RIGOROUS DESIGN MODEL FOR CO_2 ABSORBER FITTED WITH STRUCTURED PACKING

Adisorn Aroonwilas[1] , Amornvadee Veawab[1], Amit Chakma[2], and Paitoon Tontiwachwuthikul[1]

[1]Faculty of Engineering, University of Regina
Regina, Saskatchewan, Canada S4S 0A2

[2]Department of Chemical Engineering, University of Waterloo
Waterloo, Ontario, Canada N2L 3G1

Introduction

The need to alleviate the problem of global warming has resulted in environmental concern over a reduction of greenhouse gas emissions from industrial sources. Carbon dioxide (CO_2), the largest contributor to the problem, is the major target for reduction. Under these circumstances, the removal of CO_2 from industrial waste gases, which would otherwise be vented to the atmosphere, becomes important. The CO_2 removal can be achieved by a number of separation techniques, of which the most suitable process approach for removing CO_2 from high-volume waste gas streams is an absorption into the liquid solvent.

The industrial use of structured packings for CO_2 absorption has not yet been reported in the open literature. However, the potential use of the packings has been investigated.[1,2] These studies confirmed that a column fitted with structured packings yields superior performance when compared to a column using random packings. With this excellent performance, taken together with the intense environmental concern over CO_2 reduction, future use of structured packings for CO_2 absorption is anticipated

Fundamental information on the mass-transfer characteristics of the packings is required to design a CO_2 absorption column packed with structured packings. A number of research studies have been focused on determining characteristics such as mass-transfer coefficient and effective mass-transfer area for various types of structured packings. However, these have been based primarily on fitting experimental data to empirical expressions. Use of such information is therefore limited to only that particular structured packing and application.

An understanding of fluid dynamics inside the packing elements is essentially required to fundamentally describe the mass-transfer performance of structured packings. Only a few mass-transfer models have been developed so far with regard to column dynamic information. This basically indicates that the models still lack full understanding of the fluid dynamics inside the packings. The present study therefore proposes a mechanistic concept that presents the fluid dynamic and mass-transfer behavior inside the structured packings used for CO_2 absorption.

Model development

The mechanistic concept was developed on the basis of liquid irrigation features through the packing elements, which can be determined from the details of the packing geometry. The concept was also based on an integration of a number of theoretical models, that aim to determine the distribution pattern of the flowing liquid inside the packing element, effective interfacial area, mass-transfer coefficients (based on penetration theory) and other information such as thermodynamic contributions (based on electrolyte NRTL model). A Fortran-90 computer program was written for the mechanistic concept in order to simulate the CO_2 absorption performance of columns packed with structured packings. The simulation was based on the theoretical packed column design procedure for adiabatic gas absorption with chemical reaction, which was first described by Pandya (1983). The procedure accounted for heats of absorption, solvent evaporation and condensation, chemical reactions in the liquid phase, and heat-and mass-transfer resistance in both gas and liquid phases. To execute the simulation, the developed computer program required a set of input information, including feed conditions of the gas and the liquid phases (i.e. compositions, temperature and flow rates), pattern of liquid irrigation from the distributor, number and arrangement of structured packing elements in the absorption column, and geometry of the packings.

Model simulation

Simulation results. The model simulation can generate the essential required information for the absorption system design including the concentrations of CO_2 in the gas phase, concentrations of reactants in the liquid phase, mass-transfer coefficients, and the effective interfacial area at different axial positions along the packed column. The patterns of the liquid irrigation inside the structured packing elements can also be provided as shown in Figure 1.

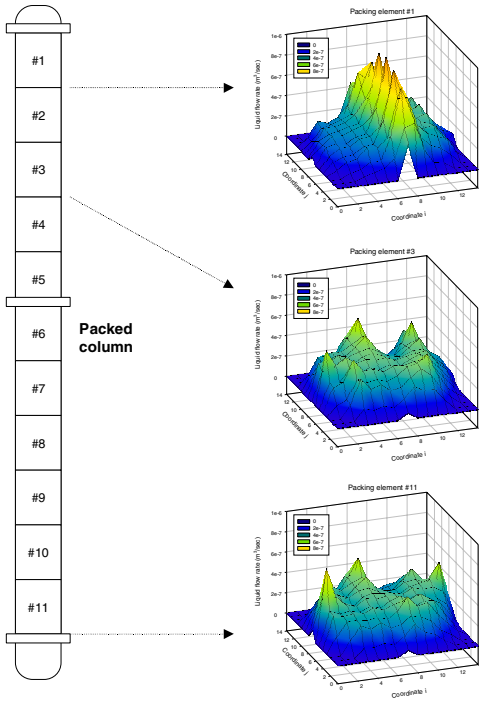

Figure 1. Examples of simulated liquid distribution plots.

Model verification. The verification of the developed concept was based on the prediction of mass-transfer performance in the CO_2-MEA absorption system. The simulation results were generally presented in terms of the gas-phase CO_2 concentration profiles along the absorption column, which were plotted against the experimental data for comparison purposes. The comparisons were made over the wide ranges of operating conditions where the thermodynamics contribution was significant in controlling the mass-transfer phenomena in the absorption system. Good agreement between the experimental and simulation results was found for all packings tested. An example of the result comparison is given in Figure 2.

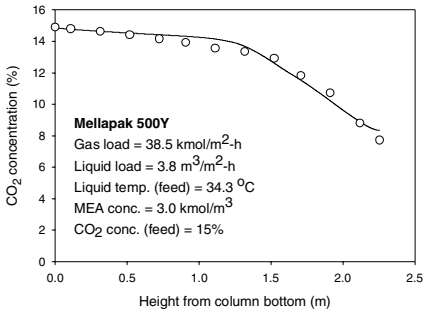

Figure 2. Comparison between the experimental (open circles) and simulated (solid lines) CO_2 concentration profiles.

Mass-transfer with different liquid loads. The liquid load was found from the simulation results that it has a significant effect on the performance of packed column. Higher liquid load enhances the CO_2 absorption efficiency due to an increasing interfacial area as evidenced by the simulation results in Figure 3.

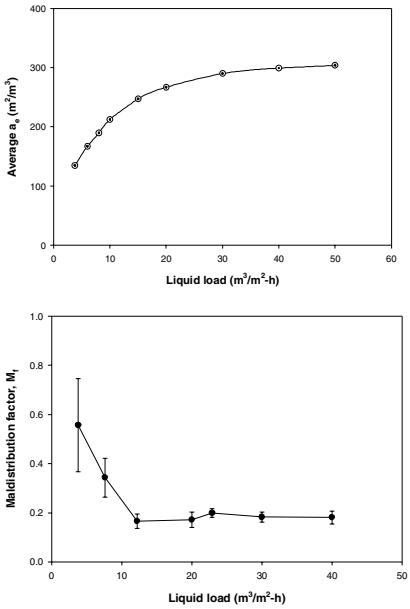

Figure 3. Simulated effective interfacial area plots of GemPak 4A structured packing (Top) and simulated maldistribution factor of Mellapak 500 Y (Bottom).

The increasing interfacial area with the liquid load is also evidenced by the quality of the liquid distribution illustrated in Figure 3. The higher maldistribution factor at the low liquid load indicates poor quality of the distribution, reflecting the lower degree of packing surface that takes part in facilitating the liquid to contact with the gas-phase. As the liquid load increases, the distribution quality is improved and the maldistribution decreases considerably. The lower maldistribution factor basically indicates a nearly uniform distribution, providing the greatest interfacial area for mass-transfer process.

Mass-transfer with different initial liquid distribution patterns. The quality of the initial liquid distribution from distributor is another important factor that has an effect on the mass-transfer performance of the packed column. Poor initial liquid distribution promotes the maldistribution phenomena, which can deteriorate the column efficiency. Figure 4 shows the simulated and experimental gas-phase CO_2 concentration profiles of the columns, operated with the two different initial liquid distribution patterns. It is apparent that the liquid distribution model well established the influence of the initial distribution on the mass-transfer performance of the column containing structured packing, i.e. the noticeable divergence between the two concentration profiles at the top packing element (element height of 0.245 m for Gempak 4A). The full-distribution pattern with the greater drip-point density generally gave higher CO_2 absorption performance than the 4H-distribution type. The lower effective interfacial area (a_e) is the primary cause of the lower absorption performance in the column with 4H-distribution.

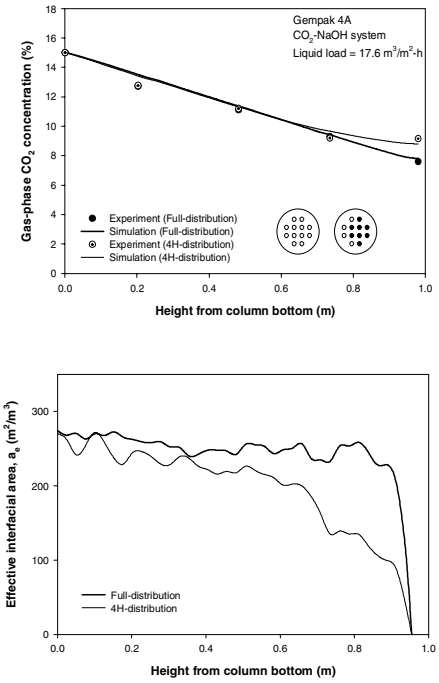

Figure 4. Gas-phase CO_2 concentration profiles based on two different initial liquid distribution patterns (Top) and their simulated effective areas.

Conclusion

The concept was developed on the basis of liquid irrigation features through the packing elements, which can be determined from the details of the packing geometry. The results of this research lead to a better understanding of the fluid dynamics within the columns fitted with structured packings. This can be used to design and simulate the CO_2 absorption process or even to optimize and customize the geometric features of new structured packings as they are developed to fit particular separation tasks.

References

1. Aroonwilas, A. (1996) High Efficiency Structured Packing for CO_2 Absorption Using 2-Amino-2-Methyl-1-Propanol (AMP): *M.A.Sc. Thesis*, University of Regina, regina, Saskatchewan, Canada.
2. Aroonwilas, A.; Veawab, A. and Tontiwachwuthikul, P. (1999) Behavior of Mass Transfer Coefficient of Structured Packings in CO_2 Absorbers with Chemical Reactions. *Industrial & Engineering Chemistry Research*. 38(5), 2044-2050.

Solid Amine CO_2 Capture Sorbents

M. L. Gray[1], Y. Soong[1], K. J. Champagne[1], R.W. Stevens, Jr.[2], P.Toochinda[2], and S. S. C. Chuang[2].

[1]US Department of Energy, National Energy Technology Laboratory, P.O. Box 10940, Pittsburgh, PA, 15236. Gray@NETL.DOE.GOV. (412) 386-4826, Fax (412) 386-4826.
[2]Chemical Engineering Department, University of Akron, Akron, OH, 44325-3906.

ABSTRACT
The capture of CO_2 from gas streams has been achieved by the utilization of amine- enriched, solid-sorbent systems. The initial solid sorbents were generated by the chemical treatment of carbon-enriched fly ash concentrates with various amine compounds. It was determined that these amine-enriched fly ash carbon concentrates performed at a 18 % CO_2 capture capacity based on commercially available sorbents. Alternative oxygen rich solids, such as, silica gel, activated carbon, and molecular sieves were examined as potential sorbents for the capture of CO_2 from gas streams. The chemical sorption performance of these solid amine sorbents will be described within this paper.

Keywords: carbon dioxide, capture, and amine sorbent

INTRODUCTION
The concentration of CO_2 in our atmosphere is promoted by the combustion of fossil fuels for the generation of electricity. Capturing CO_2 from flue-gas streams is an essential parameter for the carbon management for sequestrating of CO_2 from our environment. Current technologies[1] being considered for CO_2 sequestration include: disposal of CO_2 in deep oceans; depleted oil and gas fields; deep saline formations (aquifers); and recovery of enhanced oil, gas, and coal-bed methane. However, the current cost for the utilization of these types of technologies has proven to be too expensive. Consequently, reducing the cost for the capture of CO_2 will be a critical step in the overall carbon management program.

The physical and chemical adsorption of CO_2 can be achieved by using solvents, cryogenic techniques, membranes, and solid sorbents. The large-scale operation of these technologies is energy intensive when applied to capturing CO_2 in dilute stream, such as flue gas, which consist of 15% CO_2 by volume for most coal combustion systems. Amine-based, solvent-capture systems are the most energy efficient option, but are energy intensive due to the large amount of water needed in these system. Excessive water is required because of the corrosion and air flow problems created by the use of monoethanolamine (MEA), diethanolamine (DEA), or methyldiethanolamine (MDEA) in these aqueous-based, CO_2-capture systems. The proposed reaction sequences for using primary, secondary, and tertiary alkanolamines reacting with dissolve CO_2 are shown below.

Formation of the zwitterion ion:
(1) $R_1R_2NH + CO_2 \longleftrightarrow R_1R_2NH^+CO2^-$

Formation of amine carbamate:
(2) $R_1R_2NH + R_1R_2NH^+CO_2 \longleftrightarrow R_1R_2NH^+ + R_1R_2NCO_2^-$

Protonation of amine:
(3) $R_1R_2R_3N + H_2O + CO_2\ (aq) \longleftrightarrow R_1R_2R_3NH^+ HCO_3^-$

Solid-amine CO_2 sorbents should have similar reactions with airborne CO_2, water vapor, and the amine functional group on its surface. Consequently, these types of sorbents are being used in aircraft, submarine, and spacecraft technologies[2-4]. However, the cost of these sorbents is too expensive for large-scale applications in the utility industry. Consequently, the development of economical amine-enriched sorbents based on carbon fly ash and other oxygen rich sorbents will be discussed within this paper.

EXPERIMENTAL PROCEDURES
Samples--A fly ash containing 9.5% of unburned carbon was collected from the bag house of the 500-lbs/hr-combustion unit at the National Energy Technology Laboratory (NETL). The fly-ash sample examined in this study resulted from the combustion of a Pittsburgh-seam coal from the Black Creek mine. A column agglomeration process[5-6] developed at NETL was use for the collection of the unburned carbon samples.

The three alternative oxygen rich solid substrates that were examined as CO_2 capture sorbents were a silica gel (grade 3, 8 mesh) from Aldrich Chemical Company, a coal based activated carbon from Calgon Inc. and a 13X molecular sieve from Sud Chemie.

Amine Treatment Process--The actual conditions for incorporating the amine group into the structure of the unburned carbon samples will not be discussed in this paper due to pending patent applications.

CO_2 Capture Capacity--The chemical CO_2 capture capacities were determined by the combination of Diffuse Reflectance Infrared Transform Spectroscopy (DRIFTS) Temperature Programmed Desorption (TPD) and Mass Spectroscopy (MS) analyses. The physical adsorption of CO_2 was not analyzed due to the limitations of the experimental reactor systems. The detailed operating conditions for this procedure were previously described in the literature[7].

RESULTS AND DISCUSSION
Initially, the original fly-ash concentrates (95) were generated from the feed fly ash (59) by using the column agglomeration process. The amine treated carbon concentrates (95A, 95B, and 95C) were then examined as CO_2 capture sorbents. These samples were place in a $H_2O/CO_2/He$ stream and DRIFTS, TPD, and MS analyses determined the CO_2 capture capacity. The adsorption/desorption of CO_2 for these samples were determined over the temperature range of 25 –120 ^oC. Typical DRIFTS and TPD/MS spectra are shown in figures 1 and 2. According to the DRIFTS spectra, the formation of the corresponding carbamate-amine product was indicated by the presence of the two peaks at 1087 and 1148. The other major peaks at approximately 2380 are the physically adsorbed CO_2. The desorption of the CO_2 was observed as the temperature was increased to 120 ^oC. At this elevated temperature, the TPD/MS spectra indicates the mass numbers (m/e) for the desorption of CO_2 (m/e 44), H20 (m/e 18), O_2 (m/e 32) and CO or N_2 (m/e 28). The m/e value of 28 may be the decomposition of the surface amine compound or the breakdown of the carbamate amine product. If this is the decomposition of the surface amine compound, it will have a direct effect on the regenerable properties of these sorbents. The overall CO_2 capture capacities are summarized in Table 1.

Table 1: TPD CO_2 Desorption Data of Amine Treated Sorbents

Sample #	Treatment	μmol/g CO_2 Captured
59 Feed Fly Ash	None	24.4
95 Carbon	None	72.9
95 A Carbon	A	81.1
95 B Carbon	B	117.9
95 C Carbon	C	174.6
95C Carbon (rengenerated)	C	140.6

As shown in Table 1., the physical absorbed CO_2 in samples 59 and 95 increased with the amine chemical treatment. The best sample was 95C, which had the CO_2 capture capacity of 174.5 μmol/g, and was regenerable for an additional test (140.6 μmol/g). In comparison to commercially available sorbents with surface areas of 1000-1700 m^2/g and CO_2 capture capacities of 800-1000 μmol/g, the 95C was only able to achieve 18 % of the CO_2 capture capacity. However, the surface area of the 95C amine- enriched sorbent was only 27 m^2/g, which may account for its low CO_2 capture capacity.

Alternative oxygen-rich solid substrates tested as amine-enriched sorbents for the capture of CO_2 are summarized in Table2.

Amine Treated Samples	μmol/g CO_2 Captured	% CO_2 Capacity[1]
NETL Fly Ash	24.4	
Treated NETL Fly Ash	174.6	**615.5**
Silica Gel	4.9	
Treated Silica Gel	31.5	**531.2**
Calgon Activated Carbon	8.0	
Treated Calgon Activated Carbon	28.7	**258.7**
Sud Chemie Molecular Sieve 13X	13.6	
Treated Sud Chemie Molecular Sieve 13X	15.8	**16.1**

[1] the percentage sorbent capacity is the change of the treated support compared to the baseline support.

According to Table 2, this amine treatment can be successfully applied on a variety of oxygen rich solid substrates, such as, silica gels, activated carbons, and molecular sieves. The CO_2 capture capacities were improved for all of the solid substrates tested, however, their performance were lower then the initial NETL fly ash sample examined under these reaction conditions. It is also important to point out that our current CO_2 capture experimental procedures are based only on the chemical absorbed species; physical absorbed CO_2 is purged from the surface prior to the desorption stage. Consequently, additional work is required to refine the experimental procedures (include the physical absorbed CO_2) and to increase capture capacities to the range of 800-1000 μmol/g, which will make them competitive with existing technology. Presently, additional materials with higher surface areas are being treated with this amine process and will be reported in future publications.

CONCLUSION

The amine treatment process was successful in improving the CO_2 capture capacities of these fly-ash carbon concentrates and oxygen rich solid substrates. However, the performance of the regenerable sorbents was only able to reach 18 % of the required CO_2 capture capacity to make them competitive with the existing CO_2 sorbents. Alternative low-cost, high surface oxygen-rich solid substrates and CO_2 capture procedures are being examined and will be reported in future publications.

REFERENCES

1. DOE Report Doe/ER-30194, "Research Needs Assessment for the Capture, Utilization and Disposal of Carbon Dioxide from Fossil Fuel-Fired Power Plants," 1993.
2. US Patent 4,810,266, Zinnen, H. A., Oroskar, A. R., and Chang, C. H."CO_2 Removal using Aminated Carbon Molecular Sieves," 1989.
3. US Patent 5,492,683, Bibara P.J., Naletta T. A. "Regenerable Support Amine Polyol Sorbent," 1996.
4. US Patent 5,876,488, Bibara P. J. Filburn T. P., Nalette T. A. "regenerable Solid Amine Sorbent," 1999.
5. US Patent 6,126,014, Gray, M. L., Champagne, K. J., and Finseth, D. H. "Continuous Air Agglomeration for High Carbon Fly Ash Benefication," 2000.
6. Gray, M. L., Champagne, K. J., Soong, Y., and Finseth, D. H. "Parametric Study of the Column Agglomeration of Fly Ash," Fuel, Vol. 80, pp. 867-871, 2001.
7. Soong, Y., Gray, M. L., Siriwardane, R. V., Champagne, K. J., Stevens, Jr., R. W., Toochinda, P., and Chuang, S. S. C. "Novel Amine Enriched Solid Sorbents for Carbon Dioxide Capture," Fuel preprint, 46 (1), pp. 285, 2001.

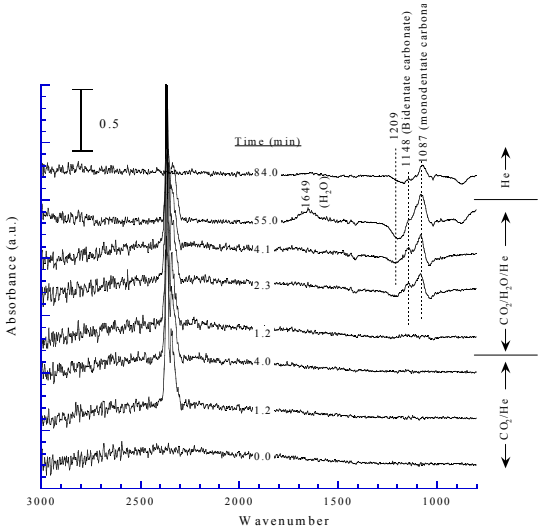

Figure 1: Typical DRIFTS CO2 absorption spectra for 95C

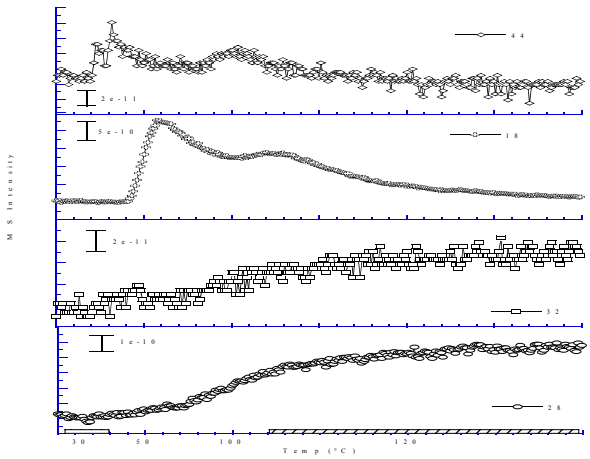

Figure 2: Typical TPD/MS spectra for 95C

A STUDY ON FACILITATED TRANSPORT MEMBRANES FOR REMOVAL OF CO_2 FROM CH_4

Ying Zhang, Zhi Wang, and Shichang Wang*

Chemical Engineering Research Center, School of Chemical Engineering and Technology, Tianjin University, Tianjin 300072, China

Introduction

The membrane separation for removal of carbon dioxide from natural gas has advantages over the conventional separation methods because of low capital, high-energy efficiency and the environmental friends. Usually, the commercially available polymeric membranes have either high permeability or high selectivity, but not both[1]. However, facilitated transport membranes (including supported liquid membranes (SLMs), ion-exchange membranes and fixed carrier membranes) selectively permeate CO_2 by means of the reversible reaction between CO_2 and the carriers in the membranes, so that they possess high permeability as well as high selectivity. The fixed carrier membranes are generally favorable compared with SLMs and ion-exchange membranes for their superior durability.

In recent years, the fixed carrier membranes, especially the CO_2 separation membranes with facilitated transport groups, amine moiety, have been investigated extensively[2-4].

We think it is more beneficial for the facilitated transport of CO_2 to introduce more kinds of carriers than one in a membrane. On the basis of this idea, we developed two kinds of membrane materials with second amine and carboxyl groups, the latter also acts as a carrier of CO_2, by the hydrolysis of polylvinylpyrrolidone(PVP) and vinyl pyrrolidone-acrylamide copolymer respectively. Then, the fixed carrier composite membranes with the materials for CO_2 separation were prepared.

Experimental

Materials. The PVP was synthesized through radical polymerization in 20% N-vinyl pyrrolidone aqueous solution by using azobisisobutyronitrile(AIBN) (it was twice recrystallized from ethanol) as the initiator at 60 °C in the inert atmosphere of nitrogen gas[5]. The PVP was hydrolyzed in an alkali solution at boiling temperature (scheme 1). The resulting polymer was precipitated by using acetone, then the polymer was dissolved in water. This aqueous solution was purified with ion-exchange resin to remove low-molecular-weight impurities and the purified polymer solution was used for membrane-casting.

The copolymer of N-Vinyl pyrrolidone and acrylamide(AAM) was prepared as the same method, but the reaction temperature is 50°C. The hydrolysis and treatment are as above (scheme 2).

Analysis. The content of active carriers (second amine and carboxyl groups) was measured by titration. The molecular weight of resulting polymer was roughly obtained from the intrinsic viscosity.

Membrane preparation and evaluation. The purified polymer solution was cast on a polysulfone(PS) support membrane by an applicator to form composite membrane. The gas permeation experiments were carried out by using a set of test cell. The effective area of the composite membrane used in the test cell is 19.26 cm^2. Prior to contacting the membrane, both the feed and the sweep (H_2) gases were passed through gas bubblers containing water. The outlet sweep gas composition was analyzed by a gas chromatography equipped with a thermal conductivity detector (HP4890, Porapak N). The fluxes of CO_2 and CH_4 were calculated from the sweep gas flow rate and its composition. The permeance is defined as the flux divided by the partial pressure difference between the upstream and downstream sides of the membrane, $R_i = N_i / \Delta P_i$, and the selectivity α was defined as the ratio of the CO_2 permeance to the CH_4 permeance. The downstream pressure in our apparatus is one atmosphere pressure.

Results and Discussion

Figures 1 and 2 show the effects of feed gas pressure on the performances of the membrane (membrane material was prepared by scheme 1). Both permeance of CO_2 and selectivity of CO_2/CH_4 decrease with the raising of feed pressure. This is the characteristic of the facilitated transport mechanism[6]. The facilitated transport mechanism with the carriers of second amine and carboxyl groups is as follow [6,7]:

$$RNH(CH_2)_3COO^- + 2H_2O + 2CO_2 \rightleftharpoons 2HCO_3^- + RNH_2^+(CH_2)_3COOH$$

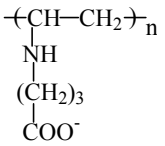

Scheme 1

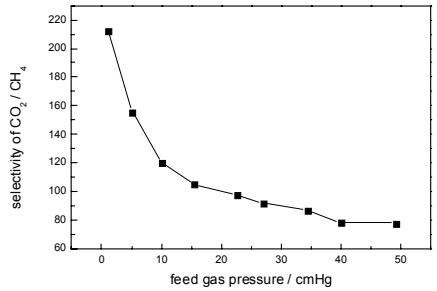

Figure 1. Effect of feed pressure on selectivity of CO_2 over CH_4 by using pure gases respectively.
Membrane material: scheme 1.Testing temperature: 27°C.

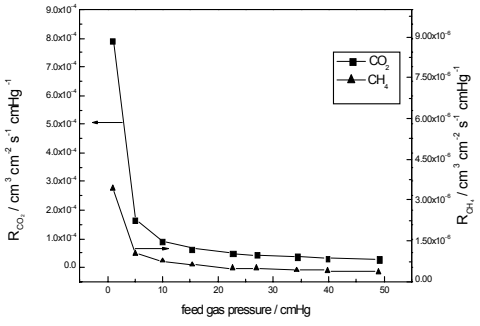

Figure 2. Effect of feed pressure on permeance by using pure gases respectively.
Membrane material: scheme 1.Testing temperature: 27°C.

CO_2 is transformed into small and easy moving ion HCO_3^-, therefore, the transport of CO_2 is enhanced by the carriers. From the standpoint of the membrane structure, the high polarity in the membrane diminishes the solubility of non-polarity component (CH_4),

this is helpful to increase the CO_2 permeation and the selectivity of CO_2 over CH_4. Furthermore, the membrane is swollen by water and forms gel. So that the diffusion coefficient is enhanced due to the decrement of movement resistance. As a result, the membrane possesses high CO_2 permeance and CO_2/CH_4 selectivity which are comparable with that of other fixed membranes in literatures[3,4].

Permeation of CH_4 is a simple solution-diffusion process. The permeance of CH_4 decreases with increasing pressure, in accordance with the "dual-mode" sorption model of gas permeation through glassy polymers [8].

The composite membrane performances were also investigated by using mixed gases (50/50 vol% CO_2/CH_4 mixture), as shown in **Figure 3** and **Figure 4**. From the Figures, it can be seen that the selectivity of CO_2 over CH_4 and permeance of CO_2 are not as good as in Figures 1 and 2. The reason may be the coupling effects between CO_2 and CH_4.

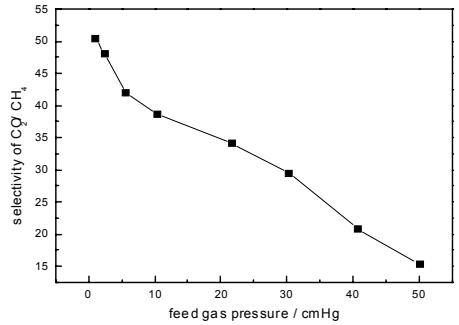

Figure 3. Effect of feed pressure on selectivity by using mixed gas. Membrane material: scheme 1.Testing temperature: 27°C. Feed gas: 50 vol% CO_2+50 vol% CH_4.

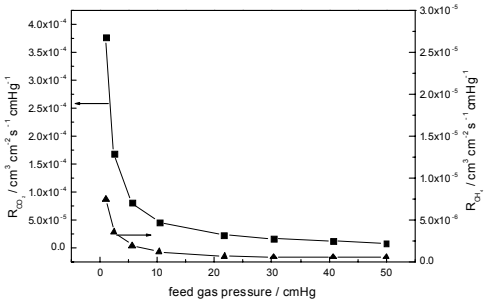

Figure 4. Effect of feed pressure on permeance by using mixed gas. Membrane material: scheme 1.Testing temperature: 27°C. Feed gas: 50 vol% CO_2+50 vol% CH_4.

The performances of the composite membrane which was prepared by scheme 2 were also investigated with mixed gas (50/50 vol% CO_2/CH_4 mixture), as shown in **Figure 5** and **Figure 6**. From the results, it can be seen that the membrane possesses better permselectiviy and it is accordance with the facilitated transport mechanism.

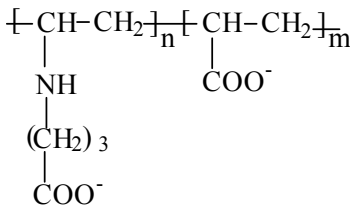

Scheme 2

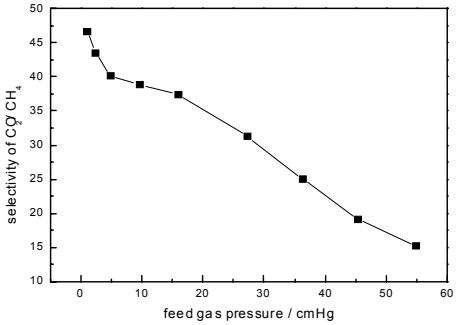

Figure 5. Effect of feed pressure on selectivity by using mixed gas. Membrane material: scheme 2. NVP: AAM =70:30(mass). Testing temperature: 20°C. Feed gas: 50 vol% CO_2+50 vol% CH_4

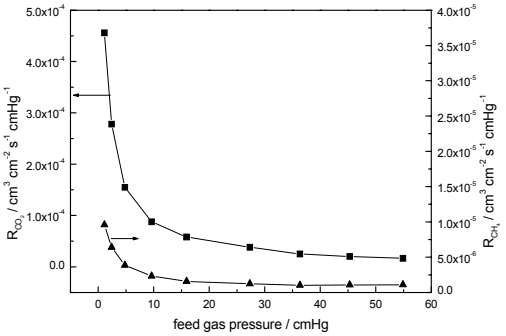

Figure 6. Effect of feed pressure on permeance by using mixed gas. Membrane material: scheme 2. NVP: AAM =70:30(mass). Testing temperature: 20°C. Feed gas: 50 vol% CO_2+50 vol% CH_4

Acknowledgement

This research is supported by the Natural Science Foundation of China (No.29976031, No.29876027), the Natural Science Foundation of Tianjin and the Foundation of Outstanding Teacher at University.

References

1. Robeson, L. M. *J. Membr. Sci*., **1991**, 62,165-185.
2. Wang, Z.; Zhen, H. F.; Li, B. A.; Ren, Y.; Wang, S. C. *J. Chem. Ind. & Eng (ch)*., **2000**, 51(6), 823-825.
3. Yoshikawa, M.; Fujimoto. K.; Kinugawa, H.; Kitao, T.; Ogata, N. *Chem. lett*., **1994,** 243-246.
4. Matsuyama, H.; Terada, A.; Nakagawara, T.; Kitamura, Y.; Teramoto, M. *J. Membr. Sci.,* **1999**, 163, 221-227.
5. Mathakiya, I.; Rakshit, A. K. *J. Appl. Polym. Sci*., **1998**, 68, 91-102.
6. Quinn, R.; Appleby, J. B.; Pez, G. P. *J. Membr. Sci.,* **1995,** 104, 139-146.
7. Matsuyama, H.; Teramoto, M.; Sakakura, H. *J. Membr. Sci.,* **1996**, 114, 193-200.
8. Houde, A. Y.; Krishnakumar, B.; Charati, S. G.; Stern, S. A. *J. Appl. Polym. Sci.,* **1996,** 62, 2181-2192.

Terrestrial Carbon Sequestration Potential

F. Blaine Metting[1], Gary K. Jacobs[2], Jeffrey S. Amthor[2] and Roger Dahlman[3]

Pacific Northwest National Laboratory[1], Oak Ridge National Laboratory[2], U.S. Department of Energy[3]

Introduction

Fossil fuel and land use change have increased the atmospheric content of CO_2 and other greenhouse gases that may be impacting climatic change. Enhanced terrestrial uptake of CO_2 during this century has been suggested as a way to reclaim the 150 or more gigatons of carbon (Gt C) lost to the atmosphere from vegetation and soil as a consequence of land use change, thus effectively "buying time" for development and implementation of long term technical solutions, such as C-free fuels (1). However, the true potential for C sequestration is unknown because of inadequate understanding of biogeochemical, microbial and plant processes responsible for ecosystem storage, particularly as they influence storage in soils, which account for two-thirds of global terrestrial organic C stocks. Technical issues associated with measurement, leakage and longevity need resolution. This presentation considers current understanding of ecosystem potential and innovative technology and addresses key scientific issues related to enhancing C sequestration potential through ecosystem management.

Ecosystem Sequestration Potential

Land use options for enhanced C sequestration at the landscape and regional scales include protection and selective management of native ecosystems, and use of appropriate and advanced management practices in manipulated ecosystems. Table 1 includes estimates of sequestration potential for major ecosystems. Sustained, long-term annual sequestration of more than 5 Gt C is speculative, of course, given that terrestrial systems today sequester only about half this amount, with the exact amount being uncertain (1).

Ecosystem	Primary Method to Increase CS*	Potential CS (GtC/y)
Agricultural lands	Management (H)	0.85 – 0.90
Biomass crop lands	Manipulation (H)	0.5 - 0.8
Grasslands	Management (M)	0.5
Rangelands	Management (M)	1.2
Forests	Management (M)	1 - 2
Wetlands	Restoration and maintenance (M)	0.1 – 0.2
Urban forest and grass lands	Creation and maintenance (M)	< 0.1
Deserts & Degraded lands	Manipulation (H)	0.8 – 1.3
Sediments and aquatic systems	Protection (L)	0.6 – 1.5
Tundra and taiga	Protection (L)	0.1 – 0.3
TOTAL		**~ 5.5 – 8.7**

Table I. Sustained Terrestrial C Sequestration Potential.
*The primary C sequestration method is rated with High (H), Medium (M), and Low (L) levels of sustained management intensity required over the long term. Global potential C sequestration (CS) rates were estimated that might be sustained over a period of up to 50 years (2).

Sequestration Potential In Managed Ecosystems

Enhancing terrestrial C sequestration with proven management practices includes converting marginal land to productive grassland or forest, increasing productivity on crop and forest land with residue management, reduced C loss with modified tillage practices, the efficient use of fertilizer, pesticide, and water, and other technologies. It is difficult to estimate global C sequestration enhancement potential because of inadequate baseline inventories. However, an analysis of the U.S. potential for soil C sequestration can be made (Table 2). Based on such information, conclusions regarding C sequestration potential of managed systems should be applicable wherever in the world local land use and economic conditions are known.

Table 2. Annual U.S. potential for C sequestration from managed forests, arable lands and pastures (2).

	Average C sequestration	
	Low estimate	High estimate
	--- Pg C / year ----	
Forestry		
Converting marginal crop/pasture to forest	0.033	0.119
Increasing timber growth on timber land	0.138	0.190
Growing short-rotation woody crops for energy	0.091	0.180
Increasing tree numbers/canopy cover in urban areas	0.011	0.034
Planting trees in shelter belts	0.003	0.006
Subtotal	0.276	0.529
Arable land		
Cropland conversion to CRP (excluding agroforestry)	0.006	0.014
Soil restoration (eroded land, mine land, salt affected soil)	0.011	0.025
Conservation tillage/residue management	0.035	0.107
Better cropping systems (fertilizer, cover crops, manure)	0.024	0.063
Subtotal	0.075	0.208
Total managed forests, arable land, pastures	0.351	0.737

Enhanced C sequestration in managed lands aims to increase the productivity of crop and forestland. In agriculture, adoption of conservation tillage practices is a viable mechanism that also reduces erosion, increases soil aggregation, and lessens loss of SOM to microbial oxidation (3). The C sequestration potential of the combined practices of no-till, mulch, and ridge tillage was estimated to be 14.1 x 10^6 MT (0.014 Gt) C/yr, with associated savings in fossil fuel equivalent to 1.6 x 10^6 MT C/yr. In addition, managing crop residues from these systems may sequester another 22.5 x 10^6 MT C/yr. As of 1997, 37% of all U.S. cropland was under some form of conservation tillage (3).

The U.S. Forest Service has estimated that 85 Mha of forested land has the potential to increase production through regeneration and stocking control. For an economic constraint of 4% annual return on investment, much of this area could sequester 0.138 Gt C/yr under appropriate management. If all timberlands were managed for C sequestration, the potential might increase to 0.19 Gt C/yr. Another strategy for sequestrating C is the conversion or reallocation of agricultural land to woody crops. Wright et al. (4) estimated that between 14-and-28 Mha of cropland are suitable for woody biomass species with a sequestration potential of between 0.09 to 0.18 Gt C/yr.

Worldwide, temperate grasslands may also be significant. To enhance production and sequestration, it is necessary to manage these lands more closely, with one option being N fertilization. However, grasslands have an inherent capacity to emit N_2O, a strong greenhouse gas. Thus, a comprehensive accounting that includes all greenhouse gas emissions and the C cost of fertilizer production and application is needed to evaluate net sequestration benefits.

Degraded lands also represent some potential for C sequestration. Worldwide, there are approximately 1965 x 10^6 ha of degraded soils;

4% from physical degradation, 56% from water erosion, 28% from wind erosion, and 12% from chemical degradation. With proper management this represents a potential to sequester between 0.81 and 1.03 Gt C/yr. (5).

New Technology for Terrestrial Carbon Sequestration

Science and technology that might drive enhanced terrestrial C sequestration includes (a) technology for soil, crop and forest management, (b) exploitation of underutilized land resources and existing biodiversity, (c) plant biotechnology, (d) microbial biotechnology, and (e) innovative chemical technology. Included is precision agriculture applied to food crops and forestry; i.e., sensor technology, aerial and satellite imaging "just in time" irrigation, fertilization, and other, yet-to-be identified innovations.

Science Needs

There are many fundamental knowledge gaps in our understanding of terrestrial C sequestration needed to identify, develop and implement new sequestration technology. Research efforts to improve basic understanding can be addressed in the context of a primary set of overarching questions in need of resolution:

- How can we best reduce the large uncertainties in global terrestrial C inventories?
- Are native ecosystem C sequestration capacities equivalent to their maximum carrying capacities?
- Is historic storage capacity of terrestrial systems equivalent to maximum inherent capacity?
- What will be the effects of climate change?
- How can ancillary benefits and risks of enhanced C sequestration be adequately quantified?
- What is the potential for plant and microbial biology in the post-genome era to impact C sequestration?

Summary

Storage of C in soils and plants has the potential to offset CO_2 emissions to the atmosphere in the coming decades while new "clean" energy production and CO_2 sequestration technologies are developed and deployed. Because they are economically important, have a rich history of directed research and can be most easily managed, forests and croplands are best suited for application of existing and new technology to enhance terrestrial C sequestration in the near term. Nonetheless, estimates of the potential for enhanced C storage, even in the United States, vary more than two-fold. In addition to proven management approaches, new management, chemical, and biological technology have the potential to impact C storage. What is needed is basic research to improve our fundamental understanding of natural phenomena controlling soil C sequestration and basic and applied research and development to bring new management and technology to the challenge.

Acknowledgement. This contribution is supported by the U.S. Department of Energy, Office of Biological and Environmental Research, provided to the DOE Consortium for Research on Enhanced Carbon Sequestration in Terrestrial Ecosystems (CSiTE).

(1) Intergovernmental Panel on Climate Change; *Climate Change 1995, Impacts, Adaptations and Mitigation of Climate Change: Scientific-Technical Analyses*; Cambridge University Press: Cambridge, **1996**.
(2) Metting, F.B.; Smith, J.L.; Amthor, J.S.; Izaurralde, R.C. *Climatic Change* **2001**, *51*, 11.
(3) Lal, R.; Kimble, J.M.; Follett, R.F.; Cole, C.V. *The Potential of U.S. Cropland to Sequester Carbon and Mitigate the Greenhouse Effect*; Ann Arbor Press: Chelsea MI, **1998**.
(4) Wright, L.L.; Graham, R.L.; Turhollow, A.F.; English, B.C. In *Forests and Global Change: Vol. 1, Opportunities for Increasing Forest Cover*; Sampson, R.N.; Hair, D.Eds.; American Forests Ass., Washington, D.C., **1992**, pp. 123-156.
(5) Lal, R.; *Climatic Change* **2001**, *51*, 35.

Thermodynamics of the Sequestration of Carbon Dioxide in Methane Hydrates in Porous Media

Joseph W. Wilder, Kal Seshadri, Duane H. Smith

U.S. Department of Energy, National Energy Technology Laboratory, Morgantown, WV 26507-0880, dsmith@netl.doe.gov, Phone:(304) 285-4069

Concerns about potential effects of rising carbon dioxide levels in the atmosphere have stimulated interest in a number of carbon dioxide sequestration studies. One suggestion is the sequestration of carbon dioxide as clathrate hydrates by injection of carbon dioxide into methane hydrates. Energy-supply research estimates indicate that natural gas hydrates in arctic and sub-seafloor formations contain more energy than all other fossil fuel deposits combined. The simultaneous sequestration of carbon dioxide into deposits of natural gas hydrates, if possible, represents a potentially efficient and cost effective option for the sequestration of carbon dioxide.

Data in the literature show that the conversion of bulk methane hydrate into carbon dioxide hydrate is thermodynamically favored. These results are not directly applicable to naturally occurring hydrates, because the hydrates in these locations are embedded in sediments. In addition, naturally occurring hydrates are normally made up of mixtures of natural gases, often predominately methane. The thermodynamics of any potential conversion of hydrates involving methane to carbon dioxide hydrate would therefore be affected by the size of the pores in which the conversion would take place, as well as the composition of the gas. We have developed a model that can be used to interpret or predict hydrate formation in porous media for any pore size distribution, allowing for the calculation of the heats of formation of these hydrates in porous media as a function of pore size and temperature. These results are applied to mixtures of methane and carbon dioxide. This allows for a preliminary assessment of the thermodynamic feasibility of converting hydrates formed from methane to carbon dioxide hydrate in porous media involving various size pores.

Introduction

The build up of carbon dioxide in the atmosphere has become of great interest due to the potential of this gas to play an important role in greenhouse effects, and its reported potential to induce global warming on the order of 2 – 5 K over the next century[1]. As a result of these concerns, researchers have suggested various methods to sequester carbon dioxide in order to remove it from the atmosphere. One sequestration scheme[2] is the injection of carbon dioxide into methane hydrate deposits, which it is suggested could result in the simultaneous sequestration of the carbon dioxide and the liberation of methane (which could then be collected and used as a clean fuel). Gas hydrates are crystalline structures that involve a lattice made up of hydrogen-bonded water molecules. This lattice includes cavities that can be occupied by gas molecules. Gas hydrates (such as methane hydrate) form under low temperature – high pressure conditions, both above and below the freezing point of water. Due to the large size of naturally occurring methane hydrate deposits, this represents a vast potential supply of methane. The simultaneous sequestration of carbon dioxide and liberation of methane represents a potentially cost-effective sequestration scheme for carbon dioxide. Since much of the worlds naturally occurring methane hydrates are in sediments below the ocean floors or in permafrost regions, it is necessary to consider the effects of porous media on the formation of gas hydrates.

Studies by Makogon[3] in sandstones suggested that the pressure required for hydrate formation increased as the pore size was decreased. Differences in chemical potentials and interfacial forces between the bulk and pore water affect hydrate formation in pores. Handa and Stupin[4] studied methane and propane hydrates in silica gel of 7.5 nm nominal pore radius, and Uchida et al.[5] investigated the properties of methane hydrate in three porous Vycor glass samples with pore radii of 25 nm, 15 nm, and 5 nm. In a recent work[6] the authors presented measurements for propane hydrate formation in silica gels of nominal pore radii of 7.5 nm, 5.0 nm, 3.0 nm, and 2.0 nm. Injection of carbon dioxide into methane hydrate deposits with the subsequent sequestration of the carbon dioxide and liberation of the methane would result in hydrates in equilibrium with a mixture of free carbon dioxide and methane. No results for hydrates in porous media formed from gas mixtures have been reported in the literature. In this work we consider the prediction of the equilibrium pressure for mixtures of methane and carbon dioxide in porous media based on a statistical thermodynamic model. The model is then used to estimate enthalpies of dissociation of hydrates formed from mixtures of carbon dioxide and methane in porous media.

Model Description

Munck et al.[7] presented a single equation involving T_f and P_f (the temperature and pressure under which the hydrate forms) that can be used to predict hydrate formation conditions under bulk conditions. This equation can be written as

$$\frac{\Delta m_W^0}{RT_0} - \int_{T_0}^{T_f} \frac{\Delta H_w}{RT^2} dT + \int_0^{P_f} \frac{\Delta V_w}{R\bar{T}} dP - \ln\left(g_w X_w\right) + \sum_i h_i \ln\left(1 - \sum_k Y_{ki}\right) = 0 \quad (1)$$

In eq (1), $\bar{T} = (T_0 + T)/2$, T_0 is the temperature of the standard reference state (T = 273.15 K, P = 0), Δm_W^0 is the chemical potential difference between the empty hydrate lattice and pure water in the reference state, h_i is the ratio of the number of cavities of type *i* to the number of water molecules in the hydrate lattice, and Y_i denotes the probability of a cavity of type *i* being occupied by the guest molecule. The probability Y_i is given in terms of the fugacity of the hydrate guest in the gaseous state (f_i) and the Langmuir adsorption constant (C_i) by $Y_{ki} = C_{ki} f_k / (1 + \sum_j C_{ji} f_j)$. Additionally, $\Delta H_W = \Delta H_W^0 + \Delta C_p^0 (T')(T - T_0)$, where ΔH_W^0 is a reference enthalpy difference between the empty hydrate lattice and the pure water phase at the reference temperature, ΔC_p^0 is the reference heat capacity difference, and ΔV_W is the volume difference between the empty hydrate and pure water (at T_0), and is assumed constant. Also note that the values used for ΔC_p^0, ΔH_W^0, and ΔV_W depend on whether the equilibrium involves liquid or solid water. In this work, the temperature dependence of the Langmuir constants will be accounted for by using the form presented by Munck et al.[7] This form is given by $C_{ki} = (A_{ki}/T)\exp(B_{ki}/T)$, where A_i and B_i are experimentally fit parameters, and are dependent on which guest molecule is present, as well as which of the hydrate structures is formed. To consider hydrate formation in porous media, eq. (1) must be modified to include the effect of the relevant interface on the activity of the water. After

making the necessary modifications in the region where the equilibria involve liquid water, eq. (1) becomes[8]

$$\frac{\Delta m_W^0}{RT_0} - \int_{T_0}^{T_f} \frac{\Delta H_w}{RT^2} dT + \int_0^{P_f} \frac{\Delta V_w}{R\bar{T}} dP - \ln(g_w X_w) + \sum_i h_i \ln(1 - \sum_k Y_{ki}) + V_L \frac{2\cos(q)s_{hw}}{RT_f r} = 0 \qquad (2)$$

In eq. (2), V_L is the molar volume of water in the pure water state, è is the contact angle between the aqueous phase and the hydrate, s_{hw} is the surface tension between the aqueous and hydrate phases (taken as 0.0267 J/m^2 as given by Clennell et al[9]), and r is the radius of the pores in the porous medium. Eq. (2) can be used for all temperatures above the ice point of water in the corresponding pore of radius r. Below the ice point one recovers eq. (1) since the current model assumes there are no surface effects between ice and hydrate.

Results and Discussion

Figure 1a shows the results of using eq. (1) to predict the hydrate equilibrium pressure for bulk mixtures of methane and carbon dioxide. Also shown in the Figure are the experimental data given in Sloan.[10] We note that all of the experimental data are in the liquid water region, and involve Structure I hydrates. We also note that for temperatures slightly above those depicted in Fig 1a as part of the calculated surface, the mixture involves liquid carbon dioxide, and the predictions become less accurate.

Surfaces similar to Fig. 1a can be constructed using eq. (2) for hydrate formation in porous media. For example, Figure 1b shows the results for pore radii of 3, 6, and 9 nm. The upper right hand corner of Fig. 1b shows a dramatic change in slope in the logarithm of the equilibrium pressure, due to the effects of the magnitude of the pressure on the state of the carbon dioxide involved in the equilibria. Also note the non-linearity of the surface in Fig. 1b for larger temperatures (and therefore pressures), which indicates the changing character of the carbon dioxide involved in the equilibria.

The equilibrium pressure of mixtures in porous media is a function of 3 variables (temperature, mole fraction, and pore radius). As a result, one can examine cross-sections of the 3 dimensional surface (which lies in a 4 dimensional space) other than the one shown in Fig. 1b. For example, in Figure 2 the logarithm of the equilibrium pressure is shown as a function of 1/T and 1/r for five values (0.0, 0.25, 0.5, 0.75, and 1.0) of the mole fraction of carbon dioxide in the mixtures. Due to the higher hydrate equilibrium pressure in porous media, changes in the state of the carbon dioxide in the mixture take place at lower temperatures than they do in the bulk. This can lead to different types of equilibria taking place at the same temperature in different size pores in the porous media. Fig. 2a shows the surfaces for pressures where both components (CO_2 and CH_4) remain in gaseous form. We note that as the mole fraction of CO_2 increases, the equilibrium pressure decreases due to the lower equilibrium pressure for hydrates formed from pure gaseous CO_2, as compared to that of those formed from pure gaseous CH_4. Higher temperatures and/or smaller pore sizes result in higher equilibrium pressures. At some of these higher pressures CO_2 liquefies. Due to the larger equilibrium pressure for hydrates formed from liquid CO_2 as compared to those for hydrates formed from either gaseous CH_4 or gaseous carbon dioxide, equilibria involving liquid CO2 have significantly higher equilibrium pressures. Under conditions where either the temperature is high enough or the pore size is small enough, mixtures with larger mole fractions of CO_2 have higher equilibrium pressures than pure methane hydrates (as seen in Fig. 2b), suggesting the presence of liquid carbon dioxide. In addition to the limitations of calculations involving liquefied components, the form of the Langmuir constants employed here may not be as accurate as more complicated forms. This potential source of inaccuracy will be investigated in future work.

As is made clear from these preliminary results, the evaluation of the potential sequestration of carbon dioxide by injection into sediment deposits containing methane hydrates may require accurate methods of predicting hydrate equilibrium pressures when the mixtures involve liquid carbon dioxide and gaseous methane. Since the determination of liquid phase densities and fugacities can

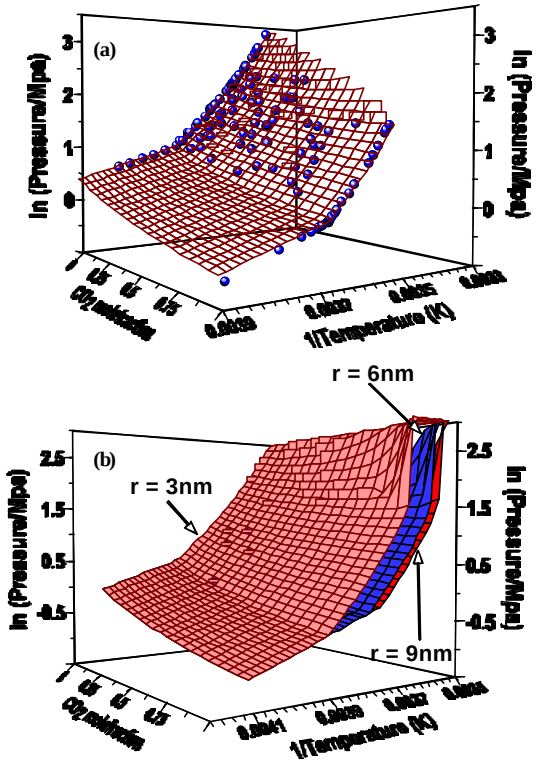

Figure 1. **(a)** Surface showing predicted equilibrium pressures for CO_2/CH_4 mixtures and experimental data for bulk hydrate formation. **(b)** Calculated surfaces for equilibrium pressures for CO_2/CH_4 mixtures in porous media with pore radii of 3, 6, or 9 nm.

involve larger errors than those for the gaseous phase,[10] great care must be taken in developing such predictions.

In addition to calculating the equilibrium pressure, eq. (2) can be used along with the Clausius-Clapeyron equation $d(\ln(P))/d(1/T) = -\Delta H/zR$ to estimate the enthalpy of formation of mixtures of carbon dioxide and methane in porous media. In the above equation, z is the gas compressibility, and is calculated using

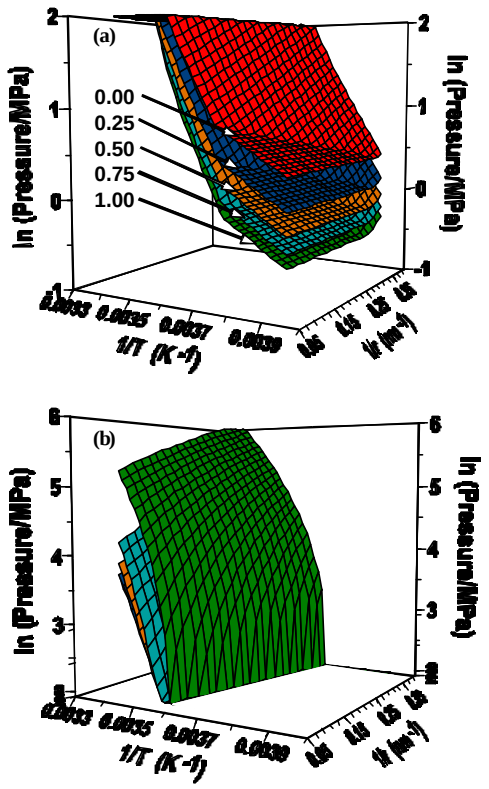

Figure 2. Calculated surfaces for equilibrium pressures for CO_2/CH_4 mixtures having CO_2 mole fractions of 0.0, 0.25, 0.5, 0.75, and 1.0 in porous media.

the Soave-Redlich-Kwong equation of state. Figure 3a shows the results of calculation of the enthalpy of dissociation for mixtures of

carbon dioxide and methane in a porous medium containing pores with 5 nm radii. Results from Figure 3a for a temperature of 273.2 K are shown in Fig. 3b, along with the results for pores having a 3 nm radius and for bulk calculations (dotted trace). We note that the very rapid changes evident in Figs 2 and 3 for pure CO_2 (a mole fraction of 1.0) are due to its liquefaction (due to the larger equilibrium pressures necessary in porous media). The calculations presented here for hydrate formation involving liquefied states may have more limitations than do those only involving gases, and as such these preliminary results will only be examined from a qualitative standpoint at this time. The difference between the enthalpy of dissociation in porous media and that in the bulk for a mixture with a mole fraction of 0.2 or greater seems to increase as the pore size decreases. For mole fractions below this there seems to be a more complicated behavior. This suggests that CO_2 sequestration in porous media via conversion of methane hydrate into CO_2 hydrate may be even more favored, thermodynamically, than it is in the bulk. While intriguing, quantitative interpretation of these results will require further investigation.

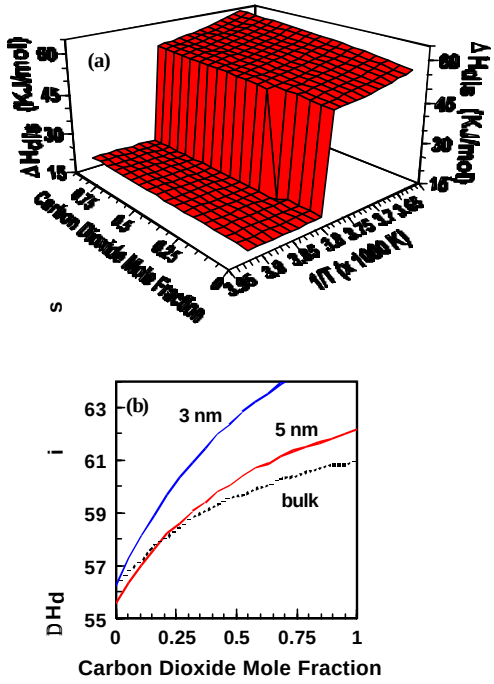

Figure 3. (a) Calculated surface showing the enthalpy of dissociation for CO_2/CH_4 mixtures in a porous medium having pore radii of 5.0 nm. **(b)** The enthalpy of dissociation at 273.2 K as a function of the mole fraction of carbon dioxide for the bulk (dotted trace) as well as in porous media with 3 and 5 nm pores.

References

1. Ravkin, A.; *Global Warming: understanding the forecast*. New York: Abbeville Press, 1992.
2. Komai, T.; Yamamoto, Y.; and Ikegami, S.; *Preprints, Am. Chem. Soc. Div. Fuel. Chem.* **1997**, *42* (2), 568.
3. Makogon, Y.F. *Hydrates of Natural Gas*, PennWell: Tulsa, 1981.
4. Handa, Y.P.; Stupin, D. *J. Phys. Chem.* **1992**, *96*, 8599.
5. Uchida, T.; Ebinuma, T.; Ishizaki, T. *Phys. Chem.* **1999**, *103*, 3659.
6. Seshadri, K.; Wilder, J.W.; Smith, D.H., *J. Phys. Chem.* B, **2001**; *105* (13); 2627.
7. Munck, J.; Skjoid-Jorgensen, S.; Rasmussen, P. *Chem. Eng. Sci.* **1988,** *43*, 2661.
8. Henry, P.; Thomas, M.; Clennell, M.B. *J. Geophys. Res.* **1999**, *104*, 23005.
9. Clennell, M.B.; Hovland, M.; Booth, J.S.; Henry, P.; Winters, W.J., *J. Geophys. Res.*, **1999**; *104*; 22985.
10. Sloan, E.D. *Clathrate Hydrates of Natural Gases,* 2nd ed.; Marcel Dekker: New York, 1997.